17

DOE/ER/61921--T1

DE-FG03-94ER61921

FINAL REPORT

A DETAILED EXAMINATION OF THE CHEMICAL, HYDROLOGICAL, AND GEOLOGICAL PROPERTIES INFLUENCING THE MOBILITY OF ^{222}RADON AND PARENT RADIONUCLIDES IN GROUNDWATER

by

Kelly Sara Sexsmith

KW final

DISCLAIMER

A thesis submitted to the Faculty and Board of Trustees of the Colorado School of Mines in partial fulfillment of the requirements for the degree of Master of Science (Environmental Science and Engineering).

Golden, Colorado

Date Oct 10, 1996

Signed: Kelly Sexsmith

Kelly S. Sexsmith

Approved: B D Honeyman

Dr. Bruce D. Honeyman
Thesis Advisor

Golden, Colorado

Date 10/11/96

Dr. John C. Emerick
Professor and Head,
Environmental Sciences and
Engineering Division

ABSTRACT

This study examines hydrological, geological and geochemical controls on ^{222}Rn variability in groundwater in the Front Range of Colorado. Specific objectives of the study are: 1) to determine if there are any correlations or spatial relationships between ^{222}Rn and the geological, geochemical and hydrogeological data; and, 2) to determine whether it is geochemically reasonable for observed ^{222}Rn levels to be the result of U and ^{226}Ra accumulation by fracture filling minerals.

Domestic-water wells were sampled and tested to determine the local aquifer characteristics and aqueous geochemistry. These tests included: water level measurements, pumping tests, field pH, specific conductivity, dissolved oxygen, temperature, alkalinity, and analysis for major anions and cations, trace metals, U and ^{222}Rn. A multivariate and staged approach was used in the data analyses. Analysis of variance tests were used to test for relationships between ^{222}Rn and the lithology of the study wells. The effects of rock-type were then removed from the chemical and hydrological variables by subtracting the mean value for each rock-type from each of the measured values within that rock-type (a residual transformation). Linear and linear multiple regression techniques were used to test for expected relationships between residual ^{222}Rn levels and these variables, and stepwise linear regressions were used to test for any unforeseen multivariate relationships in the data. Correlograms, distance-weighted average and inverse-distance-weighted average 'predictions' were used to look for spatial relationships in the data.

Groundwater ^{222}Rn levels in the study area range from 878 to 138,700 pCi/L, with a geometric mean of 6150 pCi/L. The lithology is one of the most important variables measured, accounting for 28 percent of the variance between samples. Wells in the migmatite rocks tend to have the lowest ^{222}Rn levels, while wells in the two igneous rock units: Pikes Peak Granite, and Silver Plume Quartz Monzonite have the highest ^{222}Rn

levels. In general, the regression analyses indicate that only a small portion of the variance can be accounted for by the chemical and hydrological variables. There is a weak inverse relationship between ^{222}Rn levels and transmissivity in wells with higher-than-median transmissivity levels, but not in wells with lower-than-median transmissivities. ^{222}Rn is not correlated with any of the chemical parameters, however, weak multivariate relationships are evident for ^{222}Rn and combinations of chemical and hydrological parameters. For example: 13 percent of the variance in ^{222}Rn is accounted for by a combination of uranium and bicarbonate concentrations and transmissivity. The stepwise model results are generally consistent with the chemical and radiochemical behavior of ^{222}Rn and its parents; however, these models account for a maximum of 29 percent of the variance, indicating they are not useful for predictions of ^{222}Rn levels in this system. Spatial relationships in the data are closely related to the geology; however, the results also suggest that nearby wells in the same geologic unit are more likely to have similar ^{222}Rn levels than distant wells in the same geologic unit.

Accumulation of uranium and radium to fracture surfaces is examined in Part II of this study. A conceptual model of the physical and chemical system is developed using the field data from Part I and previous studies in this area. A surface complexation model application for sorption of uranium to ferrihydrite is used to generate isotherms for a range of solution phase pH, alkalinity and uranium concentrations. These isotherms are used to calculate the sorption density, Γ, or the amount of uranium sorbed to active sites on amorphous iron-oxides along fracture margins, per mass of sorbent. The SCM modeling is verified through a series of sequential extraction tests which are used to determine the ratio of uranium to iron in amorphous iron- and manganese-oxides on the fracture surfaces from several drill-core samples. The extraction tests are also used to verify that uranium can be used as an indicator for ^{226}radium in this system.

Uranium concentrations in the fracture-filling minerals as simulated by the model are high, approximately 500x greater than the bulk rock uranium concentrations, indicating

surface accumulation of uranium is an important process for concentrating ^{222}Rn parents in favorable sites for emanation to the groundwater. Γ varies over 3 orders of magnitude in the study system, and is dependent on the solution chemistry. Uranium to iron ratios from the extraction tests are within the same order of magnitude as those simulated by the surface complexation modeling. The extraction tests verify that uranium and ^{226}Ra are correlated; thus, uranium accumulation is useful indicator for ^{226}Ra accumulation.

TABLE OF CONTENTS

LIST OF FIGURES

LIST OF TABLES

ACKNOWLEGMENTS

I wish to acknowledge and express my sincere gratitude to all of the people who have helped and supported me over the last two years. The project was funded by the Department of Energy (grant # DE-FG03-94ER61921) as part of a larger program to investigate radon in the environment. The U.S. Geological Survey provided vehicles, field equipment, and access to some specialized laboratory equipment. Additional financial support was provided by the Environmental Science and Engineering Division during my first semester through a teaching assistantship. I was also honored to receive the Laurelle DeMarco Scholarship in 1994.

My advisor, Dr. Bruce Honeyman, was a great inspiration to me throughout the project, and I feel very fortunate to have had the opportunity to work with him. He has taught me a great deal about the interaction between metals and surfaces, and encouraged me to pursue the surface chemistry aspects of this project.

Special thanks go to my co-advisor, Dr. Eileen Poeter, who gave many helpful suggestions on the hydrogeological aspects of the project and somehow always found time to sit down and work through my problems on paper. She did a wonderful job of keeping the project funded and organized, with monthly group meetings and more frequent electronic-mail correspondence. Her enthusiasm, encouragement and energy were much appreciated.

My committee members, Drs. Rich Wanty (USGS) and Robert Holub provided many helpful suggestions during the project. Dr. Wanty rescued me on my first solo sampling trip by teaching me how to 'whip' a hopelessly stuck water level indicator from a well, and has given me a great deal of practical advice since then. His insight and understanding of natural systems helped to focus my understanding of the study system and gave me some very useful ideas during the development of Part II. I had many

interesting discussions with Dr. Holub about the nature of multidisciplinary research, and appreciated his encouragement and understanding of the complexity of environmental research.

At the start of the project, I was very fortunate to have help and guidance from Pete Folger, who was in the final stages of completing his Ph.D. dissertation in this field. Pete generously shared his knowledge and experience on ^{222}Rn issues throughout the project, and his dissertation, literature collection, maps, and files were greatly appreciated. Dr. Warren Day and Dave Frishman of the U.S.Geological Survey were part of the project team during the early stages of my research and they both helped me gather the information I needed to get started. Dave Frishman was particularly helpful in compiling the geological data for the site, and getting it into a database management system for me - no small task!

I appreciated the help from Susan Steelweir of the Denver Water Board, who gave me access to the Ferndale drillcore, and for her enthusiasm and support in arranging access to the core library.

I would like to thank the "Rad-heads" and other friends for making my time here so enjoyable. Special thanks go to John Lenhart, Richard Murphy, and Charoen Sanpawanitchikit for their help in the lab, and Lee Landkamer for all his patience and help with my math, chemistry and computer stuggles. Thanks also to Chris Dick and Debra Boopsingh for assistance in the field and laboratory.

Finally I would like to thank David for his help with the statistical analyses during his too-short visits, and for his patience and understanding during the time I was away.

OVERVIEW

The purpose of this study was to examine the natural processes affecting the distribution and abundance of ^{222}Rn in groundwater. Although there are no clear indications that direct ingestion of ^{222}Rn in water poses a significant risk to human health, ^{222}Rn in well water is known to contribute to high levels of airborne ^{222}Rn in some homes (Prichard, 1987; Lawrence *et al.*, 1992). Airborne ^{222}Rn is thought to cause between 7,000 and 30,000 lung cancer deaths per year in the United States (Puskin, 1992), and is the most significant source of ionizing radiation to which the general public is exposed (Cothern, 1987).

Studies on the distribution and occurrence of ^{222}Rn are important for developing methods to predict where high levels of ^{222}Rn might be found and to develop strategies to prevent or mitigate the associated health hazards. Specific objectives of the study were:

1) to determine if there are any correlations or spatial relationships between ^{222}Rn and the geological, geochemical or hydrogeological parameters in the study area and assess the possibility of using these correlations for regional predictions of ^{222}Rn levels in groundwater (Part I); and,
2) to examine the importance of fracture filling minerals in providing local accumulation zones for ^{222}Rn parent radionuclides (Part II).

The study expands upon work completed in the Front Range of Colorado by students and faculty at the Colorado School of Mines in Golden and researchers at the US Geological Survey in Denver (Lawrence, 1990; Lawrence *et al.*, 1991; Wanty *et al.*, 1991; Lawrence *et al.*, 1992; Frishman *et al.* 1993; Folger *et al.*, 1994; Folger, 1995; Folger, *et al.* 1996a; Folger, *et al.*, 1996b). Specific findings of these earlier studies are presented in the relevant sections of this thesis.

The study was located near Pine Junction, CO, 30 km southwest of Denver (Figure 1). This area was selected for study because it is considered to have *relatively* simple geology compared to other locations in the Front Range of Colorado; it has a sufficient population density to allow sampling of existing water wells, and previous studies have found that ^{222}Rn levels in these water wells are high, often exceeding the proposed EPA groundwater standard of 3000 pCi/L (Pete Folger, *pers. comm., 1996)*. The study area is referred to as the "Elk Creek study area" throughout this document.

Previous studies on ^{222}Rn variability have shown that ^{222}Rn levels in groundwater are a function of many different parameters in the water/rock system, as shown in Figure 2 (based on Folger, 1995). Although some studies described in the literature show clear relationships between ^{222}Rn concentrations in soil gas or indoor air, and specific geological or physical parameters (e.g. Gates and Gundersen, 1989; Burkhart and Huber, 1993), there are many other air and groundwater systems for which no clear relationships have been established (Gascoyne and Barber, 1992; Lawrence, 1990). When considering the difficulties in isolating variables in a regional-scale field study, the lack of correlation of ^{222}Rn with any one variable is not surprising. In the first part of this study, the regional data are examined using multivariate and spatial statistical techniques to determine if there are any correlations or spatial relationships between ^{222}Rn and the geological, geochemical or hydrogeological parameters in the study. To date, multivariate and spatial data analyses have not been applied to a regional study of ^{222}Rn variability.

The importance of local-scale features cannot be overlooked in a multiparameter study; however, local-scale features are difficult to measure in the context of a regional study. Two important local variables are the distribution and abundance of ^{222}Rn parents (uranium and radium) in the system. Researchers have observed uranium and radium enrichment along fracture surfaces, grain boundaries and other secondary sites in rock and sediment (Tanner, 1980; Caruso and Simmons, 1985; Wathen, 1987; Gunderson, 1989; Torgerson *et al.*, 1990; Schumann, 1993; Flexser *et al.*, 1993). It has been established

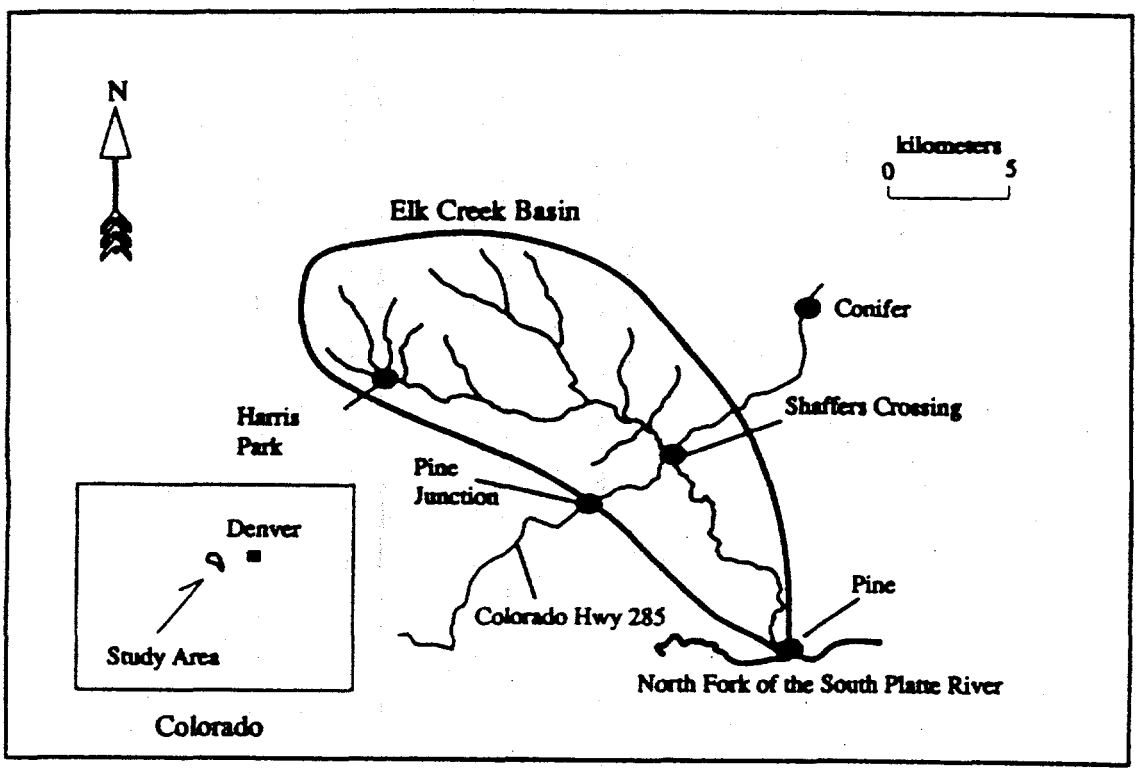

FIGURE 1 Location Map

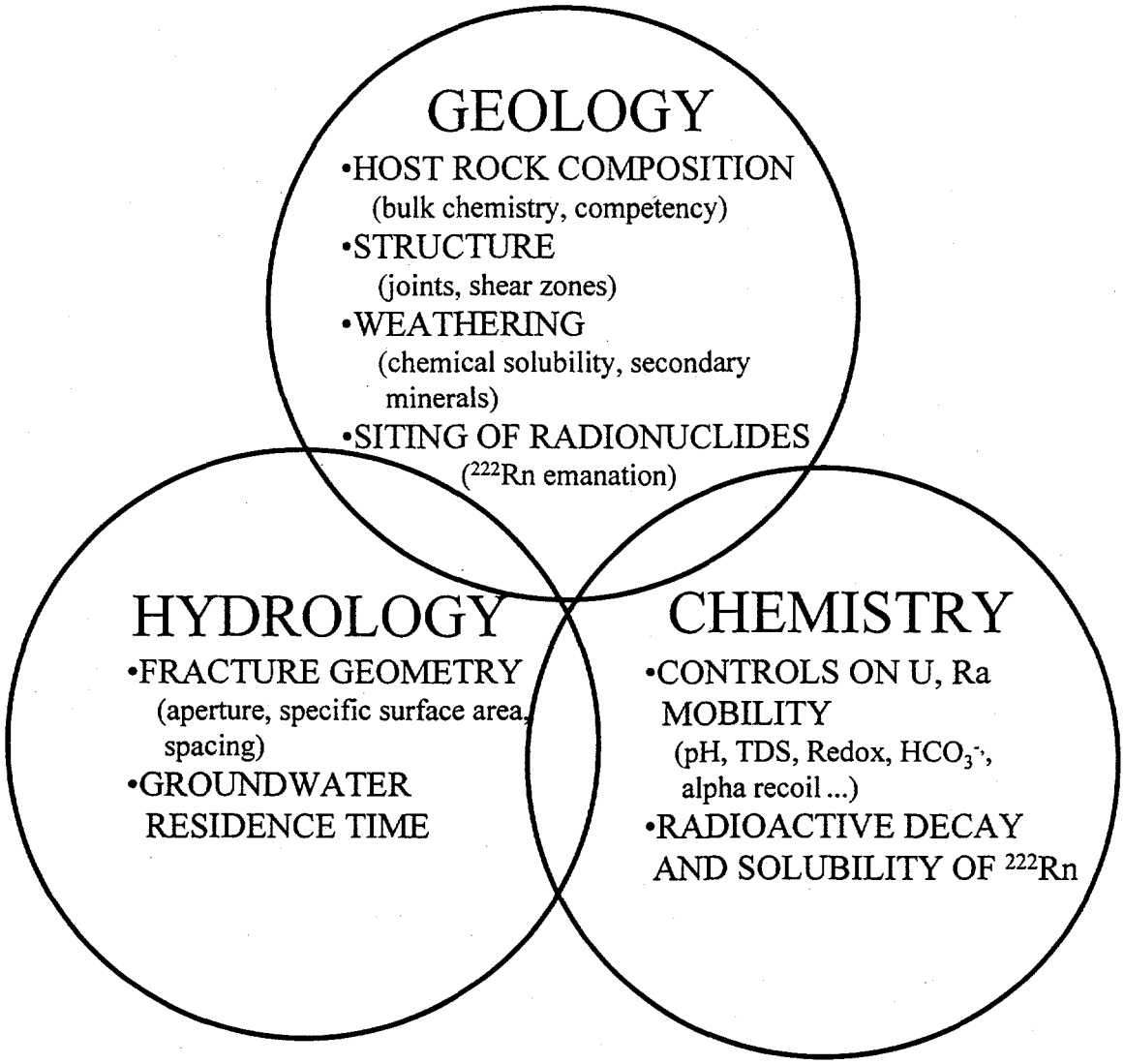

FIGURE 2 Factors Controlling ^{222}Rn Variability in Natural Systems (after Folger, 1995).

that surface enrichment of ^{222}Rn parent radionuclides enhances ^{222}Rn emanation rates over systems where the parent radionuclides are uniformly distributed through the rock mass (Krishnaswami and Seidemann, 1988; Semkow, 1990). In the Elk Creek study area, it is thought that iron oxides located along fracture margins are a likely site for the accumulation of ^{222}Rn parent radionuclides (Wanty *et al.*, 1991). The proposed process for this accumulation is sorption of uranium to the oxide mineral surfaces. Subsequent decay of ^{238}U results in an accumulation of poorly soluble decay products, including ^{222}Rn's immediate parent, ^{226}Ra. In Part II of this study, a surface complexation model describing uranium sorption to iron-oxides is used to study the accumulation of ^{222}Rn parent radionuclides in the system. The model is verified through sequential dissolution experiments carried out on fracture filling minerals from drill-core samples in the Pike's Peak granite.

PART I

ENVIRONMENTAL CONTROLS ON ^{222}RADON IN GROUNDWATER

1.0 INTRODUCTION

The literature suggests that a number of physical and chemical factors contribute to ^{222}Rn levels in groundwater. In natural systems, the details of relationships between ^{222}Rn activities and geological, chemical and hydrogeological processes are often difficult to discern because it is often not possible to isolate the contribution of one process from that of another.

The objective of this portion of this thesis is to assess the relative contribution of a range of system variables by using multivariate statistics. Specific objectives are: 1) to determine if there are any correlations or spatial relationships between ^{222}Rn and the geological, geochemical and hydrogeological data; and, 2) evaluate whether these indicators can be used to estimate ^{222}Rn levels in groundwater. Even if the results are not useful in a 'predictive' sense, they may still provide support for theoretical models of ^{222}Rn levels in groundwater.

A brief review of the controls on ^{222}Rn variability is provided in the following introductory section (Section 1.1). The multivariate approach to data analysis is discussed in Section 1.2 and the overall approach to this part of the study is outlined in Section 1.3.

1.1 Review of the Theoretical Controls on ^{222}Rn in Groundwater

Previous studies have shown that ^{222}Rn levels in groundwater are a function of many variables in the water/rock system. These were briefly outlined in the overview section, and Figure 2. The following discussion reviews the current understanding of how the

geological, hydrological and chemical parameters may influence ^{222}Rn levels in groundwater.

1.1.1 Geological

The primary geological controls on ^{222}Rn levels are the abundance and distribution of ^{222}Rn parent radionuclides (^{226}Ra and its ^{238}U-series parents) and the ^{222}Rn emanation potential of rocks and soils. Geologic controls include: bulk mineralogy, texture and porosity; structure and degree of fissuring; secondary mineralization; and trace metal and radionuclide composition. On a regional-scale map, the consistency of these features depends on the overall consistency of the geologic unit, the age and weathering history of the units and the scale of geologic mapping. In systems with spatially uniform geological characteristics, one would expect similarly uniform emanation rates. The abundance of radionuclides can be characterized using bulk chemical tests (assays) and the distribution can be characterized using thin sections and autoradioluxographs to locate sites enriched in alpha-producing radionuclides. It is important to recognize that geology is closely interrelated to the groundwater hydrology and the chemistry of the system. For example, aqueous chemistry is largely determined by the mineralogical characteristics of the host rock. Conversely, secondary mineralization in the fractures is a function of the water chemistry at some period in the geologic history of the rock. Because these factors are so closely interrelated, geology is considered a 'catch-all' parameter, encompassing many of the chemical and hydrological attributes of the groundwater system.

Previous studies in this study area have found a connection between the bedrock lithology and ^{222}Rn levels in the groundwater (Lawrence *et al.*, 1991; Frishman *et al.*, 1993). However, despite the area's apparently homogeneous properties, uranium concentrations can vary widely. For example, U concentrations varied from 2 to 25 ppm in a single outcrop of Pikes Peak Granite (Frishman *et al.*, 1993), and ranged from 2 to

250 ppm in surface samples collected in the northwest part of the study area (Lawrence *et al.*, 1991). Local uranium enrichment was also found along fracture margins (Frishman *et al.*, 1993) and were associated with iron-oxide-altered drill cuttings (Folger, 1995).

1.1.2 Hydrological

Fracture aperture and groundwater residence time are the primary hydrological controls on ^{222}Rn in groundwater in this system. Fracture aperture is thought to be inversely related to ^{222}Rn concentration in systems where ^{222}Rn parents are uniformly distributed along the fracture margins and where the groundwater velocity is slow relative to the rate of decay and ingrowth of ^{222}Rn (Rumbaugh, 1983). Above a minimum limiting value (Renshaw, 1995), the fracture aperture is related to transmissivity by the cubic law as shown in equation 1 (Tsang, 1992). Thus, it is expected that transmissivity would also be inversely related to radon.

$$b = \left(\frac{12T\mu}{\nu}\right)^{\frac{1}{3}} \qquad (1)$$

where:

b	=	fracture width or aperture (m)
T	=	transmissivity (m^2/s)
μ	=	dynamic viscosity ($kg/m \cdot s$)
ν	=	specific weight of water ($kg/s^2 \cdot m^2$)

An earlier field study in the Elk Creek area showed that water samples from highly transmissive wells tended to have lower ^{222}Rn levels, but ^{222}Rn levels in poorly transmissive wells were not always high (Lawrence *et al.*, 1991). Detailed studies in a well-field in the northwest part of the study area showed that differences in fracture aperture could explain differences in ^{222}Rn concentration within, but not between hydraulically connected well pairs (Folger, 1995). A more clear relationship was found

between ^{222}Rn and transmissivity in a relatively uniformly fractured bedrock in Eastern Pennsylvania (Rumbaugh, 1983).

In systems where the groundwater residence time is shorter than the characteristic time of ^{222}Rn ingrowth and decay, there is a "dilution effect", where radon levels reflect the average hydrological condition in the aquifer and never have time to reach secular equilibrium (radioactive equilibrium between the parent radionuclide and its daughter) in the local fracture system. Thus, at high groundwater velocities (and consequently short residence times), the expected relationship between ^{222}Rn and fracture aperture breaks down. Groundwater velocity is difficult to ascertain in fractured flow systems; consequently, it is not possible to directly measure the effects of groundwater velocity on the results. Numerical modeling of ^{222}Rn transport through fracture networks has shown that there is a complex relationship between groundwater residence time, fracture geometry and ^{222}Rn in systems with uniform surface concentration of ^{226}Ra (Folger, 1995; this study Appendix A). An illustration of this interrelationship is shown in Figure 3. It should be noted that in the numerical model, boundary conditions constrained the relationship between residence time and fracture aperture such that fracture segments with wide apertures had longer residence times. This relationship is not expected in the field.

1.1.3 Chemical

^{222}Rn is a noble gas formed by the decay of ^{226}Ra, a member of the ^{238}U series of naturally occurring radionuclides. Although it is highly soluble in water, ^{222}Rn has a low partial pressure and tends to degas on exposure to air. Because it is a noble gas, it does not interact to an appreciable extent with other constituents in the water/rock system. Rather, its activity is controlled by that of its parent, ^{226}Ra, its rate of decay, and the groundwater residence time:

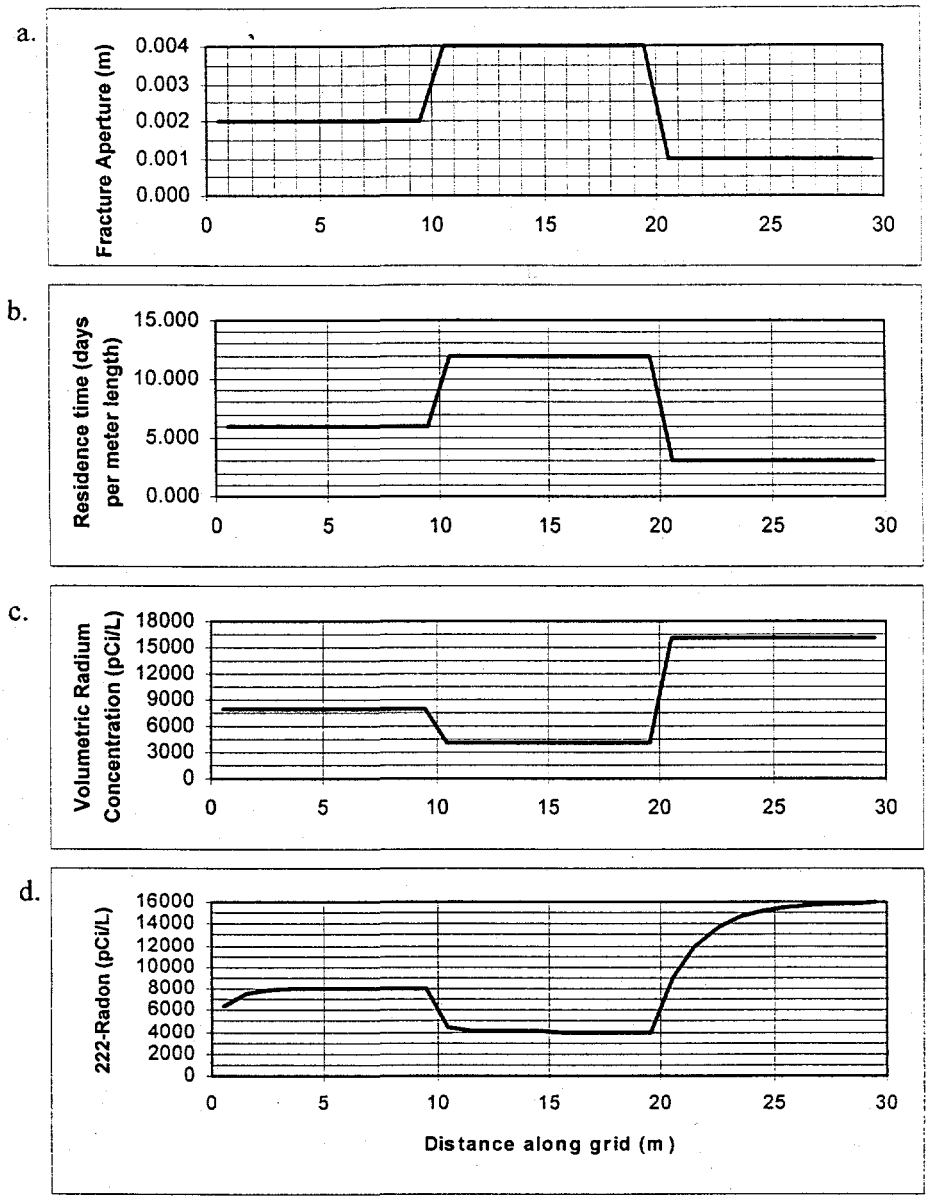

FIGURE 3 Relationship of fracture aperture, residence time and ^{226}Ra concentration to radon ingrowth and decay: a) fracture aperture in three connected fracture segments; b) corresponding residence times in the fracture segments; c) corresponding volumetric ^{226}Ra concentration based on a uniform surface concentration of 8000 pCi/L; and, d) resulting radon profile as water moves through the fracture.

$$A_{Rn} = \frac{\lambda_{Rn}}{\lambda_{Rn} - \lambda_{Ra}} \cdot A_{Ra}{}^{o} (e^{-\lambda_{Ra} t} - e^{-\lambda_{Rn} t}) + A_{Rn}{}^{o} e^{-\lambda_{Rn} t} \quad (2)$$

where:
- A_{Rn} = activity of ^{222}Rn in system as a whole (pCi)
- A_{Ra} = activity of ^{226}Ra in system as a whole (pCi)
- λ_{Rn} = decay constant for ^{222}Rn
- λ_{Ra} = decay constant for ^{226}Ra
- t = groundwater residence time

In systems where the residence time is sufficiently long that ^{222}Rn has reached secular equilibrium with its parent, ^{226}Ra, equation 2 is reduced to the following:

$$A_{Rn} = A_{Ra}{}^{o} (e^{-\lambda_{Ra} t} - e^{-\lambda_{Rn} t}) \quad (3)$$

Numerous examples in the literature have shown that ^{222}Rn is not in secular equilibrium with ^{226}Ra in the water phase of natural groundwater systems (Tanner, 1964; Hammond *et al.*, 1988; Lawrence *et al.*, 1991; Gascoyne and Barber, 1992). This indicates that ^{222}Rn must be supported by ^{226}Ra on the aquifer solids, and suggests that water chemistry would have little or no influence on the ^{222}Rn results. In some systems, however, the water chemistry may indirectly reflect parent radionuclide enrichment in the solid phase. In particular, there may be relationships between ^{222}Rn and the water chemistry parameters in systems where the parent radionuclide concentration is controlled by surface reactions (sorption/desorption).

In the Elk Creek groundwater system, uranium occurs primarily in the +6 oxidation state, i.e. as uranyl species (UO_2^{2+}, $UO_2CO_3^{o}$, UO_2OH^{-} etc.). Uranyl species are considered to be more mobile than reduced forms of uranium; however, in the pH range of 3 to 8, they are highly surface active and tend to form strong complexes with aquifer solids. Surface uranium concentrations are a function of the mineralogy on fracture

surfaces, competing ligands (primarily carbonate in the Elk Creek System), pH and aqueous uranium concentrations. In systems which have been closed for geologically significant lengths of time, it is reasonable to assume that U on the surface would be in secular equilibrium with all of its daughters, including ^{226}Ra. Thus, the water chemistry parameters controlling uranium mobility might also be correlated with ^{222}Rn.

Radium mobility is controlled by a combination of alpha recoil processes (Osmond and Cowart, 1992) and geochemical processes (Gascoyne, 1992). Radium is an alkaline-earth metal, and occurs primarily as Ra^{2+} in natural waters (Hem, 1992). Ra forms soluble complexes with nitrate, chloride, and iodate, and poorly soluble complexes with sulfate and carbonate. Ra is also surface active, although to a lesser degree than U. Sorption tends to increase with increasing pH, and decrease in the presence of 0.1 to 1 milli-molar levels of calcium and other divalent cations (Riese, 1982). Ra activities are generally much lower than uranium in natural waters, reflecting the poor mobility of their immediate parents (^{230}Th, ^{228}Th, ^{227}Th) (Hem, 1992).

Previous studies in this area have not yielded any meaningful correlations between radon and any of the other dissolved constituents in the water (Lawrence, 1990). However, as discussed below, it was not possible to isolate the chemical parameters from the hydrological parameters in this complex natural system, thus a multivariate approach to data-analysis is needed to detect any of the expected relationships.

1.2 Multivariate and Spatial Controls

Although some studies described in the literature have found clear relationships between ^{222}Rn concentrations in soil gas or indoor air and specific geological or physical parameters (Wathen, 1987; Beck and Brown, 1987; Gates and Gundersen, 1989; Burkhart and Huber, 1993), there are many soil gas, air and groundwater systems where no clear relationships have been established (Gascoyne and Barber, 1992; Lawrence, 1990). To

date, multivariate statistics have not been used to test for relationships between radon and the geological, hydrological and chemical variables in a regional study of radon. Although the results of multivariate statistics are sometimes difficult to conceptualize, the methods provide better insight into the complexities of natural systems, and can be used to evaluate the importance of the processes described in the preceding sections. Multivariate statistical techniques are well developed in the ecological field, where there are many similarities in the form and objectives of data analysis (James and McCulloch, 1990). For example, categorical data (e.g., lithology) is often mixed with numerical data (e.g., transmissivity), and it is often desirable to consider the spatial attributes of the samples. Another difficulty encountered in this type of data is the interdependency of variables, i.e. autocorrelation. Autocorrelation effects can be minimized through careful interpretation of the statistical results.

As discussed previously, geology encompasses many aspects of the groundwater system. Since geology is a spatial attribute, it is important to consider the influence of geology on ^{222}Rn in an appropriate spatial context. Spatial statistical techniques (geostatistics) have been used for many years in the mineral exploration and mining field (Bonham-Carter *et al.*, 1988) and for ecological studies (Legendre and Fortin, 1989; Rossi *et al.*, 1992) to examine spatially dependent relationships. In this study, spatial data analysis methods are used to examine spatial relationships in the data, both with and without the more obvious association with geology.

1.3 Approach to the Study

Domestic water wells throughout the study area were sampled and tested to determine the local aquifer characteristics and aqueous chemistry. The results were pooled with data from two previous studies in the same area (Lawrence, 1990; Folger, 1995), and analyzed using multivariate and spatial statistics. Controls on radon variability were

examined at three scales: variability contributed by measurement error, geological variability and variability within geological units.

The following chapter (Chapter 2) describes the sampling and data analysis methods. Chapter 3 presents the results of the field studies and statistical analyses examining controls on ^{222}Rn variability. A discussion of the results is provided in Chapter 4. The findings of the study are summarized in Chapter 5. Citations for Part I are provided in the overall reference list of the thesis.

2.0 METHODS

2.1 Field Studies

Forty-three domestic-water wells in the Elk Creek drainage basin were sampled and tested to determine the local aquifer characteristics and aqueous geochemistry. Tests included: water level measurements, pumping tests, field pH, specific conductivity, dissolved oxygen, temperature, alkalinity, major anions and cations, trace metals, U and ^{222}Rn. The sample locations are shown in Figure 4.

2.1.1 Geological Data

Geological data was taken from USGS 1:24,000 scale geological maps (Bryant, 1974a,b; 1976a,b).

2.1.2 Hydrogeological Measurements

Forty-two of the sample locations were drilled wells, with total depths ranging from 30 to 200 meters. One of the samples (95-CO-21) was a large cistern fed directly by a sub-surface spring. Where possible, well records obtained from the Colorado State Engineer's Office were used to determine the well geometry, aquifer characteristics and specific capacity data of the wells as recorded by the driller. Drilled wells in this area are typically 20 cm diameter through the overburden and loose rock and 15.2 cm diameter at depth. The upper 6 to 16 meters are usually cased with an 16.8 cm diameter steel casing. A smaller (10.2 cm diameter) perforated, polyvinyl chloride (PVC) casing extends through the steel casing to the bottom of the hole. All of the wells were equipped with a dedicated submersible pump, which was connected to a pressure tank at the surface.

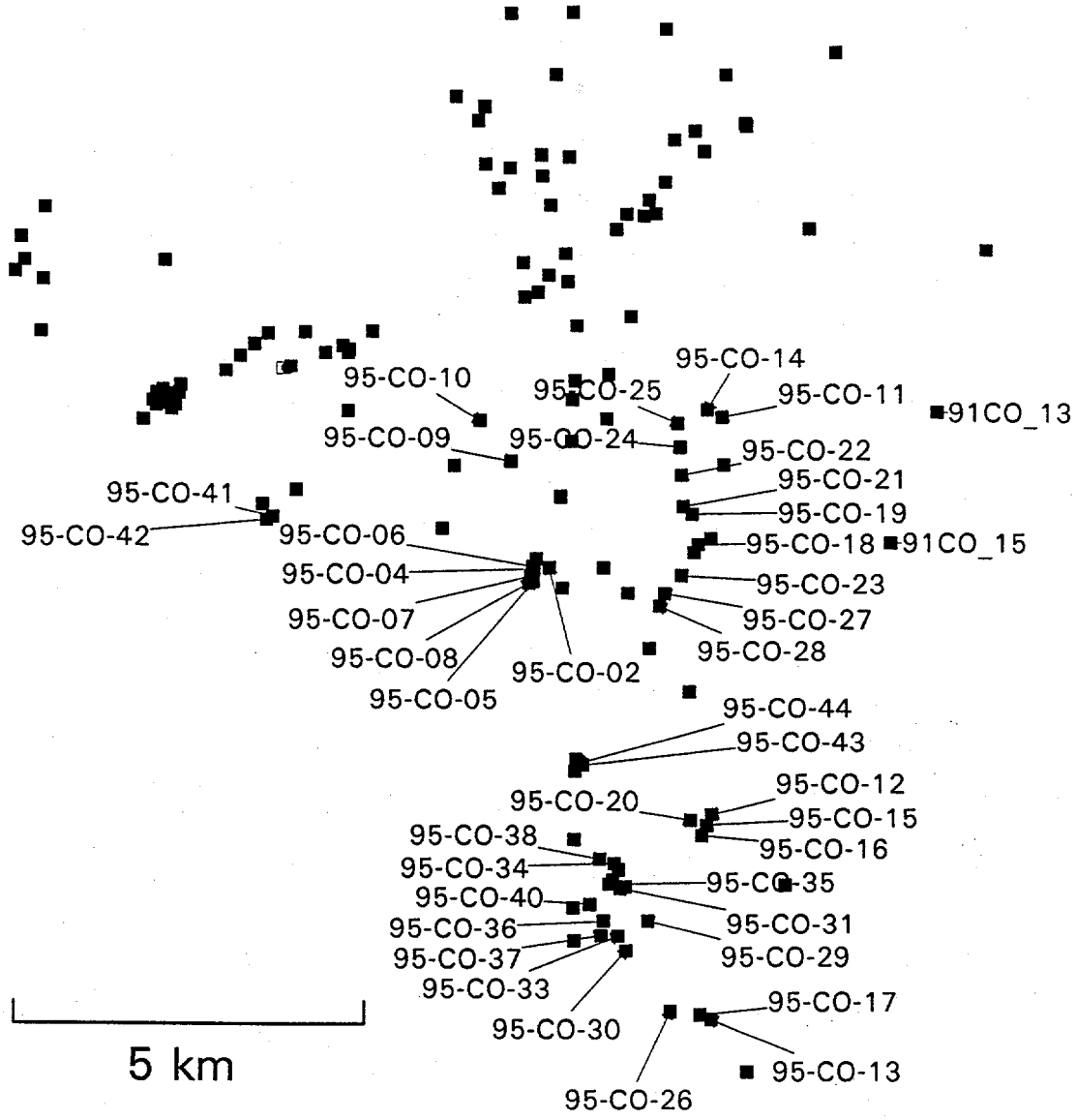

FIGURE 4 Sample Location Map showing relative locations of the 1995 samples. The latitude and longitude of the samples are provided in Appendix B.

Single-well aquifer tests were completed on 37 of the 43 wells according to the following procedure: 1) The water level was recorded using an electronic water-level indicator. Measurements were taken over a period of 10 to 15 minutes prior to the test to ensure that steady-state or static conditions had been established. 2) An outdoor spigot connected to the pressure tank was used to control the flowrate from the pressure tank. The total volume of water and the flowrate at various time intervals were determined using an impeller-type flowmeter (Carlon JLP or Neptune TM). In some cases, the flowrate was measured using the 'bucket and stopwatch' method. The flowrate was typically fixed at a constant value between 3 and 23 liters per minute. In some cases, the flow rate had to be adjusted to avoid pumping the well dry or because insufficient drawdown was observed. 3) The time and the drawdown at the well were recorded over a period of 1 to 2 hours. Since the submersible pump turned the well on and off according to the pressure level in the pressure tank, the time-drawdown curves all have cyclic patterns reflecting actual pumping and intervals of recovery. In interpreting the results, average drawdown curves were used (Lawrence, 1990). 4) The water was turned off after approximately 2 hours of pumping and the water level during this recovery period was recorded. In rapidly recovering wells, the water level was measured until it approached the static level measured at the beginning of the test. In slowly recovering wells, the water level was measured for as long as possible (usually 1-2 hours).

Several techniques were used to calculate the transmissivity, including:

- estimation using specific capacity data from the pumping tests and driller's logs;
- Theis graphical method for evaluating the time/drawdown data; and,
- Jacob semilog method for time/drawdown and time/recovery data.

An estimation of the transmissivity could be made for some wells using either the specific capacitance data available on the driller's logs or equivalent results from the

pumping tests (Czarnecki and Craig, 1985). The transmissivity was estimated by rearranging the Theis equation as shown in equation 4:

$$f(T) = T - \frac{Q}{s}\frac{2.3}{4\pi}\log\frac{2.25Tt}{r^2S} \qquad (4)$$

where:

T	=	transmissivity (m^2/s)
Q	=	pumping rate (m^3/s)
s	=	drawdown (initial - final water level) (m)
t	=	pumping time (s)
r	=	borehole radius (m)
S	=	storativity or specific yield

Equation 4 was then solved iteratively for a T which allowed $f(T)$ to approach zero. The calculations were done using a Quick-BASIC routine.

Theis curve matching was done using either the graphical procedure described in Freeze and Cherry (1979) or AQUIX-4S (EnviroTools Ltd., 1993), a software package which uses an inverse modeling procedure to match the Theis curve to the drawdown data, and then optimizes the fit using a ridge regression technique. Semilog plots prepared using a basic spreadsheet package were used to evaluate the time/drawdown data (Freeze and Cherry, 1979), and the time/recovery data (U.S. Department of the Interior, 1985), and were found to be preferable to the curve matching procedure because they provided better insight on the presence of boundary conditions in the data.

Where possible, all of the above methods were used in the estimations. The best estimate of transmissivity was selected and recorded in the database after evaluating the goodness-of-fit, the influence of boundary conditions and the validity of the method.

2.1.3 Groundwater Sampling

Field measurements and water samples were collected from each of the 43 study wells. Sampling was usually done during the later part of the pumping test to ensure that fresh formation waters were collected. Samples were usually collected from a garden hose attached to the spigot used to control the flow-rate. The hose drained into a clean wash-bucket which was allowed to overflow at some distance from the well. Samples and field measurements were taken as close to the hose outlet as possible to avoid interaction with the atmosphere (losses of ^{222}Rn, or CO_2 and O_2 transfer).

Temperature, pH, specific conductivity and dissolved oxygen were measured in the field. The pH and temperature were recorded using a Beckman Model Φ10 pH meter with automatic temperature correction. The specific conductivity was recorded using a Markson CDM-1 meter, with manual temperature compensation. Dissolved oxygen was measured using a Hach DR 2000 meter. After the field readings had stabilized (usually after 1 hour), samples were collected for subsequent laboratory analysis of major anions and cations, uranium and ^{222}Rn. The sampling protocol is summarized in Table 1.

2.1.4 Previous Field Studies

Data from previous studies in this area (Lawrence, 1990; Folger 1995) were combined with data from the 43 samples collected in 1995. Sampling and analytical methods were generally consistent among the studies. One important change was made in the way geologic units were assigned. Lawrence (1990) examined nearby outcrops and assigned the local geological characteristics to his samples, while subsequent investigations (Folger, 1995; this study) assigned geological units on the basis of geological maps. For consistency, the 1988/89 data were re-evaluated using the geologic maps.

TABLE 1 Field Sampling Protocol

Sample	Size/Bottle Type	Collection Procedure	Preservation
cations and total uranium	125 mL, LDPE* bottle	filtered **	HNO_3 to ≈ pH 1
anions	30 mL, LDPE bottle	filtered **	refrigerated
alkalinity determination	125 mL, LDPE bottle	collected with zero headspace,	refrigerated, analyzed within 24 hours of collection
^{222}radon	10 mL samples in 20 mL glass liquid scintillation vials, with polyseal caps	***	tightly capped, analyzed within 24 hours

Notes: * low density polyethylene

** filtered through a 0.45 μm cellulose acetate membrane filter.

*** The collection procedure is based on the U.S. EPA procedure (Cecil and Gesell, 1992). The flowrate was reduced to less than 1 gpm, and a pipette was used to slowly collect 10 mL of sample from the hose outlet. The pipette tip was immediately submersed and the contents were released into a scintillation vial containing 10 mL of a mineral-based scintillation cocktail with 2,5-diphenyloxazole (PPO) and p-bis-lo-methylstryrylbenzene (bis-MSB) as fluors. The vial was immediately capped and sealed with a polyseal cap, shaken, and placed in a cardboard shipping tube for transport back to the laboratory. A duplicate sample was taken at each location.

Selected data collected by Lawrence (1990) were used to assess the relative importance of variability *within* wells (i.e. sampling error and temporal changes), compared to the variability *between* wells (i.e. spatial variability). In his study, Lawrence sampled 28 wells twice, once during the 1988 field season and once in 1989. Duplicate samples were collected during both of the time periods. This nested sampling design is illustrated in Figure 5.

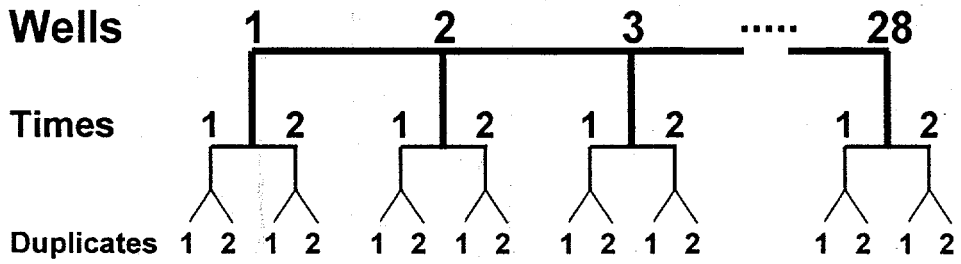

FIGURE 5 Nested sampling design used to assess the relative importance of temporal and sampling variability.

2.2 Analytical Methods

Alkalinity was determined in the laboratory within 24 hours of sample collection according to the standard USGS method I-1030-78 (Skougstad *et al.*, 1979). The pH was recorded after each addition of titrant using an Orion Model 720A pH meter equipped with a Ross electrode. The titrant consisted of commercially prepared analytical grade 0.02 N ± 0.0002 sulfuric acid. The titration was carried past the endpoint, to a pH of about 3.0. The endpoint was defined as the inflection point on the titration curve, typically about pH 4.5. Alkalinity was calculated as follows:

$$Alk(as\ CaCO_3\ in\ mg/L) = \frac{1000}{mL\ sample} \times (50.05)(0.02N) \times mL\ acid\ to\ endpoint \quad (5)$$

Radon concentrations were determined using the liquid scintillation technique (Pritchard and Gesell, 1977; Hahn and Pia, 1991). A series of 4 radon standards were prepared using a nominal ^{226}radium standard obtained from Isotope Products Laboratory. These standards were allowed to ingrow ^{222}Rn for 21 days, and were then calibrated against traceable standards at the U.S. Geological Survey National Water Quality Laboratory in Arvada, Colorado. Samples were analyzed within 24 hours of collection and decay corrected. The samples were shaken vigorously and then allowed to equilibrate in the dark for at least 3 hours prior to counting for 50 minutes with a Packard Model 1600 Liquid Scintillation Analyzer. Calibration of the instrument was achieved by counting the standards and a background sample each time a field sample was analyzed. The ^{222}Rn concentration was calculated as follows:

$$C_{Rn-222} = \frac{(cpm\ of\ sample - cpm\ of\ background) \times 1000\left(\frac{mL}{L}\right)}{CF \times decay\ factor \times volume\ sample\ (mL)} \quad (6)$$

where:

C_{Rn-222}	=	concentration of radon in pCi/l
cpm	=	counts per minute
CF	=	calibration factor in cpm/pCi (net cpm of most similar nearest standard/^{222}radon activity of the standard)
decay factor	=	$e^{-\lambda t}$ where λ is the decay constant (ln 2/3.824 days^{-1}) and t is the time between sample collection and the counting period in days.

Anions, including F^-, Cl^-, NO_3^-, PO_4^{2-} and SO_4^{2-}, were determined using a Dionex Model 2120 Ion Chromatograph. Phosphate was not detected in any of the samples. Cations were analyzed using a Perkin Elmer Optima 3000 inductively coupled plasma atomic emission spectrometer (ICP-AES). A suite of elements was measured, which included detectable levels of Na, Li, Ca, Mg, Ba, Sr, Cu, Mn, and Zn in most of the wells, and detectable levels of Fe, K, Ag, Cd, B, Si, Cr, Ni, Al, Mo, and Ti in some of the wells. Total uranium concentrations were measured using a Scintrex UA-3 laser fluorimeter and calibrated using the standard addition method.

2.3 Data Analysis

2.3.1 Data Transformation

Data with values less than the analytical detection limit were given values of one-half the detection limit for statistical analyses. Temperature, pH, dissolved oxygen and silicon data were normally distributed and were used without further transformation. The remaining chemical variables and transmissivity were log-normally distributed and were ln-transformed for the statistical analyses.

A commercially available statistics package, SYSTAT was used for the statistical analyses except where indicated.

2.3.2 Determining The Relative Importance of Sampling Error and Temporal Variation Within Wells

Three sources of variation in radon measurements were examined using the 1988/89 radon data from Lawrence (1990; described in Section 2.1.4). The nested data were used to examine the relative importance of: sampling and measurement error between duplicates collected at the same time in a well; temporal variations, resulting from

different hydrological conditions, pumping stresses or seasonal factors; and, variations between wells (the focus of this study). Variance partitioning techniques (Burdick and Graybill, 1992) were used to calculate the percentage of variance due to each of the three sources. Expected mean squares (MS) from ANOVA tables are used in the calculations. In brief, the variance partitioning in this design is calculated as follows (Sit, 1995):

$$\text{variance due to sampling error:} \quad \sigma_e^2 = MS_e \tag{7}$$

$$\text{variance due to temporal factors:} \quad \sigma_t^2 = \frac{MS_t - \sigma_e^2}{a}$$

$$\text{variance between wells:} \quad \sigma_w^2 = \frac{MS_w - \sigma_e^2 - a\sigma_t^2}{a \cdot b}$$

where: $a = 2$, the number of duplicates collected at a well
$b = 2$, the number of times that the wells were sampled.

The data collected by Folger (1995) and in this study are assumed to show a similar variance distribution.

2.3.3 Variation Between Rock-types

A single factor ANOVA was used to test for significant differences in ^{222}Rn levels between rock-types. Tukey tests were then used to test for significant pairwise differences between rock-types. Variance partitioning was used to calculate how much of the variance in Rn levels was due to rock-type. In this single factor analysis, the adjusted r-squared value in the ANOVA table is a direct measure of the percentage of variance due to rock-type.

2.3.4 Variations Within Rock-types

Regression techniques were used to test for relationships between measured variables and ^{222}Rn levels within rock-types, i.e., the variance that is not accounted for by rock-types. The basic approach was to factor out the effects of rock-type by using residuals, which are calculated by subtracting the mean value for each rock-type from each of the measured values within that rock-type. Residuals were calculated for the log-transformed chemical variables, log-transformed ^{222}Rn and log-transformed transmissivity. This procedure allowed the samples from all rock-types to be pooled into a single dataset. An alternative approach would have been to analyze each of the categories separately; however, the use of residual data improves the sample size for multivariate analyses, and ensures that any relationships are general and can be applied to all of the geologic units.

Two groups of analyses of variation within rock-type were done: 1) tests of relationships predicted *a priori* on the basis of previous studies; 2) exploratory analysis of the whole dataset to test for significant unknown relationships.

A priori relationships:

A priori relationships are relationships that might be expected from previously established theory or from the results of field studies at other locations. The background pertaining to these *a priori* relationships was reviewed in Section 1.1. *A priori* relationships were tested using linear regression techniques. The following single-variable relationships were tested: 1) ^{222}Rn vs. transmissivity (as a measure of aperture width); and, 2) ^{222}Rn vs. factors known to control U and ^{226}Ra transport and mobility (pH, Dissolved Oxygen, Specific Conductivity, CO_3^{2-}, F^-, U, and ^{226}Ra). Since the factors controlling ^{222}Rn levels in a field setting cannot be isolated, the possibility of multivariate relationships was also tested. Multivariate models tested were ^{222}Rn vs. (U, CO_3^{2-} and transmissivity), and ^{222}Rn vs. (^{226}Ra, specific conductivity - as a measure of total

dissolved solids, and transmissivity). Some of the models were tested separately for wells with high (>median) and low (<median) transmissivities. These tests were done because there is a partial relationship between residence and time and transmissivity: low transmissivity wells tend to have lower than average residence times. However, hydraulic gradients are independent of the transmissivity, and are equally important in determining the residence time, so transmissivity alone is not necessarily a good indicator of residence time.

Unknown Relationships:

Exploratory methods were used to test for relationships in the data that have not been considered previously. Stepwise regression was used to search for the best-fit predictive model given the large number of predictor variables. The stepwise procedure fits a linear model to all possible variables, then removes variables that contribute least to the success of the model. After several iterations of removal and addition, it settles on a "best-fit" model in which all the included variables have significant partial regression coefficients. These methods are appropriate for exploring for new relationships in the data. However, independent data should be used to verify the findings. The variables in the step-wise procedure included all of the chemical and hydrological variables as possible predictors of within-rock-type variability of ^{222}Rn. Step-wise regressions were done on the complete dataset, and on low and high transmissivity wells.

2.3.5 Spatial Patterns in Radon Levels Within and Between Rock-types

Correlograms

Spatial patterns in ^{222}Rn levels were examined using correlograms (Legendre and Fortin, 1989). Correlograms are a plot of correlation coefficients (r) for pairs of wells in

various classes of distances between wells (correlation lengths). The trend of the datapoints can give insight into the degree of spatial correlation between neighboring wells, and can be used to find the distance to which significant spatial relationships extend. Correlograms were prepared according to the methods in Legendre and Fortin (1989). A Quick-BASIC routine was written to perform the calculations. Spatial trends were examined for the complete dataset, for the residual log-transformed ^{222}Rn data to see if any spatial patterns remained after the effects of geology were removed, and for high and low transmissivity groups. In all cases, distance-pairs were located within the same geologic unit. The analyses were based on distance pairs for all directions assuming only isotropic relationships were present.

Spatial Models

Two spatial models for predicting radon levels from nearby wells within a given geological unit were developed. In the first model, all ^{222}Rn measurements within a 2 km radius of each well (in the same geologic unit) were averaged, and then plotted against the measured ^{222}Rn level at that well. A linear regression was used to describe the relationship between measured and predicted values. This model was tested for the overall dataset and for the residual data after rock-type means were removed. In the second model, the predicted values are based on a distance weighted average (inverse square) of neighboring wells in the same geologic unit. A Quick-BASIC routine was written to perform the calculations. This model was tested for the complete dataset, for the residuals after rock-type means, and at high and low transmissivities.

3.0 RESULTS

Results from the field and analytical testing are presented in Appendix B. Section 3.1 provides a summary of the field and analytical results, and Section 3.2 presents the results of the statistical analyses examining controls on ^{222}Rn variability.

3.1 Field Sampling and Analytical Results

3.1.1 Geology

Each of the study wells was assigned a geologic unit based on the USGS 1:24,000 scale geologic maps (Bryant, 1974a,b; 1976a,b). A simplified map of the geology is shown in Figure 6. As shown on the figure, there are three major geological units in the study area: Early Proterozoic Migmatites, X_m (1,700 Ma) and two Middle Proterozoic intrusive bodies, Silver Plume Quartz Monzonite, Y_{sp} (1,440 Ma), and Pikes Peak Granite, Y_{pp} (1,100 Ma) (Bryant, 1974a,b;1976a,b). In the northeast part of the study area, the migmatite was intruded with numerous small bodies of Silver Plume Granite and was mapped as a distinct subunit (X_{ms}) by Bryant (1974b) to distinguish it from the relatively continuous migmatite in the southern part of the study area. Two other migmatite subunits were found in the study area: amphibolite migmatite (X_{ma}), and sheared migmatite in the Kennedy Gulch Shear Zone (X_{kgs}) . The distribution of study wells by these geologic units is shown in Table 2.

The geology of the study area is reviewed in Lawrence *et al.*, (1991) and Frishman *et al.*, (1993). In brief, the migmatites are variable in composition, with mixed layers of biotite and granitic gneiss, biotite shist and amphibolite. Bulk uranium concentrations in this unit average about 3 ppm. Silver Plume Quartz Monzonite is a coarse to fine-grained muscovite-biotite-quartz monzonite. No data were available on bulk rock uranium concentrations in this unit. The Pikes Peak Granite is a medium to coarse-grained,

hornblende-biotite granite. Despite its uniform appearance, uranium concentrations vary substantially within a very short distance, with values ranging from 2 to 250 ppm, and an average value of about 5 ppm (Frishman *et al.*, 1993). A system of northwest trending shear zones extends throughout the study area. These zones are associated with intense iron oxide alteration and iron staining. Fracture densities are generally higher in these areas, and hydraulic transmissivities are correspondingly higher. Extensive erosion since the Laramide Orogeny has resulted in the formation of sub-horizontal unloading joints throughout the study area which provide the main pathways for groundwater flow in the unsheared areas (Hicks, 1987).

TABLE 2 Distribution of Study Wells According to Geology

Geologic Unit	Number of Study Wells
Migmatite:	
type (X_m)	27
amphibolite (X_{ma})	9
mixed with Silver Plume QM (X_{ms})	14
Kennedy Gulch Shear Zone (X_{kgs})	4
Silver Plume Quartz Monzonite (Y_{sp})	26
Pikes Peak Granite (Y_{pp})	62

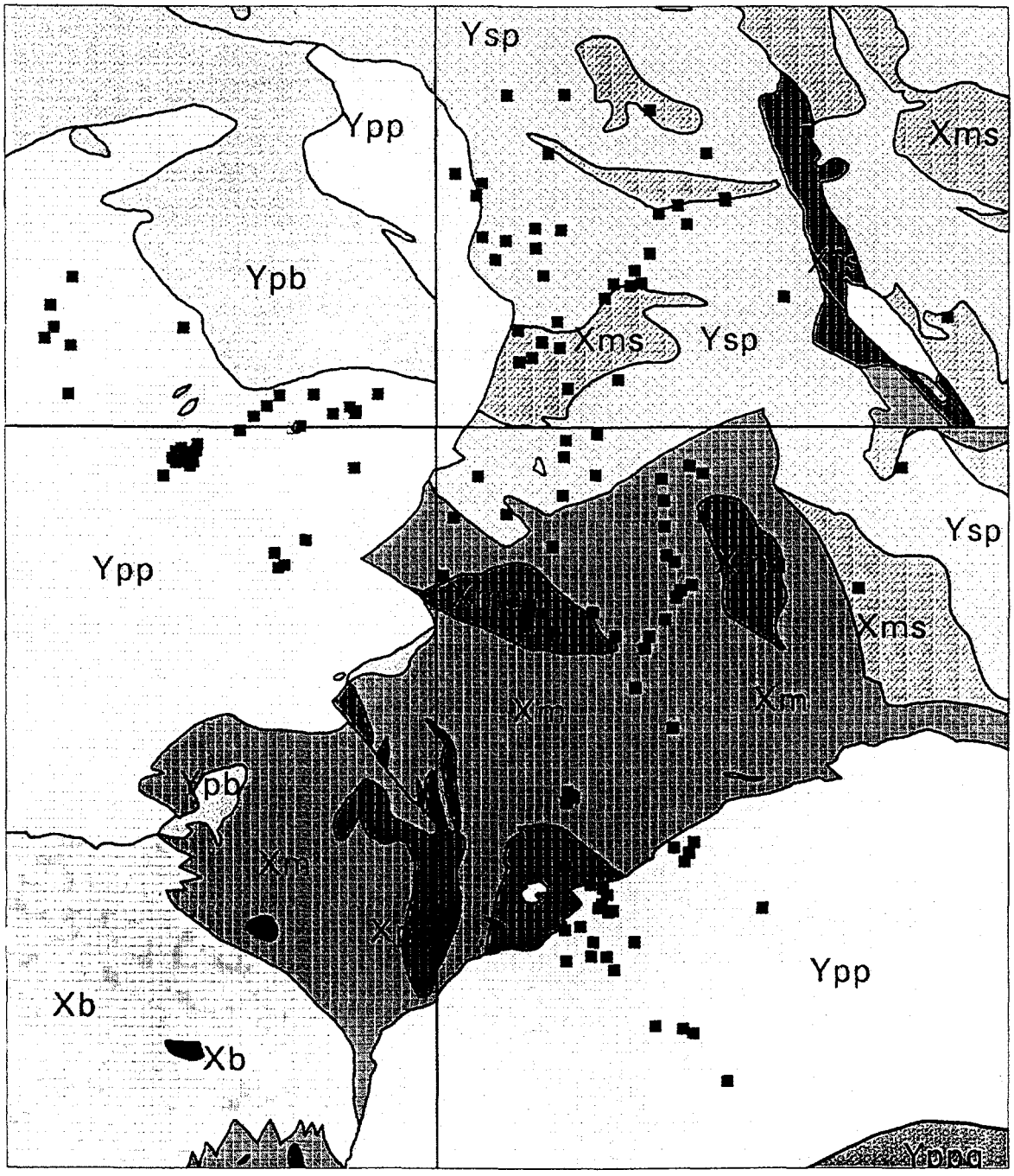

FIGURE 6 Geological Map of the Study Area (Bryant, 1974a,b; 1976a,b). Dark blue squares denote sample locations

3.1.2 Hydrogeological

Transmissivity

The transmissivity data are log-normally distributed. Transmissivity values range from 0.13 to >2000 ft^2/day, with a geometric mean of 12.1 ft^2/day. There does not appear to be any spatial pattern in transmissivity; however, the Kennedy Gulch Shear Zone samples (n = 4) have higher than average transmissivities.

Fracture aperture

Fracture apertures were calculated from the transmissivity data (Section 1.0, equation 1). Fracture apertures range from 0.06 to 1.5 mm, with a geometric mean of 0.27 mm.

Groundwater Velocities

Hydraulic gradients were estimated from potentiometric surface maps prepared by Lawrence *et al.* (1990), and Folger (unpublished map). These were used in conjunction with estimated aquifer thickness and porosities to calculate a range of probable groundwater velocities. Groundwater velocities calculated by this method vary from 0.4 to 80 ft/day (standard deviation around the geometric mean of 5.2 ft/day). Groundwater modeling has shown that pumping of domestic water wells may increase gradients, and therefore velocities to several hundred feet per day in the immediate vicinity of the pump wells (Appendix A).

3.1.3 Chemical

Accuracy Checks

The accuracy of the chemical data from this phase of the study was assessed by calculating the cation-anion balance of the major elements:

$$\% \ Error = \frac{\sum cations - anions}{\sum cations + anions} \times 100\% \qquad (8)$$

The error is within 5% for 36 of the 43 samples, between 5 and 10% for 5 of the 43 samples, and 12 and 17% for the remaining 2 samples.

Field Data

The field pH, specific conductivity, dissolved oxygen , and temperature data are summarized in Table 3. Specific conductivity data is log normally distributed, thus geometric means are presented for this parameter.

Field pH levels are in the neutral range, with values ranging from 5.8 to 8.4. The highest average pH levels are in the migmatite groundwater samples. Specific conductivity levels vary considerably, but are highest in the migmatite groundwater samples, indicating there is a higher total dissolved solids content in these groundwater samples. Dissolved oxygen levels are similar in samples from all of the geologic units, with average values in the range of 5 to 6 mg/L. The dissolved oxygen measurements reflect oxidizing conditions in the water. Average groundwater temperatures are in the range of 8 to 10 °C. There is however a high degree of uncertainty associated with these measurements, particularly for low capacity wells which were pumped at low flow rates to minimize drawdown. It is considered that temperature measurements in the low transmissivity wells err towards high readings since most of the wells were sampled during the summer.

TABLE 3 Summary of Field Data

Parameter	Migmatite (X_m, X_{ma}, X_{kgs})	Silver Plume (Y_{sp})	Undifferentiated (X_{ms})	Pikes Peak (Y_{pp})
pH*	7.31 ± 0.43 (6.49-8.19)	6.73 ± 0.57 (5.8-7.91)	7.00 ± 0.73 (5.91-8.42)	7.1 ± 0.56 (5.8-8.42)
Specific Cond. ** (μmhos/cm)	368 (75-1200)	114 (26-650)	110 (42-280)	192 (41-1000)
Dissolved Oxygen (mg/L)*	4.7 ± 2.3 (0.3-9.1)	5.1 ± 2.5 (0.8-9.4)	5.3 ± 3.2 (1.1-12.5)	6.4 ± 2.8 (<0.1-12.2)
Temperature (°C)*	9.5 ± 1.4 (6.2-13.2)	7.7 ± 7.7 (5.3-10.0)	8.3 ± 1.6 (6.4-11.7)	10.2 ± 2.1 (3.3-15)

Notes: * Mean ± Standard Deviation (minimum - maximum)
** Geometric Mean (minimum - maximum)

Major Element

The major element data are summarized in Table 4. Major element concentrations are low compared to groundwaters from sedimentary basins in the Denver region (Lee and Fetter, 1994). The highest concentrations of Ca^{2+}, Mg^{2+}, Na^{+}, HCO_3^{-}, SO_4^{2-}, and Cl^{-} are found in migmatite groundwater samples. Ca^{2+} and HCO_3^{-} are the dominant ions in most of the samples. Isolated samples with high SO_4^{2-} and/or NO_3^{2-} seem to be associated with horses or cattle. Samples with anomalously high Cl^{-} levels may reflect contamination from household water softeners which are used by a small percentage of homeowners in

the area. High F^- levels are common in groundwater samples from the Pikes Peak granite with

TABLE 4 Summary of Major Element Data by Rock-type

Parameter	Migmatite (X_m, X_{ma}, X_{kgs})	Silver Plume (Y_{sp})	Undifferentiated (X_{ms})	Pikes Peak (Y_{pp})
Ca^{2+} (mg/L)	42 (8.9-210)*	13 (2.9-35)	14 (0.7-48)	20.5 (5.0-100)
Mg^{2+} (mg/L)	10 (2.7-23)	3.3 (0.8-10)	4.1 (0.014-16)	3.8 (0.8-25)
Na^+ (mg/L)	11 (4.9-44)	6.3 (2.9-13)	9.6 (4.7-57)	6.5(2.0-26)
HCO_3^- (mg/L)	160 (38-330)	51 (14.4-180)	68 (17-160)	71 (16-250)
SO_4^{2-} (mg/L)	16 (3.2-490)	4.7 (1.7-12.0)	6.2 (3.5-14)	9.3 (2.3-31)
Cl^- (mg/L)	7.9 (1.2-110)	3.1 (0.6-49)	4.5 (0.8-180)	3.5 (0.75-97)
F^- (mg/L)	0.6 (0.2-3.4)	0.6 (0.2-3.2)	0.6 (0.2-2.9)	2.5 (0.8-4.3)
NO_3^{2-} (mg/L)	2.3 (<0.1-110)	2.8 (0.4-27)	3.6 (0.5-22)	2.1 (<0.1-19)

Note: * Geometric Mean (minimum - maximum

average values exceeding the recommended range of 0.8 to 1.7 mg/L (for children with developing teeth and bones).

Trace Element Data

Ba, Sr, Li, Fe, Mn, Cu, and Zn are at detectable levels in most of the study wells. A summary of the results is provided in Table 5. Ba and Sr are at significantly higher concentrations in the migmatite groundwater samples than in samples from the igneous or

undifferentiated rocks. These alkaline-earth metals are in the same group as Ca, Mg and Ra, and are therefore potentially important indicators for Ra mobility in the system. Fe levels are close to the detection limits in most wells, further supporting the assumption that these waters are oxidizing. Mn levels are generally lower in the migmatite samples than in the other wells. Cu and Zn levels are highest in samples from the Silver Plume Quartz Monzonite; however, high levels are found in wells throughout the study area. High Cu and Zn concentrations may be the result of contamination by household plumbing (eg., zinc solder, copper pipes) rather than natural variation in the aquifer. Other trace metals found in the study wells included (B, Ag, Cr, Cd, Ni, Mo, and Ti), however these metals are below analytical detection limits in most of the wells, and are of interest from a water quality standpoint only to the individual well users.

TABLE 5 Summary of Trace Element Data by Rock-type

Parameter	Migmatite (X_m, X_{ma}, X_{kgs})	Silver Plume (Y_{sp})	Undifferentiated (X_{ms})	Pikes Peak (Y_{pp})
Ba^{2+} (µg/L)	68 (12-240)*	12 (2.5-61)	25 (3.5-100)	21 (<det-320)
Sr^{2+} (µg/L)	320 (56-5500)	51 (12-130)	110 (31-480)	97 (20-1100)
Li^{+} (µg/L)	4.1 (<det-13)	4.8 (2.0-9.3)	6.3 (4.0-11)	7.3 (2.0-37)
Fe^{3+} (mg/L)**	0.01 (<0.0015-0.2)	0.05 (0.01-0.7)	0.04 (0.02-0.35)	0.015 (0.0015-1.2)
Mn^{3+} (µg/L)**	1.4 (0.12-21)	5.5 (0.5-48)	4.5 (0-130)	3.7 (0.12-1200)
Cu^{2+} (µg/L)**	23 (2.7-130)	51 (10-180)	43 (13-330)	28 (0-320)
Zn^{2+} (µg/L)**	28 (1.5-1400)	65 (2.0-3400)	21 (0-430)	21 (1.5-2200)

Notes: * Geometric mean (minimum-maximum)
** Oxidation state assumed

Radionuclides

The radionuclide data are summarized in Table 6. U levels are highly variable, with slightly lower than average levels in groundwater samples from the Pikes Peak Granite compared to the other sample groups. The highest U levels are found in the undifferentiated Migmatite/Silver Plume samples (X_{ms}), and in the Silver Plume QM samples. The highest U concentration measured in the study is 61 times greater than the EPA recommended level of 20 μg/L for U in drinking water, and 23% of the study wells have U levels exceeding 20 μg/L. ^{226}Ra levels are typically in the range of 0.03 to 3 pCi/L, with average levels of less than 1 pCi/L in all the geological units. The MCL for ^{226}Ra is 3 pCi/L. ^{222}Rn levels are highly variable, ranging from 878 to 138,700 pCi/L with an overall geometric mean of 6150 pCi/L. A histogram of ^{222}Rn levels is shown in Figure 7. It is evident from the figure that most of the samples have ^{222}Rn levels exceeding the EPA proposed MCL of 3000 pCi/L. The controls on ^{222}Rn variability are examined in the following section.

TABLE 6 Summary of Radionuclide Data by Rock-type

Parameter	Migmatite (X_m, X_{ma}, X_{kgs})	Silver Plume (Y_{sp})	Undifferentiated (X_{ms})	Pikes Peak (Y_{pp})
U (μg/L)	8.8 (0.33-79)*	7.8 (<0.14-620)	6.9 (0.33-1220)	4.5 (0.42-180)
^{226}Ra (pCi/L)	0.46 (0.1-2.9)	0.32 (0.03-2.7)	0.71 (0.09-12)	0.42 (0.09-3.2)
^{222}Rn (pCi/L)	3040 (880-11560)	7900 (970-138700)	9910 (4130-36280)	7820 (1340-22740)

Note: * Geometric mean (minimum-maximum)

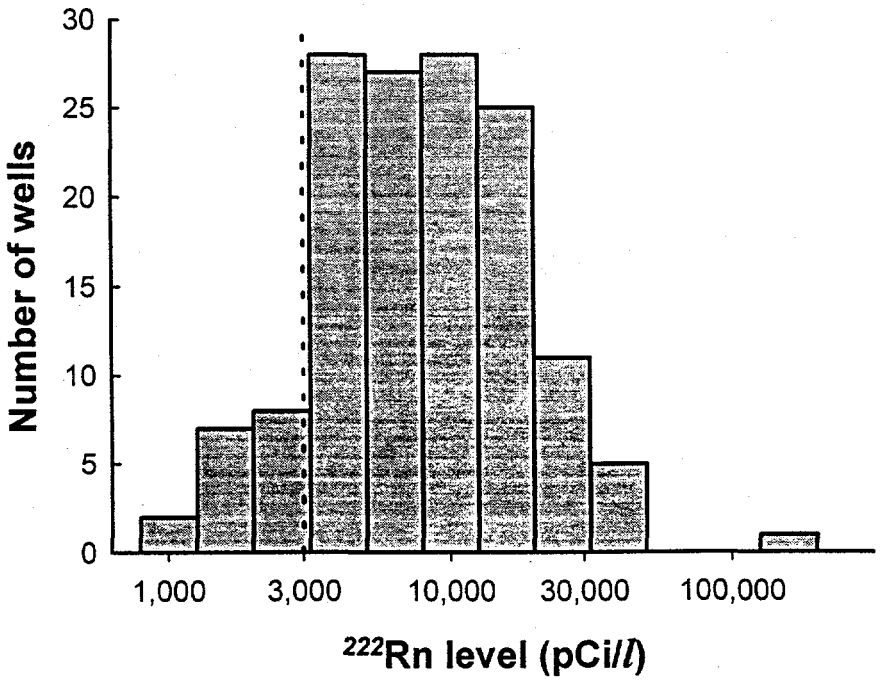

FIGURE 7 Histogram of ^{222}Rn levels in the Study Area. Dashed line at 3000 pCi/L indicates the proposed MCL for ^{222}Rn levels in groundwater.

3.2 ^{222}Rn Variability in Domestic Water Wells

3.2.1 Importance of Sampling Error and Temporal Variations Within Wells

Sampling error was assessed using the variance partitioning techniques described in Section 2.3.2. The results are presented in Table 7. Sampling and measurement errors are negligible, comprising only 0.1 percent of the variance*1. Temporal variations are also very small, comprising 3 percent of the overall variance. The true variance between wells is 96.9 percent, indicating that sampling error is not an important part of the variance in this study.

TABLE 7 ANOVA Table with Variance Component Calculations for Determining the Importance of Sampling and Measurement Error

Source	SS	DF	MS	Expected MS	Variance	% Variance
Well	101.223	27	3.749	$\sigma_e^2 + a\sigma_t^2 + ab\sigma_w^2$	0.9228	96.9
Time (within well)	1.630	28	0.058	$\sigma_e^2 + a\sigma_t^2$	0.0285	3.0
Error (duplicates)	0.046	56	0.001	σ_e^2	0.001	0.1
Sum					0.9523	100

Notes: SS = sum of squares
DF = degrees of freedom
MS = mean squares
σ^2 = variance (subscripts: e - duplicates, t - time, w - well).

---

*1. variance (σ^2) = $\frac{\sum (x - \bar{x})^2}{n-1}$, where x is the sample value, $\bar{x}$ is the average value of all samples, and n is the number of samples. The variance is a measure of the overall deviation about the mean. (The standard deviation is the square root of the variance.)

3.2.2 Geological Variability

Six lithologic sub-units were considered in this study: 1) Migmatite (X_m) ; 2) Amphibolite (X_{ma}); 3) Silver Plume Quartz Monzonite (Y_{sp}); 4) Mixed Silver Plume and Migmatite (X_{ms}); 5) Pikes Peak Granite (Y_{pp}); and 6) Migmatite within the Kennedy Gulch Shear Zone (X_{kgs}). Box and whisker plots shown in Figure 8 illustrate the range of ^{222}Rn variability within and between these units.

Analysis of variance and Tukey tests show that mean ^{222}Rn levels in X_m and X_{ma} are significantly different from Y_{sp}, Y_{pp} and X_{ms}. Average ^{222}Rn levels in the Kennedy Gulch Shear zone are more similar to the X_m/X_{ma} group, but are not significantly different from the $Y_{sp}/Y_{pp}/X_{ms}$ group, however the lack of significance is largely due to sample size limitations.

Variance partitioning analysis shows that rock-type accounts for 28 percent of the variance between wells, indicating that map-scale geologic designations are an important control on ^{222}Rn variability. However, 72 percent of the variance is still unexplained. The following sections present the results of tests to evaluate whether a portion of the variance within geological units can be explained using the chemical and hydrological parameters measured in this study.

3.2.3 Variation within rock-type.

In this section, the data are presented as residuals after rock-type, i.e., they reflect the differences remaining after the effects of rock-type have been removed. Recall from Section 2.3.4 that residuals are calculated as the value of a sample less the mean of all samples from the same rock-type. Residuals greater than zero indicate samples that are greater than the mean of the sample's rock-type. For example, in Figure 9, the well labeled Y has a residual ln radon value of 1.0. This means the ln radon value at that well was 1.0 ln radon units higher than the mean ln radon value for that rock-type (equation 7):

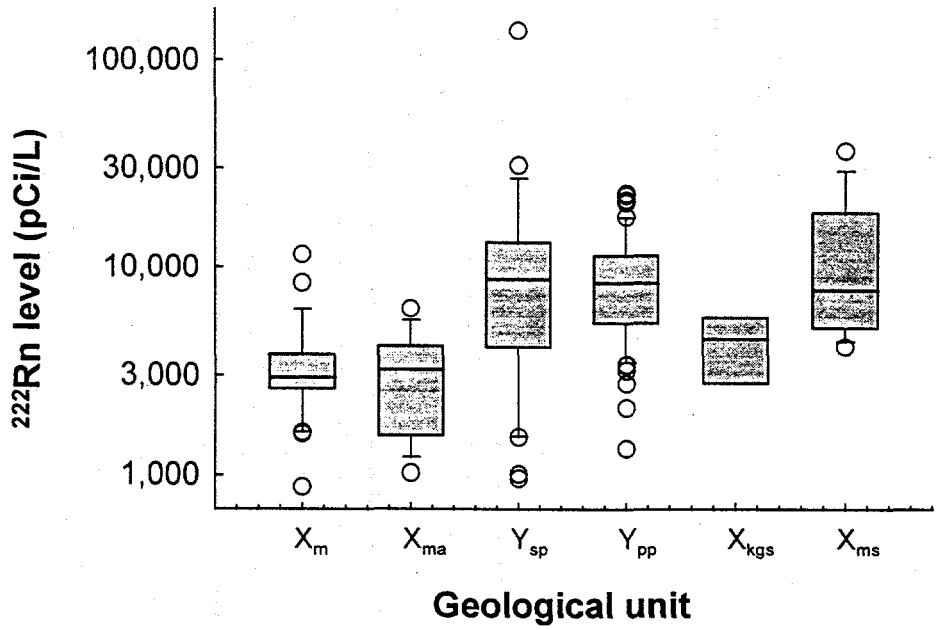

FIGURE 8 Box and whisker plots of Rn variability by geology. Geological units are: migmatite (X_m); amphibolite (X_{ma}); Silver Plume quartz monzonite (Y_{sp}); Pikes Peak granite (Y_{pp}); migmatite - Kennedy Gulch shear zone (X_{kgs}); unifferentiated migmatite/Silver Plume QM (X_{ms}).

$$ln\ residual^{222}Rn = ln^{222}Rn\,(sample\ in\ rock\ i) - average\ ln^{222}Rn(rock\ i) \quad (9)$$

Because the effects of rock-type have been removed by using residual values, all the samples can be used together.

A priori models

^{222}Rn vs. transmissivity:

Figure 9a shows that there is no overall relationship between transmissivity and ^{222}Rn levels. However the figure suggests that a more clear relationship may be found in wells with higher than average transmissivities. Figure 9b shows the data from high transmissivity wells only (wells with greater than the median transmissivity). These data show a significant inverse relationship, with lower radon levels in the high transmissivity wells ($r^2_{adj} = 0.09$, $p = 0.01$)*2.

^{222}Rn versus factors controlling U and Ra transport

Because ^{222}Rn is a noble gas and it is not in secular equilibrium in the water phase of the system, no direct correlations with the other aqueous chemical parameters are

---

*2. r^2_{adj} = coefficient of determination: a measure of the proportion of variance in the dependent variable (y values) that can be explained by a linear regression model (Devore and Peck, 1986). The adj subscript indicates an adjustment has been made to the r^2 value to show the proportion that would be expected when applying the linear model to a new set of samples from the same population (Wilkinson *et al.*, 1992). This adjustment is conservative: it results in slightly lower values than are traditionally reported.

p = p-value, the smallest level of significance at which the null hypothesis can be rejected. The null hypothesis in a linear regression is there is no relationship. P-values of less than 0.05 indicate there is a significant relationship at the 95% confidence level.

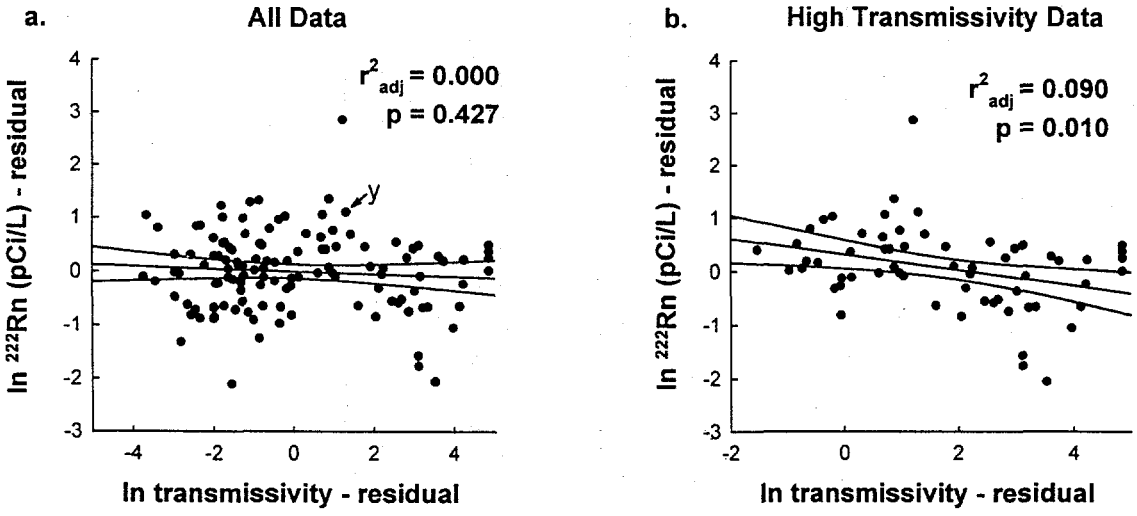

FIGURE 9 Residual ln ^{222}Rn versus residual ln transmissivity: a) all wells b) high transmissity wells (> median). Lines are the regression line and 95% confidence intervals. (Note: the high T group of wells are those above the median, therefore some of them fall below the mean, and there are some negative residuals.)

expected. However, some chemical parameters are indicative of parent radionuclide solubility and transport, and may have *indirect* relationships with ^{222}Rn. Possible indirect relationships include: pH, dissolved oxygen, specific conductivity, fluoride, bicarbonate/carbonate, uranium and radium. The results of single variate linear regressions between Rn and these parameters are presented in Table 8. Scatterplots of the data are shown in Figures 10, 11 and 12. The results show there are no significant single variable relationships between ^{222}Rn and these chemical parameters.

TABLE 8 ^{222}Rn versus Chemical Parameters Known to Influence Uranium and Radium Mobility

Independent Variable*	adjusted r-squared	p-value**
pH	0.003	0.23
Dissolved Oxygen	0.000	0.613
Specific Conductivity	0.012	0.102
F^-	0.000	0.313
CO_3^{2-}	0.008	0.147
U	0.000	0.451
^{226}Ra	0.009	0.208

Notes: * all variables are residuals of the ln-transformed data.

** none of the relationships tested are significant at the 95% confidence level.

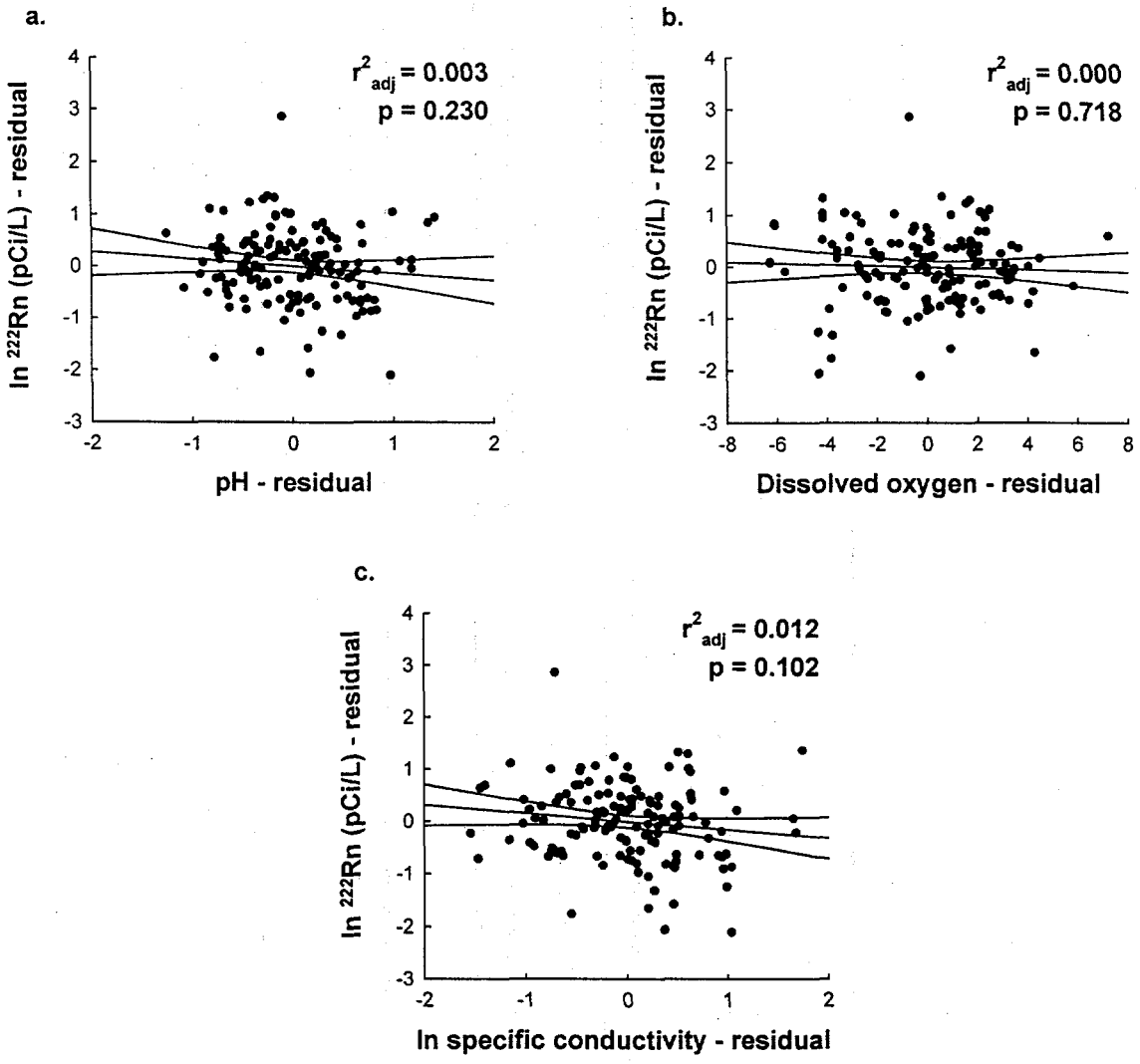

FIGURE 10 ln ^{222}Rn residuals versus field measurements: a) ln ^{222}Rn residuals (pCi/L) versus pH residuals; b) ln ^{222}Rn residuals (pCi/L) versus dissolved oxygen residuals (mg/L); c) ln ^{222}Rn residuals (pCi/L) versus ln specific conductivity residuals (μmhos/cm).

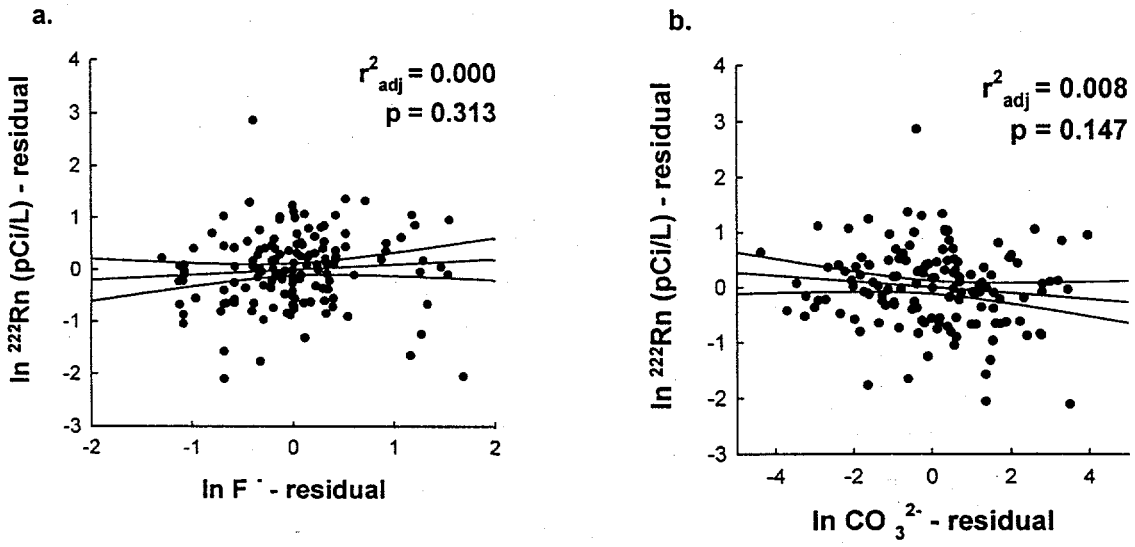

FIGURE 11 ln ^{222}Rn residuals versus ln fluoride and ln carbonate residuals: a) ln ^{222}Rn residuals (pCi/L) versus ln fluoride residuals (mg/L) b) ln ^{222}Rn residuals (pCi/L) versus ln carbonate residuals (mg/L).

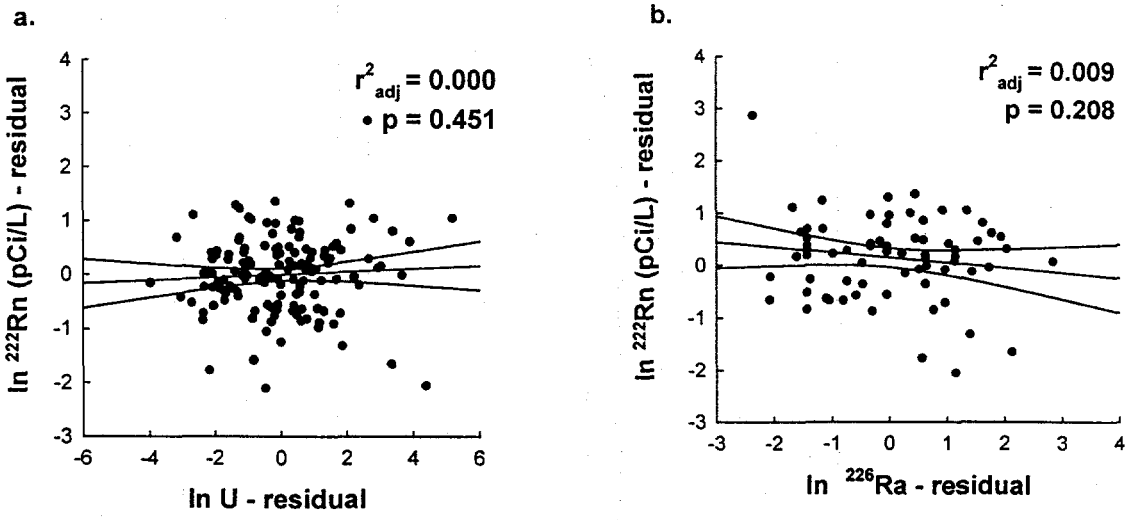

FIGURE 12 ln ^{222}Rn residuals versus radionuclides: a) ln ^{222}Rn residuals (pCi/L) versus ln U residuals (μg/L); b) ln ^{222}Rn residuals versus ln ^{226}Ra residuals (pCi/L).

^{222}Rn versus the combined effects of uranium, carbonate and transmissivity:

The results of a multivariate linear regression considering the combined effects of uranium, carbonate and transmissivity are shown in Table 9. The results show a weak relationship between radon and these three parameters where high radon levels would be expected for samples with high uranium, low carbonate and low transmissivities. There is a significant relationship when all the samples are considered ($r^2_{adj} = 0.087$, $p = 0.003$), a somewhat better fit in the subset of high transmissivity wells ($r^2_{adj} = 0.130$, $p = 0.013$), and a poor and not statistically significant fit in the subset of low transmissivity wells ($r^2_{adj} = 0.067$, $p = 0.074$). The chemical variables add to the hydrological model above by explaining slightly more of the variance than transmissivity does by itself. A graph of radon and the dominant variables, transmissivity and carbonate is shown in Figure 13. Because the relationship explains only a small portion of the variance ($r^2_{adj} = 0.13$), the relationships between dominant variables and ^{222}Rn shown in this and subsequent dominant variable figures are not readily apparent. The arrows on the figures were added to show the expected trend based on the model coefficients. Larger symbols depicting higher ^{222}Rn levels tend to be found in the region of the graph labeled 'Higher ^{222}Rn'.

^{222}Rn versus the combined effects of radium, specific conductivity and transmissivity:

The results of a multivariate linear regression considering the combined effects of radium, specific conductivity and transmissivity are shown in Table 10. The results indicate there are no statistically significant relationships between radon and these variables, however there is a weak relationship in the high transmissivity wells which explains a small portion of the variance. In this model, high specific conductivity, low ^{226}Ra activity and low transmissivity would favor high ^{222}Rn levels ($r^2_{adj} = 0.139$, $p = 0.063$). Since ^{226}Ra data are only available for about half of the wells sampled, the lack of statistical significance is partially a function of the small sample size.

TABLE 9 ^{222}Rn as a Function of Uranium, Carbonate and Transmissivity

Variable*	Coefficient	Partial p-value**	Adjusted r-squared	Overall p-value
All Transmissivities (n= 122)			0.087	0.003
Transmissivity	-0.048	0.122		
U	0.106	0.037		
CO32-	-0.177	<0.0005		
Constant***	0.009	0.887		
Low Transmissivity (n = 60)			0.067	0.074
Transmissivity	-0.094	0.390		
U	0.112	0.082		
CO32-	-0.147	0.021		
Constant***	-0.174	0.393		
High Transmissivity (n = 61)			0.130	0.013
Transmissivity	-0.146	0.013		
U	0.081	0.344		
CO32-	-0.174	0.033		
Constant***	0.269	0.060		

Note: * all variables are residuals after rock-type means of the ln transformed data.
** the partial p-value reflects the significance of the individual variables in a multiple regression, the overall p-value reflects the significance of the overall model.
*** the constant in a linear regression is the y-intercept.

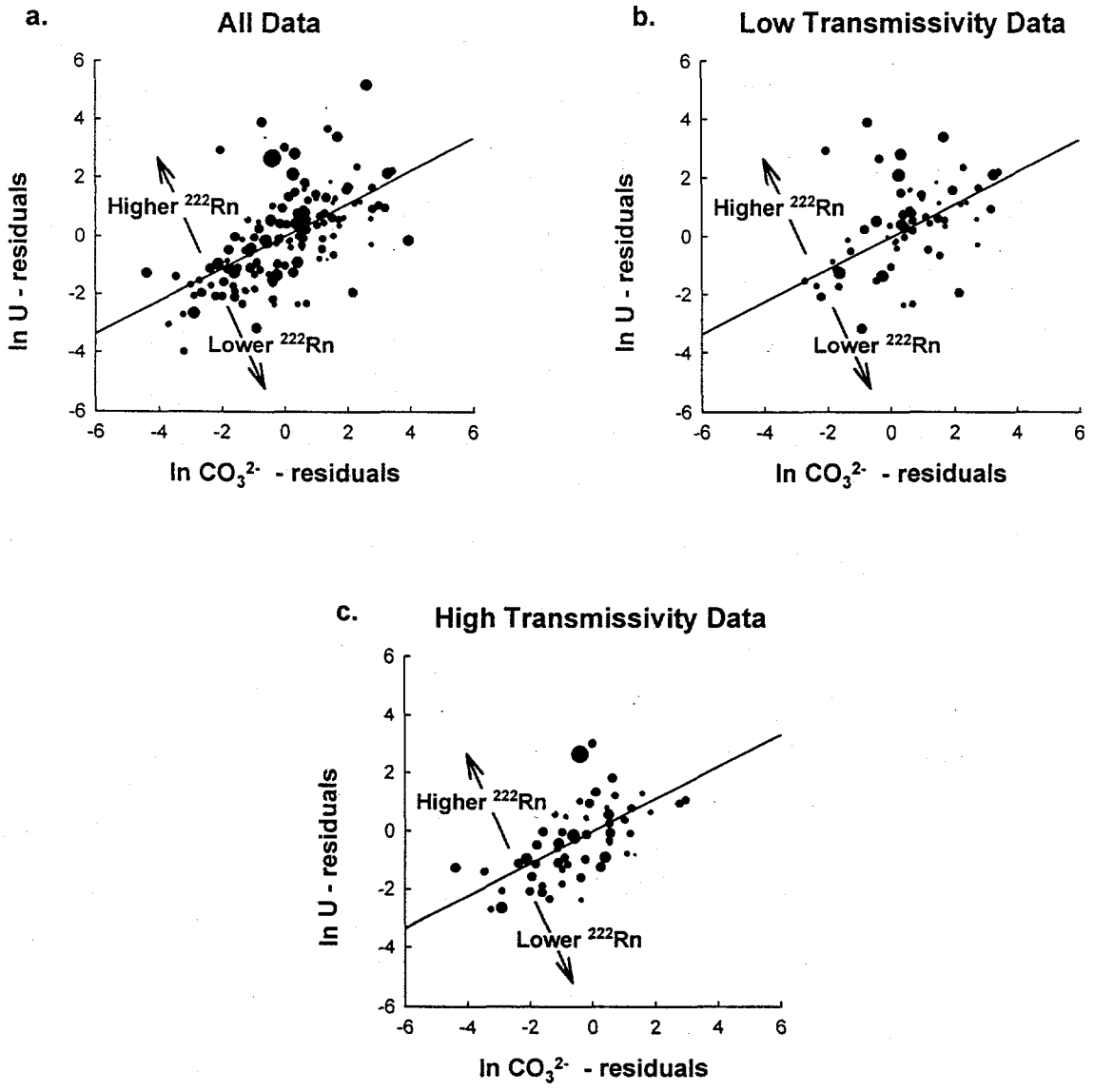

FIGURE 13 Graph of dominant variables in the uranium/carbonate/ transmissivity model ln U residuals (μg/L) and ln CO_3^{2-} residuals (mg/L) versus ln ^{222}Rn residuals (pCi/L): a) all data; b) low transmissivity data; c) high transmissivity data. Point size is proportional to ^{222}Rn levels, and arrows indicate the trend of the relationship.

TABLE 10 ^{222}Rn as a Function of ^{226}Ra, Specific Conductivity and Transmissivity

Variable*	Coefficient	Partial p-value	Adjusted r-squared	Overall p-value
All Transmissivities (n= 64)			0.030	0.187
Transmissivity	-0.092	0.053		
^{226}Ra	-0.116	0.210		
Specific Conductivity	-0.094	0.613		
Constant	0.117	0.236		
Low Transmissivity (n = 31)			0.000	0.724
Transmissivity	-0.005	0.975		
^{226}Ra	0.020	0.865		
Specific Conductivity	-0.293	0.274		
Constant	0.146	0.660		
High Transmissivity (n = 33)			0.139	0.063
Transmissivity	-0.220	0.052		
^{226}Ra	-0.234	0.101		
Specific Conductivity	0.143	0.591		
Constant	0.411	0.052		

Notes: * all variables are residuals of the ln transformed data.

** there are several missing ^{226}Ra values in the data resulting in lower sample sizes than in the previous models.

Exploratory models

A model to predict ^{222}Rn at all transmissivities:

Stepwise regression methods were used identify combinations of variables that gave the best overall prediction of radon. The resulting model suggests that ^{222}Rn is partially a function of U, Na, Ba, Li, and Sr ($r^2_{adj} = 0.18$, $p < 0.0005$). The regression results are shown in Table 11. Figure 14a shows the relationship between ^{222}Rn and the dominant variables: Sr and Na for all the transmissivity data.

TABLE 11 A Model to Predict ^{222}Rn at All Transmissivities

Variable*	Coefficient	Partial p-value	Adjusted r-squared	Overall p-value
All transmissivities (n=142)			0.175	<0.0005
U	0.110	0.005		
Na	0.547	0.001		
Ba	-0.168	0.004		
Li	0.228	0.038		
Sr	-0.461	<0.0005		
Constant	0.000	0.995		

Notes: * all variables are residuals of the ln transformed data.

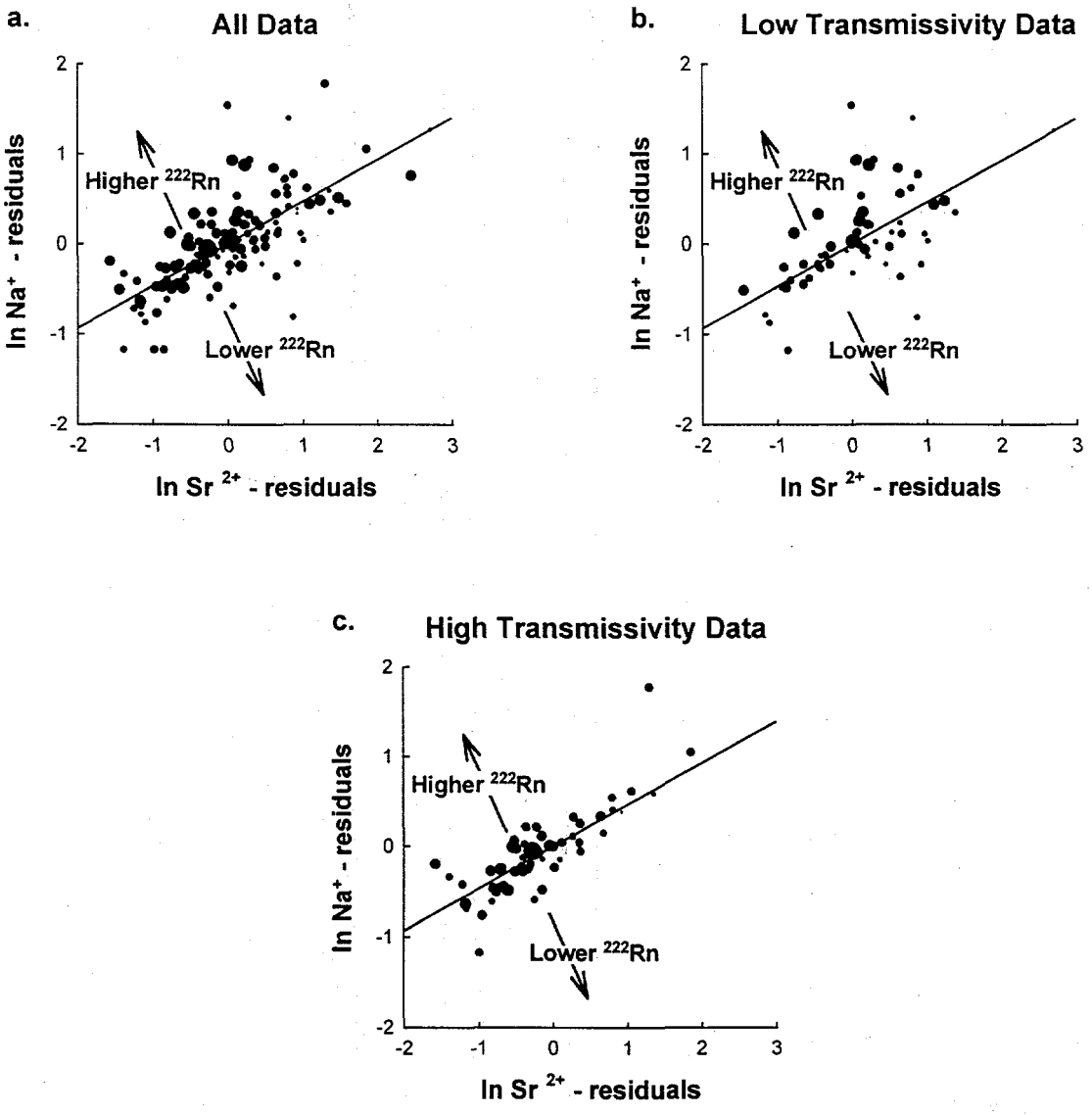

FIGURE 14 Graphs of dominant variables in the 'all' and 'low' transmissivity exploratory models, ln Na residuals (mg/L) and ln Sr residuals (μg/L) versus ln ^{222}Rn residuals (pCi/L): a) all data; b) low transmissivity data; c) high transmissivity data (shown for contrast). Point size is proportional to ^{222}Rn levels, and arrows indicate the expected trend of the relationship.

A model to predict ^{222}Rn in low transmissivity wells:

Stepwise regression methods were used identify combinations of variables that gave the best-fit prediction of radon at low transmissivities (less than median). The resulting model suggests that ^{222}Rn is partly a function of U, pH, Na, F, and Sr ($r^2_{adj} = 0.29$, $p < 0.0005$). The regression results are shown in Table 12. Figure 14b shows the relationship between ^{222}Rn and Na and Sr for the low transmissivity wells.

TABLE 12 A Model to Predict ^{222}Rn in Low Transmissivity Wells

Variable*	Coefficient	Partial p-value	Adjusted r-squared	Overall p-value
Less than median transmissivity (n= 62)			0.29	<0.0005
U	0.104	0.064		
pH	-0.345	0.045		
Na	0.505	0.006		
F	0.362	0.017		
Sr	-0.541	<0.0005		
Constant	-0.078	0.344		

Note: * all variables are residuals of the ln transformed data.

A model to predict ^{222}Rn in high transmissivity wells:

Stepwise regression was also used to identify combinations of variables that gave the best fit prediction of radon at high transmissivities (greater than median). The resulting model suggested that Rn is partly a function of Ba, Li, temperature and transmissivity ($r^2_{adj} = 0.29$, $p < 0.0005$). The regression results are shown in Table 13. Temperature and transmissivity are the dominant variables. A graph of radon versus the dominant variables, temperature and transmissivity is shown in Figure 15.

TABLE 13 A Model to Predict ^{222}Rn in High Transmissivity Wells (all variables considered).

Variable*	Coefficient	Partial p-value	Adjusted r-squared	Overall p-value
Greater than median transmissivity (n= 62)			0.29	<0.0005
Ba	-0.132	0.113		
Li	0.264	0.134		
Temp	-0.176	0.012		
Trans	-0.18	<0.0005		
Constant	0.298	0.015		

Note: * all variables are residuals of the ln transformed data.

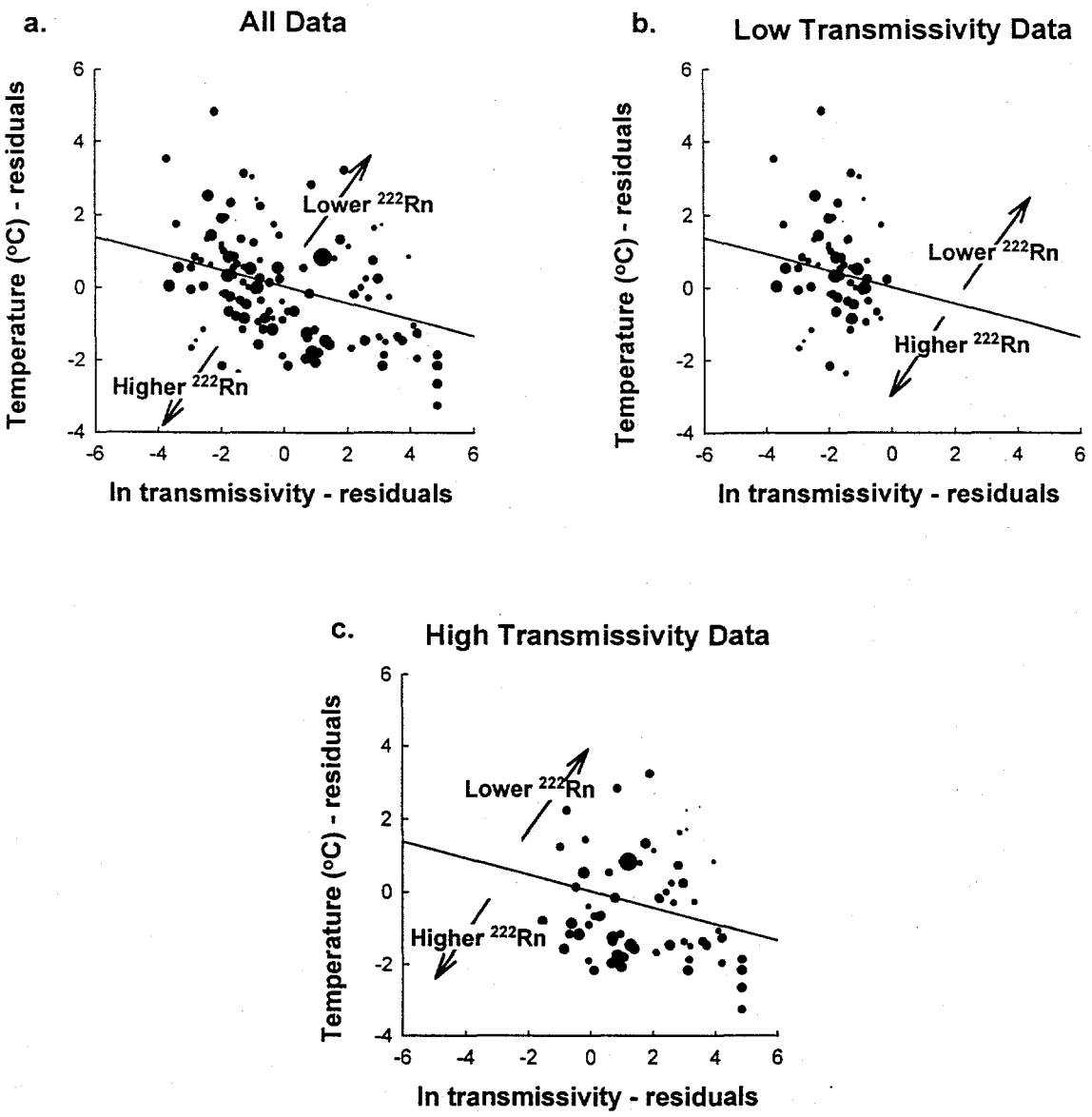

FIGURE 15 Graphs of dominant variables in the high transmissivity exploratory model, temperature residuals (°C) and ln transmissivity residual (ft^2/day) versus ln ^{222}Rn residuals (pCi/L): a) all data (for contrast); b) low transmissivity data (for contrast); c) high transmissivity data. Point size is proportional to ^{222}Rn levels, and arrows indicate the trend of the relationship

A second stepwise regression was run for the high transmissivity data in which the effects of temperature and transmissivity were removed (i.e., a chemical model). This regression shows a relationship between Rn and a combination of Ca, specific conductivity, U and bicarbonate, (r^2_{adj} = 0.20, p = 0.002). Ca and U are the dominant variables. The regression results are shown in Table 14.

TABLE 14 A Model to Predict ^{222}Rn in High Transmissivity Wells (chemical variables only)

Variable*	Coefficient	Partial p-value	Adjusted r-squared	Overall p-value
Greater than median transmissivity (n= 64)			0.20	0.002
Ca	-0.743	0.012		
SpCond	0.425	0.061		
U	0.179	0.021		
HCO_3^-	-0.453	0.043		
Constant	0.162	0.087		

* All variables are residuals of the ln transformed data

3.2.4 Spatial Variability Within and Between Geological Units

Correlograms

Correlograms showing spatial patterns in the data within and between rock units are shown in Figure 16. The data show a strong spatial relationship between wells in the same geological unit (Figure 16a). Graphs of residual data shown in Figure 16b,c,d show that weak spatial patterns remain even after the effects of rock-type are removed. The

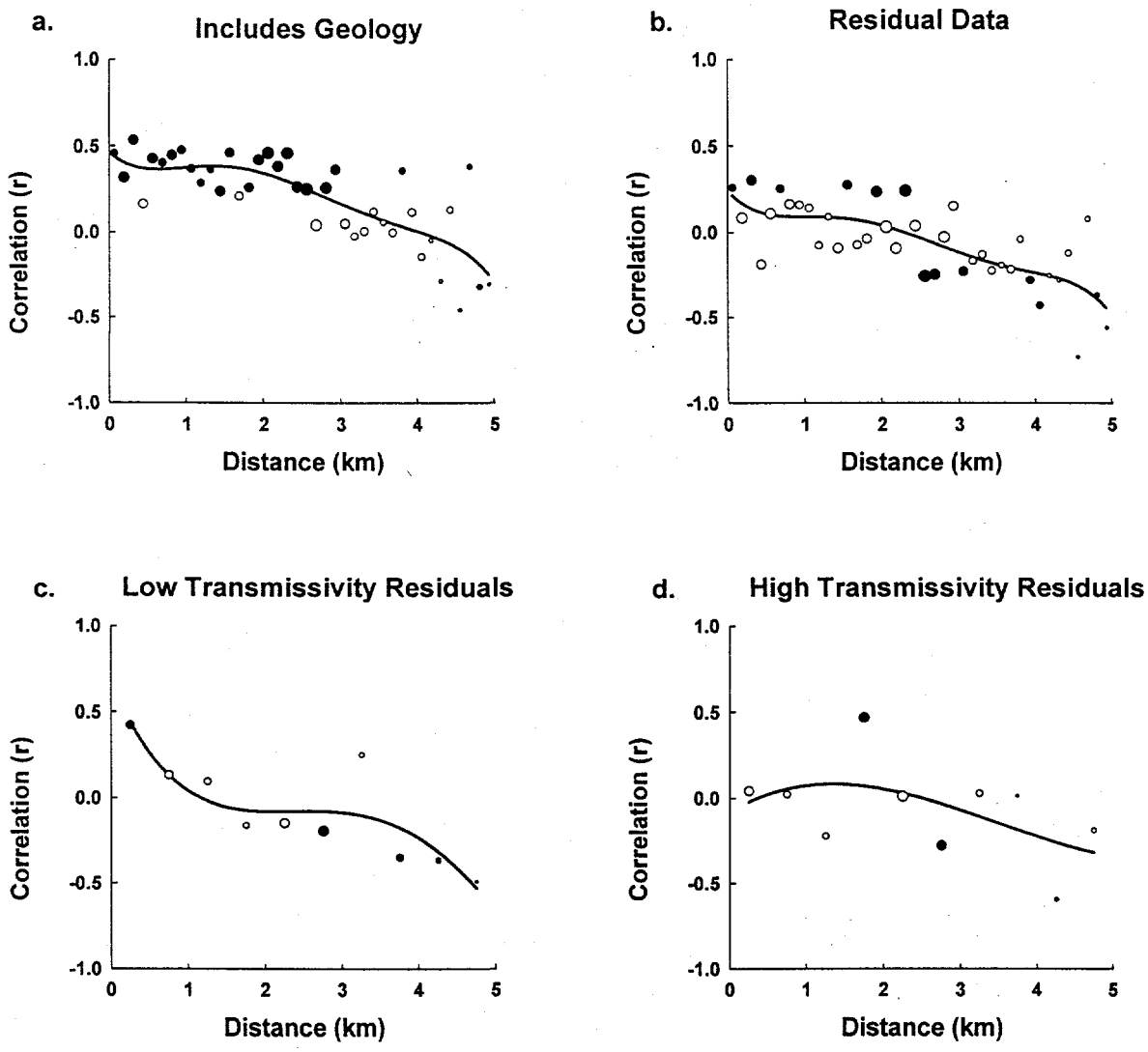

FIGURE 16 Correlograms showing spatial correlations in ^{222}Rn activities at various distance classes: a) includes geology, b) residual data, c) residual low transmissivity data, d) residual high transmissivity. Closed circles represent statistically significant points, open circles are not significantly different from zero. Circle size reflects the sample size.

relationship appears to extend for a distance of 2 km in the overall dataset (Figure 16b), but is much stronger in a subset of low transmissivity wells (Figure 16c), and non-existent in high transmissivity wells (Figure 16d). The low transmissivity wells show a significant relationship in the 0 to 500 meter distance class, and a weak relationship in the 500-1000 meter distance class. There are no significant spatial patterns beyond 1 km.

Spatial models

Two spatial models for predicting radon levels from nearby wells within a given geological unit were examined.

1) 2 km distance model:

The 2 km distance model is based on an average of all ^{222}Rn measurements within a 2 km radius within the same geologic unit. Graphs of the predicted radon levels versus the measured values is shown in Figure 17. Figure 17a shows the results before the effects of rock-type are removed, and Figure 17b shows spatial correlations remaining after the effects of rock-type are removed. The results show a significant spatial relationship when the effects of rock-type are included ($r^2_{adj} = 0.33$, $p < 0.0005$), and a less important, but significant relationship when the effects of rock-type are removed ($r^2_{adj} = 0.07$, $p = 0.001$).

2) Inverse-squared model:

The inverse squared model is based on a distance weighted mean of nearby wells within the same geological unit. Graphs of the predicted radon levels versus the measured values is shown in Figure 18. Figure 18a shows the results before the effects of rock-type are removed, part b shows spatial correlations remaining after the effects of rock-type are removed and Figures 18c and 18d show the spatial patterns remaining after

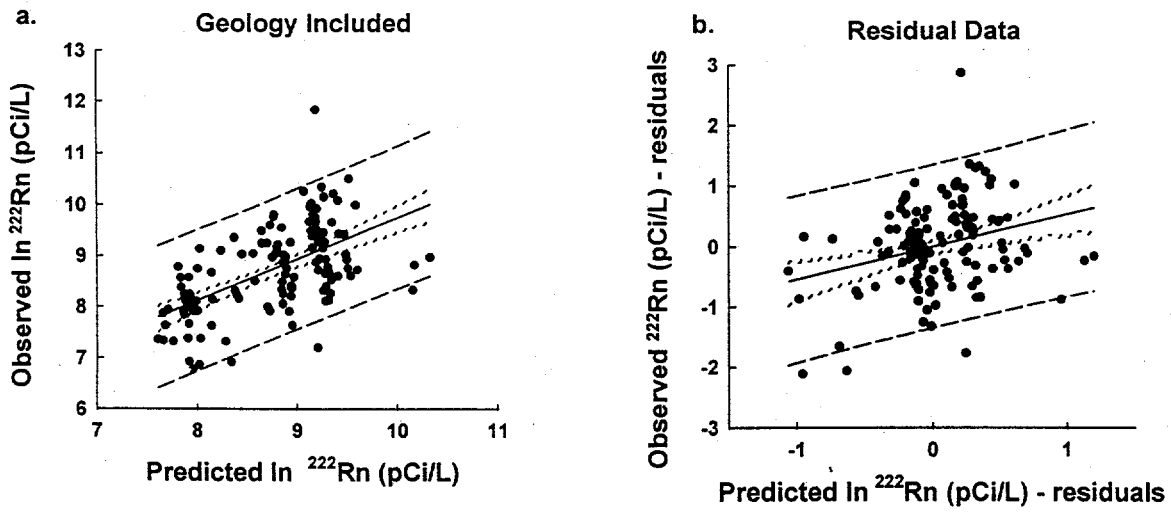

FIGURE 17 Observed ln ^{222}Rn residuals (pCi/L) versus predicted ln ^{222}Rn residuals in the 2-km spatial model a) geology included, b) residual data after rock type means. Solid lines are the regression line, dotted lines represent the 95% confidence intervals on individual predictions and dashed lines represent 95% confidence intervals on individual predictions.

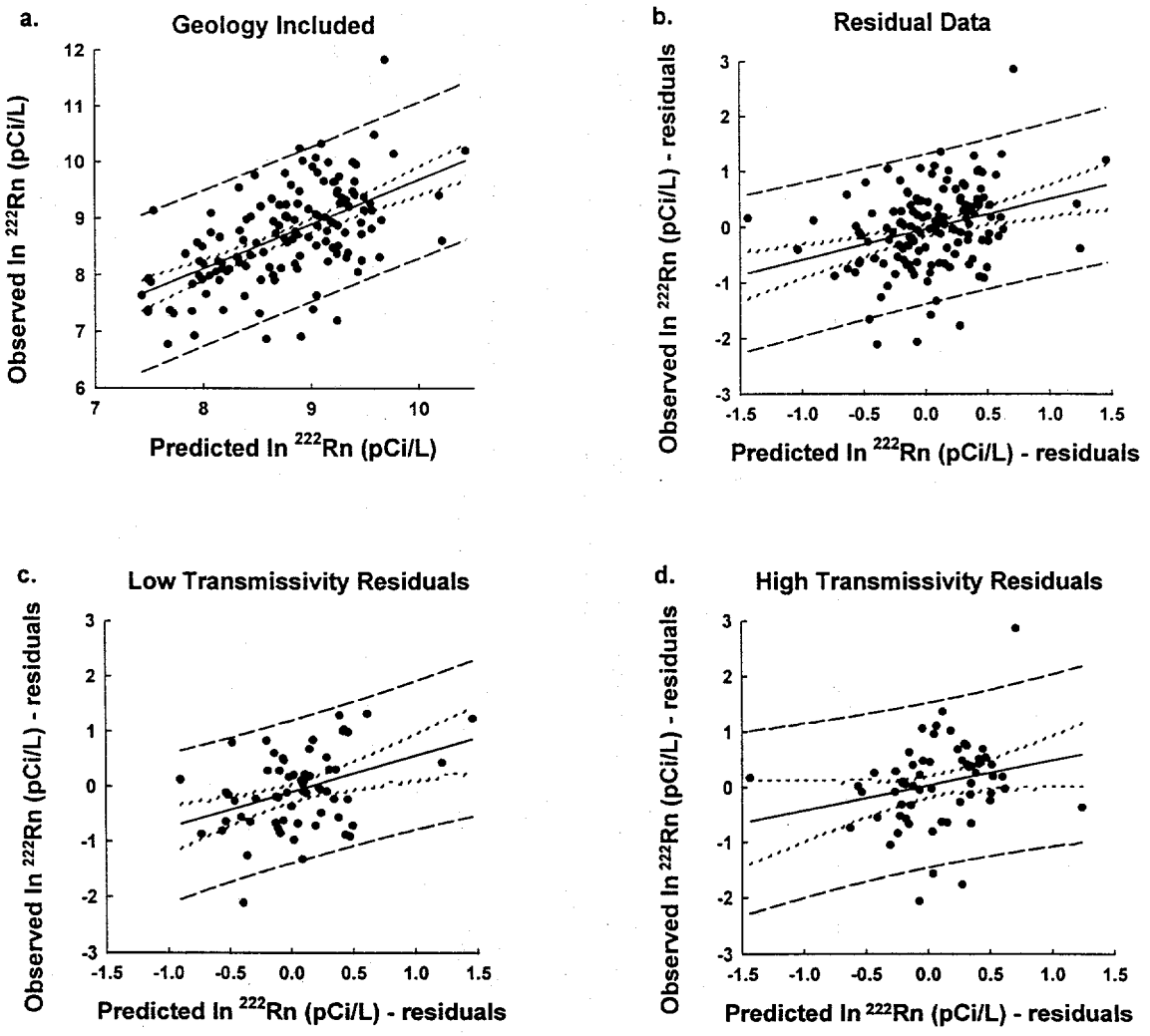

FIGURE 18 Observed ln ^{222}Rn residuals (pCi/L) versus predicted ln ^{222}Rn residuals in the inverse-distance-squared model: a) geology included; b) residual data after rock type means; c) low transmissivity data; and, d) high transmissivity data. Solid lines are the regression line, dotted lines represent the 95% confidence intervals on individual predictions and dashed lines represent 95% confidence intervals on individual predictions.

the effects of rock-type have been removed for low and high transmissivity wells respectively. The results show a significant spatial relationship when the effects of rock-type are included ($r^2_{adj} = 0.33$, $p < 0.0005$), and a less important, but significant, relationship when the effects of rock-type are removed ($r^2_{adj} = 0.094$, $p < 0.0005$). As would be expected from the correlogram results, the residual results for low-transmissivity wells show a better inverse-distance-squared relationship than the high-transmissivity wells (low transmissivity: $r^2_{adj} = 0.139$, $p = 0.002$; high-transmissivity: $r^2_{adj} = 0.042$, $p = 0.060$).

4.0 DISCUSSION

The Elk Creek study area is located in a geologically complex area. Three major lithologic groups were included in the study, including: Migmatite (X_m), Silver Plume Quartz Monzonite (Y_{sp}) and Pikes Peak Granite (Y_{pp}). The Migmatite is further divided into four subgroups: Migmatite (X_m), Amphibolite (X_{ma}), Kennedy Gulch Shear Zone (X_{kgs}) and Undifferentiated Migmatite intruded by Silver Plume QM (X_{ms}). The water chemistry is generally undersaturated with respect to common minerals, and is dominated by calcium and bicarbonate. Water samples from the Migmatite tend to have a higher total dissolved solids content and slightly higher pH than water samples from the igneous rocks. Migmatite water samples also have significantly higher calcium, strontium, barium and bicarbonate concentrations than do water samples from igneous rocks, indicating that U and ^{226}Ra should be more mobile in these waters. The regional groundwater system behaves as a porous medium on a large scale, although it is a heterogeneous fracture flow system. Transmissivity levels vary over 5 orders of magnitude, but there are no significant differences in transmissivity levels between the different lithologic units. The complexity of the regional system makes it impossible to isolate the effects of chemistry, hydrology and geology on ^{222}Rn levels. Controls on ^{222}Rn variability were, therefore, studied in concert, using a multivariate approach to data analysis.

Controls on Radon Variability in Domestic Water Wells

Radon variability was examined at three different levels in this study: the variance due to sampling error and temporal variations at a specific well site, the variance between samples from different geological units, and the variance remaining after the effects of geology are isolated. The results presented in Section 3.2.1 showed that the error due to

sampling and temporal variations is small (<3%) compared to the true variance between wells.

Geology is an important control on radon variability, with map-scale lithologies explaining 28% of the variance between wells. Comparisons between the lithologic groups have shown that the igneous rocks and the mixed Migmatite/Silver Plume Quartz Monzonite (Y_{pp}, Y_{sp}, and X_{ms}) have the highest ^{222}Rn levels. ^{222}Rn levels are somewhat lower in the Migmatites (X_m, X_{ma}, X_{kgs}), however most of the samples still exceed the proposed EPA MCL of 3000 pCi/L. From a management point of view, lithology is the most practical indicator of ^{222}Rn levels in groundwater. Geologic maps are readily available and the lithology of a given well site can be determined with reasonable certainty without sampling or expensive testing procedures. A potentially useful tool to planners is a cumulative probability graph of ^{222}Rn levels for geologic units (Figure 19). Using this diagram, it is possible to determine the probability that a well will exceed a certain radon level, for example, the proposed MCL of 3000 pCi/L. It is evident from the figure that there is a 60% probability that wells in amphibolite migmatite (X_{ma}) will be under the proposed 3000 pCi/L MCL, whereas there is only a 7% chance that wells in the Pikes Peak Granite will be below this level.

While lithology is important, the majority of the variance between wells is still unexplained. The variation within lithologic units was examined by factoring out the macro-scale effects of lithology from the hydrological and chemical data (see Section 2.3.4). The expected or *a priori* controls on radon were examined using linear regression and multiple linear regression techniques. These are considered to be relatively robust because the relevant variables are selected prior to the statistical analysis.

It has been established that fracture aperture should be inversely related to ^{222}Rn levels in simple systems where the source concentrations are uniformly distributed along the fracture margins, and where groundwater residence times are long compared to the

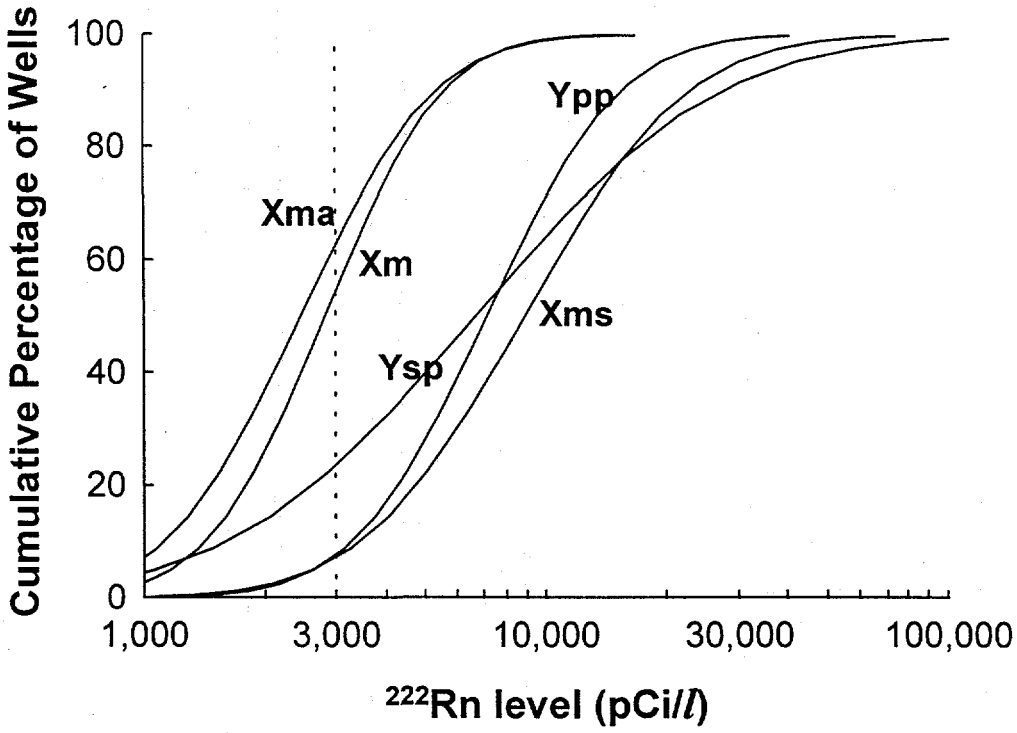

FIGURE 19 Cumulative probability plot of ^{222}Rn levels by geology. Geological units are: migmatite (X_m); amphibolite (X_{ma}); Silver Plume QM (Y_{sp}); Pikes Peak granite (Y_{pp}); unifferentiated migmatite/Silver Plume QM (X_{ms}). The dashed line indicates the proposed 3000 pCi/L MCL for ^{222}Rn in groundwater.

half-life of ^{222}Rn. Since transmissivity is related to fracture aperture, the same inverse relationship is expected between ^{222}Rn and transmissivity. Single variate correlations between ^{222}Rn and transmissivity showed no relationship for the overall database, however, there was a weak but significant inverse relationship in a sub-set of high transmissivity wells (> median). This finding suggests that the aperture model has some applicability in the higher transmissivity wells, but not the low transmissivity wells. The scatter in the high transmissivity data can be attributed to variations in parent radionuclide enrichment or residence time effects. The complete lack of a relationship in the low transmissivity data is not well understood. Possible explanations are: 1) that groundwater residence times may be higher on average in high transmissivity wells (see Appendix A); and/or, 2) low transmissivity wells are drawing water *through* small aperture fractures near the well, but *from* connected fractures of variable aperture width at some distance from the well, while high transmissivity wells are drawing water that is more representative of the local water-rock system. A study of the boundary conditions encountered during the pumping tests might help to resolve this second issue.

As discussed previously, correlations between ^{222}Rn and the chemical parameters are only expected if the aqueous chemistry reflects fracture surface enrichment of parent radionuclides. Possible indicator parameters for U and ^{226}Ra transport and mobility include: pH, dissolved oxygen, specific conductivity (as an indication of total dissolved solids), F, U, and ^{226}Ra. Single variate regressions between radon and these chemical parameters did not show any significant correlations. The two *a priori* models which considered the effects of multiple variables: U/CO_3^{2-}/transmissivity, and ^{226}Ra/specific conductivity/transmissivity were slightly better at explaining the within well variance; however, they still only were able to explain a small portion of the variance. The U/CO_3^{2-}/transmissivity model accounted for 9% of the overall within well variance ($p = 0.003$), and 13% of the variability in the high transmissivity wells ($p = 0.013$). The model coefficients were consistent with the theoretical framework, showing an inverse

relationship with transmissivity and CO_3^{2-} and a positive relationship with U. While this model is highly significant, it does not explain enough of the variance to make effective predictions of ^{222}Rn levels. It does however suggest that the water chemistry is a partial reflection of parent radionuclide enrichment in the fracture system. The ^{226}Ra/specific conductivity/transmissivity model was not significant at the 95% confidence level.

Exploratory methods were used to search for multivariate relationships in the data that had not been considered previously. However, because these methods look for relationships in a large pool of possible variables, they may identify relationships in the data that have no physical meaning. Consequently the results must be interpreted with caution and verified using independent datasets. Exploratory models were included in this investigation because they may be useful for guiding further studies. The exploratory models were developed for the complete dataset, low and high transmissivities.

The overall exploratory model found that ^{222}Rn was partly a function of U, Na, Li, -Ba, and -Sr ($r^2_{adj} = 0.175$, $p < 0.0005$). Na and Sr were the dominant variables. This model is consistent with the theoretical understanding of uranium and radium mobility. The positive relationship with U is consistent with the idea that higher solution concentrations reflect higher fracture surface concentrations. Barium and strontium are divalent cations, which behave similarly to ^{226}Ra. These metals may either: 1) help to mobilize ^{226}Ra by displacing it from the fracture filling minerals in an ion-exchange mechanism, so lower concentrations of these cations could indicate relatively higher ^{226}Ra concentrations on the fracture surfaces; or, 2) they may behave as surrogates for ^{226}Ra behavior and thus lower concentrations in the water phase may indicate favorable conditions for ^{226}Ra, Sr and Ba sorption. The positive correlation between Rn and Na and Li is not well understood. It is interesting to note that this model did not select transmissivity as a controlling variable. This overall model was somewhat better at predicting ^{222}Rn levels than the *a priori* models were, however it still only explains 17.5% of the variance within geologic units.

An exploratory model was also developed for low-transmissivity wells. In this model, ^{222}Rn was found to be a function of U, Na, F, -pH and -Sr ($r^2_{adj} = 0.29$, $p = 0.0005$). Na and Sr were the dominant variables. This model is also consistent with the theoretical understanding of U and Ra mobility. In systems with low carbonate, C_T, U(VI) mobility decreases with increasing pH through the sorption of uranyl species to mineral surfaces. As C_T increases, the formation of non-adsorbing uranyl-carbonato species at high pH (typcially greater than *ca.* 6) results in the enhanced mobilization of U(VI) relative to low C_T and low pH conditions. The positive relationship with F is not well understood; however, F may be associated with weathering of biotite. This weathering also leads to the formation of iron-oxyhydroxides, which are a potential site for uranium sorption (Wanty, *pers. comm.*, 1996). Higher levels of F might indicate a higher portion of these sites, and therefore increased parent radionuclide enrichment. This model was more successful than the overall model, explaining 29% of the variance. While this is still not sufficient for accurate prediction of ^{222}Rn levels, it does indicate the importance of chemical parameters in this system.

A very different relationship was evident in the high-transmissivity wells. In these wells, ^{222}Rn was a function of Li, -Ba, -temperature and -transmissivity ($r^2_{adj} = 0.29$, $p < 0.0005$). Temperature and transmissivity were the dominant variables. While this model is highly significant, the reasons for the relationship are not clear. One possibility is the temperature dependency of Henry's Law constant governing gas solubility. Since gases are less soluble at higher temperatures, there may be a greater tendency for ^{222}Rn to escape from waters with higher than average temperatures during sampling. The temperature measurements are considered to be a poor reflection of the true groundwater temperature in the low transmissivity wells, but this dataset includes high-transmissivity wells that were generally pumped at sufficient flow rates to give reasonable temperature estimates. The results suggest that future investigations should pay more attention to this variable, possibly by using a downhole temperature recorder, or measuring temperature

inside the house where it is less affected by ambient temperatures. If temperature and transmissivity are excluded from the exploratory variables, the step-wise regression settles on a model where ^{222}Rn is a function of U, specific conductivity, $-HCO_3^-$, and -Ca ($r^2_{adj} = 0.20$, $p = 0.002$). U and Ca are the dominant variables. The positive relationship with specific conductivity is not consistent with the idea that Ra is more mobile, and therefore has a lower affinity for surfaces in high-TDS waters, but this parameter is relatively less important in the system than the U and Ca.

The predictive capability gained by the chemical models is limited. At best, only 29% of the variance within geological units (recall 'within-geologic' variance was 72% of the overall variance) can be explained using the exploratory models. An additional 28% of the variance can be predicted by considering the effects of geology. This means that (0.29 x 0.72) + 0.28, or about 49% of the overall variance could be predicted. From a practical standpoint it is more difficult to test for the hydrological and chemical parameters than it is to test for Rn in established wells, and these parameters obviously cannot be measured before a groundwater well is drilled at a site. The results, do, however support the theoretical understanding of controls on ^{222}Rn variability. In fact the correlation coefficients (r-squared values) are surprisingly high considering that the effects of groundwater residence time and the distribution of surface radionuclides could not be measured in this study.

The correlograms and spatial models showed that geology was the primary spatial control on ^{222}Rn variability. Predictions based on the 2 km-distance average and the inverse-square weighted average both explained 33% of the variance. This is slightly higher than predictions based on geology alone, indicating that there are additional spatial controls in the local aquifer system. The two-km distance average and the inverse-squared weighted average models still showed significant relationships in the residual data (after the effects of geology were removed), however they were relatively unimportant in terms of their predictive capability. The best "residual" predictions were

obtained using the inverse-distance-squared model for the low transmissivity wells, where 14% of the variance within geology could be explained (Figure 18c). Since this model puts a higher weight on the nearest wells, the correlation between the observed and predicted values probably reflects similarities in the water chemistry between neighboring wells. Spatial predictions would have limited application in assessing risk levels in an area, since predictions based on geology would be almost as successful and easier to apply.

5.0 CONCLUSIONS

The Elk creek study area is characterized by groundwater ^{222}Rn levels, which vary from 878 to 138,700 pCi/L. The focus of this part of the study was to examine regional-scale controls on ^{222}Rn variability. Each of the study wells was characterized in terms of its geology (lithology), hydrology (transmissivity) and aqueous chemistry data. A statistical approach was used to look for correlations between ^{222}Rn and these variables. In addition, spatial relationships were examined using correlograms and 'nearest neighbor' models.

The majority of the variance in groundwater ^{222}Rn levels is due to variations between sample wells rather than related temporal or sampling error at a specific well site. The lithology of the well site is the most important variable considered, accounting for 28% of the variance between samples. The variations in ^{222}Rn levels within the geologic units were examined by factoring out the effects of lithology. ^{222}Rn is weakly and inversely related to transmissivity in a subset of high transmissivity wells, but not in low transmissivity wells. None of the chemical variables are correlated with ^{222}Rn levels in the single-variable tests. A multivariate model of ^{222}Rn as a function of uranium and bicarbonate concentration, and transmissivity is significant at the 95% confidence level, but only accounts for a small portion of the variance. Exploratory models are somewhat more successful in explaining the variance within geological units, but even the most successful of these can only account for 29% of the variance within geologic units. Spatial relationships in the data are primarily due to lithologic variation; however, the results suggest that nearby wells in the same geologic unit are more likely to have similar ^{222}Rn levels than distant wells in the same geologic unit. These results suggest that a predictive model of ^{222}Rn levels in groundwater in this area is not practical. The probability distribution of ^{222}Rn levels shown in Figure 19 is the most useful indicator of risk.

The weak relationships evident in the multivariate models suggest that surface accumulation of ^{222}Rn parents is reflected by the aqueous chemistry parameters. Without a method for direct measurement of the surface accumulation of ^{222}Rn parents in the local fracture system, this cannot be proven, but it does contribute to the growing weight of evidence that surface processes play an important role in providing generation sites for ^{222}Rn in this system.

PART II
DEVELOPMENT OF A MODEL TO UNDERSTAND THE ROLE OF PARENT MINERAL ACCUMULATION IN THE FRACTURE SYSTEM

1.0 INTRODUCTION

1.1 The Role of Surface Enrichment in Enhancing ^{222}Rn Emanation

Part I of this thesis provided evidence that local-scale processes are responsible for a significant portion of the ^{222}Rn variability in groundwater. The distribution of ^{222}Rn parent radionuclides (U and ^{226}Ra) has been identified as an important local scale variable by a number of researchers (Wathen, 1987; Wanty *et al.*, 1991). In particular, parent radionuclide enrichment at the mineral/water interface is known to enhance ^{222}Rn emanation because there is a higher rate of ^{222}Rn production in the enriched zone and better transfer efficiency to the water phase (Krishnaswami and Seidemann, 1988; Semkow, 1990; Schumann, 1993). The study by Krishnaswami and Seidemann (1988), comparing escape to production ratios for several Rn and Ar isotopes, provides strong evidence that parent radionuclide enrichment along grain boundaries is a more likely explanation for high ^{222}Rn emanation rates than the nanopore network theory proposed by Rama and Moore (1984). Through modeling, Semkow (1990) demonstrated that emanation rates are greatly enhanced in systems where ^{226}Ra is concentrated on the surface of the particles. Field studies reviewed by Schumann (1993) suggest that surface concentrations of parent radionuclides are a common factor associated with the high emanation rates observed in many soil and groundwater systems.

Uranium and radium enrichment has been observed along fracture surfaces, grain boundaries and other secondary sites in rock and soil by several researchers (Tanner, 1980; Caruso and Simmons, 1985; Wathen, 1987; Gates and Gunderson, 1989; Torgerson

et al., 1990; Schumann, 1993; Flexser *et al.*, 1993). Previous work in the Elk Creek study area found that parent radionuclide enrichment is associated with metal oxides situated along fracture margins (Wanty *et al.*, 1991; Lawrence *et al.*, 1991; Frishman *et al.*, 1993), and in altered, iron stained rocks near water-bearing fractures (Folger, 1995).

Without surface enrichment, it seems unlikely that typical granitic rocks could support the radon levels found in the air and water of many of these systems. To illustrate this point, radon emanation from the Pikes Peak granite was calculated assuming a "uniform" distribution of uranium. The calculations presented in Table 15 show that ^{222}Rn emanation to groundwater would be very small (on the order of 0.6 pCi/L) without one of the following: 1) a very large surface area; 2) higher bulk uranium concentrations than are actually present; or, 3) an enriched surface.

Since iron oxides and other common fracture-filling minerals are considered to be excellent sorbents for heavy metals and radionuclides, the concentration of ^{222}Rn parents on mineral surfaces has been attributed to sorption reactions between aqueous species and the secondary mineral surfaces (Langmuir, 1978; Krishnaswami *et al.*, 1982; Wanty *et al.*, 1991). The partitioning of uranium (and by association, ^{226}Ra) can be described using surface complexation models (SCM's). Background pertaining to surface complexation modeling is briefly reviewed in Section 1.2.

This part of the study examines the surface enrichment process in two ways: 1) concentration of U in the fracture-filling minerals is examined in the framework of a surface complexation model (SCM); and, 2) extraction tests are carried out on iron oxide coated fractures to determine the extent of enrichment in the iron oxide minerals.

TABLE 15 Calculation of ^{222}Radon Emanation Rates from a Uniformly Distributed Source

A useful conversion factor:

$$[\ ]\frac{mg}{kg}\times\frac{1kg}{10^6 mg}\times\frac{0.99275\ g^{238}U}{gU}\times\frac{1mole\ ^{238}U}{238gU}\times 6.023x10^{23}\ \frac{atoms}{mole}\times\frac{\ln 2}{4.51x10^9\ yrs}\times\frac{1yr}{3.1536x10^7\ \sec}$$
$$\times\frac{1Ci}{3.7x10^{10}}\frac{\sec}{decay}\times 10^{12}\ \frac{pCi}{Ci}$$

$$[\ ]\frac{mg}{kg}\times 0.3309 - - - - > pCi/g$$

calculations:

5 ppm U in bulk-rock x 0.3309 = 1.65 pCi/g ^{238}U

1.65 pCi/g x 2.7 g/cm^3 x (100 cm/m)^3 = 4,467,000 pCi/m^3

4,467,000 pCi/m^3 x 37 Bq/pCi = 165,285,000 Bq/m^3 = 165,285 kBq/m^3

Assume 1 fracture has 2 m^2 bulk surface area/m^2 area (2 sided fracture), and that the recoil distance is 40 nm (Flügge and Zimens, 1939 *in* Semkow, 1990):

40 nm x 1 m/10^9 nm x 2m^2 = 8x10^{-8} m^3 (volume within the recoil range).

8x10^{-8} m^3 (4,467,000 pCi/m^3) = 0.357 pCi

In a 0.2 mm aperture fracture, the volume of water in a 1 m^2 segment is 0.2 liters assuming 30% emanation:

0.357 pCi x 0.3 ÷0.2 L = 0.54 pCi/L

Measured ^{222}Rn values in a 0.2 mm aperture fracture were actually 11,000 pCi, thus:

11,000/0.54 ≅ 20,000 x greater than expected.

1.2 Surface Complexation Approach to Modeling Parent Radionuclide Enrichment

There is a wide range of approaches to describing the accumulation of chemical species at the particle/solution interface. At one end of the spectrum are site specific, empirical models using distribution coefficients or isotherms, which account for sorption processes for a limited set of geochemical conditions. In contrast, surface complexation models, which are based on a more theoretical understanding of the processes occurring at the mineral surface, are applicable over a broad range of chemical conditions. Because the surface complexation approach accounts for chemical variability, it provides better insight into the chemical processes occurring at the mineral/water interface.

The basic idea behind surface complexation models is that surface species are formed between specific functional groups on the mineral surface and dissolved species. The formation of the surface complexes can be described using mass law equations in a similar manner to complexation reactions in homogeneous systems. A 'correction factor' derived from electric double layer theory must be applied to the mass law constants to account for surface charges arising from the surface reactions. Over the past 30 years, 4 basic types of models have been developed. The main differences between these 'molecular hypotheses' are the way in which free energy of adsorption is resolved into chemical and electrostatic terms. When considering ideal laboratory systems, the selection of a specific model framework is important for defining the chemical interactions. However, in practice, all of the models are considered adequate for modeling transport and adsorption of ions in natural waters. Recent reviews of the surface complexation modeling approach are found in Davis and Kent (1990) and Dzombak and Morel (1990).

In this study, uranium sorption to fracture-filling minerals (iron oxides) is examined within the framework of a surface complexation model. This framework will be used to

bound the extent of uranium adsorption required to produce the observed ^{222}Rn levels over the range of chemical conditions found at the study site. In essence, the SCM will be used as a heuristic device to test the hypothesis that local-scale enrichment of ^{222}Rn parents is needed to produce the observed ^{222}Rn levels in groundwater. In established systems it is reasonable to assume that surface concentrations of ^{238}U would be related to the surface concentrations of its decay products, including ^{226}Ra, the immediate parent of ^{222}Rn. Uranium was selected as an indicator of parent radionuclide enrichment for this study because its interaction with geological materials has been well studied (Ho and Miller, 1985; Hsi and Langmuir, 1985; Milton and Brown, 1987; Payne and Waite, 1991; Prikryl *et al.*, 1994; Payne *et al.*, 1994; Waite *et al.*, 1994).

1.3 Objective and Approach

A surface complexation model (SCM) describing uranium sorption to iron and manganese oxides is used to study chemical controls on parent radionuclide enrichment. The objective is to test the hypothesis that fracture mineralization provides sufficient local accumulation zones for ^{222}Rn parent radionuclides.

The approach followed in the study is outlined below:

1) A conceptual model of the water-rock system is developed using field data and concepts described in previous studies (Lawrence, 1990; Folger, 1995). The conceptual model defines the geology, mineralogy, fracture geometry, hydraulic residence time, specific surface area and water chemistry of the system, and is the basic framework for understanding small-scale processes in the system (Section 3.0).

2) Uranium sorption to ferrihydrite is described using the surface complexation model framework described in Waite *et al.* (1994) (Section 4.0). Uranium accumulation is determined for fractures in the vicinity of each study well as follows:

- FITEQL Version 3.2 (Herbelin and Westall, 1996) is configured to describe uranyl sorption to ferrihydrite (Waite *et al.*, 1994) and then used to generate an isotherm for the pH and bicarbonate concentration measured for each of the water samples.

- The sorption density, Γ (moles U sorbed/moles sites), is determined graphically from the isotherm and equilibrium uranium concentration (U_{eq}) measured in each of the water samples.

- Γ's are converted to concentration or activity units (μg U/g sorbent or pCi ^{238}U/g sorbent).

3) By assuming that ^{238}U, ^{226}Ra and ^{222}Rn are in secular equilibrium, ^{222}Rn levels measured in each well can be used to constrain how much of the enriched iron needs to be present in the local fracture system to produce a desired ^{238}U sorption density.

4) By considering the geometric assumptions in the conceptual model, the mass of required sorbent can be converted to a mass per unit surface area or a thickness, giving the problem physical meaning (Section 4.3.2).

5) Sequential extraction experiments are performed on fractured drill core samples to show the association between uranium, ^{226}Ra and the iron and manganese oxides on the fracture surfaces, and to verify the results of the sorption modeling (Section 5).

2.0 METHODS

2.1 Drill Core Sampling and Preparation

Drill core samples were available from a project carried out in 1984 by the Denver Water Board. The drilling project was located adjacent to the Platte River approximately 6 km downstream of Pine, in similar terrain and geological conditions to the Elk Creek Study Area. A total of 9 drillholes ranging in depth from 130 to 248 feet were available for sampling. Three of the holes were selected for sampling based on drill-logs prepared by the Denver Water Board. 40 samples, including 32 iron-stained fractures, 6 chlorite-coated fractures, and 2 freshly broken rock samples were collected.

Each of the samples was described on the basis of host rock appearance, fracture filling mineral appearance, color, thickness and degree of crystallinity. The samples were then prepared for the leaching experiments as follows: 1) core segments were either sawed using a water cooled, hand operated rock saw or broken with a hammer to reduce the fragments to a manageable size for leaching (approximately 5 cm diameter x 1 cm deep). The samples were then rinsed in deionized water to remove any dust or rock powder, and left to air dry overnight. A metal pick was used to scrape off a small amount of the fracture filling mineral for XRD analysis. A chemically resistant vinyl ester polymer (Dudick Inc., Protecto-Coat 800) was then applied to the un-mineralized surfaces of the rock to isolate them from the chemical extraction. The bulk surface area of the exposed fracture filling minerals was estimated and the mass of the fragment was measured on an analytical balance.

2.2 Sequential Extraction Procedure

Selected core samples were subjected to a modified sequential extraction procedure based on sequential extraction procedures developed for soils (Tessier *et al.*, 1979; Yong

et al., 1993). Significant modifications to the Tessier *et al.* procedure were: 1) the addition of sodium carbonate to desorb uranium from surface sites on the fracture (Torma *et al.*, 1986); 2) larger sample and extractant volumes to accommodate the relatively large rock fragments; and, 3) longer leaching times to allow sufficient reaction to occur on the relatively smaller surface area available for leaching. All of the extraction solutions were prepared using Nanopure water and analytical grade or better reagents.

A total of 27 sequential extraction experiments were done, including: 1 epoxy control (an iron-stained fragment coated with epoxy), 1 fresh host-rock control, 3 altered host-rock controls, 2 smectite-coated fracture samples and 19 iron and manganese oxide-coated samples. The extraction steps were: 1) exchangable fraction; 2) desorption fraction; 3) bound to carbonates; 4) bound to iron and manganese oxides. The modified procedure was completed as follows:

1) Exchangeable Fraction: ion-pair or outer-sphere complexes (Extraction #1):

The extractant consisted of a concentrated salt solution. Since $MgCl_2$ was found to interfere with the laser fluorimetry method for analyzing uranium, a 1 M $MgNO_3$ solution was substituted. Rock fragments selected for the extraction were placed in a glass beaker and submerged in sufficient salt solution to completely submerge the exposed fracture surface (20, 30 or 40 mL). The samples were then placed on an orbital shaking table at 90 rpm for 21 hours and then allowed to settle for 10 to 15 minutes. Solutions were decanted into acid washed, 40 mL polycarbonate centrifuge tubes and then centrifuged at 3500 rpm for 20 minutes. The supernatant fluid was transferred to a 30 mL LDPE (low density polyethylene) bottle and stored for further analyses. Any particles separated in the centrifuge were transferred back into the beaker by rinsing with 20 mL of deionized water. The beaker was then gently agitated to rinse the larger rock fragment and any other sediments of the first extractant. This rinse water was

then returned to the centrifuge tubes, centrifuged for 20 minutes at 3500 rpm and then discarded. Any sediments remaining in the centrifuge tube were transferred back to the beaker with a known volume of the subsequent extractant and the next leach cycle was initiated.

2) Desorption Fraction (Extraction #2):

The extractant consisted of a 0.5 M $NaHCO_3/Na_2CO_3$ solution. In this extraction, strong carbonato complexes are formed with the uranyl ion, which would tend to desorb uranium from surface sites on the fracture. The sample was submerged in an appropriate volume of extractant and agitated on the shaking table for a period of 24 hours. The supernatant was recovered and the rock and particles were rinsed as described above.

3) Associated with Carbonates (Extraction #3):

The extractant used was a 1M NaOAc solution adjusted to pH 5.0 with HOAc. Samples were shaken for a period of 24 hours, with periodic pH adjustment. The pH was reasonably stable after the first adjustment, indicating that there was not significant buffering by the fracture minerals. The supernatant was recovered and the rock and particles were rinsed as described above.

4) Associated with Iron and Manganese Oxides (Extraction #4):

The extractant selected was a 0.04M $NH_2OH \cdot HCl$ (hydroxylamine-hydrochloride) in 25% HOAc. Samples were submerged in 40 mL of the extractant, covered and heated to approximately 90 °C in a water bath. This temperature was maintained for approximately 6 hours, the samples were allowed to cool overnight, and then reheated for an additional 6 hours the next day. The samples were in contact with the leach solution for a total of 48 hours, and were

heated for a total of 12 hours. The supernatant was recovered and the rock and particles were rinsed as described above. Under these relatively aggressive conditions, the integrity of the epoxy was compromised as was evidenced by lack of the original water resistance and by flaking in some cases.

2.3 Analytical Work

Seven of the fracture-mineral samples were submitted to the Geological Sciences Department at the Colorado School of Mines for mineralogical analyses by x-ray diffraction (XRD). Total uranium concentrations were measured using a UA-3 Scintrex Uranium Analyzer. A 28-element suite of metals, including detectable levels of Ag, Al, B, Ba, Be, Ca, Cd, Co, Cu, Fe, K, Li, Mg, Mn, Mo, Na, Ni, Pb, Sr, Ti, V, and Zn, was analyzed on a Perkin Elmer Optima 3000 inductively coupled plasma atomic emission spectrometer (ICP-AES). ^{226}Ra analyses were completed by Hazen Research using alpha spectroscopy. U assays of the bulk-rock samples were completed by Hazen Research using laser fluorimetry methods.

2.4 FITEQL Modeling

The computer code FITEQL, Version 3.2 (Herbelin and Westall, 1996), was used to generate adsorption isotherms from an SCM model of uranium sorption to ferrihydrite. The chemical reactions and equilibrium constants used in the code were based on an application of a surface complexation model describing uranyl adsorption to ferrihydrite (Waite *et al.*, 1994). A printout of the input and output FITEQL files is provided in Appendix C. Isotherm generation in FITEQL is a tedious process in that the computer code must be executed for each starting uranium concentration. A quick-basic program, BATS, was written to automate the process, and to create a spreadsheet-importable results file. A hardcopy of BATS is provided in Appendix D. The sorption density (Γ)

was determined by inspection using the isotherm and the uranium concentration measured (U_{eq}) in the field samples.

3.0 DEVELOPMENT OF A CONCEPTUAL MODEL

3.1 Overview of Conceptual Model

A conceptual model of the water-rock system is illustrated in Figure 20. The system is defined as a 1 m^3 block of granite or migmatite. A water bearing fracture extends through this control volume. The fracture is viewed as a simple parallel plate with a uniform aperture width. The hydraulic residence time has been given a value of 30 days to allow ^{222}Rn to reach secular equilibrium with the wall rocks. Secondary weathering products (primarily iron and manganese oxides) coat the fracture surfaces. Adsorption/desorption reactions are in a state of equilibrium, i.e., the chemistry of water entering and leaving the fracture system is the same. ^{226}Ra and ^{222}Rn are in secular equilibrium, and ^{222}Rn concentrations in the aqueous phase are controlled by the fracture geometry and ^{226}Ra on the fracture surfaces.

It is proposed that uranium enrichment along the fracture surfaces is controlled by: 1) mineralogy and surface chemistry of the fracture filling minerals; 2) aqueous uranyl concentration and speciation; and, 3) ligands that compete for uranyl (primarily bicarbonate) in the aqueous phase.

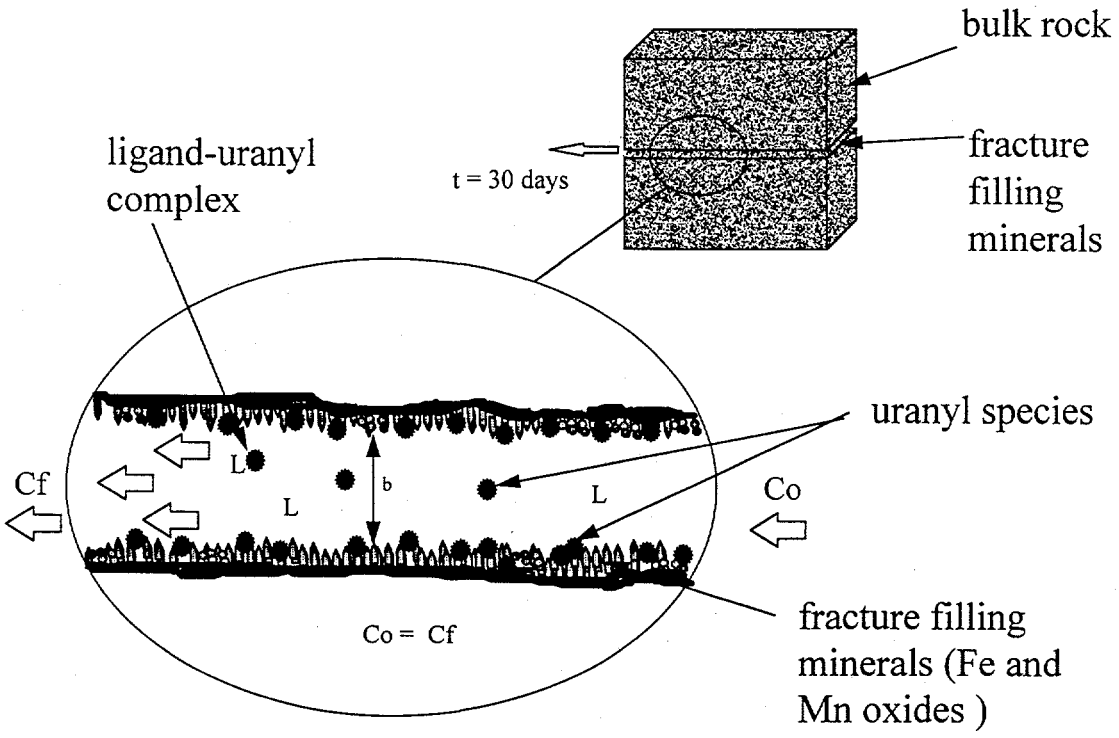

FIGURE 20 Conceptual Model of Fracture System. b = aperture width; L = ligand (e.g., CO_3^{2-}); C_o = concentration of U(VI) species entering the control volume; C_f = concentration of U(VI) species leaving the control volume. ^{222}Rn parent species are 'enriched' on fracture walls through association with fracture-filling minerals.

3.2 Field Evidence to Support the Conceptual Model

The conceptual model is based on the field studies completed in the study area (Lawrence, 1990; Folger, 1995; this study). Data used in developing the model includes:

- regional geological and geochemical data from surface sampling and mapping studies (Bryant, 1974a,b; Bryant, 1976a,b; Frishman *et al.*, 1993);
- bulk-rock geochemistry and chemical-extraction data from drill cuttings in the immediate vicinity of the water-bearing fracture (Folger, 1995);
- mineralogical (XRD) and chemical-extraction data from drill core samples in the Pikes Peak Granite;
- water chemistry data from domestic-water wells; and,
- hydrogeological data, including pumping tests, to determine the transmissivity of the well, and limited geophysical logging to determine the portion of the water that was derived from the main water-bearing fracture.

Surface chemistry parameters (surface area and surface site density) used in the conceptual model could not be determined from the available field data, but have been estimated using physical arguments and qualitative information from thin-section work.

The following sections describe the interpretation of the data and details of the conceptual model.

3.2.1 Geology/Structure

The three major lithologic units were considered in this part of the study: Early Proterozoic Migmatites (1,700 Ma), and two Middle Proterozoic intrusive bodies, Silver Plume Quartz Monzonite (1,440 Ma), and Pikes Peak Granite (1,100 Ma) (Bryant; 1974). The migmatites are variable in composition, with mixed layers of biotite and granitic gneiss, biotite shist and amphibolite. Bulk uranium concentrations in this unit average

about 3 ppm. Silver Plume Quartz Monzonite is a coarse to fine-grained muscovite-biotite quartz monzonite. The unit contains numerous inclusions of migmatite and are situated in close proximity to migmatites in the northeast portion of the study area. No data are available on bulk-rock uranium concentrations in this unit. The Pikes Peak Granite is a medium to coarse-grained, hornblende biotite granite. Despite its uniform appearance, uranium concentrations vary substantially within a very short distance, with values ranging from 2 to 250 ppm, and an average value of about 5 ppm (Frishman *et al.*, 1993).

A system of northwest trending shear zones extends throughout the study area. These zones are associated with intense iron oxide alteration and iron staining. Fracture densities are generally higher in these areas, and hydraulic transmissivities are correspondingly higher. Extensive erosion since the Laramide Orogeny has resulted in the formation of sub-horizontal unloading joints throughout the study area which provide the main pathways for groundwater flow in the unsheared areas (Hicks, 1987).

3.2.2 Mineralogy

Minerals present in the study area which are potential sorbents include: feldspars, silica, smectite, titanium oxides, iron oxides and manganese oxides. Previous work by Lawrence (1990) showed that radionuclides occur in three distinct sites: iron oxides, decomposition products of biotite (e.g. chlorite), and as discrete grains of zircon, titanite, allanite or monazite. The iron oxides are located primarily along the fracture margins and are, therefore, thought to dominate the sorptive capacity of the system. Figure 21 shows a thin section and an alpha-track map of the same thin section, illustrating the concentration of alpha emitters along fracture margins that are coated with iron oxides (Frishman *et al.*, 1993). The specific mineralogy of the iron oxides has not been determined; however, at

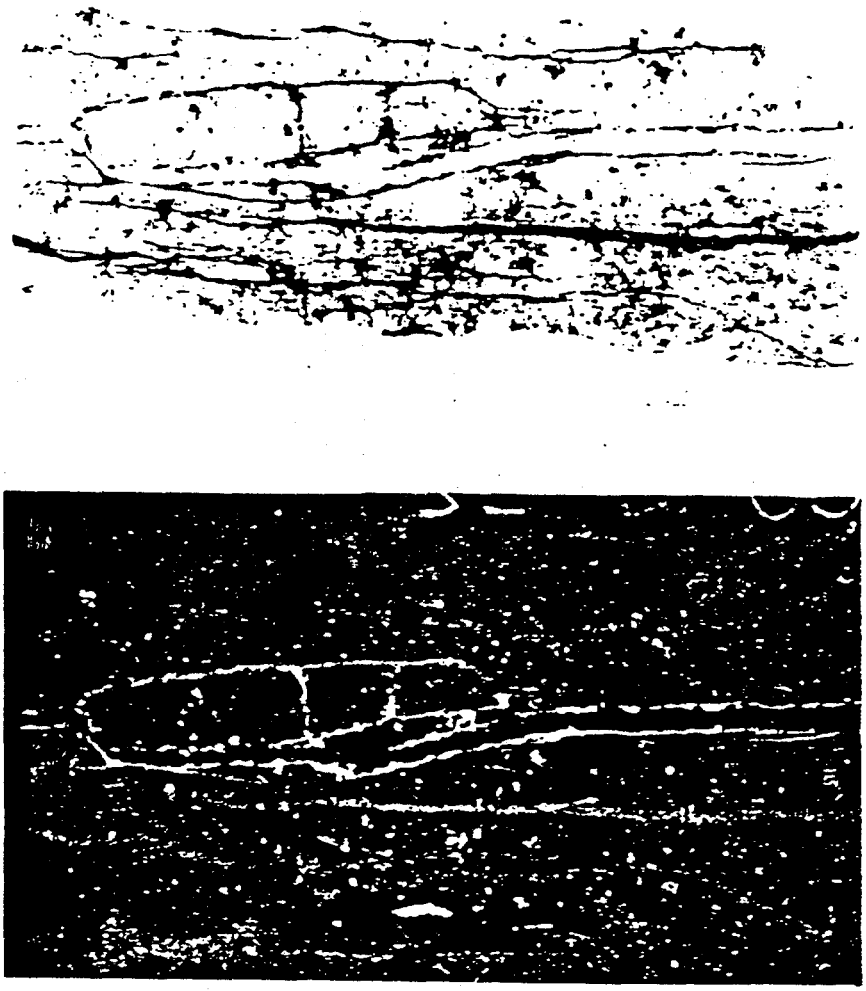

FIGURE 21 Photographs illustrating uranium/thorium residence in sample 91-CO-38: a) transmitted light, showing dark iron oxide coatings along fractures; b) alpha-track map of same section, showing the tracks left by alpha particles (after etching with NaOH). (Frishman *et al.*, 1993)

the temperature and pressures present in the system, goethite (α-FeOOH) is likely the most stable iron oxide phase (Schwertmann and Taylor, 1977).

XRD analyses of fracture coatings from the drill core samples (see Section 5.1) were not conclusive in identifying the mineralogy of the iron-stained coatings. Trace amounts of goethite were observed in most of the iron-stained samples, but the diffractograms showed low intensity dispersed peaks indicating poor crystallinity or low abundance. Since no other dominant crystalline minerals were present, it was inferred that amorphous minerals made up the bulk of the coating material. A light green clay observed on some fractures was identified as smectite. These fractures were often intact in the core boxes, and may have been "healed" or isolated from groundwater flow.

Sequential extraction tests showed that substantial amounts of manganese were present in the hydroxylamine-hydrocholoride/acetic acid extractant (discussed in Section 5.3). Since this extraction is known to attack both iron and manganese oxides (Chao, 1984), and because manganese metal is not strongly sorbed by iron oxides (Millward and Moore, 1991), it is likely that the manganese was present as either amorphous or poorly crystalline manganese oxides.

In summary, the mineralogical evidence shows that iron and manganese oxides are the primary fracture filling minerals. Although the specific mineral forms could not be identified, it is inferred that iron oxides are either poorly crystalline goethite or amorphous (ferrihydrite) and the manganese oxides are amorphous. These two mineral groups are expected to dominate the sorptive behavior of the system. Smectite was also identified as a fracture filling mineral but is considered to be a weak sorbent relative to iron and manganese oxides (Ticknor, 1994), and did not appear to be located on hydraulically transmissive fractures.

3.2.3 Fracture Geometry

Evidence from the geophysical logging shows that one or two fractures contribute most of the flow to a well (Folger, 1995). A review of driller's logs in the area also shows limited water bearing zones in the subsurface. By assuming only one of these fractures contributes most of the flow to a well, transmissivity data can be used to determine the fracture aperture. The calculation is based on the cubic law (Tsang, 1992):

$$b = \left(\frac{12T\mu}{\nu}\right)^{\frac{1}{3}} \qquad (1)$$

where:

b	=	fracture width or aperture (m)
T	=	transmissivity (m^2/s)
μ	=	dynamic viscosity ($kg/m \cdot s$)
ν	=	specific weight of water ($kg/s^2 \cdot m^2$)

Fracture apertures calculated by this method range from 0.06 to 1.5 mm, with a median value of 0.2 mm. It should be noted that the bulk fracture aperture represents a minimum fracture aperture, as the pumping test data tends to reflect the more constricted parts of a fracture wall (Tsang, 1992). In interpreting the model, this parameter is used in a comparative sense; thus, as long as a consistent method is used to calculate the aperture, the general conclusions will not be affected. A more serious limitation exists for wells with multiple fractures. From a hydrological standpoint, the aperture width in the individual fractures would be less; thus, the overall bulk specific surface area (see following section) would be greater. If only one of the fractures supplied ^{222}Rn to the well, the ^{222}Rn level in the well would vary according to the portion of the flow that fracture contributes. In the absence of specific data showing the number of water-bearing fractures for all of the study wells, it is assumed that there is one major water-bearing fracture per well.

3.2.4 Bulk Specific Surface Area

The bulk specific surface area is defined here as the bulk, 'macroscopic' surface area of reactive minerals exposed to a given volume of water (e.g., m^2/L). Assuming a completely smooth fracture surface, the bulk specific surface area is 2 m^2 divided by the fracture aperture (mm) x 1 m^2. For example, a fracture with an aperture of 0.2 mm (the median fracture) would have a bulk specific surface area of 10 m^2/L. This purely geometric approach does not account for the additional surface area resulting from micropores and crystal surfaces. The true available surface area is likely several orders of magnitude larger (Paces, 1973; Wanty *et al.*, 1991). Visual inspections of the drill core samples indicate that the coatings on Pikes Peak Granite are: <0.1 mm to 0.3 mm thick. The additional surface area resulting from the fine crystalline texture would contribute substantially to the small scale surface area. For example, an SEM photograph (Figure 22) shows the surface of a mass of goethite crystals formed in a comparable depositional environment. It is clear from this photograph that the surface area is very high.

To derive input parameters for the surface complexation model, it was to assumed that the sorbent is ferrihydrite with a surface area of 600 m^2/g. The mass concentration of ferrihydrite was then calculated as the quotient of the bulk specific surface area (m^2/L) and the ferrihydrite surface area (m^2/g). The resulting ferrihydrite mass concentration represents a minimum amount of sorbent - basically a thin coating over the "smooth" fracture wall.

FIGURE 22 Scanning electron micrograph of soil goethites from a pore coating in a laterite on acid igneous rock, Cameroun (Schwertmann and Taylor, 1977).

3.2.5 Site Density

Site densities were based on laboratory data and modeling studies on ferrihydrite (Waite *et al.*, 1994) rather than any *ex situ* determination from the drill core data. The ferrihydrite was conceptualized as having a small number of high-affinity (strong) sites distributed amongst a larger number of low-affinity (weak) sites. A strong site density of 0.0018 moles of sites/mole of iron, and a weak site density of 0.873 moles of sites /mole of iron were used in the sorption modeling calculations, as is consistent with Waite *et al.* (1994). In calculations where the amount of sorbent (ferrihydrite) is converted to an equivalent mass or a surface area of goethite, a value of 20 sites/nm^2 goethite (James and Parks, 1982) is used for the conversion.

3.2.6 Groundwater Residence Time

Groundwater residence times are inversely proportional to groundwater velocity. This parameter is difficult to measure in fracture flow systems, and cannot be determined on a well-specific basis using single-well aquifer tests. Velocities in the study area are considered to be high with a geometric mean of 1.6 m/day, and a standard deviation ranging from 0.11 to 24 m/day. Velocities were determined through two-well aquifer tests and flow modeling completed by Folger (1995) and, derived from the steep hydraulic gradients inferred by water level measurements throughout the study area. Pumping stresses only serve to steepen gradients in the vicinity of water wells, and may result in local velocities of 150 to 400 m/day.

The effect of residence time on ^{222}Rn in-growth and decay was explored in two groundwater modeling exercises (Folger, 1995; Appendix A). These examinations indicate ^{222}Rn levels do not reach secular equilibrium with parent radionuclides in the host rocks in systems with either steep gradients, short flow-paths, or pumping stresses. In such systems, small-aperture fracture segments have less of an impact on the overall

radon concentration than wide-aperture fractures because groundwater residence times are larger in the latter. Steep gradients and negligible residence times were found in the immediate vicinity of pumping wells, suggesting that variations in parent radionuclide concentrations near wells have almost no influence on the resulting water quality. One implication of this finding is that rock samples collected from the fracture zone in a borehole may not be in radiochemical equilibrium with the water sampled in that same borehole (unless the sample represents conditions at some distance from the well).

Although it is recognized that the residence time of water in fractures is probably very short in the field, a residence time of 30 days is assigned to the conceptual model (i.e., sufficient time to assume that secular equilibrium between ^{222}Rn and its parent nuclide, ^{226}Ra, has been reached). Since this work attempts to demonstrate that there is a significant accumulation of parent radionuclides, the assumption of a 30 day residence time is conservative in that the amount of enrichment would be underestimated where there is insufficient residence time to allow full ingrowth of ^{222}Rn. The assumption of a 30 day residence time allows this study to focus on the chemical processes leading to enrichment.

3.2.7 Water Chemistry

A discussion of the water chemistry results was presented in Part I of this study. In brief, the water chemistry is typical of waters in granitic terrane, with low total dissolved solids (TDS), moderate alkalinity, and near neutral pH's. Dissolved oxygen levels vary, but are close to saturation (7.5 mg/L at this temperature and elevation). Dissolved oxygen levels can be used to calculate the redox condition of the water and consequently the oxidation state of the uranium (Langmuir, 1978). Based on pE/pH conditions of the system, the uranium should occur as uranium (VI) species. The bicarbonate alkalinity of the system is an important variable because the uranyl ion forms complexes with

carbonate species and these species are more weakly sorbing than are the uranyl ion or uranyl hydroxy species. At high pH levels, carbonate acts as a competing ligand for uranium and may shift the distribution of uranium from mineral surfaces to the solution phase.

Table 16 shows key chemical variables considered in the model: pH, HCO_3^- and uranium. The data are presented according to the major rock-types. Bicarbonate levels are highest in the migmatites, with median values of 2 to 3 times greater than those measured in the Silver Plume and Pikes Peak wells. pH levels were also somewhat higher in the migmatite wells. Uranium levels varied considerably, with the highest values measured in the Silver Plume wells.

3.3 Conceptual Model Assumptions

The application of any model necessitates assumptions and simplifications about the system under study. This is particularly true for natural systems where sampling limitations may restrict the collection of sufficient data to characterize the system. Some of the problems encountered in characterizing the Elk Creek system are discussed in Section 3.2. This section discusses the further implications of the assumptions which are part of the application of surface complexation models to analysis of the system.

3.3.1 Multiple Sorbents

A disadvantage to surface complexation models is that only one or two sorbents can be considered in the model platforms as currently configured. However, it has been shown that a single sorbent often dominates the sorptive behavior of a system (e.g., Honeyman, 1984). Several examples in the literature illustrate that amorphous ferric oxyhydroxides often dominate the sorption of metal cations in multiple sorbent systems (Payne and Waite, 1991; Payne *et al.*, 1994; Ticknor, 1993; and Gascoyne and Barber, 1992),

TABLE 16 Range of Key Chemical Parameters in Pikes Peak and Migmatite

Component	median concentration	minimum concentration	maximum concentration
Migmatite			
HCO_3^- (mg/L)	176	76	326
pH	7.3	6.60	8.19
U (µg/L)	10	1.6	79
Silver Plume Quartz Monzonite			
HCO_3^- (mg/L)	56	14	177
pH	6.65	5.8	7.91
U (µg/L)	5.3	0.14	619
Pikes Peak Granite			
HCO_3^- (mg/L)	73	16	252
pH	7.00	5.8	8.4
U (µg/L)	4.1	0.42	175

particularly when fracture surfaces are coated with these minerals. As discussed in Section 3.2, iron and manganese oxides are found in the Elk Creek system and comprise a substantial portion of the exposed surface area. Ticknor, (1993) tested uranium sorption for 10 fracture filling minerals and found that chlorite, geothite, hematite, kaolinite and muscovite all had distribution coefficients (R_d values) in excess of 1500 ml/g, while other fracture filling minerals commonly found in bedrock (including smectite) had a relatively low sorptive strength. Experimental limitations prevented further distinction between these sorbents. Since the oxides and smectite are the only minerals found in significant quantities on fracture surfaces in this study, Ticknor's observations support the use of a dominant sorbent in the surface complexation model. An extensive review of the literature failed to locate data on uranium sorption to manganese oxides, thus ferrihydrite was the only sorbent that could be considered in the SCM model. However, it is recognized that manganese oxides contribute to the sorption and this is addressed in the interpretation of the model.

3.3.2 Variations in Mineral Form

The degree of crystallinity, site density, exposed surface area and mineral composition affect the sorptive capacity and intensity of metal binding of the system. These parameters have not and probably cannot be characterized in the Elk Creek system. The application of the SCM approach in this study is not to mimic the actual system but to provide a heuristic device for evaluating the significance of accumulation centers to ^{222}Rn generation. Even if present day conditions could be established, the geochemical conditions during deposition are probably of equal, if not greater, importance. Over the large time scales that this system has evolved (*ca.* 1,100 m.y.), the mineralogical and elemental distributions in and around fractures and cracks represent a varied history of fluid movement and fluid composition (Latham, 1994). Since the geochemical conditions

favoring uranium solubility and iron oxide formation are similar, it is reasonable to assume that oxide deposition and uranium sorption could occur simultaneously. Freshly formed oxides have been shown to have higher surface areas and sorptive capacities than do more developed crystalline forms (Payne *et al.*, 1994), so laboratory data generated for amorphous or freshly synthesized minerals may be adequate to characterize these older systems.

It has also been shown that iron oxides as a group exhibit similar metal ion binding characteristics, on a per-surface-site basis. For example, Hsi and Langmuir (1985) carried out uranium sorption experiments using ferrihydrite, geothite, and natural and synthetic hematite. The data from these experiments (Figure 23) exhibit very similar sorption edges, despite a considerable range in sorbent site density, specific surface area and crystal morphology (see table accompanying Figure 23). This observation implies that model constants derived for any ferric oxyhydroxide should be applicable to other ferric oxyhydroxides provided that the appropriate corrections have been made for mineral specific characteristics (site density, specific surface area etc.).

3.3.3 Mineral Distribution

The distribution of iron minerals in the system is a key concern regarding the utility of this model. It is not possible to examine the distribution of iron minerals using the available data. The strongly weathered nature of the rock prevents the use of road cuts or trenches to quantify iron distributions, and drill core does not provide a large enough surface area to adequately characterize the fractures. It should be clear that the model can only explain differences in radon levels related to variations in the amount of enrichment that can occur, not those attributed to the abundance or distribution of enriched iron in the system.

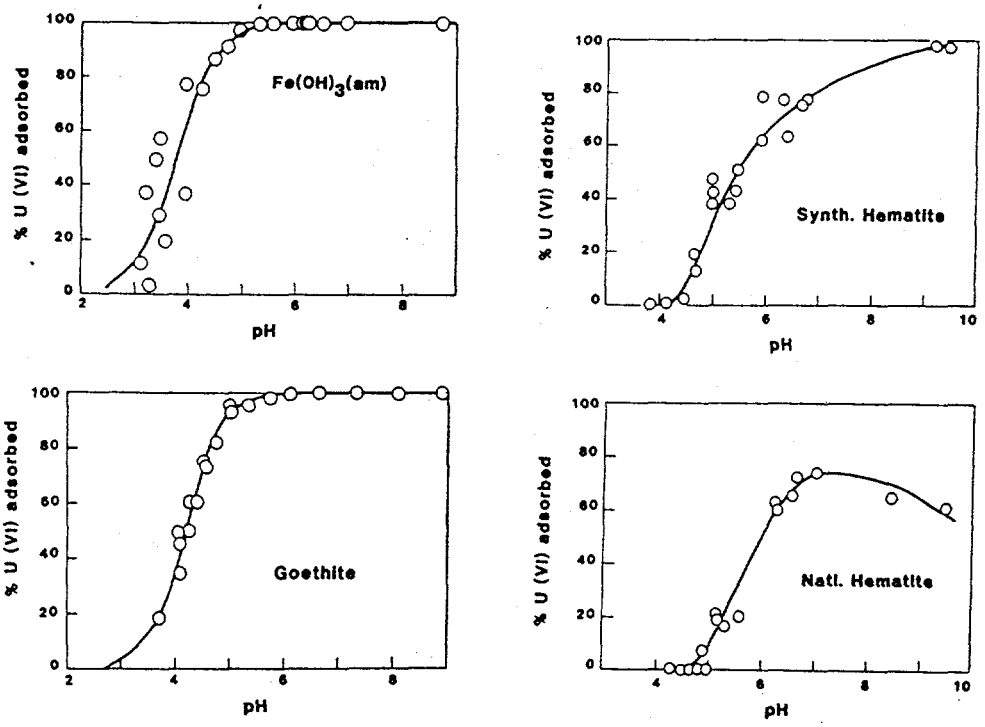

Physical and surface properties of starting materials:

Material	Particle Shape	Particle Size	SA (m^2/g)	N_s (sites/nm^2)	PZC	IEP	Wt % H_2O
$Fe(OH)_3$ (am)	Spherical	2 nm	306	20*	7.9±0.2	-	13
α-FeOOH	Rod-like	1 cm length	45	18*	8.5±0.3	8.9±0.2	11.5
Synthetic α-FeOOH	Spherical	0.3 μm	3.1	19	7.5±0.5	7.2±0.5	2
Natural α-FeOOH	Irregular	1 μm	15	15	7.8±0.5	7.0±0.5	1

Notes: * 1.05×10^{-3} mol/g
** 1.35×10^{-3} mol/g

FIGURE 23 Adsorption of uranyl to ferrihydrite, goethite, synthetic and natural hematite (Hsi and Langmuir, 1985).

3.3.4 Competing Ions

U (VI) species are more surface active compared to other ions typically found in groundwaters. These uranyl species typically outcompete other solutes for mineral surface sites. For example, Hsi and Langmuir (1985) examined the effect of competing cations on uranyl adsorption and found that Ca and Mg levels of 10^{-3} M did not significantly affect uranyl adsorption. The extent to which other solutes will effectively compete with U for the occupation of surface sites will depend on the concentration of ions and the relative intensity of ion binding to those sites.

3.3.5 Complexing Ions or Competing Ligands

Uranyl forms complexes with several inorganic ligands and with natural organic matter. These ligands include carbonate, fluoride, phosphate and humic and fulvic acids. Of these, carbonate is the most abundant in the Elk Creek system. The effect of carbonate activity on uranium sorption is well documented, and has been considered in the model. Fluoride is present only in groundwaters within the Pikes Peak granite, and is present at levels below 4 mg/L, and phosphate was consistently below the detection limit of 1 mg/L. The dissolved organic carbon content of groundwaters in the Elk Creek basin has not been measured; however, groundwater DOC values are typically very low in crystalline rocks, with median values of 0.5 mg/L (Thurman, 1985).

3.3.6 Geochemical History of System

As discussed previously, the Elk Creek system has been evolving for approximately 1,100 million years. It is therefore reasonable to assume that the current fracture system reflects a considerable history of chemical and mineralogical changes brought on by regional tectonic events and by more recent, local scale weathering processes.

The assumptions of chemical and secular equilibrium in the system are a central assumption in the simulation of local scale uranium enrichment and the extrapolation of results to understanding chemical controls on ^{222}Rn variability. It is thought that the system has been in a relatively stable configuration for several million years: there is no evidence of recent faulting and the area was not subject to glaciation.

3.3.7 Hydrogeological Factors

The extension of the surface complexation model results to simulating groundwater ^{222}Rn levels also depends on our ability to understand the hydrological characteristics of the system. The simplified cubic law assumptions may not adequately describe the surface area to volume ratios found in the system. Multiple water-bearing fractures, variations in hydraulic gradient and velocity, the effects of pumping wells and differences in the length of flow paths are all relevant factors that have not been considered in this study.

4.0 SURFACE COMPLEXATION MODELING

4.1 Review of Waite *et al.* (1994) Model Describing Uranium Sorption to Ferrihydrite

The literature provides several examples of the application of surface complexation models to describe the sorption of uranium to iron oxides (Hsi and Langmuir, 1985; Payne and Waite, 1991). A recent application by Waite *et al.* (1994) for uranium (VI) adsorption onto ferrihydrite was selected for this study because of its excellent supporting evidence and thorough documentation. The Waite *et al.* application used the diffuse layer model (Dzombak and Morel, 1990) as the framework for describing sorption reactions. Uranium (VI) solution speciation is based on reaction constants taken from Grenthe *et al.* (1992); these are summarized in Table 17. Simulated aqueous speciation of U(VI) is shown in Figure 24. Although several polynuclear complexes are present in solution, Waite *et al.* showed through 'extended x-ray adsorption fine structure' spectroscopy (EXAFS) that constraints imposed by surface coordination prevent all but free uranyl and uranyl carbonate from binding to the surface. A typical experimental adsorption 'edge' for U(VI) species binding to ferrihydride is presented in Figure 25. The edge shows the characteristic "metal-like" behavior in the low pH range, where UO_2^{2+} is thought to be the dominant sorbent, and the desorption edge in the high pH range, where non-sorbing, negatively charged uranyl complexes dominate the system. Waite *et al.* (1994) postulated a series of surface reactions which were consistent with the EXAFS data and sorption experiments (Table 18). Reaction constants were determined in FITEQL, Version 3.1, (Herbelin and Westall, 1994).

TABLE 17 Aqueous Phase Reactions (after Grenthe *et al.*, 1992)

$UO_2^{2+} + OH^- = UO_2OH^+$	Log K = 8.8
$UO_2^{2+} + 2OH^- = UO_2(OH)_2^o$	Log K = 16.0
$UO_2^{2+} + 3OH^- = UO_2(OH)_3^-$	Log K = 22.0
$UO_2^{2+} + 4OH^- = UO_2(OH)_4^{2-}$	Log K = 23.0
$UO_2^{2+} + 4OH^- = UO_2(OH)_4^{2-}$	Log K = 11.2
$2UO_2^{2+} + OH^- = (UO_2)_2(OH)^{3+}$	Log K = 11.2
$2UO_2^{2+} + 2OH^- = (UO_2)_2(OH)_2^{2+}$	Log K = 22.37
$3UO_2^{2+} + 4OH^- = (UO_2)_3(OH)_4^{2+}$	Log K = 44.1
$3UO_2^{2+} + 5OH^- = (UO_2)_3(OH)_5^+$	Log K = 54.44
$3UO_2^{2+} + 7OH^- = (UO_2)_3(OH)_7^-$	Log K = 67.0
$4UO_2^{2+} + 7OH^- = (UO_2)_4(OH)_7^+$	Log K = 76.1
$UO_2^{2+} + CO_3^{2-} = UO_2CO_3^o$	Log K = 9.7
$UO_2^{2+} + 2CO_3^{2-} = UO_2(CO_3)_2^{2-}$	Log K = 17.0
$UO_2^{2+} + 3CO_3^{2-} = UO_2(CO_3)_3^{4-}$	Log K = 21.63
$2UO_2^{2+} + CO_3^{2-} + 3OH^- = (UO_2)_2CO_3(OH)_3^-$	Log K = 40.82
$\beta\text{-}UO_2(OH)_2 = UO_2^{2+} + 2OH^-$	Log K = -23.07

Note: Constants are for I = 0.

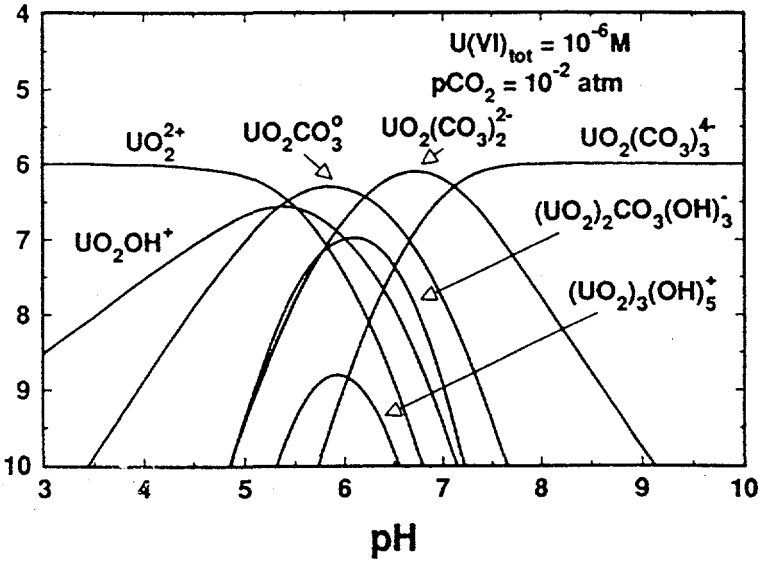

FIGURE 24 Dissolved Speciation of U(VI) at a total concentration of 10^{-6} M in an open system equilibrated with a partial pressure of CO_2 of 10^{-2} atm, ionic strength = 0.1 (Waite *et al.*, 1994)

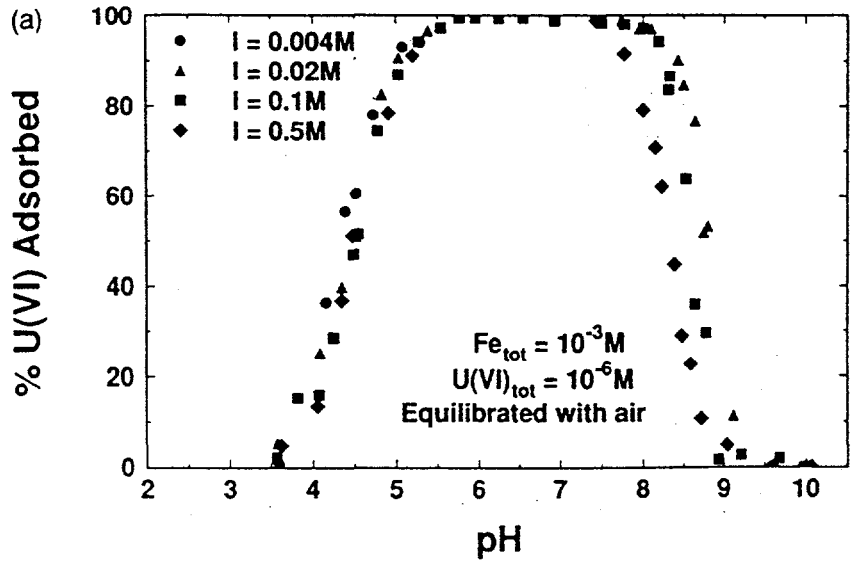

FIGURE 25 Adsorption of 10^{-6} M U(VI) on ferrihydrite (10^{-3} M as Fe), as a function of pH and ionic strength. Open system. (Waite *et al.*, 1994).

4.2 Application of Ferrihydrite Sorption Model (Waite *et al.*, 1994) to the Conceptual Model System

The Waite *et al.* (1994) model for uranium sorption to ferrihydrite was used to generate adsorption isotherms for the conceptual model system discussed in Section 3.0. FITEQL Version 3.2 (Herbelin and Westall, 1996) was used for the calculations since it is capable of handling the bidentate complexes proposed in the Waite *et al.* model. In addition to the basic model parameters (speciation constants, reactions, surface species etc.) described in Section 4.1, the ferrihydrite site density, concentration and specific surface area assumptions from the conceptual model were entered into the computer code. The conceptual model assumptions used in FITEQL are summarized in Table 19. As discussed in the methods section, a quick-basic routine, BATS, was used the generate batch input files to generate isotherms at various pH and bicarbonate concentrations.

TABLE 19 Summary of FITEQL Model Parameters from Field Data

sorbent	ferrihydrite
pH	variable (see Table 16)
$H_2CO_3^*$	variable (see Table 16, Appendix E)
ferrihydrite conc.	0.01083 g/L $FeO_3 \cdot H_2O$
bulk specific surface area	6.5 m^2/L
site density (Waite et al., 1994):	
weak	0.873 moles sites/moles ferrihydrite (1.6E-7 moles sites/L)
strong	0.0018 moles sites/moles ferrihydrite (7.77E-5 moles sites/L)

The adsorption isotherms generated using the Waite *et al.* model and FITEQL are used to calculate the adsorption density, Γ, (moles UO_2 sorbed/moles sites) for various pH, HCO_3^- and U_T concentrations. Since Γ is normalized to the number of sorption sites, it is essentially independent of the absolute number of sorption sites and the geometry of the fracture.

Gamma (Γ) can also be used to calculate any of the following results:

- uranium activity per mole of sites;
- uranium concentration or activity in ferrihydrite;
- uranium surface concentration or activity for iron minerals where site density is expressed in sites per mass (e.g. hematite);
- uranium surface concentration or activity per unit surface area for iron minerals where site density is expressed in sites/nm^2 (e.g. goethite).

Within the bounds of the conceptual model framework, radon levels in the water can be used to constrain the surface area or mass of the enriched sorbent that must be present in the system. These calculations are useful for evaluating whether the enrichment scenario is physically and geologically reasonable.

4.3 SCM Model Results

4.3.1 Isotherms

A typical adsorption isotherm from the FITEQL model is shown in Figure 26. Isotherms generated with the Waite *et al.* model have a characteristic shape that reflects the contribution of the strong and weak binding sites. At low equilibrium uranium concentrations, the slope of the isotherm is equal to one. In this region, strong sites dominate the sorptive behavior. At about $10^{-8.5}$ molar U, the strong sites begin to fill up, and by about 10^{-7} molar U_{eq} they are completely occupied. In this region, the isotherm

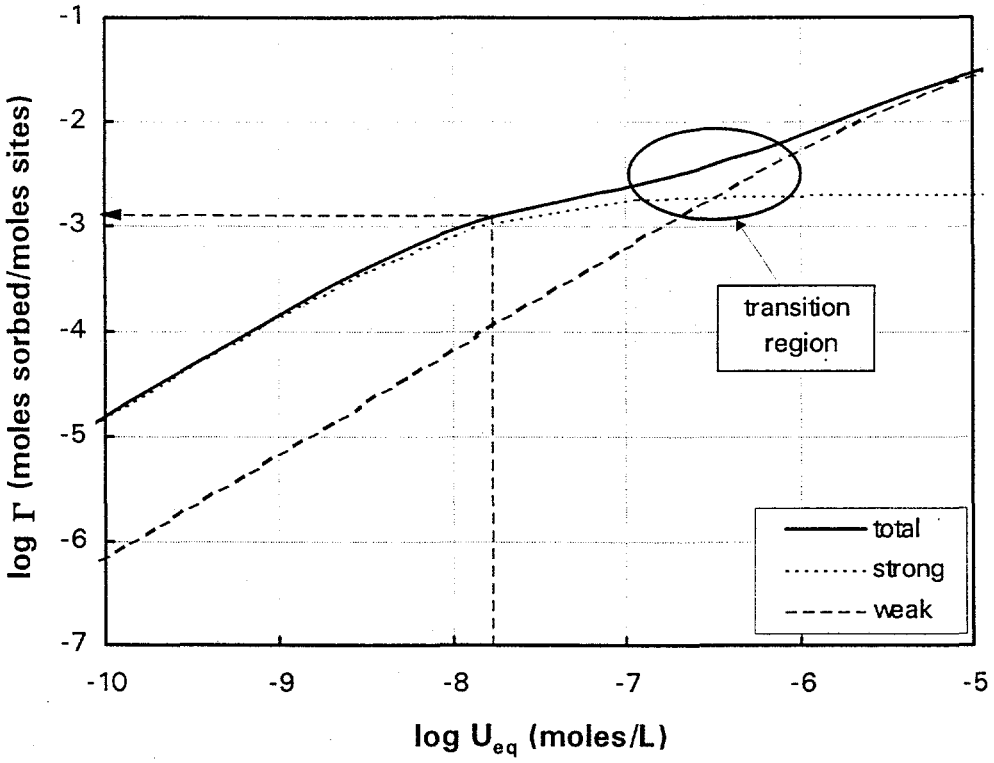

FIGURE 26 Model Adsorption Isotherm for Example Well 91-CO-38: alkalinity = 0.9 mM, pH = 7.1, U_{eq} = 4 µg/L. Lines represent the result of computations using FITEQL and the configuration of Waite et al. (1994), Section 4.1.

has a slope of about one-half. Weak sites then begin to dominate the sorption. Solubility limitations are not shown on the figure; however, it is recognized that schoepite (a uranyl oxide mineral) would reach saturation and limit U_T concentrations to about 10^{-6} moles U/liter (Langmuir, 1978). Above this threshold, precipitation and sorption would regulate solution concentrations, and the fracture walls would exhibit greater enrichment than expected from an adsorption model. Fortunately, the measured U concentrations are below this threshold.

The adsorption isotherms generated using the Waite *et al.* model are consistent with experimental isotherms found in the literature. For example, an isotherm presented in Langmuir (1978) is plotted alongside a model-generated isotherm with the same pH and bicarbonate concentration in Figure 27.

pH and alkalinity were varied over the range observed for water samples from the three geological units considered in this part of the study: Migmatite, Silver Plume Quartz Monzonite and Pikes Peak Granite. The isotherms are shown in Figures 28, 29 and 30. The results show that variations in alkalinity and pH account for an order of magnitude range in Γ within a given rock unit. When combined with the variations in measured uranium concentrations, Γ may range as much as 3 orders of magnitude. The region of interest shown on each of the isotherm figures corresponds to the range of measured U, pH and alkalinity values in each rock-type. These results show considerable overlap in Γ values. However, it is apparent from the figures that migmatite has lower Γ values, and less variability than the granites. The results show that wells with high alkalinity, high pH and low uranium should have less uranium sorbed to the fracture walls than wells with low alkalinity, low pH and high uranium.

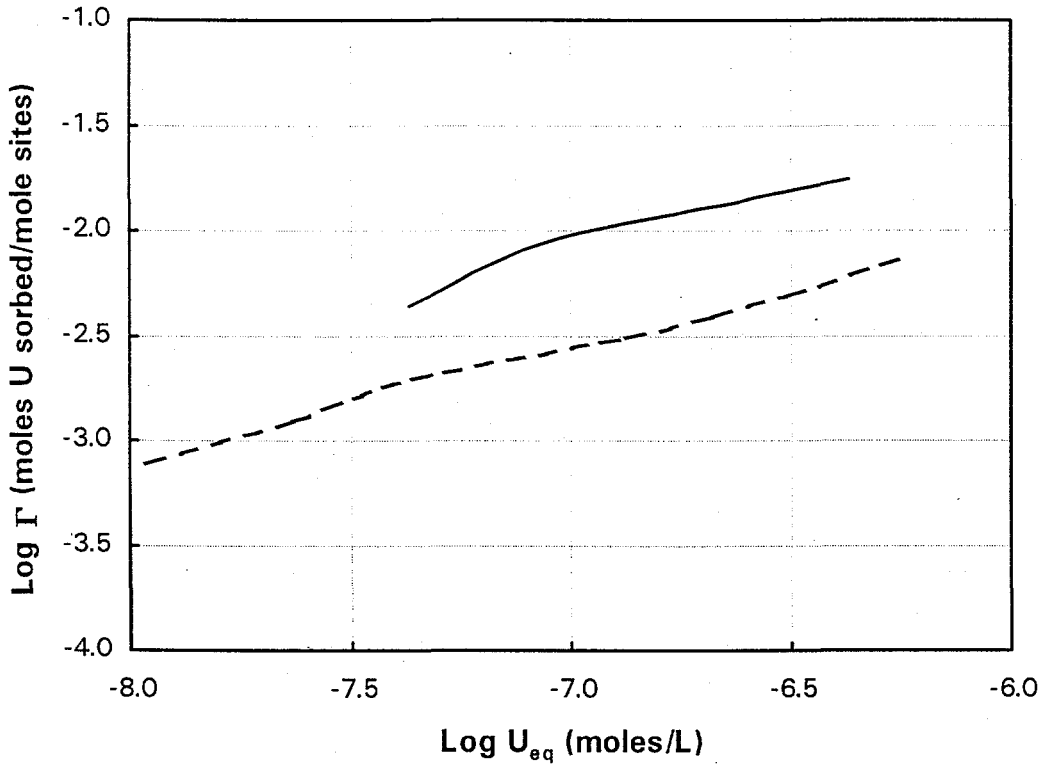

FIGURE 27 Comparison of model isotherms to experimental data. Solid line represents experimental data (Langmuir, 1978), dashed line represents model isotherm (see Figure 26). Experimental and model conditions: pH = 7.23, $C_T = 10^{-8}$, 1.03 g/L ferrihydrite, 285 m^2/g, 0.873 weak sites/mole Fe, 0.0018 sites/mole Fe.

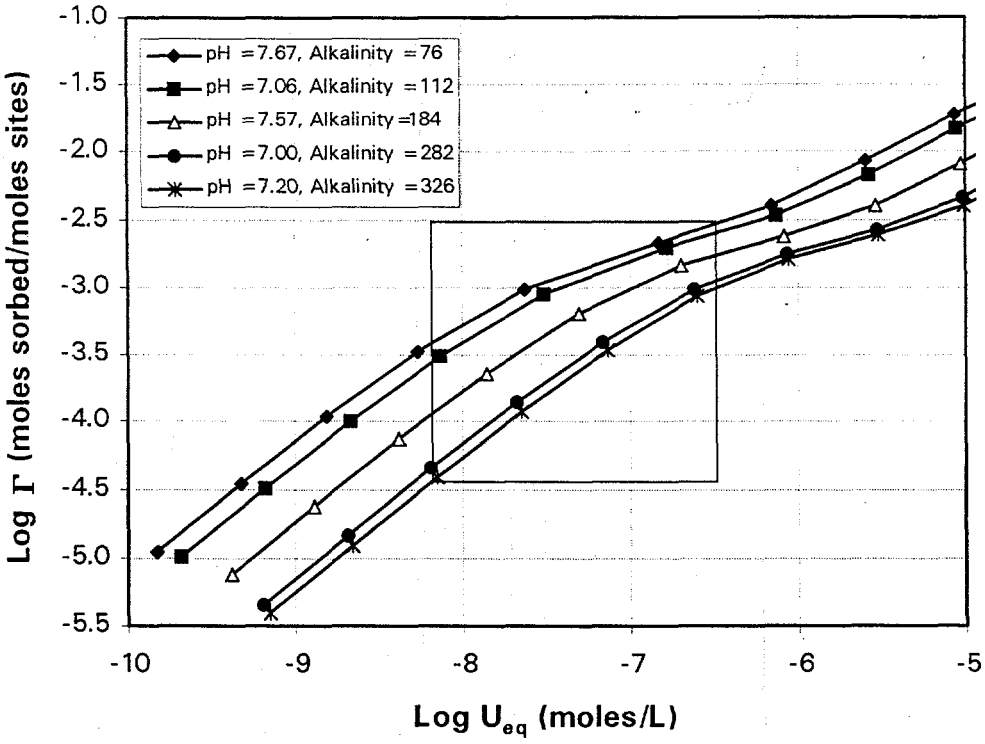

FIGURE 28 Uranium Adsorption Isotherms (after Waite *et al.*, 1994) for Migmatite groundwater samples. Isotherms represent the range of pH and alkalinity measured in these samples. Gamma is further constrained by the range of equilibrium uranium concentrations, as indicated by the square region on the figure.

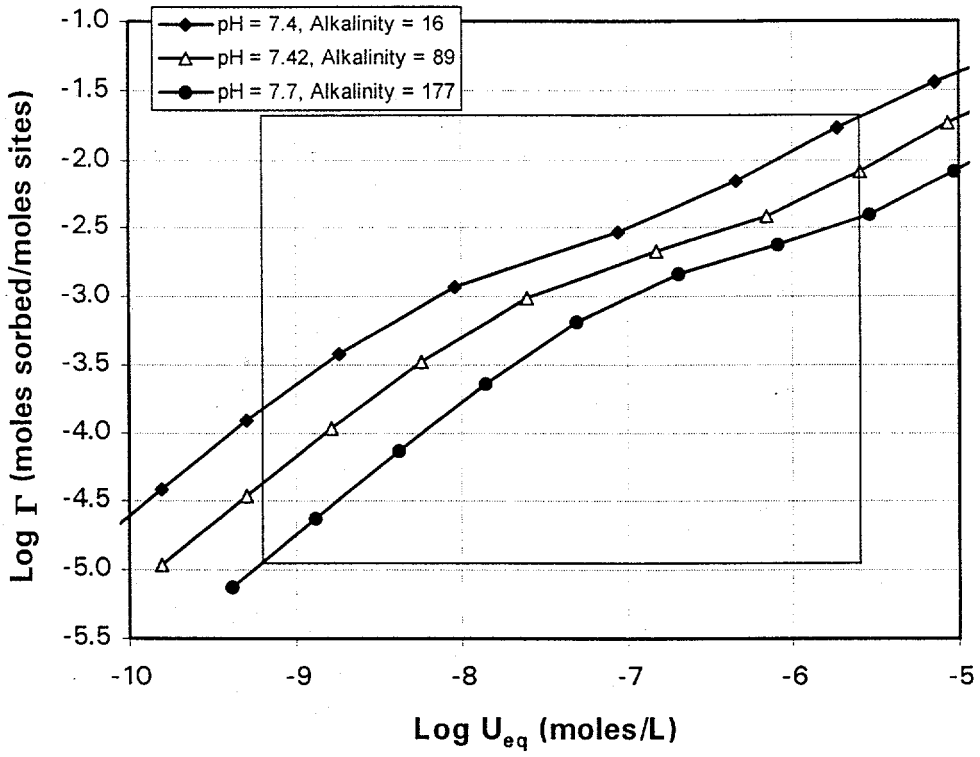

FIGURE 29 Uranium Adsorption Isotherms (after Waite *et al.*, 1994) for Silver Plume Quartz Monzonite groundwater samples. Isotherms represent the range of pH and alkalinity measured in these samples. Gamma is further constrained by the range of equilibrium uranium concentrations, as indicated by the square region on the figure.

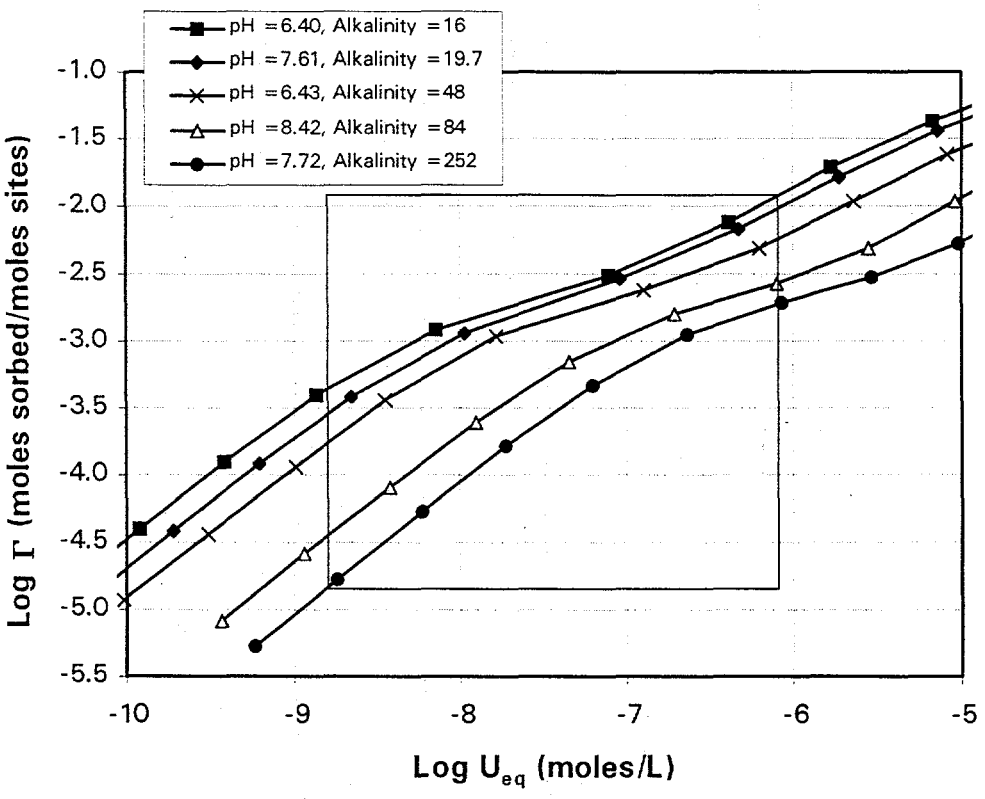

FIGURE 30 Uranium Adsorption Isotherms (after Waite *et al.*, 1994) for Pikes Peak Granite groundwater samples. Isotherms represent the range of pH and alkalinity measured in these samples. Gamma is further constrained by the range of equilibrium uranium concentrations, as indicated by the square region on the figure.

4.3.2 Uranium Enrichment Calculations

Results from a typical Pikes Peak water supply well (91-CO-38) are used to show that mineral surface enrichment results can be interpreted in the context of the conceptual model. First, the sorption density (Γ) is determined graphically using the adsorption isotherm shown in Figure 26. Sorption density is then converted to moles of U sorbed per mole of ferrihydrite as follows (using a Γ of 1.26×10^{-3} moles U sorbed/mole site as an example):

$$\frac{1.26 \times 10^{-3}\ moles\ U\ sorbed}{moles\ sites} \times \frac{0.875\ moles\ sites}{mole\ Fe_2O_3 \cdot H_2O} \times \frac{238\ g\ U}{mole\ U}$$

$$\times \frac{1\ mole\ Fe_2O_3 \cdot H_2O}{178 g\ Fe_2O_3 \cdot H_2O} = \frac{1.47 \times 10^{-3}\ g\ U}{g\ Fe_2O_3 \cdot H_2O} \Rightarrow \frac{1470\ mg\ U}{kg\ Fe_2O_3 \cdot H_2O}$$

The U(VI) surface concentration can be converted to a specific activity (e.g., pCi ^{238}U/g of ferrihydrite) by multiplying by 0.3309 (see conversion in Table 15) to give a surface activity of approximately:

$$\frac{500\ pCi\ ^{238}U}{g\ Fe_2O_3 \cdot H_2O}$$

Assuming that the ^{222}Rn emanation efficiency is 50 percent, and that secular equilibrium exists between uranium and all of its daughters, the measured radon can be used to estimate how much iron oxide would have to be present on the fracture to support the ^{222}Rn activity:

- *on a volume basis (assuming a radon activity of 11,000 pCi/liter):*

$$\frac{11000\ pCi\ ^{222}Rn/liter}{(500 pCi\ ^{238}U / g\ Fe_2O_3 \cdot H_2O) \times 0.5} = \frac{44\ g\ Fe_2O_3 \cdot H_2O}{liter}$$

- *on a surface basis (assuming a bulk specific surface area of 6.5 liters/m^2):*

$$\frac{44\ g\ Fe_2O_3 \cdot H_2O}{liter} \times \frac{1\ liter}{6.5\ m^2} = \frac{6.8\ g\ Fe_2O_3 \cdot H_2O}{m^2}$$

Assuming a density of 1.5 g ferrihydrite/cm^3, the ferrihydrite would have to be about 0.0045 mm thick to support the observed radon levels. This thickness is both physically and geologically reasonable.

Recall from Section 1.1 that the recoil distance is approximately 40 nm, or about one-hundreth of the above thickness. The calculations shown above assume that half of the radon produced in the 4.5 μm layer of enriched iron escapes to the solution phase of the system. Thus, it is important to recognize that the surface layer is porous and that the porosity contributes to the "roughness" or the true surface area of the fracture surface. The surface roughness can also be estimated from the sorption modeling data. First, the mass concentration of ^{238}U is converted to a volume based concentration as follows:

$$\frac{500\ pCi^{238}\ U}{g\ Fe_2O_3 \cdot H_2O} \times \frac{1.5\ g}{cm^3} \times \left(\frac{100\ cm}{m}\right)^3 = \frac{7.5 \times 10^8\ pCi\ ^{238}U}{m^3}$$

The volume of this enriched ferrihydrite that is within the recoil range of a smooth 1 m^2 fracture (with 2 m^2 of bulk surface) is 8 x 10^{-8} m^3 (see Table 1); thus the activity of ^{238}U within the recoil range is:

$$\frac{7.5 \times 10^8\ pCi\ ^{238}U}{m^3} \times (8 \times 10^{-8} m^3) = 60\ pCi\ ^{238}U$$

Following the above example, the radon concentration resulting from this smooth fracture assuming an emanation efficiency of 50%, would be:

$$60\ pCi \times 0.5 \times \frac{6.5\ m^2}{liter} \times \frac{1}{2\ m^2} = \frac{100\ pCi\ ^{222}Rn}{liter}$$

Finally, the actual ^{222}Rn activity in this example fracture is 11,000 pCi/L, so the surface roughness must be 110 times greater than for a perfectly smooth fracture surface.

Similar enrichment calculations were performed for a range of samples from each of the geologic units. Approximate Γ values were determined by fitting regression lines through a high, low and median alkalinity isotherm, and calculating Γ from the uranium

and the regression equations. The "best" Γ was then determined by interpolating on the basis of bicarbonate alkalinity. This method introduces some error because the interpolation does not consider pH; however, it is considered sufficiently accurate to show the range of surface concentrations in these samples. The results of the sorption calculations are presented in Appendix E and summarized in Table 20.

TABLE 20 Uranium Enrichment Calculations

Rock	Log Γ (moles U/moles sites)	mg U/kg $Fe_2O_3 \cdot H_2O$
Migmatite	-3.30 (-3.80, -2.92)*	680 (200-1400)
Silver Plume QM	-3.10 (-4.22,-2.19)	2000 (70-7500)
Pikes Peak Granite	-3.17 (-4.27,-2.14)	1200 (60-8500)

*average (min-max)

4.3.3 Relationship between Surface Concentrations and Measured Radon Activities

The enrichment results Γ (moles U/moles sites) were plotted against measured radon levels to test for any correlations between the model and field results. The results are shown in Figure 31. There is no apparent correlation between measured ^{222}Rn and the model-based Γ's. Figure 32 shows a second scatterplot with Γ plotted against the measured radon level multiplied by the fracture aperture. This essentially factors out the effects of aperture width; however, there is still no relationship between the model and field results. Variations in the amount and distribution of sorbent in the system, dilution effects caused by insufficient residence times, and/or error introduced by multiple fractures can easily explain the lack of correlation.

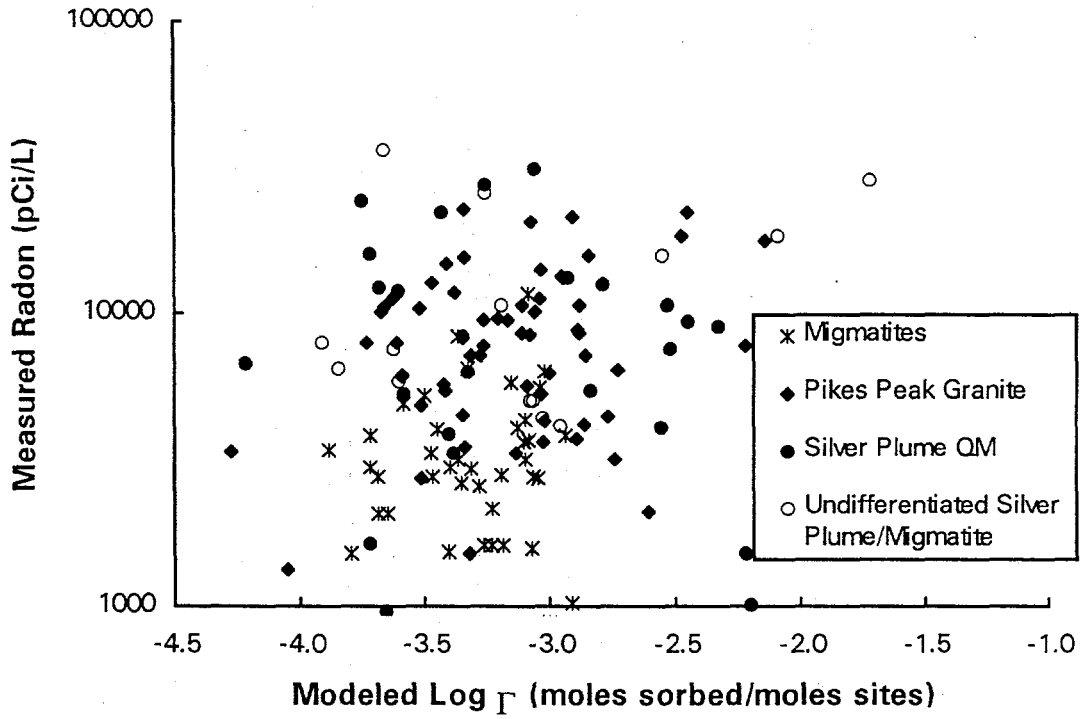

FIGURE 31 Scatterplot of ^{222}Rn versus sorption density (Γ). Notice the clustering of migmatite samples towards low ^{222}Rn and low Γ's compared to the wider scatter seen in the other rock groups.

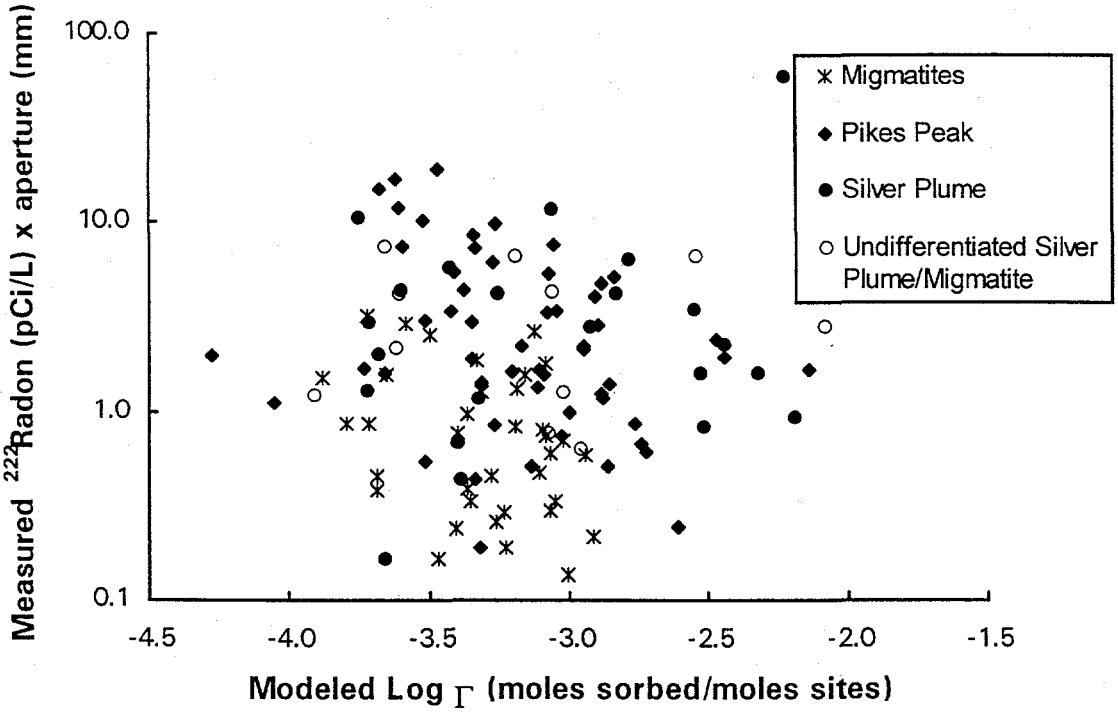

FIGURE 32 Scattterplot of (^{222}Rn x fracture aperture) versus sorption density. By multiplying the ^{222}Rn activity by the fracture aperture, the "dilution" effect caused by different fracture apertures is removed. As in Figure 31, migmatite clusters in the low ^{222}Rn, low Γ portion of the graph.

4.4 Discussion of Model Results

Isotherms generated with the Waite *et al.* (1994) model are consistent with laboratory isotherms prepared under the same conditions (e.g., Langmuir, 1978). The position of the model isotherms varies according to the pH and carbonate content of the water. According to the model, wells with high bicarbonate alkalinity, high pH (7 to 8.5) and low uranium should have less uranium sorbed to the fracture walls than wells with low alkalinity, low pH (5.5 to 7) and high uranium. These chemical variables account for order of magnitude differences in the sorption density, Γ. When combined with the variability in aqueous U concentrations, Γ can vary as much as three orders of magnitude.

The sorption density, Γ, can be converted to a concentration of U in a given mass of iron oxide. The calculations presented in Section 4.3.2 show that U concentrations in the iron oxides would be in the range of 60 to 8500 mg U/kg $Fe_2O_3 \cdot H_2O$. This is 15 to 2000 times greater than the bulk-rock concentration of 5 ppm U. Because the iron oxides are located at the water/rock interface, the enrichment of U (and by association, ^{226}Ra) would contribute substantially to ^{222}Rn fluxes in this system. Although there are no correlations between Γ and the measured ^{222}Rn levels, the magnitude of uranium surface enrichment is sufficient to support the observed range of ^{222}Rn activities in the water. Comparisons between the major geologic groupings are consistent with the observed ^{222}Rn levels in these units. For example, surface enrichment is generally lower in the migmatites than in the igneous rocks, and ^{222}Rn levels are also lower in this unit.

Experimental work to verify the model results is presented in the following section. The main target of the verification is to determine the magnitude of uranium enrichment in fracture-filling iron and manganese oxides.

5.0 EXPERIMENTAL RESULTS AND MODEL VERIFICATION

This section presents the results of experimental work on drill core samples from the Pikes Peak Granite. Testing included x-ray diffraction tests (XRD) to determine the fracture mineralogy, uranium assays and sequential extraction tests.

5.1 Fracture Mineralogy

Results from the 7 drill-core samples submitted for XRD analysis are shown in Table 21. The results indicate that the fracture filling minerals described as "iron-stained, limonite or hematite coated" are likely amorphous to weakly crystalline iron oxides. Goethite was the only crystalline iron oxide mineral that could be found in the core samples. The light green fracture filling mineral was identified as smectite on the basis of a glycol test (which tests for the swelling properties of this clay). Small amounts of quartz, microcline, orthoclase, albite, and muscovite were found in the samples, and were probably fragments of host rock minerals incorporated into the samples during preparation.

5.2 Bulk-rock Chemistry

Uranium assays were done on 23 of the core samples. The results show that bulk-rock uranium concentrations are within the normal range for Pikes Peak Granite, with values ranging from <0.16 to 1.7 ppm U. There were no correlations between the bulk-rock U concentrations and extractable uranium concentrations.

TABLE 21 Results of X-Ray Diffraction Tests on Fracture Filling Minerals from Drill Core Samples

Sample ID	Hand Sample Description	Minerals identified in XRD testing*
KSS-FD1-D	light green clay, tr limonite	Quartz, Orthoclase, Albite, Smectite
KSS-FD1-Q	light green clay	Muscovite, tr.Quartz, Orthoclase (tr. microcline), Smectite
KSS-FD5-D	limonite and hematite, (rusty to reddish)	Muscovite, Quartz, Orthoclase, Albite, tr.Goethite
KSS-FD5-F	limonite, tr. clay (light yellow to rusty)	Goethite, Muscovite, Quartz, orthoclase, albite, tr. smectite
KSS-FD5-J	hematite, tr. clay (reddish)	Goethite, smectite, quartz, orthoclase
KSS-FD6-A	thick vein filling, limonite (yellow to dk. red)	Fluorite, feldspar, tr. geothite, tr. quartz
KSS-FD6-K	limonite, tr. light green clay	Quartz, orthoclase, tr. smectite, tr. goethite

* low intensity peaks are consistent with these phases being present in small amounts

5.3 Sequential Extraction Test Results

The sequential extraction results are presented in Appendix F, and summarized in the following sections.

5.3.1 Uranium Distribution

The distribution of extractable uranium is shown in Table 22 and Figure 33. The results from the iron oxide-coated samples show that most of the uranium is associated with iron and manganese oxides, which are dissolved in the 4th extraction (65%). A substantial portion (19%) is associated with the second extraction: desorption of uranium at or near the rock/water interface. Fourteen percent of the uranium was associated with the carbonate fraction and only 2 percent was removed by the first extractant. The controls and smectite-coated samples show slightly lower percent removals in the first 3 extractions and significantly lower total extractable uranium levels.

TABLE 22 Percent Distribution of Extractable Uranium

Samples	Extraction #1	Extraction #2	Extraction #3	Extraction #4
Controls (n=5)	1.2 (0.3-1.8)*	3.7 (2.1-5.7)	10 (3.1-22)	85 (71-93)
Smectites (n=2)	0.7 (0.6, 0.7)	7.3 (6.5, 8.0)	15 (12, 17)	77 (74, 80)
Iron oxides (n=19)	2.0 (0.2-16)	19 (3.1-39)	14 (7.0-20)	65 (51-86)

* average (min-max)

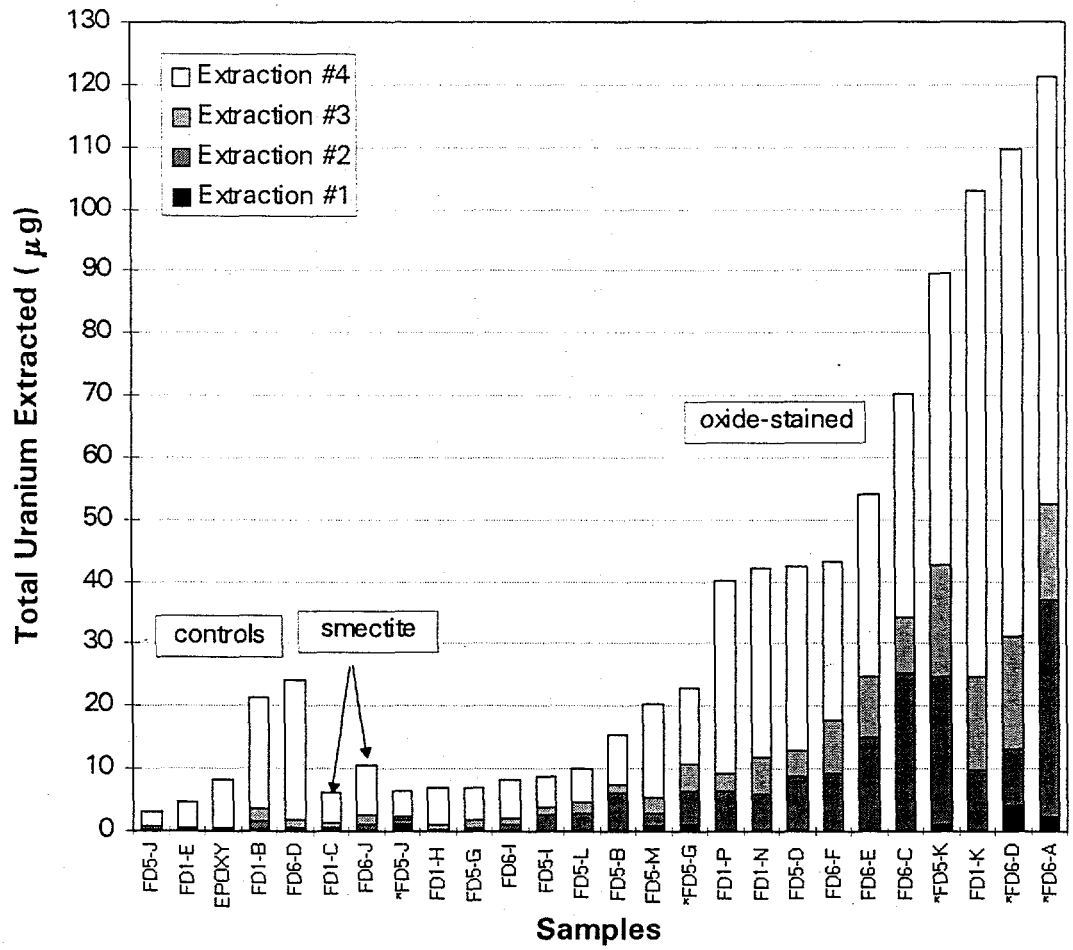

FIGURE 33 Distribution of uranium in sequential extraction tests. Asterisks indicate phase I samples which were not treated with epoxy.

5.3.2 Association between Uranium and Iron and Manganese Oxides

Average extractable iron and manganese levels were 8.4 and 9.3 mg, respectively, in the oxide-coated fractures. The relatively high portion of manganese released in the extractions is attributed to the presence of amorphous manganese oxides.

The extractable uranium was correlated with extractable iron and manganese levels as shown in Figure 34a-d. Figure 34a, extractable U is plotted against extractable Fe+Mn for all of the iron-coated fractures (n=19). Six outliers are evident on the plot: the first 3 (FD6-A, FD6-D, FD1-K) have proportionately high extractable U compared to the other samples and the second 3 (FD1-P, FD5-K, FD5-L) have proportionally higher manganese. Two of the high U samples are from the first set of tests where no epoxy was used to isolate the fractures, and the third was normal in appearance. Two of the high manganese samples had black to purple oxide coatings, indicating they are enriched with manganese oxides, while the third was from the first set of tests where no epoxy was used to isolate the fractures. These differences justify outlier removal from the dataset. However, the variability in enrichment is considered to be "real" rather than experimental. When the outliers are removed, (Figure 34b) there is a strong correlation between extractable uranium and the sum of the extractable iron and manganese (r^2_{adj} = 0.79, $p < 0.0005$). Extractable U is also correlated reasonably well with extractable manganese ($r^2_{adj} = 0.668$, $p < 0.0005$) (Figure 34c), and partially correlated with extractable iron ($r^2_{adj} = 0.37$, $p = 0.016$) (Figure 34d).

The strong relationship between U and Fe+Mn provides evidence that both the iron and manganese oxides are important sorbents for uranium. For comparison with the sorption model results, the total extractable U to equivalent ferrihydrite, birnessite, and ferrihydrite+birnessite ratios were calculated. These results are presented in Table 23. Equivalent calculations are not appropriate for the controls or the smectite samples since there is no expected association between the extractable uranium and the small amount of

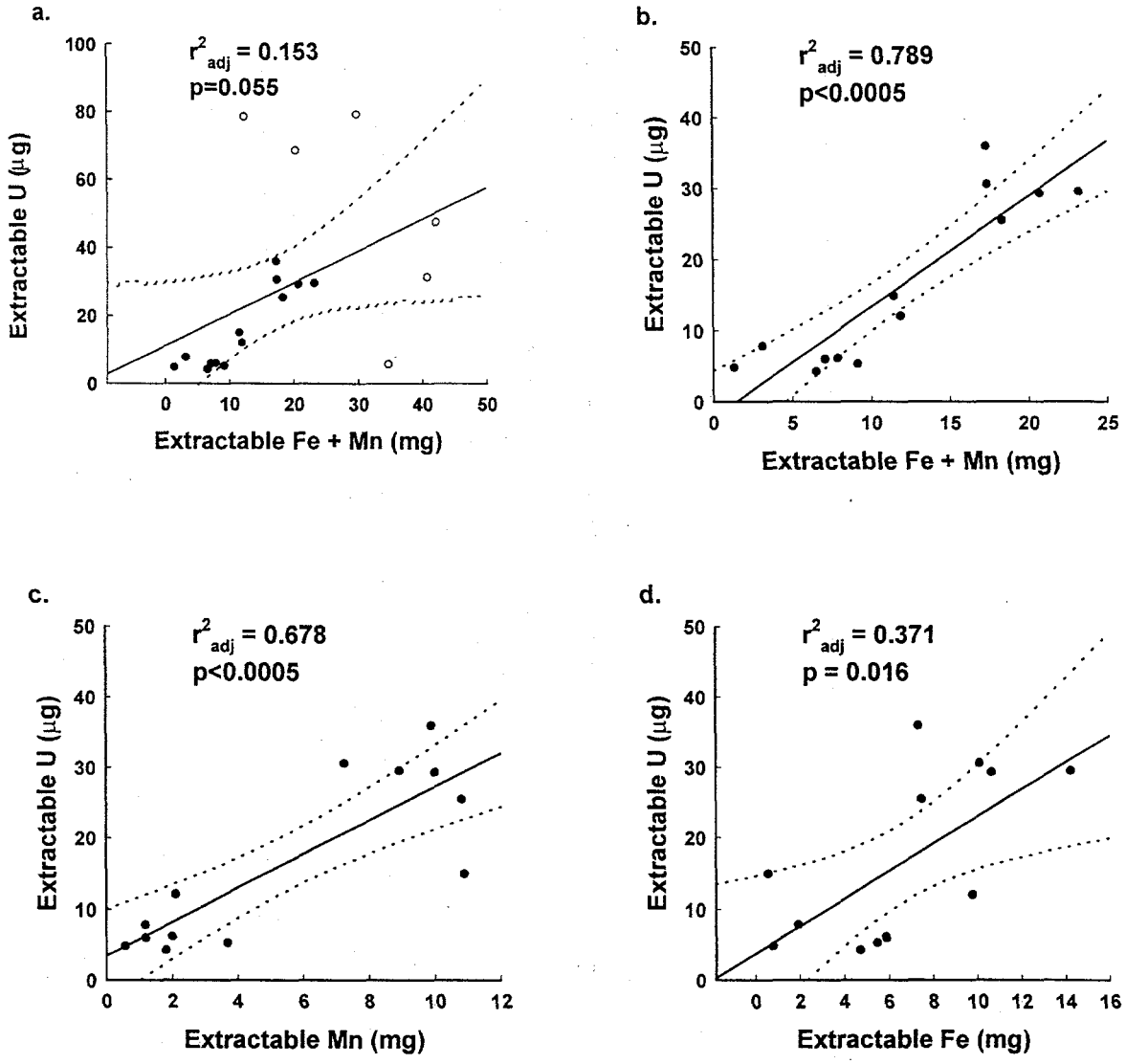

FIGURE 34 Relationship between extractable U and Fe/Mn in the fourth extraction: a) extractable U versus Fe + Mn (open circles represent the outliers removed in parts b-d); b) extractable U versus Fe + Mn (outliers removed - see text); c) extractable U versus Mn (outliers removed); d) extractable U versus Fe (outliers removed).

iron and manganese leached from these samples. The extraction ratio for ferrihydrite ranges from 300 to 11200 μg U/g $Fe_2O_3 \cdot H_2O$, with an average value of 2200 μg U/g $Fe_2O_3 \cdot H_2O$. These are comparable to the model results which indicate enrichment in the Pike's Peak study wells would range from 60 to 8500, with average values of 1200 μg U/g $Fe_2O_3 \cdot H_2O$.

TABLE 23 Extractable U to Sorbent Ratios for Iron-coated Fracture Surfaces

Sorbent	Extraction Ratio (μg U to g sorbent)
$Fe_2O_3 \cdot H_2O$	2200 (300-11200)*
MnO_2	5900 (300-41400)
$Fe_2O_3 \cdot H_2O + MnO_2$	1100 (100-2700)

* average (min-max)

5.3.3 Relationship between Extractable Uranium and Radium Levels

Measured total extractable radium activities were typically lower than calculated total extractable uranium activities: in the iron-coated fracture samples the average activity ratio of ^{226}Ra to ^{238}U activity was 57 percent; in the smectite-coated fractures the average ratio was 53 percent, and in the control samples the average ratio was 50 percent. Considering ^{226}Ra is mobilized by alpha recoil and is generally more mobile than U, it is not surprising that there is less ^{226}Ra in the system. There was a reasonable correlation between extractable ^{226}Ra and ^{238}U levels in the iron-coated fractures ($r^2_{adj} = 0.45$, $p = 0.003$), and the relationship was stronger if the three high-U samples described earlier

were removed from the dataset ($r^2_{adj} = 0.88$, $p < 0.0005$). Scatterplots of the data with and without the outliers are shown in Figures 35a and 35b.

5.3.4 Surface Radionuclide Concentrations

The bulk or macro-scale surface area exposed to the leach solutions was estimated and was used in conjunction with the leach extraction results to calculate a surface radionuclide concentration. The surface concentration is the activity of uranium or radium extracted from a given bulk surface area of fracture: it is essentially the parent radionuclide activity available for emanation into the fracture void. The bulk surface area is geometrically equivalent to the bulk surface area described in Section 3.2.

The surface concentrations are summarized in Table 24. The results show that surface concentrations are highest in the iron oxide coated fracture samples, but are still substantial in the control and smectite-coated samples. The surface concentrations are consistent with the high radon concentrations observed in groundwaters in this study area. For example, a typical well (91-CO-38) in the Pikes Peak granite had a radon concentration of 11000 pCi/L, and a bulk specific surface area of 6.5 m^2/L (determined from transmissivity data). Assuming that secular equilibrium between surface ^{226}Ra and aqueous ^{222}Rn had been established, the fracture surfaces would need to have 1650 pCi/m^2 to support the observed ^{222}Rn activity. If groundwater residence times are not sufficient to allow the assumption of secular equilibrium, or if ^{222}Rn emanation is less efficient, higher surface concentrations would be required. The average ^{226}Ra surface concentration of 3900 pCi/m^2 is therefore consistent with field data.

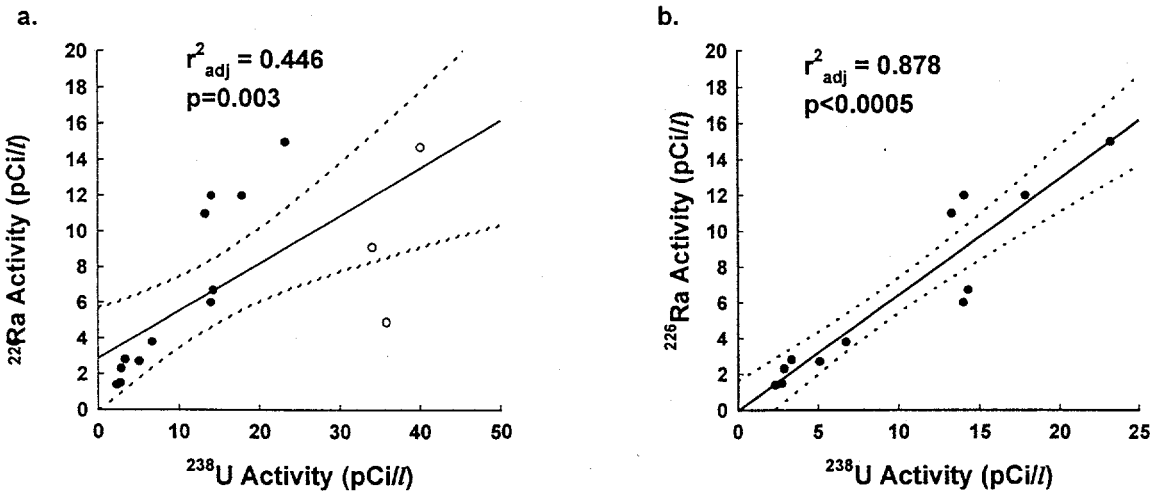

FIGURE 35 Relationship between extractable ^{238}U and ^{226}Ra: a) all data, (open circles represent the outliers removed in part b); and, b) high ^{238}U outliers removed.

TABLE 24 Surface Radionuclide Concentrations

Sample Type	pCi U/m^2	pCi $^{226}Ra/m^2$
Controls (n = 5)	2300 (520-4800)	900 (470-1800)
Smectite-coated fractures (n = 2)	1600 (1100-2100)	870 (620-1100)
Iron-coated fractures (n = 19)	7800 (1200-41400)	3900 (700-15200)

* average (min-max)

5.3.5 Trace Metal Accumulation in Fracture Minerals

In addition to U and ^{226}Ra, several other trace metals were associated with the fracture filling minerals. The only implication of this finding to this study is that they may occupy sorption sites on the fracture filling minerals. The ICP-AES metals results are presented in Appendix F.

Cd, Co, Cu, Ni, Zn and Mo were found in the first extraction solution which removes exchangeable ions on the mineral surfaces. The second extraction was specific for the desorption of uranium from mineral surfaces, and only mobilized significant concentrations of Cr, Cu, and Mo. Metals associated with the carbonate phase included: Be, Cd, Co, Cu, Mo, Ni, and Zn. Metals associated with the iron and manganese phase included Ag, Be, Cd, Co, Cu, Mo, Ni, Pb and Zn. This final extraction liberated substantial amounts of the trace metals, especially Co, Pb and Zn, indicating that the iron and manganese oxides are important sorbents for these metals as well as for U and ^{226}Ra. This is consistent with many other studies showing the importance of these sorbents in regulating metal concentrations in natural waters (e.g. Morgan and Stumm, 1964; Murray, 1975; Chao and Theobald, 1976; Zasoski and Burau, 1988).

5.4 Discussion of Experimental Results and Model Validation

The extraction tests provide strong and direct evidence of an association between uranium, radium and the iron and manganese fracture-filling minerals. Visual observations and XRD analyses provided evidence that the fracture-filling minerals on the core samples were amorphous iron and manganese oxides. The presence of manganese oxides in the system was confirmed by the high concentrations of Mn in the fourth extraction which is known to attack iron and manganese oxides.

The distribution of uranium in the various extractants showed that most of the extractable U was strongly associated with the iron and manganese oxides, 20 percent was desorbed using a strong bicarbonate-carbonate solution, and the rest was associated with the carbonate phase.

The ratio of extractable U to extractable iron and manganese is consistent with the modeling results presented in Section 4.0, which show that uranium to ferrihydrite ratios would be in the range of 60 to 8500 μg U/g $Fe_2O_3 \cdot H_2O$ in the Pikes Peak Granite. Uranium to ferrihydrite ratios in the extraction experiments ranged from 300 to 11200 μg U/g $Fe_2O_3 \cdot H_2O$. The consistency between the experimental and model results suggests the conceptual model assumptions provided a reasonable framework to study parent enrichment in this system. The total extractable ^{238}U and ^{226}Ra activities were strongly correlated. ^{226}Ra activities were approximately half the ^{238}U activities, reflecting the differences in their chemical and radiochemical behavior. This finding supports the assumption that uranium can be used as an indicator of radium enrichment: a critical assumption in the application of the SCM model results to inferences about ^{222}Rn generation sites.

The experimental results were also used to derive equivalent surface concentrations (pCi/m^2 ^{226}Ra or ^{238}U). The surface area is the bulk surface area measured directly from the exposed surface on the core samples, and is analogous to the bulk surface area defined in Section 3.2.4. Average surface concentrations of 3900 pCi/m^2 are more than sufficient to support measured ^{222}Rn levels given a typical fracture geometry or bulk specific surface area.

6.0 CONCLUSIONS

It has been shown that surface accumulation of uranium is an important process for concentrating ^{222}Rn parents in favorable sites for ^{222}Rn emanation to the groundwater. A surface complexation model which takes solution phase pH, alkalinity and uranium concentration into account was used to calculate the sorption density, Γ, or the amount of uranium sorbed to active sites on amorphous iron oxides along fracture margins. Γ can range over 3 orders of magnitude and represents high uranium concentrations in the iron phase of the system. Sequential extraction tests on iron oxide coated fractures show the concentrations predicted by the model are reasonable. The results suggest uranium concentrations in the fracture filling minerals may be up to 500x the bulk-rock concentrations. The extraction tests also verify that uranium can be used as an indicator for ^{226}Ra in this system. Surface area based concentrations from the extraction experiments are also very high, and are capable of supporting ^{222}Rn activities.

REFERENCES

Asikainen, M. (1980) State of disequilibrium between ^{238}U, ^{234}U, ^{226}Ra and ^{222}Rn in groundwater from bedrock. *Geochemica et Cosmochimica Acta.* **45**, 201-206.

Aspinall, R. and N. Veitch (1993) Habitat mapping from satellite imagery and wildlife survey data using a Baysian modeling procedure in a GIS. *Photogrammetric Engineering and Remote Sensing,* **59(4)**, 537-543.

Beck, P.J. and D.R. Brown (1987) Hydrogeologic Controls on the Occurance of Radionuclides in Groundwater of Southern Ontario. In *Radon in Groundwater: Proceedings of the NWWA Conference, April 7-9, 1987, Somerset, New Jersey* (ed. Graves, B), pp. 449-473. Lewis Publishers Inc., Michigan.

Bonham-Carter, G.F., F.P. Agterberg and D.F. Wright (1988) Integration of geological datasets for gold exploration in Nova Scotia. *Photogrammetric Engineering and Remote Sensing.* **54(11)**, 1585-1592.

Bryant, B. (1974a) Reconnaissance geologic map of the Pine quadrangle, Jefferson County, Colorado. U.S. Geological Survey Misc. Field Studies Map MF-598.

Bryant, B. (1974b) Reconnaissance geologic map of the Conifer quadrangle, Jefferson County, Colorado. U.S. Geological Survey Misc. Field Studies Map MF-597.

Bryant, B. (1976a) Reconnaissance geologic map of the Bailey quadrangle, Jefferson County and Park Counties, Colorado. U.S. Geological Survey Misc. Field Studies Map MF-816.

Bryant, B. (1976b) Reconnaissance geologic map of the Meridian Hill quadrangle, Jefferson County, Colorado. (unpublished source)

Burdick, R.K. and F.A. Graybill (1992). *Confidence intervals on variance components.* Marcel Dekker Inc.

Burkhart, J.F. and T.P. Huber (1993) Correlation of indoor radon concentrations to commonly available geologic data. *Environmental Management,* **17 (2)**, 249-256.

Cecil, L.D. and T.F. Gesell (1992) Sampling and analysis for radon-222 dissolved in groundwater and surface water. *Environmental Monitoring and Assessment* **20,** 55-66.

Chao, T.T. (1984) Use of parital dissolution techniques in geochemical exploration. *Journal of Geochemical Exploration,* **20**, 101-135.

Chao, T.T. and P.K. Theobald (Jr.) (1976) The significance of secondary iron and manganese oxides in geochemical exploration. *Economic Geology*, **71,** 1560-1569.

Cothern, R.C. (1987) Estimating the Health Risks of Radon in Drinking Water. *Journal of the Americal Waterworks Association,* April 1987, 153-158.

Czarnecki, J.B. and R.W. Craig (1985) A program to calculate aquifer transmissivity from specific capacity data for programmable calculators. *Ground water,* **23(5)**, 667-672.

Davis, J.A. and D.B. Kent (1990) Surface Complexation Modeling in Aqueous Geochemistry. In *Reviews in Mineralogy, Vol.23: Mineral Water Interface Geochemistry.* (eds. Hochella, M.F.(Jr.), A.F. White), pp. 177-260. Mineralogical Society of America, Washington, D.C.

Devore, J. and R. Peck (1986) *Statistics: The Analysis and Exploration of Data.* West Publishing Co., St. Paul. 699 pages.

Dzombak, D.A. and F.M.M. Morel (1990) *Surface Complexation Modeling: Hydrous Ferric Oxide*. John Wiley and Sons, New York. 393 pages.

EnviroTools Ltd. (1993) *AQUIX-4S Pump and Slug Test Analysis: (Software and Model Documentation Package).* International Ground Water Modeling Center (IGWMC), Golden, Colorado.

Flexser, S., H.A. Wollenberg and A.R. Smith, (1993) Distribution of radon sources and effects on radon emanation in granitic soil at Ben Lomond, California. *Environmental Geology,* **22**, 162-177.

Folger, P.F., P. Nyberg, R.B. Wanty and E. Poeter, (1994) Relationships between ^{222}Rn dissolved in groundwater supplies and indoor ^{222}Rn concentrations in some Colorado Front Range houses. *Health Physics*, **67(3)**, 245-253.

Folger, P.F. (1995) *A Multidisciplinary Study of the Variability of Dissolved ^{222}Rn in Ground Water in a Fractured Crystalline Rock Aquifer and its Impact on Indoor Air.* PhD. Dissertation T-4696, Colorado School of Mines.

Folger, P.F., Poeter, E., Wanty, R.B., Frishman, D. and Day, W., in press, Controls on Radon Variations in a Fractured Crystalline Rock Aquifer Evaluated Using Aquifer Tests and Geophysical Logging. *Ground water*, 34(2), 250-276.

Folger, P.F., Poeter, E., Wanty, R.B., Day, W. and Frishman, D., in review, Radon Transport in a Fractured Crystalline Rock Aquifer: Results from Numerical Simulations, *In press for 1997 Journal of Hydrology.*

Freeze, R.A. and J.A. Cherry (1979) *Groundwater.* Prentice Hall, New Jersey. 604 pages.

Frishman, D. W.C. Day, P.F. Folger, R.B. Wanty, P.H. Briggs and E. Poeter (1993) Bedrock geologic controls on radon abundances in domestic water, Conifer, Colorado. In *Proceedings of the 1993 International Radon Conference, September 20-22, 1993, Denver, Colorado,* 20-30.

Gascoyne, M. (1992) Geochemistry of the actinides and their daughters. In *Uranium Series Disequilibrium: Applications to Earth, Marine and Environmental Sciences. Second Edition* (eds. M. Ivonovich and R.S. Harmon). Ch. 2, pp. 34-61. Clarendon Press, Oxford.

Gascoyne, M. and J.H. Barber (1992) The mobility of U, Ra and Rn in a granitic batholith on the Canadian Sheild. *Radiochimica Acta,* Vol 58/59, pp. 281-284.

Gates A.E. and L.C.S. Gundersen (1989) Role of ductile shearing in the concentration of radon in the Brookneal zone, Virginia. *Geology,* **17**, 391-394.

Grenthe I., J. Fuger, R.J.M. Lemire, A.B. Muller, C.N-T. Cregu, H. Wanner (1992) *Chemical Thermodynamics of Uranium.* (Eds. H. Wanner and I. Forest). Elsevier Science Publishing Company, New York.

Hahn, P.B. and S.H. Pia (1991) Determination of radon in drinking water by liquid scintillation counting, Method 913.0 (Draft). Radioanalysis Branch, Nuclear Radiation Assessment Division, Environmental Monitoring Systems Laboratory, U.S. Environmental Protection Agency. Las Vegas, Nevada.

Hammond. D.E., B.W. Leslie, T.-L. Ku and T. Torgerson (1988) ^{222}Rn concentration in deep formation waters and the geohydrology of the Cajon Pass borehole. *Geophysics Research Letters*, **15(9)**, 1045-1048.

Hem, J.D. (1992) Study and Interpretation of the Chemical Characteristics of Natural Water. Third Edition. *U.S. Geological Survey Water Supply Paper 2254.*

Herbelin, A. and J. Westall (1994) *FITEQL: A Computor Program for Determination of Chemical Equilibrium Constants from Experimental Data, Version 3.1.* Department of Chemistry, Oregon State University, Corvallis: Report 94-01.

Herbelin, A. and J. Westall (1996) *FITEQL: A Computor Program for Determination of Chemical Equilibrium Constants from Experimental Data, Version 3.2.* Department of Chemistry, Oregon State University, Corvallis: Report 96-01.

Hicks, J.R. (1987) Hydrogeology of igneous and metamorphic rocks in the Shaffers Crossing area and vicinity near Conifer Colorado. M.S. Thesis T-3319, Colorado School of Mines. 174 pages.

Ho, C.H. and N.H. Miller (1986) Adsorption of uranyl species from bicarbonate solution onto hematite particles. *Journal of Colloid and Interface Science*, **110(1)**, 165-171.

Honeyman, B.D. (1984) *Cation and Anion Adsorption at the Oxide/Solution Interface in Systems Containing Binary Mixtures of Adsorbents: An Investigation of the Concept of Adsorptive Additivity.* Ph.D. Dissertation, Stanford University.

Hsi, C-K and D.D. Langmuir (1985) Adsorption of uranyl onto ferric oxyhydroxides: Application of the surface complexation site binding model. *Geochimica et Cosmochimica Acta*, **49**, 1931-1941.

James, F.C. and C.E. McCulloch (1990) Multivariate analysis in ecology and systematics: panacea or Pandora's box. *Annual Reviews in Ecology and Systematics*. **21**, 129-166.

James, R.O. and G.A. Parks (1982) Characterization of aqueous colloids by their electircal double layer and intrinsic surface chemical properties. *Surface and Colloid Science*, **12**, 119-216.

Krishnaswami, S., W.C. Graustein, K.K.Turekian and J.F. Dowd (1982) Radium, thorium and radioactive lead isotopes in groundwaters: Application to the in situ determination of adsorption-desorption rate constants and retardation factors. *Water Resources Research,* **18(6)**, 1633-1675.

Krishnaswami S. and D.E. Siedmann (1988) Comparative study of ^{222}Rn, ^{40}Ar, ^{39}Ar and ^{37}Ar leakage from rocks and minerals: Implications for the role of nanopores in gas transport through natural silicates. *Geochimica et Cosmochimica Acta,* **52**, 655-658.

Langmuir, D. (1978) Uranium solution-mineral equilibria at low temperatures with application to sedimentary ore deposits. *Geochimica et Cosmochimica Acta,* **42,** 547-569.

Latham, A.G. (1994) Diffusion-sorption modeling of natural u in weathered granite fractures: potential and problems. In *Fourth International Conference on the Chemistry and Migration Behaviour of Actinides and Fission Products in the Geosphere. Charleston, SC, December 12-17, (1993).* 701-710.

Lawrence, E.P. (1990) *Hydrogeologic and Geochemical Processes Affecting the Distribution of ^{222}Rn and Its Parent Radionuclides in Ground Water.* MSc.Thesis. T-3923, Colorado School of Mines.

Lawrence, E., E. Poeter and R.B. Wanty (1991) Geohydrologic, geochemical and geologic controls on the occurrence of radon in groundwater near Conifer, Colorado, USA. *Journal of Hydrology*, **127**, 367-386.

Lawrence, E.P., R.B. Wanty and P. Nyberg (1992) Contribution of ^{222}Rn in domestic water supplies to ^{222}Rn in indoor air in Colorado homes. *Health Physics*, **62(2)**, 171-177.

Lee, K. and C.W. Fetter (1994) Hydrology Laboratory Manual. Macmillan Publishing Co. New York. 135 pages.

Legendre, P. And M-J Fortin (1989) Spatial Pattern and Ecological Analysis. *Vegetatio.* **80**,107-138.

Millward, G.E. and R.M. Moore (1982) The adsorption of Cu, Mn and Zn by iron oxyhydroxide in model estuarine solutions. *Water Res.* **16**, 981-985.

Milton, G.M. and R.M. Bròwn (1987) Adsorption of uranium from groundwater by common fracture secondary minerals. *Canadian Journal of Earth Science*, **24**, 1321-1328.

Morgan, J.J. and W. Stumm (1964) Colloid-chemical properties of manganese dioxide. *Journal of Colloid Science*, **19,** 347-359.

Murray, J.W. (1975) The interaction of metal ions at the manganese dioxide-solution interface. *Geochimica et Cosmochimica Acta,* **39,** 505-519.

Osmond, J.K. and J.B. Cowart (1992) Ground Water. In *Uranium Series Disequilibrium: Applications to Earth, Marine and Environmental Sciences. Second Edition.* (eds. M. Ivonovich and R.S. Harmon, eds). Ch. 9, pp. 290-330. Claredon Press, Oxford.

Paces, T. (1973) Steady state kinetics and equilibria between groundwater and granitic rock. *Geochimica et Cosmochimica Acta,* **37**, 2641-2663.

Payne, T.E. and T.D. Waite (1991). Surface complexation modeling of uranium sorption data obtained by isotope exchange techniques. *Radiochemica Acta.* **52/53**, 487-493.

Payne, T.E., J.A. Davis and T.D. Waite (1994). Uranium retention by weathered schists: The role of iron minerals. *Radiochemica Acta.* Vol. 66/67, pp. 301-307.

Prikryl, J.D., R.T. Pabalan, D.R. Turner and B.W. Leslie (1994) Uranium sorption on α-alumina: Effects of pH and surface-area/solution-volume ratio. *Radiochemica Acta,* **66/67**, 295-300.

Prichard, H.M. and T.F.Gesell (1977) Rapid measurements of ^{222}Rn concentrations in water with a commercial liquid scintillation counter. *Health Physics*. **33**, 577-581.

Prichard, H.M. 1987. The transfer of radon from domestic water to indoor air. *Am. Water Works Assoc. J.* **79,** 159-161.

Puskin, J.S. (1992) An analysis of the uncertainties in estimates of radon-induced lung cancer. *Risk Analysis*, **12(2)**, 277-285.

Rama and W.S. Moore (1984). Mechanism of transport of U-Th series radioisotopes from solids into groundwater. *Geochimica et Cosmochimica Acta, **48**, 395-399.*

Renshaw, C.E. (1995). On the relationship between mechanical and hyraulic apertures in rough-walled fractures. *Journal of Geophysical Research,* **100 (b12)**, 24,629-24,636.

Riese, A.C. (1982). *Adsorption of Radium and Thorium onto Quartz and Kaolinite: A Comparison of Solution/Surface Equlibria Models.* Ph.D. Thesis T-2625, Colorado School of Mines.

Rossi, R.E., D.J. Mulla, A.G. Journel and E.H. Franz (1992) Geostatistical tools for modeling and interpreting ecological spatial dependence. *Ecological Monographs*, **62**, 277-314.

Rumbaugh, J.O., III (1983) *Effect of Fracture Permeability on Radon-222 Concentrations in Ground Water of the Reading Prong, Pennsylvania.* M.S. Thesis, Pennsylvania State University, 111 pages.

Schumann, R. (1993) The radon emanation coefficient: An important tool for geologic radon potential estimations. In *Proceedings of the 1993 International Radon Conference, Sept 20-22, Denver Colorado.*

Schwertmann, U. and R.M. Taylor (1977) Iron oxides. In *Minerals in Soil Environments* (eds. J.B. Dixon, S.B. Weed, J.A. Kittrick, M.H. Milford and J.L. White) pp. 145-180.Chapter..

Semkow, T.M. (1990) Recoil-emanation theory applied to radon release from mineral grains. *Geochimica et Cosmochimica Acta,* **54**, 425-440.

Sit, V. (1995) *Analyzing ANOVA Designs - Biometrics Information Handbook No. 5.* B.C. Ministry of Forests, Victoria, B.C.

Skougstad, M.W., M.J. Fishman, L.C. Friedman, D.E. Erdmann and S.S. Duncan (eds.) (1979) *Chapter A1 - Methods for Determination of Inorganic Substances in Water and Fluvial Sediments: Techniques of Water-Resources Investigations of the United States Geological Survey.* U.S. Department of the Interior, Geological Survey, United States Government Printing Office, Washington.

Tanner, A.B. (1964) Physical and chemical controls on the distribution of radium-226 and radon-222 in ground water near Great Salt Lake, Utah. In: The Natural Radiation Environment. (Eds. J.A.S. Adams and W.M. Lowder), pp. 253-276. University of Chicago Press, Chicago.

Tessier, A., P.G.C. Campbell and M. Bisson, (1979) Sequential extraction procedure for the speciation of particulate trace metals. *Analytical Chemistry*, **51(7)**, 844-851.

Thurman, E.M. (1985). *Organic Geochemistry of Natural Waters*. Developments in Biogeochemistry Series. Martinus Nijhoff/Dr. W. Junk Publishers, Boston. 497 pages.

Ticknor, K.V. (1993) Actinide Sorption by Fracture-Infilling Minerals. *Radiochimica Acta,* **60**, 33-42.

Ticknor, K.V. (1994) Uranium Sorption on Geological Materials. *Radiochimica Acta,* **63**, 229-236.

Torgerson, T., J. Benoit and D. Mackie (1990) Controls on groundwater Rn-222 concentrations in fractured rock. *Geophysical Research Letters,* **17(6)**, 845-848.

Torma, A.E., N.R. Pendleton and W.M. Fleming (1986) Sodium carbonate-bicarbonate leaching of a New Mexico uranium ore and removal of long half-life radionuclides from the leach residue. *Uranium*, **2**, 17-36.

Tsang, Y.W. (1992) Usage of "equivalent apertures" for rock fractures as derived from hydraulic and tracer tests. *Water Resources Research*, **28(5)**, 1451-1455.

U.S. Department of the Interior, (1985) *Ground Water Manual: A Guide for the Development and Management of Ground-Water Resources*. U.S. Dept. of Interior, Bureau of Reclamation.

Waite, T.D., J.A. Davis, T.E. Payne, G.A. Waychunas, N. Xu (1994) Uranium (VI) adsorption to ferrihydrite: Application of a surface complexation model. *Geochimica et Cosmochimica Acta*, **58(24)**, 5465-5478.

Wanty, R.B., E.P. Lawrence, L.C.S. Gundersen (1991) A theoretical model for the flux of Radon-222 from rock to groundwater. *GSA Special Paper No. 271*, 73-78.

Wanty, R.B., C.A. Rice, D. Langmuir, P. Briggs and E.P. Lawrence (1991) Prediction of uranium adsorption by crystalline rocks: the key role of reactive surface area. In *Materials Research Society Symposium Proceedings*. **212**, 695-702.

Wathen, J.B. (1987). The effect of uranium siting in two-mica granites on urnaium concentration and radon activity in ground water. In *Radon in Groundwater: Proceedings of the NWWA Conference, April 7-9, 1987, Somerset, New Jersey* (ed. Graves, B). Lewis Publishers Inc., Michigan. pp. 31-46.

Wilkinson, L., M-A. Hill, J.P. Welna and G.K. Birkenbeuel (1992) *SYSTAT: Statistics Manual*. 750 pages.

Yong, R.N., R. Galvez-Cloutier and Y. Phadungchewit (1993) Selective sequential extraction analysis of heavy-metal retention in soil. *Can. Geotech. J.*, **30**, 834-847.

Zasoski, R.J. and R.G. Burau (1988) Sorption and sorptive interaction of cadmium and zinc on hydrous manganese oxide. *Soil Science Society of America Journal,* **52,** 81-87.

APPENDIX A

THE EFFECTS OF GROUNDWATER RESIDENCE TIME ON ^{222}RADON INGROWTH AND DECAY

NUMERICAL MODELING OF FLOW AND ADVECTIVE-REACTIVE TRANSPORT IN A MULTI-FRACTURE SYSTEM

ABSTRACT

Fracture flow was modeled in a multiple fracture groundwater system to determine the effects of hydraulic gradient, pumping stresses, and fracture geometry on groundwater velocities. Groundwater residence times through the system were determined for several different starting conditions and pumping stresses. The effect of groundwater residence time on the ingrowth and decay of ^{222}Rn through the fracture system was examined using a simple, spreadsheet-executable, advective transport model. The results show that radon levels do not always reach secular equilibrium with parent minerals in the host rocks in systems with steep natural gradients, shorter flow-paths, or pumping stresses. In such systems, small-aperture fracture segments have less of an impact on the overall radon concentration than large aperture fractures, because groundwater residence times are relatively smaller in small aperture fractures. Steep gradients and negligible residence times were found in the immediate vicinity of pumping wells located near the constant head boundary. This result suggests that enrichment or depletion of source minerals near the well would have almost no influence on the resulting quality of water drawn from the well.

A-1 INTRODUCTION

A-1.1 Problem Description

^{222}Rn is a short-lived daughter of ^{226}Ra, a natural series radionuclide in the ^{238}U decay series. In groundwater systems, radon activity levels are usually supported by radium present on mineral surfaces in the aquifer. In systems where the rate of groundwater movement is slow compared to the rate of radon decay (i.e. 30 days), radon and radium will reach secular equilibrium, where their activity levels are equal. In systems where the groundwater residence times are less than 30 days, the rate of radon ingrowth and decay along the flowpath can have a significant influence on ^{222}Rn activity levels in the groundwater.

The residence time of a parcel of water moving through the fracture system can be calculated from head distributions obtained from numerical flow models. In the flow model, the effects of fracture geometry, transmissivity, hydraulic gradient, and stresses imposed by pumping wells can be examined. Rate dependent chemical processes can be modeled using radioactive decay laws (as discussed in Section 3). Since only a few of the model variables can be measured in a complex field setting, modeling is an important tool for simulating the range of possible conditions in the aquifer and examining response of the system to each variable.

A-1.2 Modeling Objective and Approach

The focus of this paper is to examine the effects of groundwater residence time and fracture geometry on radon ingrowth and decay as water moves through a fracture system. MODFLOW is used to model flow through a multiple segment fracture system to determine the head distribution along the fracture under a variety of starting conditions and stresses. The head distribution from each of the flow scenarios is then exported to a

spreadsheet to calculate the hydraulic gradient, groundwater velocity, residence time, and ^{222}radon activity in each of the grid cells.

A-2 ANALYTICAL AND NUMERICAL MODELING OF FLOW

A-2.1 Review of Two Fracture Model

A conceptual model of a two-fracture system was developed from a detailed field and modeling study carried out by Folger (1995). Pump tests and geophysical logging of the boreholes provided evidence for a fracture system connecting two of the wells: 92CO-14 and 92CO-16. Pumping tests were used to measure the transmissivity in each of the wells, and by inference, the fracture in the immediate vicinity of the wells. The schematic representation of the flow system is further simplified into a form suitable for numerical modeling, as shown in Figure A-2. A brief review of the assumptions behind the conceptual model is provided below.

Hydraulic gradient: The difference in heads measured at the two wells was 1.5 meters, however the flow path between the wells is not known. The hydraulic gradient between the wells could range from 0.044 to 0.0001, depending on whether the flowpath is the linear distance between the wells (34 meters), or whether it follows an arbitrarily longer flow-path.

Fracture Geometry: The average hydraulic fracture aperture for each of the wells was determined using transmissivity data from the pump tests. The fracture aperture was determined using the cubic law:

$$b = \left(\frac{12T\mu}{\gamma} \right)^{\frac{1}{3}} \qquad \text{(A-1)}$$

where:
- b = fracture width or aperture (units)
- T = transmissivity
- μ = dynamic viscosity
- γ = specific weight of water

The hydraulic apertures calculated for the two study wells were 0.38 and 0.24 mm.

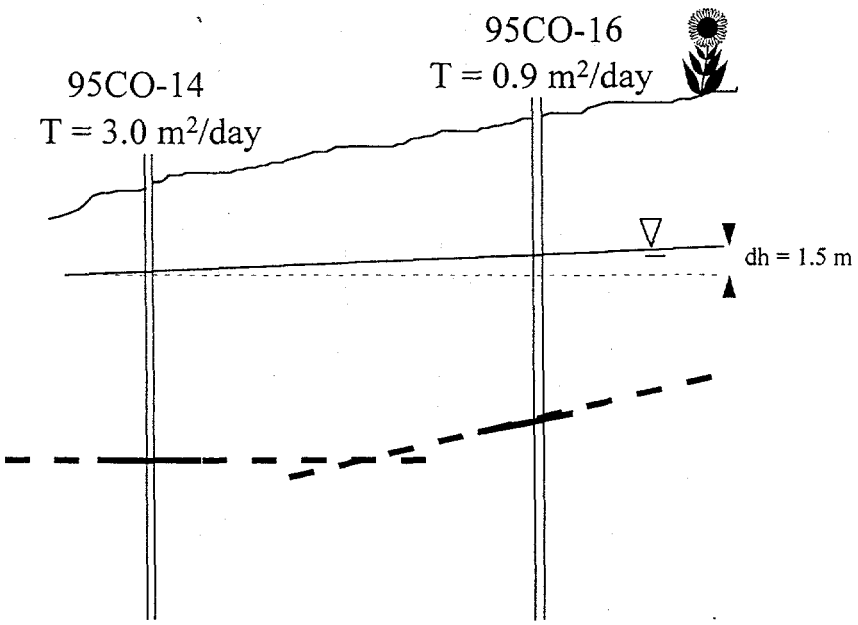

Plan View

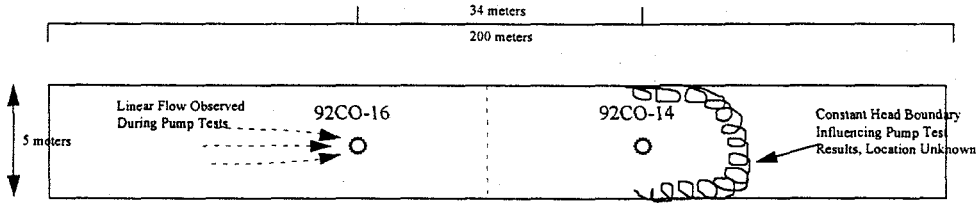

Cross Section

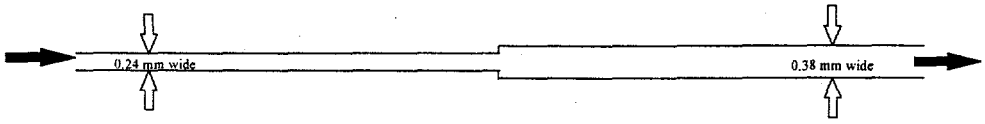

FIGURE A-1 Conceptual model of the fracture system: a) schematic cross-section, b) conceptual model.

Boundary Conditions: The pump test data were used to establish boundary conditions for the fracture system. Data from well 92CO-14 showed evidence of a "constant head" boundary after only 8 minutes of pumping, which supported the placement of a constant head boundary near to this well. The data from 92CO-16 showed evidence of liner flow behavior, suggesting that the system could be modeled as a 'finite' channel, rather than a radially symmetric disk.

A-2.2 Development of a Multi-fracture Model

For the purposes of evaluating radon ingrowth and decay in this study, a longer flow path, with more variations in hydraulic apertures was desirable. Consequently the two-fracture system was modified to incorporate 8 additional fracture segments. Since no specific field data was available for the extension, it is purely hypothetical, with randomly selected transmissivities from field pumping tests done in other parts of the aquifer. The additional fracture segments were added to the left, or western boundary of the model, where they would have the least impact on the well with the nearby "constant head boundary".

A fracture profile is shown in Figure A-2, illustrating the changes in transmissivity and fracture aperture through the model.

A-2.3 Analytical Modeling of the Flow System

In the absence of pumping wells, the head distribution across this simple model can be determined using a simple analytical model based on Darcy's law. The equivalent transmissivity (harmonic mean) along the fracture system is calculated, then Darcy's law is used to calculate the flow (q) at any point perpendicular to the flowpath:

$$T_{eq} = \frac{D_T}{\sum \frac{d_i}{T_i}} \qquad \text{(A-2)}$$

$$q = T_{eq}\left(\frac{\Delta h}{\Delta l}\right) \qquad \text{(A-3)}$$

where:			
	T_{eq}	=	equivalent transmissivity
	D_T	=	total distance along fractures
	d_j	=	distance along fracture reach j
	T_j	=	transmissivity along fracture reach j
	q	=	flow
	Δh	=	head difference
	Δl	=	length difference

Since conservation of mass must be maintained in the system, q is the same at any point in the system. Darcy's law can then be applied to each of the fracture sections to get Δh across each section:

$$\Delta h = \frac{q}{T} \cdot \Delta l \qquad \text{(A-4)}$$

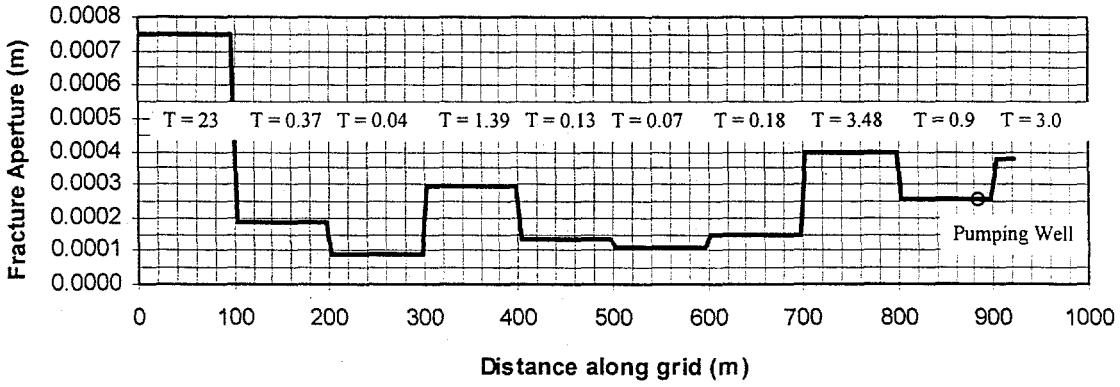

FIGURE A-2 Schematic Diagram of the Multi-fracture System.

The head distribution within each uniform section is then linear along that section. Groundwater velocities are also calculated using Darcy's law, $v = Ki$. This velocity is considered to be the average linear velocity since the porosity is assumed to be equal to 1. In this system, K is equal to the transmissivity (T) over the fracture aperture (b).

A-2.4 Numerical Modeling of the Flow System

A numerical model of the flow system was developed from the conceptual model illustrated in Figures A-1 and A-2. A block centered, finite difference code, MODFLOW (McDonald and Harbaugh, 1988), was used for the flow modeling.

Grid Design

The grid design and boundary conditions are based on the numerical model developed by Folger (1995) for his two-fracture system, and was extended to include the multiple fractures. The grid design is summarized below:

Geometry: The fracture system is modeled as a single confined layer with seven, one meter wide rows in the y direction, and 185 columns of 5 meters width in the x direction. The confined layer can be visualized as having a 10 segments with the apertures shown in Figure A-2. However MODFLOW is set-up as a confined aquifer, so that each segment is actually assigned its corresponding transmissivity (also shown in Figure A-2), and the code does not directly consider the layer thickness. The grid geometry was fixed in all of the model runs, however one set of simulations was done using 1 meter grid lengths to assess the influence of a shorter flow path.

Boundary Conditions: Constant head boundaries are assigned to all rows in columns 1 and 185, and rows 1,2 and 6,7 in column 184. The constant head cells in columns 184 and 185 are assigned a reference head of 1.0 meter, and the constant head cells in column 1 are assigned a value of $1.0 + \Delta h$, where Δh is the change of head across

the 925 meter long system. Rows 1 and 7, columns 2 to 183 are assigned no flow boundaries (i.e. they are inactive). These extra grid cells are not specifically needed by MODFLOW, as the default is a no-flow boundary.

Model Variables

The primary variable influencing residence time is the hydraulic gradient across the model. Since there is no direct measure of this value, there is considerable room for variation. As discussed previously, the steady state gradient without pumping could range from 0.044 to 0.0001 in the two-fracture part of the system. Hydraulic gradients of 0.01 to 0.0001 over the original two fracture portion of the system were used in model simulations and the overall gradient was adjusted accordingly.

Stresses

Well 92CO-16 was the pump well in all of the simulations with pumping. This well is located in column 177, in the center of the grid, 20 meters from the intersection with the farthest right fracture segment. Various pumping scenarios were used in the model runs, including no pumping and steady-state pumping to simulate normal household usage. Pumping will be the most significant stress imposed on the system. Scenarios included are:

1) *No pumping.* Flow through the aquifer under steady-state conditions without pumping was simulated in these runs. Simulations were done for hydraulic gradients of 0.065 and 0.0065.

2) *Domestic pumping.* Average domestic water usage rates for a household of four in this area are estimated to be approximately 0.8 m^3/day. The effects of sustained pumping at this rate on the hydraulic gradients is

examined in a steady state simulation. Hydraulic gradients of 0.065 and 0.00065 were simulated.

3) *Shorter Flow-path length.* The effects of a shorter flow path were simulated with and without pumping at a hydraulic gradient of 0.065.

The results of numerical model simulations of the multifracture system are presented in Section 4.

A-3 ANALYTICAL MODELING OF INGROWTH AND DECAY

A-3.1 Theoretical Background

The concentration of ^{222}radon in groundwater is thought to be supported by the available concentration of ^{226}radium in the aquifer solids. In systems where the groundwater residence time is high compared to the half-life of ^{222}radon, i.e. greater than 30 days, the activity of ^{222}radon and its parent ^{226}radium are approximately equal. This condition is known as secular equilibrium, and it applies to any radioactive decay chain where the half life of the parent nuclide is much longer than its daughter. In systems where the groundwater residence time is less than 30 days, the rate of ingrowth and decay is governed by the following expression:

$$A_{Rn} = \frac{\lambda_{Rn}}{\lambda_{Rn} - \lambda_{Ra}} \cdot A_{Ra}{}^{o} \left(e^{-\lambda_{Ra} t} - e^{-\lambda_{Rn} t}\right) + A_{Rn}{}^{o} e^{-\lambda_{Rn} t} \qquad \text{(A-5)}$$

where:

A_{Rn}	=	activity of ^{222}radon (pCi/L)
A_{Ra}	=	activity of ^{226}radium (pCi/L)
λ_{Rn}	=	decay constant for ^{222}radon
λ_{Ra}	=	decay constant for ^{226}radium
t	=	residence time

A schematic illustration of ingrowth and decay as radon moves through a fracture system is shown in Figure A-3. As shown in the figure, the fracture aperture varies through the system. As a result, the volume (V), residence time (τ), and the surface area to volume ratio changes across the system. Small-aperture fractures will have lower volumes, lower residence times and higher surface area to volume ratios than large-aperture fractures. If we assume a constant surface concentration of ^{226}radium is present in the fracture walls (pCi/m^2), the amount of ^{226}radium per volume of water (pCi/L) will also vary through the system, such that fractures with smaller apertures will tend to have

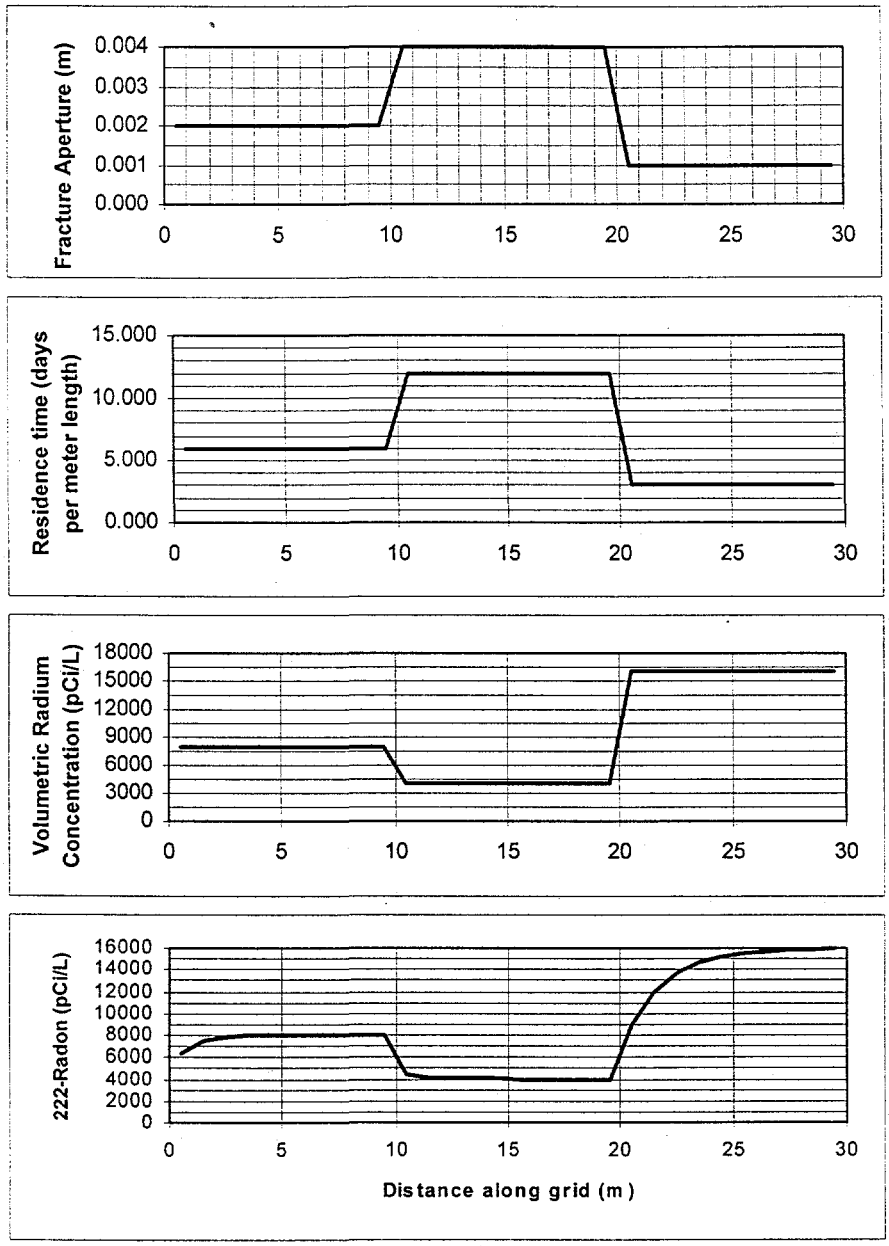

FIGURE A-3 Relationship of fracture aperture, residence time and ^{226}Ra concentration to radon ingrowth and decay: a) fracture aperture in three connected fracture segments; b) corresponding residence times in the fracture segments; c) corresponding volumetric ^{226}Ra concentration based on a uniform surface concentration of 8000 pCi/L; and, d) resulting radon profile as water moves through the fracture

higher volumetric ^{226}Ra concentrations. The volumetric ^{226}Ra concentration profile in the multifracture system is based on a ^{226}Ra surface concentration of 2000 pCi/L, and is shown in Figure A-4.

As water moves through the fracture system, ^{222}Rn levels in the water will approach the volumetric ^{226}radium concentration in each fracture reach according to equation 5, but will only reach secular equilibrium if the residence time in the segment is greater than about 30 days. As shown in Figure A-3, radon levels along the fracture are influenced by a combination of geometry, groundwater residence times and volumetric radium concentrations. The effect of hydraulic gradient, stresses imposed by pumping, and differences in the flow path length add a greater degree of complexity to the system.

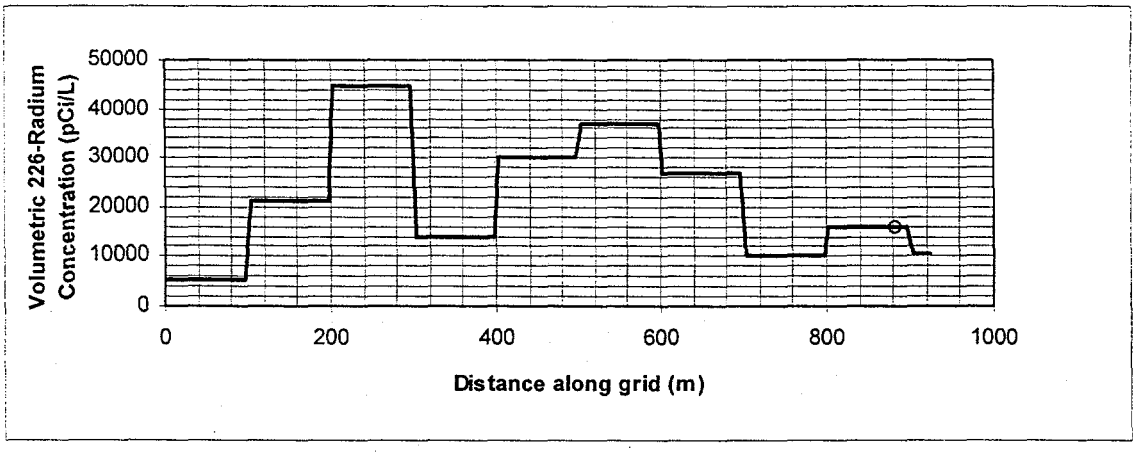

FIGURE A-4 Volumetric ^{226}Ra concentrations along fracture profile.

A-3.2 Modeling Methodology

A spreadsheet based analytical model of advective-reactive transport was used to assess the effects of residence time and fracture geometry on the ingrowth and decay of ^{222}radon in the multi-fracture flow system defined in Section A-2. The structure of the spreadsheet model is described below. In brief:

1) hydraulic heads are extracted from the MODFLOW output file and are imported into column A of the spreadsheet.

2) the hydraulic gradient (column B) is calculated from the head difference between each node pair and the cell length (column C).

3) the transmissivity in each cell (column D) is used to calculate the fracture aperture (column E), the specific surface area (column F, surface area/volume ratio), and the hydraulic conductivity (column G).

fracture aperture: (see equation A-1)

specific surface area:
$$A_{sp} = \frac{SA}{V} \tag{A-6}$$

where: A_{sp} = specific surface area
SA = fracture surface area
V = volume (b x SA)

hydraulic conductivity:
$$K = \frac{T}{b} \tag{A-7}$$

where: K = hydraulic conductivity

4) velocity is calculated from product of the hydraulic conductivity (K) and the hydraulic gradient (i) (column H). The porosity of the fracture is assumed to be 1.

$$v = Ki \qquad \text{(A-8)}$$

5) the residence time is calculated from the cell length divided by the velocity (column I).

6) the surface concentration of ^{226}radium is entered as a constant in column J. From this and the specific surface area, the volumetric ^{226}radium concentration is determined (column K).

7) finally, the radon concentration is determined using equation A-5. The initial radon activity ($A_{Rn}{}^{o}$) is taken from the upgradient cell in the spreadsheet (usually the previous row). The constant head boundaries are given a value of 3000 pCi/L.

The results of the analytical transport model are presented in Section A.4.

A-4 RESULTS AND DISCUSSION

This section presents the flow and transport modeling results for each of the simulations.

A-4.1 Steady State Simulations

Simulations without pumping

MODFLOW simulations were done at hydraulic gradients of 0.00065 and 0.065, corresponding to gradients of 0.0001 and 0.01 across the original portion of the fracture. The results of the two simulations are presented in Figures A-5 and A-6. As expected, the shape of the head profile was identical for the two runs, but the much steeper gradient in the second simulation resulted in substantially higher groundwater velocities (up to 120 m/day), and lower residence times through the system. The effect of the steeper gradient on the resulting ^{222}radon profile through the fracture was significant. In the simulation with a gradient of 0.00065, radon levels reached secular equilibrium with the volumetric radium concentrations in all of the fracture segments, giving the blocky radon profile shown in Figure A-5c. In contrast, velocities were so fast in the simulation with a gradient of 0.065, that radon levels did not reach secular equilibrium in any of the fracture segments. As shown in Figure A-6c, the radon levels increased to an average volumetric level, and then changed only slightly in response to aperture differences. The simulations show that in systems with high groundwater velocities, there is a considerable averaging effect.

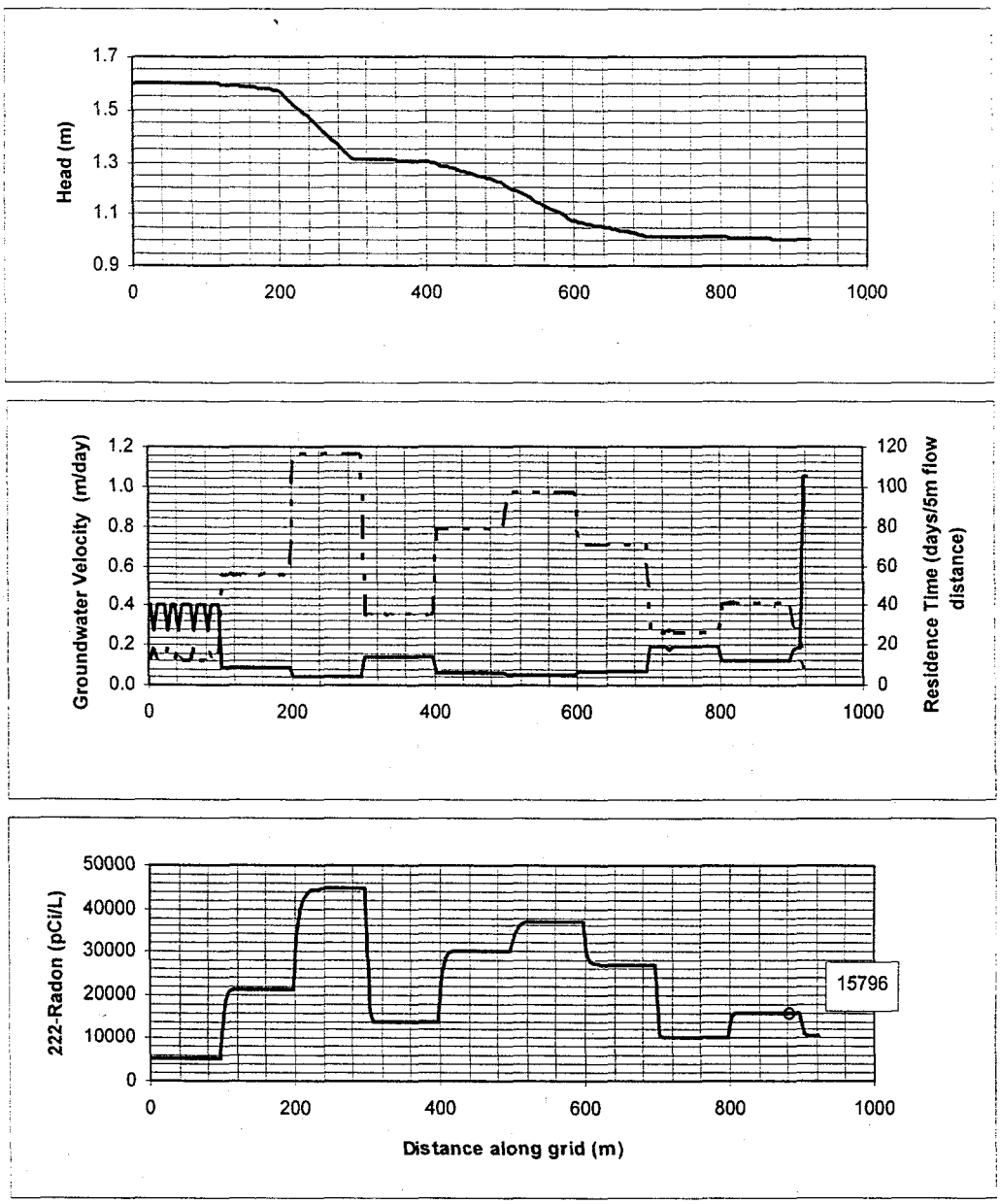

FIGURE A-5 Simulations in the absence of pumping with a natural gradient of 0.00065: a) head distribution; b) groundwater residence time (solid line) and groundwater velocity (dashes), and, c) radon profile through fracture.

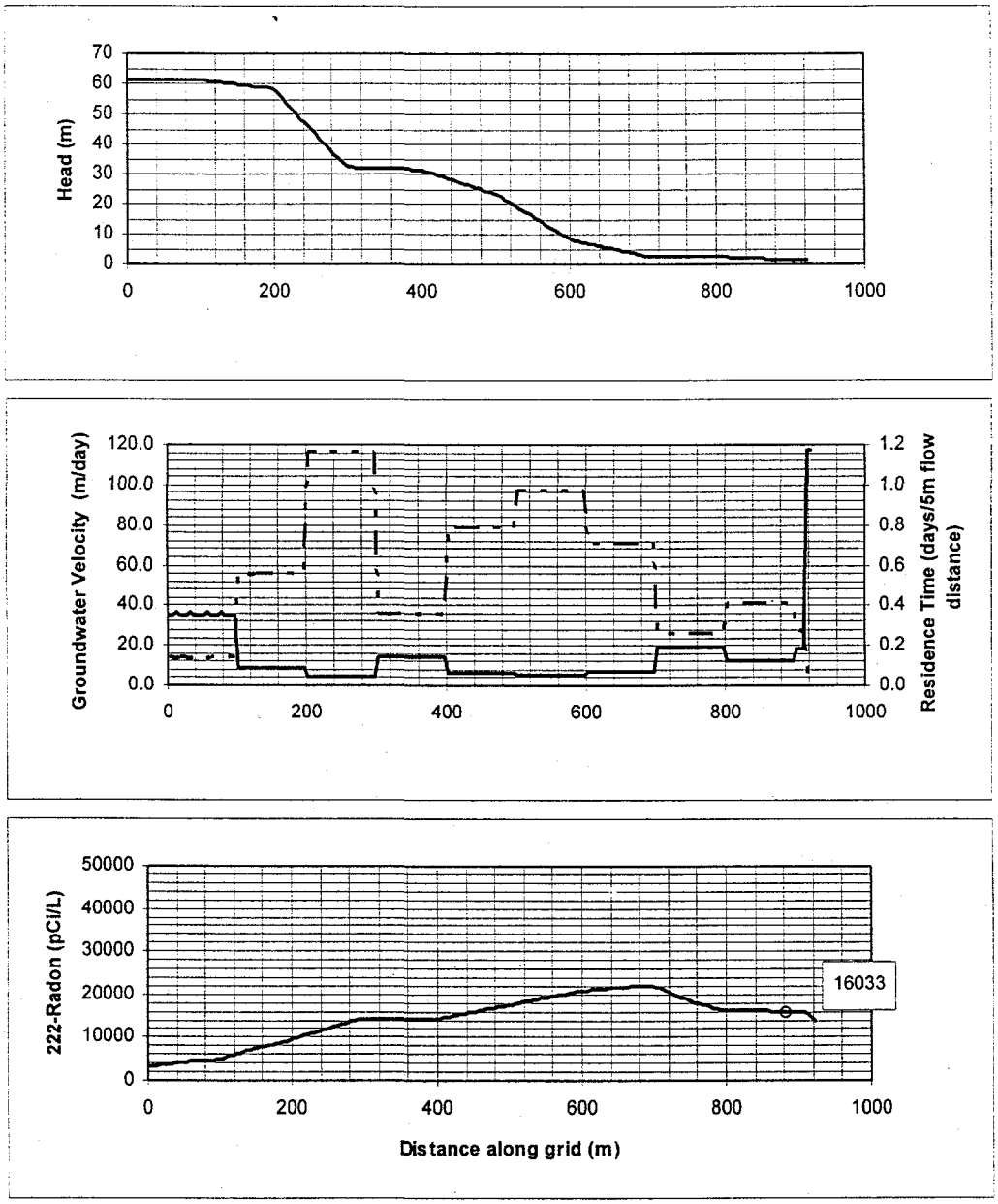

FIGURE A-6 Simulations in the absence of pumping with a natural gradient of 0.065: a) head distribution; b) groundwater residence time (solid line) and groundwater velocity (dashes), and, c) radon profile through fracture.

Simulations for domestic water use of 0.8 m^3/day

Steady state changes to the hydraulic gradient resulting from long-term domestic water use were simulated in this run. A single well, located in the eastern portion of the fracture (cell 177), was pumped at a continuous rate of 0.8 m^3/day. Two simulations were done, using overall hydraulic gradients of 0.00065 and 0.065 respectively. The results are presented in Figures A-7 and A-8.

The total drawdown observed in the first simulation was approximately 3.0 meters, resulting in a substantial change to the hydraulic gradient through the system. As a result of the pumping, groundwater residence times in the fracture system decreased by about 25x, and became negligible in the immediate vicinity of the well. As expected, this had a considerable impact on radon activity levels. As shown on Figure A-7c the residence time in a given fracture segment is not always sufficient for the establishment of secular equilibrium between ^{222}Rn and ^{226}Ra. The effect is most noticeable in fractures segments with narrow apertures and lower residence times. Since these segments have the highest volumetric radium levels, the overall effect is to lower the average radon activity levels in the fracture. In contrast, the pumping well had little influence on residence times and radon levels in the system with an already high hydraulic gradient. The most significant effect was observed within 40 meters of the well, where the hydraulic residence time became negligible. The main effect on radon activity levels was mixing of the fracture waters with waters from the constant head boundary, which was assigned an arbitrary radon concentration of 3000 pCi/L.

In both simulations, the results suggest that sources for radon ingrowth close to an actively pumped domestic water well would have little influence on the observed radon concentrations.

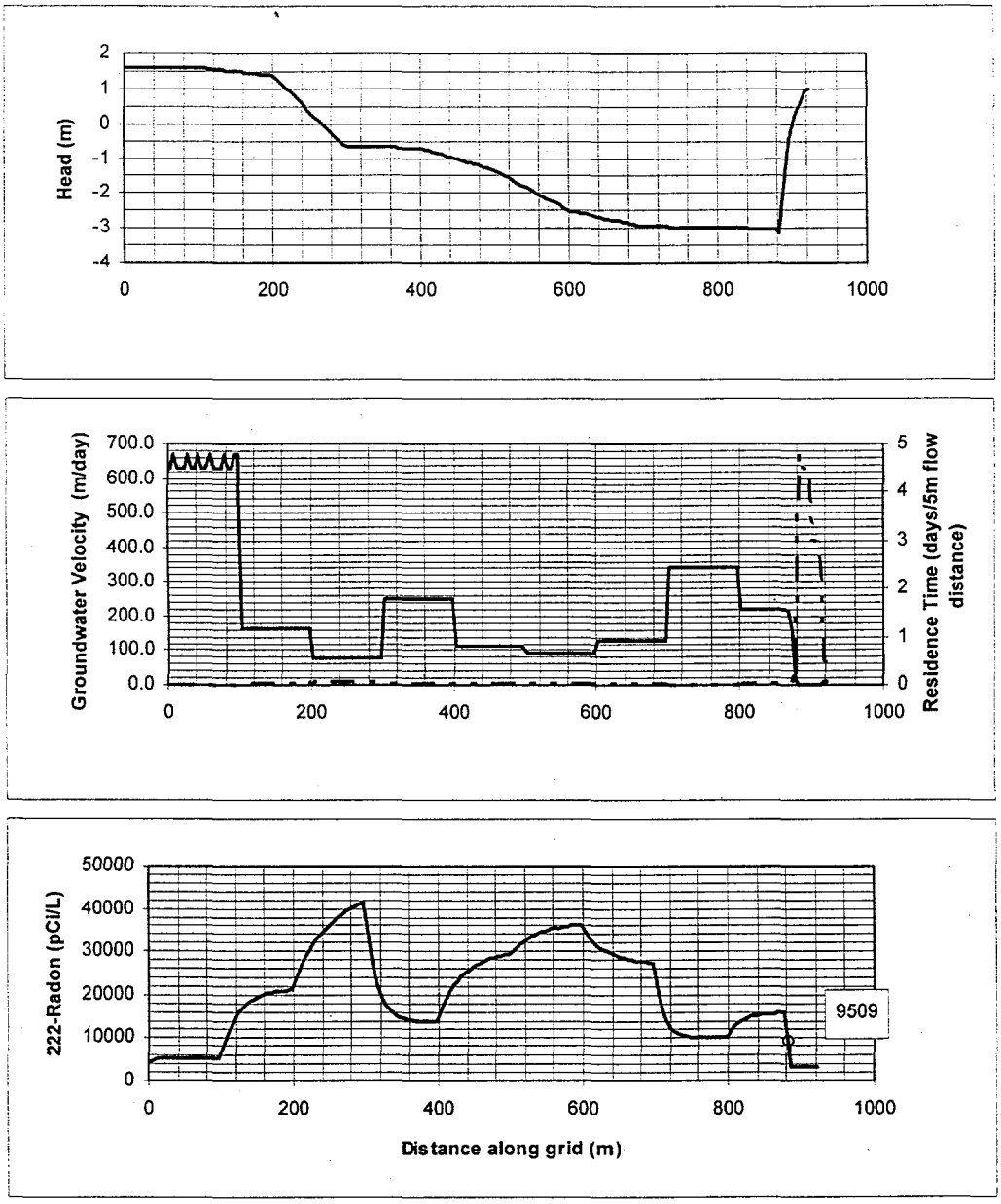

FIGURE A-7 Simulations at domestic water use rates of 0.8 m^3/day with a natural gradient of 0.00065: a) head distribution; b) groundwater residence time (solid line) and groundwater velocity (dashes); and, c) radon profile through fracture.

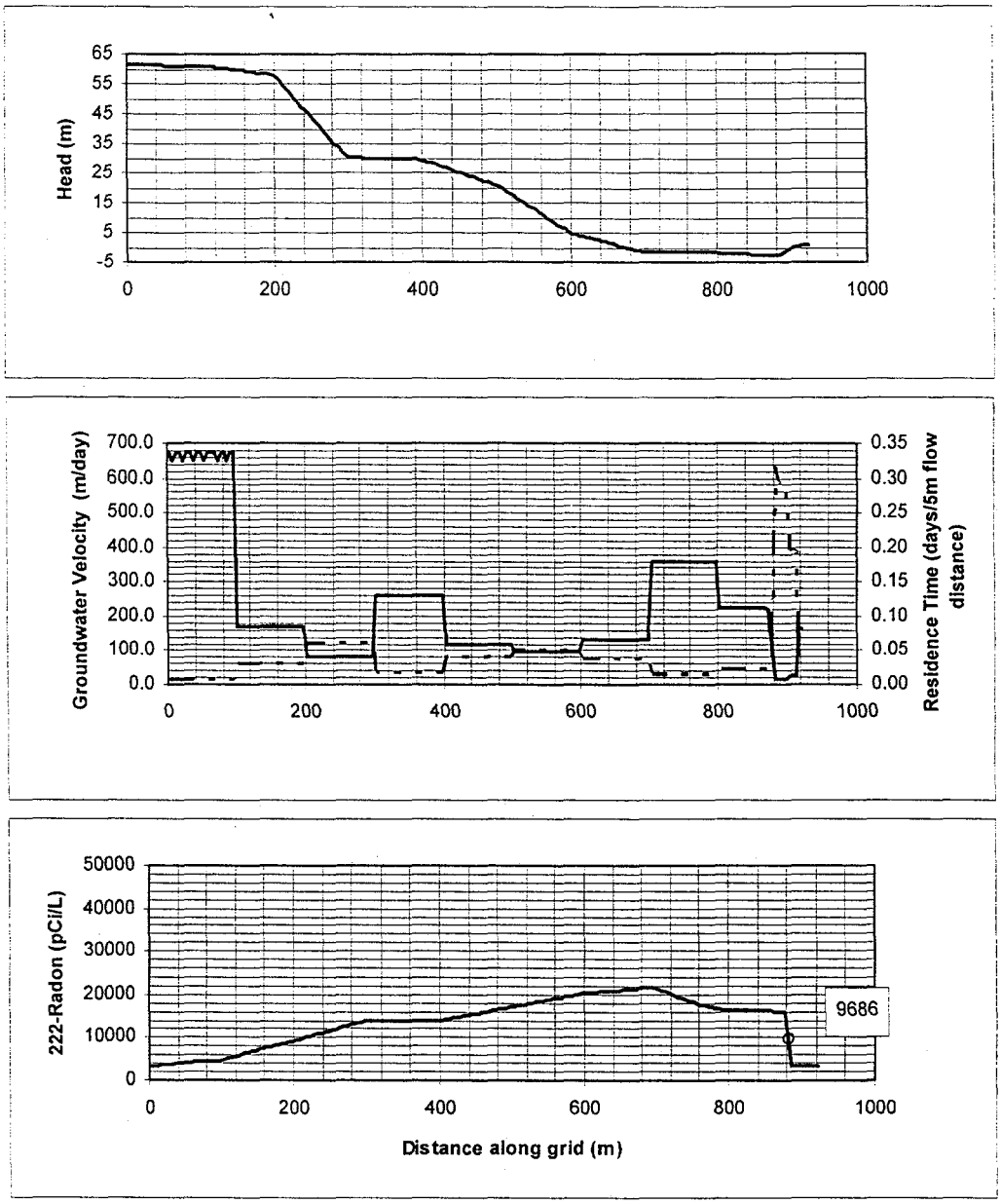

FIGURE A-8 Simulations at domestic water use rates of 0.8 m^3/day with a natural gradient of 0.00065: a) head distribution; b) groundwater residence time (solid line) and groundwater velocity (dashes); and, c) radon profile through fracture.

Simulations with shorter flow path lengths

Two steady state simulations were done using a column length of 1 meter, (1/5th the previous value), to simulate the effects of a shorter flow path on radon ingrowth and decay. Both simulations were done using a hydraulic gradient of 0.00065, such that the results could be directly compared to those shown in Figures A-5 and A-7. The results of these simulations are shown in Figures A-9 and A-10. The first simulation represents steady state conditions in the absence of pumping. As expected, the residence time per unit length was the same as that determined previously, however since the flow-path is shorter, there is less time to reach secular equilibrium in a given fracture segment. As shown in Figure A-9c, this results in more gradual transitions in radon levels between fracture segments. If the flowpaths were any shorter, or the gradient any higher, these results would be subject to the same smoothing process that occured in the steep gradient runs discussed previously. The second simulation shows the effects of pumping at a rate of 0.8 m^3/day in this short flow path model. As shown in Figure A-10, the total drawdown at the well is less than that observed in the longer model, on the order of 1 meter. This change is a direct result of moving the constant head boundaries closer to the well. Although the drawdown is small compared to the longer grid, it is still substantial compared to the natural hydraulic gradient. As a result, the hydraulic residence time is much lower, and radon levels do not reach their full potential in a given fracture segment. The net effect is averaging of the total radon activity levels along the fracture profile.

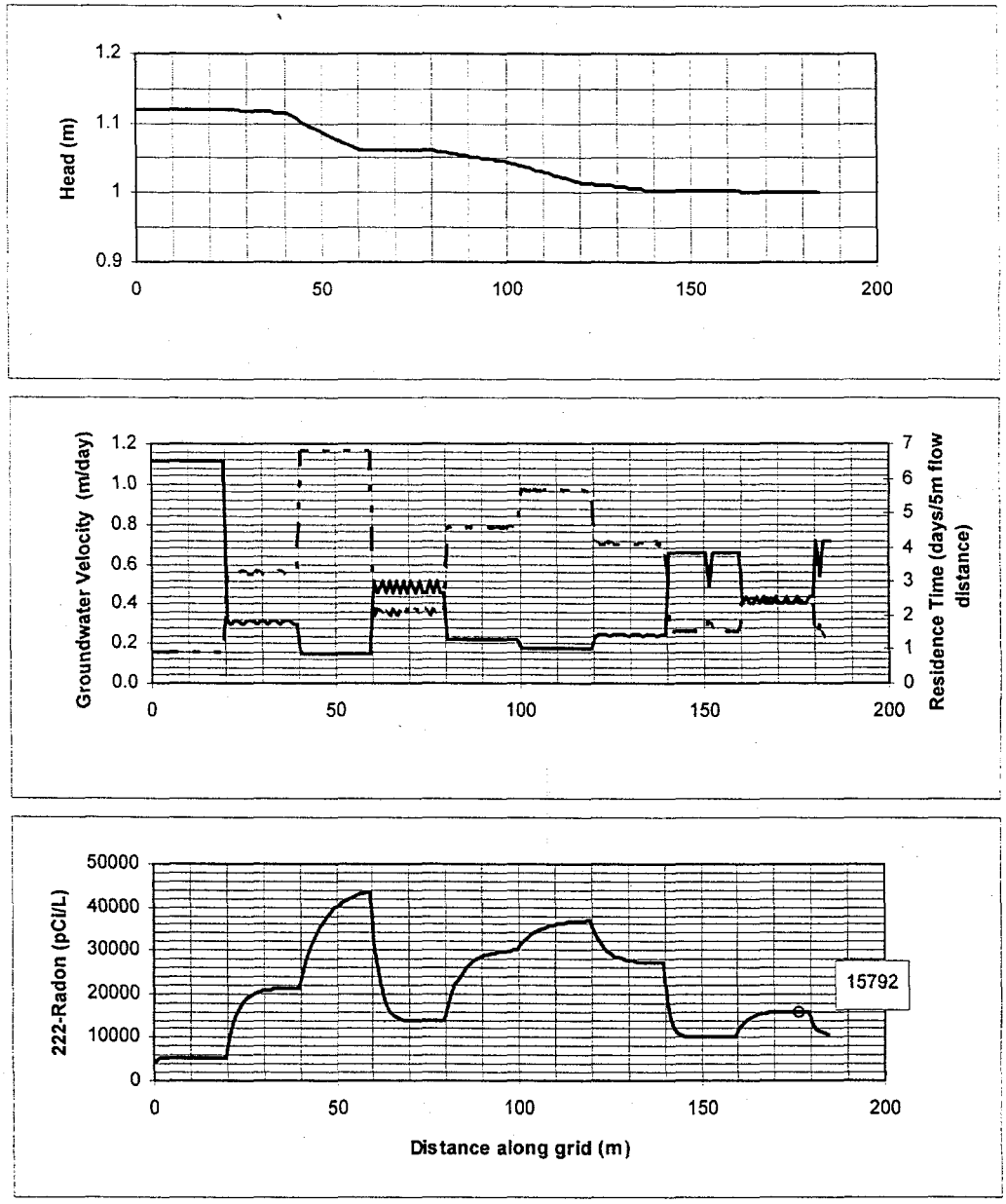

FIGURE A-9 Simulations of a system with a shorter flow path at a natural gradient of 0.00065: a) head distribution; b) groundwater residence time (solid line) and groundwater velocity (dashes); and, c) radon profile through fracture.

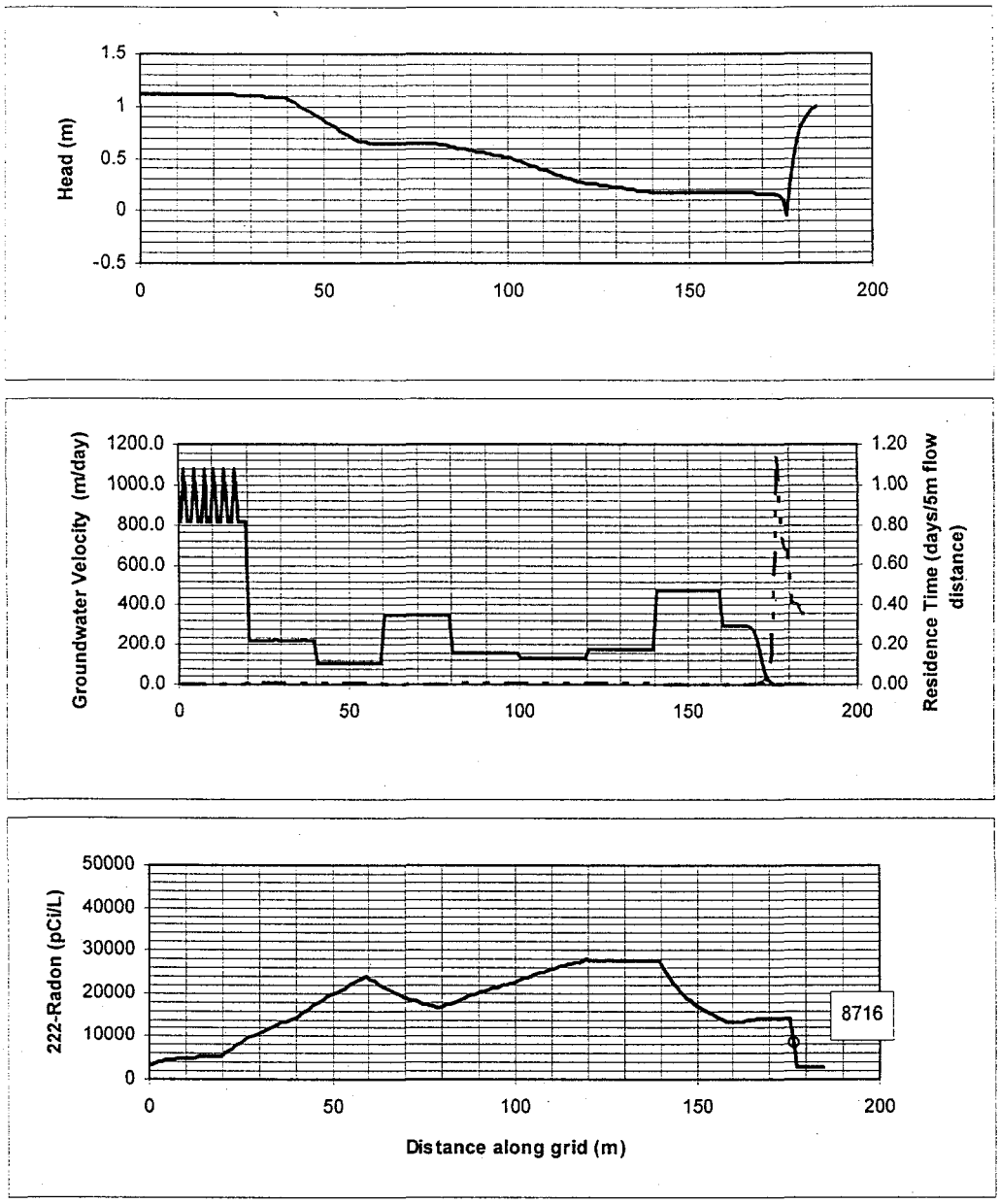

FIGURE A-10 Simulations at domestic water use rates of 0.8 m^3/day with a natural gradient of 0.00065: a) head distribution; b) groundwater residence time (solid line) and groundwater velocity (dashes); and, c) radon profile through fracture.

A-5 SUMMARY AND CONCLUSIONS

Fracture flow was modeled in a multiple fracture groundwater system to determine the effects of hydraulic gradient, pumping stresses, and fracture geometry on groundwater velocities. The steady state head distribution in this system could be modeled using a simple analytical model based on Darcy's law. As expected, fractures with small apertures tended to have higher gradients than fractures with large apertures. Although fracture segments with smaller apertures have lower hydraulic conductivitys, they have higher head losses, resulting in higher velocities and lower residence times. Groundwater velocities are inversely proportional to the fracture apertures.

Numerical modeling was undertaken to determine the head distribution under a variety of starting conditions and pumping stresses. From this, the residence time distribution for each of the model simulations along the fracture profile was determined, and used to examine the ingrowth and decay of ^{222}radon through the fracture system. The results show that radon levels do not always reach secular equilibrium with parent minerals in the host rocks in systems with steep natural gradients, shorter flow-paths, or pumping stresses. In such systems, narrow fracture segments have less of an impact on the overall radon concentration than wide ones, because groundwater residence times are relatively smaller in narrow fractures. Steep hydraulic gradients and negligible residence times were found in the immediate vicinity of pumping wells located near to the constant head boundary. This result suggests that enrichment or depletion of source minerals near to the well would have almost no influence on the resulting water quality.

APPENDIX B

SAMPLING AND TESTING RESULTS

Appendix B - Sampling and Testing Results

Sample$	LAT	LONG	Rock	pH	DO	Temp	SpCond	^{222}Rn	U	^{226}Ra	Ca	Mg	Na	HCO3	SO4	Cl	NO3	F	Ba	Cu	Fe	Li	Mn	Si	Sr	Zn	Trans
			Type		(mg/L)	°C	(umhos/cm)	(pCi/L)	(µg/L)	(pCi/L)	(mg/L)	(mg/L)	(mg/L)	(mg/L)	(mg/L)	(mg/L)	(mg/L)	(mg/L)	(µg/L)	(µg/L)	(mg/L)	(µg/L)	(µg/L)	(mg/L)	(µg/L)	(µg/L)	(ft^2/day)
88-CO-22	39.52639	105.36656	3	7.40	9.1	5.3	26	3890	0.73	.	4.5	1	2.9	16	4.4	3.3	.	0.6	8.6	82	0.04	2.7	2.3	5.9	16	13	3.216
88-CO-23	39.52333	105.36434	3	6.23	7.1	7.5	41	11930	0.93	.	7.4	1.7	4	32	4.8	0.8	1.5	0.8	3.2	170	0.05	3.5	.	6.7	25	11	30.82
88-CO-24	39.52593	105.36242	3	6.72	7.1	7.2	28	15850	0.33	0.1	2.9	0.8	3.8	21	4.3	1.3	1.0	1.0	.	58	0.04	4.4	4.5	9.2	12	2400	4.154
88-CO-25	39.51353	105.36022	7	5.91	5.9	11.7	42	6541	0.33	.	5.1	1.4	4.7	20	4.8	5.8	2.7	.	8.3	330	0.02	.	16	7.4	31	150	.
88-CO-26	39.51474	105.35314	3	7.40	6.2	7.4	60	4100	28.0	0.04	11	2.9	5	53	3.3	0.8	2.6	0.3	8	.	0.04	4	.	8.7	35	21	388.6
88-CO-27	39.52113	105.35567	3	5.90	7.55	6.2	36	24040	0.54	0.06	4.3	1.6	3.9	19	4.1	5.0	3.9	0.6	2.5	180	0.23	5	7.4	7.6	28	160	50.92
88-CO-29	39.53208	105.36769	4	6.30	6.7	8.2	41	6190	0.57	.	6	1.2	4.6	22	3.9	5.0	0.9	0.8	7.9	87	0.06	.	3.2	7.2	24	40	1058.6
88-CO-30	39.54599	105.36216	3	5.80	2.6	7.6	180	6800	0.14	0.42	18	4.1	13	17	5.8	48.6	5.3	.	36	78	0.67	.	48	6.9	110	33	.
88-CO-31	39.52005	105.33799	3	6.62	4.35	8.5	56	138700	110.0	0.03	10	2.6	6	44	3.9	7.2	.	0.4	2.7	68	0.04	4.8	.	11	39	13	46.9
88-CO-32	39.51801	105.34459	7	7.10	4.15	6.5	56	15670	26.0	3.3	11	3.3	5.8	61	4.5	0.9	.	0.5	8	14	0.35	4.6	1	9.7	51	7.1	45.56
88-CO-33	39.52737	105.35253	3	7.91	2.37	8.5	140	7590	71.0	1.8	15	8.7	7.1	104	5.5	1.2	.	2.1	.	77	0.04	6.2	.	7.3	100	6.6	0.804
88-CO-34	39.52761	105.35718	3	7.10	8.2	7.2	46	8390	0.87	.	6.8	1.8	4.5	14	7.6	4.4	15.8	0.4	4.9	95	0.18	.	4.8	6.4	39	40	.
88-CO-35	39.51192	105.35591	7	7.60	7.15	6.8	50	5070	3.1	0.25	10	2.7	4.8	52	3.5	0.8	1.0	0.2	6.2	.	0.04	5.7	.	10	34	4.6	388.6
88-CO-36	39.51113	105.35271	7	6.15	8.1	8	52	5900	0.45	0.17	8	1.9	5.2	18	5.2	11.8	7.8	.	25	140	0.06	.	1.6	7.2	48	13	227.8
88-CO-37	39.53510	105.37148	4	5.80	6.5	8.2	45	14800	1.3	0.09	8.4	0.9	5.3	16	4.0	11.8	3.0	3.1	.	150	0.02	4.7	3	7.4	20	11	30.82
88-CO-38	39.53799	105.32622	3	6.70	3.65	9	215	12500	48.0	0.27	29	8.9	8.9	103	10.4	8.6	26.9	0.3	29	130	0.03	6.1	30	10	98	64	81.74
88-CO-39	39.54092	105.30792	7	7.70	3.66	9.5	175	4130	22.0	0.53	26	11	7	150	5.6	2.7	5.8	0.6	3.5	13	.	4.6	.	8.9	110	400	2.144
88-CO-40	39.54396	105.33632	7	7.08	2.9	9.3	135	7930	0.67	0.09	0.7	0.2	45	111	5.5	2.5	.	0.5	.	36	.	.	.	10	.	9	2.278
88-CO-41	39.54613	105.35174	3	6.71	3.8	8.2	72	22100	3.1	.	15	4.6	6.4	79	3.4	1.0	4.4	0.3	.	51	0.02	9.3	1	13	49	230	11.256
88-CO-42	39.49433	105.38979	4	6.28	2.55	12.4	110	1340	0.51	0.74	21	2.8	6.6	82	5.3	2.4	.	1.8	27	16	1.2	4.3	1200	8.8	96	88	348.4
88-CO-43	39.48339	105.35396	2	7.11	7.95	10.5	360	4110	32.0	.	66	15	12	234	24.5	15.3	19.4	0.3	39	24	0.08	.	8.2	7	220	80	160.8
88-CO-44	39.47622	105.33172	2	6.60	7.5	10.5	182	1510	1.6	0.28	33	8.4	8.9	114	14.7	15.0	8.7	0.3	24	29	0.03	.	1.9	11	190	17	109.88
88-CO-45	39.48751	105.32674	1	6.63	2.8	8.4	170	3830	3.1	0.12	33	9.2	5.8	149	7.7	2.6	6.0	0.2	140	25	0.01	5.3	.	14	140	6.2	375.2
88-CO-46	39.47749	105.29886	7	6.96	1.35	7.9	160	4410	15.0	.	27	6.2	8.3	119	6.5	2.4	6.8	0.3	100	.	0.03	5.5	2.6	9.8	120	95	14.74
88-CO-47	39.50980	105.35768	7	6.58	6.3	6.4	66	7590	1.10	0.18	12	4.6	5.3	68	3.7	1.0	3.1	.	7.3	35	0.02	6.1	.	11	85	8.7	14.74
88-CO-48	39.51816	105.31244	5	7.45	5.7	7.9	180	2070	4.2	0.23	36	11	6.1	177	5.2	2.3	4.1	0.2	14	21	0.04	.	.	12	130	230	268
88-CO-49	39.51539	105.28280	7	7.05	3.6	9.4	280	5060	25.0	0.32	48	7.7	10	163	14.1	21.6	8.3	.	100	73	0.02	11	130	8.8	300	9.1	2.144
88-CO-50	39.49436	105.29122	3	6.88	6	9.4	180	1640	3.4	.	29	9.4	9.3	138	9.5	8.2	4.5	0.3	59	50	0.01	5.3	1.4	11	130	18	308.2
88-CO-51	39.50915	105.36003	7	8.00	2	6.5	110	28400	1220.0	1.8	18	6.2	7.5	92	10.2	1.1	.	2.0	43	14	.	.	.	6.4	130	430	.
89CO-03	39.49339	105.34629	3	6.40	9.4	5.5	140	1516	222.2	2.7	23	4.4	8.8	58	7.4	7.7	5.2	1.9	54	30	0.1	5	2	7.9	130	56	.
89CO-04	39.49590	105.35199	3	6.50	3.2	7.8	140	9340	158.7	1	14	3.1	8.8	86	7.9	14.1	0.6	0.4	16	5	0.05	2	8	9.5	68	9	8.71
89CO-05	39.50669	105.34221	3	6.40	3.0	7.5	100	10590	111.1	1	17	3.2	6.7	76	4.8	0.6	.	0.7	16	24	0.04	8	2	11	54	2300	2.144
89CO-06	39.49826	105.35157	3	6.90	0.8	10.0	165	1012	618.6	1	24	7.8	8.8	131	4.0	1.8	.	3.2	42	58	0.05	8	20	7.7	94	49	469
89CO-07	39.50543	105.35128	7	6.62	12.5	10.2	120	18404	336.4	4.2	19	4.1	9.1	78	7.4	4.3	1.5	1.8	59	5	0.06	4	1	7.4	130	14	2.144
89CO-08	39.49915	105.34595	3	6.00	4.9	9.0	85	8995	144.9	0.6	11	2.2	7.2	35	4.6	7.8	4.8	0.6	19	120	0.07	4	10	9.5	55	75	3.484
89CO-09	39.51998	105.34291	3	6.47	4.2	6.3	145	5496	21.5	0.2	17	4.9	7.1	62	4.2	13.2	2.3	0.8	12	12	0.04	5	.5	8.2	67	73	281.4
89CO-10	39.51972	105.33998	7	6.10	7.9	8.1	155	10640	1.7	12.2	46	16	57	17	6.6	177.0	3.4	0.2	70	74	0.02	8	3	7.8	400	12	147.4
89CO-11	39.53384	105.36665	3	6.48	5.7	5.9	650	30934	6.7	0.5	9.3	1.9	6.3	49	1.7	0.6	0.4	1.0	8	24	0.01	6	.5	10	30	2	33.5
89CO-12	39.52185	105.33920	3	6.30	6.6	8.0	100	27240	2.2	0.1	10	2.9	8.2	27	2.2	18.1	0.8	0.0	3	44	0.02	2	4	12	57	210	2.278
89CO-13	39.52966	105.33490	5	6.62	5.2	6.3	75	5837	2.2	0.5	9	2.7	5.8	38	3.2	5.4	2.7	0.3	100	5	0.1	2	4	9.2	56	24	11.792
89CO-14	39.53077	105.33147	7	6.71	7.0	8.8	200	36288	1.8	0.7	25	8.6	10	102	8.6	11.4	21.8	0.4	29	28	0.03	9	3	10	110	30	5.36
89CO-15	39.53169	105.32308	2	7.68	8.6	9.0	750	0	0.2	.	6.6	1.8	7	22	3.3	12.0	.	0.5	14	5	0.21	2	12	6.5	37	4	.
89CO-16	39.53141	105.32284	7	8.42	1.1	7.0	205	25691	5.8	0.71	21	11	16	137	7.0	7.3	0.5	2.9	99	5	0.03	8	10	6	480	1	.
89CO-17	39.52813	105.32987	5	6.49	6.6	6.2	80	3440	0.3	2.9	8.9	3.5	4.9	50	4.7	1.9	.	0.3	38	15	0.03	2	4	8.6	68	86	52.26
89CO-18	39.52414	105.33643	3	7.42	1.3	8.5	120	12283	1.1	.	14	5.2	6.2	89	1.8	0.8	.	1.0	3	5	0.03	8	4	10	39	3400	2.814
89CO-19	39.53799	105.35473	5	7.45	5.4	8.0	140	5573	8.3	.	15	8.7	7.3	101	10.4	1.2	.	0.9	32	20	0.07	4	8	6.4	140	1400	.
89CO-20	39.52490	105.35701	3	6.01	8.4	6.5	610	6368	1.7	.	5.5	1.6	4.9	17	2.8	3.8	7.3	0.2	6	61	0.01	2	3	6.6	33	34	3.752
91-CO-01B	39.51377	105.44412	4	6.40	8.40	8.0	82	10465	0.6	0.10	9	2	5	35	5.4	0.97	3	2.2	3	60	0.025	6	.5	11	39	3	2.144
91-CO-03B	39.47427	105.35861	1	7.70	4.90	9.6	450	3825	40.0	0.40	53	11	8	210.5	15.6	9.4	6.5	0.85	67	5	0.07	5	.5	5	190	4	2.144
91-CO-05	39.50279	105.39063	4	6.93	2.80	10.1	260	10700	20.0	3.20	22	10	9	130.4	5	1.8	2.3	3.1	47	80	0.2	10	7	7	110	8	0.804
91-CO-06	39.50463	105.38565	4	7.90	0.70	9.7	320	7200	24.0	1.10	23	14	11	165.6	4.3	0.87	.	3.5	220	5	0.025	10	2	6	110	1.5	4.422
91-CO-07	39.50013	105.39944	4	6.99	3.25	10.2	310	10700	11.0	0.10	27	8	8	149.4	8.9	4.8	3.2	2.6	40	10	0.025	10	20	10	120	20	1.206
91-CO-08	39.49987	105.40004	4	6.71	6.00	8.3	180	10100	1.7	0.40	16	4	6	126	9.4	3.2	4.7	2.7	7	10	0.09	10	2	10	78	10	2000
91-CO-09	39.49956	105.41040	4	6.88	6.50	8.7	180	9534	1.8	0.00	16	3	5	43.55	13	3.5	13	2.1	2	5	0.025	5	.5	7	69	3	656.6
91-CO-10	39.49988	105.40082	4	6.60	6.50	8.0	220	12770	1.5	0.00	17	4	6	67.5	9.2	3.1	5.4	2.6	5	5	0.06	10	.5	11	80	10	2000
91-CO-11	39.48418	105.39854	4	7.00	8.10	8.8	200	10404	0.9	0.20	21	3.4	5.1	56	14.11	6.63	18.57	1.76	18	17	0.05	4	5	8.2	99	10	576.2
91-CO-12	39.50300	105.40565	4	7.00	2.23	10.2	290	22211	75.0	1.60	19	9	9	112.8	6.5	2.4	4	3.8	40	5	0.025	10	.5	8	62	4	0.402
91-CO-13	39.43298	105.31634	4	7.30	0.10	13.0	320	8490	9.7	1.30	32	5.8	12	143	4.94	1.82	0	2.86	160	5	0.1	29	49	7.8	280	1.5	37.52
91-CO-14	39.51381	105.42069	4	6.40	12.20	3.3	60	5471	0.8	0.00	5	0.8	2	16	4.8	0.75	2.5	2	3	5	0.1	6	5	6	24	10	.
91-CO-15	39.47153	105.35368	1	7.80	6.70	9.8	440	2145	15.4	0.60	48	13	9.5	218	14.93	3.75	2.78	0.46	99	15	0.1	5	5	5.9	240	3	1.474
91-CO-16	39.50190	105.39364	4	7.50	2.20	9.9	360	13411	22.0	2.90	27	11	15	182	3.1	1.1	.	3.4	210	20	0.025	10	34	8	180	270	2.814
91-CO-17	39.50228	105.38955	4	6.26	10.00	7.5	110	11262	0.6	0.30	8	1	4	31.2	5.1	0.77	2.2	2.4	1	20	0.025	7	.5	11	37	10	.
91-CO-18	39.50189	105.38975	4	6.35	7.20	7.5	200	11428	0.9	0.10	15	3	4	51.9	7.7	3.7	9.7	1.8	2	40	0.025	9	5	9	84	10	2000
91-CO-19	39.51232	105.44572	4	6.40	10.60	8.5	76	4877	0.8	0.00	9	1	4	31	5.6	0.82	1.7	2.3	1	40	0.025	8	.5	10	38	5	0.804

Appendix B - Sampling and Testing Results

Sample$	LAT	LONG	Rock Type	pH	DO (mg/L)	Temp °C	SpCond (umhos/cm)	^{222}Rn (pCi/L)	U (µg/L)	^{226}Ra (pCi/L)	Ca (mg/L)	Mg (mg/L)	Na (mg/L)	HCO3 (mg/L)	SO4 (mg/L)	Cl (mg/L)	NO3 (mg/L)	F (mg/L)	Ba (µg/L)	Cu (µg/L)	Fe (mg/L)	Li (µg/L)	Mn (µg/L)	Si (mg/L)	Sr (µg/L)	Zn (µg/L)	Trans (ft^2/day)
91-CO-20	39.51135	105.44101	4	6.84	8.10	9.5	105	13203	5.8	0.10	13	2	4	51.2	5.9	1.1	1	2.7	1	30	0.025	6	.5	7	40	6	2.68
91-CO-21	39.49326	105.42434	4	6.71	7.70	12.8	110	6151	0.7	0.00	13	3	5	44.5	11.5	1.2	0.7	2.5	8	5	0.025	5	2	10	58	44	.
91-CO-22	39.51688	105.44470	4	6.55	10.40	6.9	84	7969	0.6	0.00	9	1	2	30.5	5.7	1	4.3	1.8	1	40	0.025	5	1	7	36	7	2000
91-CO-23	39.50442	105.40329	4	6.62	6.30	9.0	180	9460	4.3	0.10	17	5	8	73.2	11.2	1.5	1.4	3.8	8	60	0.025	10	2	12	68	310	8.04
91-CO-24	39.50457	105.44146	4	6.60	9.80	9.7	140	7242	1.5	0.70	11	2	2	36	10.4	1	1.7	2.2	10	60	0.025	2	6	7	41	10	4.556
91-CO-25	39.49664	105.42207	4	6.38	8.50	8.9	140	22740	1.7	0.00	12	2	5	40.3	9.9	1.3	1.3	2.8	2	50	0.025	7	.5	11	48	6	32.16
91-CO-26	39.52071	105.44073	4	7.55	2.60	8.7	250	2100	29.0	1.70	24	5	6	99	2.5	1.1	3.3	2.8	66	10	0.025	10	2	8	91	8	0.938
91-CO-27	39.47238	105.35853	1	7.65	9.10	9.3	330	3646	17.0	0.00	44	9	10	177.5	26	3.2	6.7	0.6	110	10	0.06	2	.5	5	190	1.5	1.34
91-CO-28	39.47218	105.35931	1	7.85	7.70	10.2	380	2746	19.0	0.00	42	11	10	171	24	4.4	11	0.8	99	10	0.025	4	.5	5	230	9	1.072
91-CO-29	39.47306	105.35883	1	7.90	1.90	10.0	400	3198	6.1	0.20	27	12	27	164.5	19	13	2.6	3.2	94	5	0.025	9	5	6	880	310	1.072
91-CO-30	39.49314	105.36752	3	7.70	4.80	9.5	320	966	4.8	0.00	35	10	9	177	8.7	1.2	.	0.3	61	10	0.06	4	.5	9	130	730	2.948
91-CO-31	39.47532	105.35805	1	7.25	7.90	8.6	1100	1604	15.0	0.00	89	22	13	183	43	58	110	0.5	99	5	0.025	4	.5	6	420	20	335
91-CO-32	39.48792	105.36235	3	6.40	1.70	8.5	150	5315	2.1	0.00	13	3	6	65	6.7	1.1	0.7	0.3	10	5	0.7	8	21	10	55	20	.
91-CO-33	39.47797	105.32892	2	7.10	7.80	9.3	420	2081	2.7	0.00	43	9	10	166	14	11	13	0.3	71	5	0.06	2	0.5	7	260	56	3.618
91-CO-34	39.46372	105.33918	2	7.88	4.25	9.4	390	1022	39.0	0.00	41	12	9	200	21	1.5	1.6	0.4	78	100	0.025	2	10	5	580	1.5	5.762
91-CO-35	39.45807	105.33239	2	7.30	2.20	10.8	360	1543	8.3	0.00	50	7	9	199	14	3.8	0.6	0.8	120	70	0.025	7	6	9	930	20	2.278
91-CO-36	39.49049	105.35213	3	7.51	3.40	8.3	320	3329	5.8	0.00	35	7	8	132	12	11	5.1	0.2	43	30	0.06	6	43	8	98	1600	1.34
91-CO-37	39.40890	105.32273	4	7.61	0.83	12.4	2950	1517	1.7	0.00	220	3	200	64	860	130	.	4	10	5	0.025	250	580	11	2700	20	1.206
91-CO-38a	39.50458	105.39713	4	7.10	7.50	8.0	95	11268	4.0	0.40	19	4	8	.	9.6	1.9	0.2	3.8	5	30	0.2	10	7	12	78	73	17.42
91-CO-40	39.52332	105.36429	3	7.00	6.40	6.1	86	13200	7.2	0.50	11	2	4	47.75	3.3	0.7	1.4	1.5	6	20	0.025	5	0.5	7	23	9	6.03
91-CO-41	39.48336	105.35395	2	7.00	6.30	9.3	665	4052	19.0	1.40	77	17	16	282	21	24	35	0.2	54	10	0.025	2	4	8	300	51	.
91-CO-42	39.47414	105.35582	2	7.55	2.00	11.7	340	6321	17.1	0.90	33	7.2	16	144	23.4	3.19	1.14	1.8	53	18	0.2	8	21	6	430	40	0.804
92-CO-01	39.50148	105.40805	4	6.90	3.60	9.3	90	21216	7.8	0.60	15	3.1	7.3	64.8	2.3	4.52	1.66	2.55	9	68	0.05	6	5	12	45	19	4.422
92-CO-09	39.43365	105.34525	4	7.75	0.30	10.7	200	17551	133.0	2.10	22	1.3	10	77.5	12.6	3.5	1.1	3.3	85	5	0.05	36	5	4.9	290	200	0.536
92-CO-10	39.43276	105.34317	4	.	.	11.5	.	3837	27.0	1.10	.	.	.	.	11.4	24.8	12.3	3.7	.	.	.	.	.	.	.	.	1.34
92-CO-11	39.49707	105.42107	4	7.40	8.70	8.6	115	15603	1.3	0.10	13	2.3	4.9	42.5	11.27	1.59	1.24	2.60	7	5	0.1	4	5	9.2	42	16	64.32
92-CO-13	39.49509	105.42215	4	6.60	8.50	11.3	150	3391	0.4	0.10	16	2.9	5.1	143	11.41	1.41	11.24	2.35	7	170	0.1	6	5	11	72	10	119.26
92-CO-14	39.49459	105.41960	4	6.32	7.80	8.8	240	11809	1.5	0.30	22	3.8	5.9	35.8	10.2	21.21	12.01	1.89	6	5	0.1	5	5	8.7	77	11	32.16
92-CO-15a	39.49651	105.42028	4	7.30	.	10.7	140	7745	1.6	0.80	.	.	.	41	12.02	1.63	1.68	2.49	.	.	.	.	.	.	.	.	0.804
92-CO-16	39.49516	105.41899	4	6.90	8.70	9.0	120	20527	3.0	0.30	11	1.4	3.4	34.7	6.46	2.07	1.89	2.19	3	5	0.05	2	5	6.7	30	20	10.854
92-CO-17	39.49528	105.42132	4	6.80	7.10	8.5	180	5748	1.2	0.20	17	2.9	5.7	49.1	8.61	10.39	7.59	1.86	5	5	0.6	5	66	9.1	65	14	129.98
92-CO-18	39.49571	105.42271	4	7.90	.	10.0	300	3355	8.3	0.90	22	7.8	26	158	5.91	1.88	1.5	3.46	220	10	0.2	26	46	8.9	220	11	2.144
92-CO-19	39.47394	105.35840	1	7.60	2.70	9.9	350	3714	21.5	0.60	41	13	10	194	9.73	4.7	1.34	1.77	79	11	0.05	7	5	5.7	270	1.5	4.69
92-CO-20	39.47420	105.34677	2	7.30	1.00	10.3	280	3197	18.6	0.10	33	14	12	175	14.76	7.49	0.65	1.95	92	5	0.05	7	5	6.2	610	290	.
92-CO-21	39.47092	105.34268	2	7.35	2.30	10.5	330	4361	26.7	0.90	26	23	11	217	9.77	3.63	1.56	0.59	44	5	0.05	8	5	5.7	280	1.5	3.752
93-CO-01	39.49578	105.41965	4	7.61	7.50	9.7	90	4464	6.7	0.40	13	1.5	2.7	19.7	6.53	1.2	0.97	2.54	8	5	0.1	2	5	5.3	32	4	4.288
93-CO-02	39.49670	105.41835	4	7.30	5.90	9.3	160	17279	8.0	0.40	.	.	.	.	8.66	1.78	0.91	2.92	.	.	.	.	.	.	.	.	8.576
93-CO-04	39.49762	105.41811	4	7.40	5.80	9.5	120	15771	7.8	0.00	.	.	.	55	9.23	1.5	1.12	2.7	.	.	.	.	.	.	.	.	21.44
95-CO-02	39.42639	105.34719	4	7.42	6.0	11.7	282	7743	175.0	.	39	5.3	10.1	122	11.4	10.1	2.16	3.21	192	8.1	0.002	12.5	0.12	6.26	476	20	.
95-CO-03	39.44928	105.35137	1	7.2	0.5	.	740	11560	79.0	.	80	20.7	30.0	327	35.6	30.4	1.07	1.51	104	13.9	0.002	5.0	3.9	7.22	459	20	2.3
95-CO-04	39.44137	105.33220	4	7.45	3.3	.	503	14055	24.0	.	53	10.1	13.7	215	29.6	3	0.1	2.07	30	7.2	0.002	13.7	9.5	8.89	1132	488	.
95-CO-05	39.44215	105.32868	4	7.04	9.0	.	217	4514	4.1	.	37	7.8	9.7	137	21.6	10.1	0.1	0.95	74	9.8	0.002	2.3	0.12	8.72	219	20	178
95-CO-06	39.43946	105.33031	4	6.98	5.6	11.0	235	2743	2.9	.	41	8.2	11.6	148	21	9.3	1.16	0.84	75	19.7	0.005	3.6	19.9	9.09	377	20	820
95-CO-07	39.44851	105.35028	1	7.55	2.6	9.0	490	2757	32.4	.	61	10.7	21.5	233	32	16.3	0.18	1.35	39	48.0	0.07	2.9	8.0	7.81	811	20	6.2
95-CO-08	39.44071	105.32952	4	7.24	7.8	11.0	95	4286	3.4	.	12	1.9	3.3	35	9.8	2.2	0.14	3.41	20	160.4	0.01	10.2	2.1	6.57	103	20	.
95-CO-09	39.42572	105.35172	4	7.3	6.9	.	310	3669	3.7	.	30	3.2	6.6	45	15.1	14.5	9.69	2.52	58	31.5	0.002	12.6	7.3	6.74	133	2158	5
95-CO-10	39.43887	105.35173	2	7.3	6.4	12.0	1900	3304	.	.	281	71.3	40.0	290	114	248.3	114.4	1.9	330	65.3	0.002	8.7	6.2	6.30	2274	359	1.3
95-CO-11	39.43251	105.34399	4	7.19	9.3	10.9	320	10125	5.8	.	32	6.2	8.3	90	11.7	13.7	4.47	3.82	15	18.8	0.002	14.5	1.3	6.55	141	20	262
95-CO-12	39.43491	105.34426	4	7.2	8.5	13.3	370	8613	5.6	.	37	6.3	6.3	101	13.7	14.6	4.76	3.73	27	176.9	0.002	10.3	4.1	7.39	160	20	4.4
95-CO-13	39.43632	105.34739	4	7.33	8.2	12.5	570	9667	8.5	.	53	9.6	11.3	170	16.8	10.7	6.29	3.44	170	14.0	0.002	11.3	0.12	7.65	185	20	2.9
95-CO-14	39.43576	105.34502	4	8.25	5.6	15.0	320	8815	11.7	.	34	4.3	6.5	111	11.1	2.4	1.56	3.48	99	13.4	0.002	12.3	0.12	5.80	106	20	1.7
95-CO-15	39.44881	105.35075	1	7.35	5.6	10.5	820	8430	14.8	.	64	14.2	31.6	250	38.7	21.1	3.77	0.65	101	11.0	0.002	3.3	0.6	5.65	388	20	0.93
95-CO-16	39.43046	105.34912	4	7.72	6.2	12.4	1000	8290	11.5	.	103	24.6	18.5	253	27.1	97.3	6.34	1.4	244	3.4	0.002	5.0	2.0	7.51	621	908	7.4
95-CO-17	39.42833	105.34674	4	6.47	8.7	11.6	430	5677	7.9	.	37	8.0	7.5	84	16.2	25.7	4.41	3.13	93	30.5	0.002	11.5	14.9	7.01	191	20	13.2
95-CO-18	39.43312	105.34584	4	7.14	7.7	13.2	497	3176	22.2	.	40.26	10.752	7.34	107	13.1	18.5	5.62	4.28	197.13	48.33	0.002	8.99	7.79	5.33	165.47	20	5.7
95-CO-19	39.42631	105.34435	4	7.81	.	10.9	510	4213	13.7	.	42.50	8.402	9.16	116	15.1	25.5	7.84	2.97	316.49	68.91	0.002	8.41	97.10	4.35	385.25	20	1.1
95-CO-20	39.41664	105.33563	4	8.13	0.1	13.4	250	8631	13.0	.	34.48	4.752	6.74	121	10.5	2.4	0.1	3.17	204.22	1.75	0.017	10.24	71.70	5.64	108.89	20	106
95-CO-21	39.41567	105.32880	4	7.75	7.2	14.5	190	5352	4.5	.	19.94	3.901	4.01	67	10	1	0.73	3.53	37.43	240.49	0.002	2.75	0.38	4.31	52.38	20	.
95-CO-22	39.41626	105.33062	4	7.62	5.2	12.1	260	6290	8.0	.	30.32	10.327	7.95	107	23.9	7.5	2.21	3.58	188.69	41.30	0.002	2.12	0.43	5.54	124.24	20	2.4
95-CO-23	39.42442	105.34307	4	7.33	9.3	8.3	260	7216	4.1	.	37.79	6.633	6.78	126	13	5.3	2.42	2.15	95.45	12.92	0.004	6.50	1.97	6.97	137.89	79	367
95-CO-24	39.42836	105.33936	4	8.42	0.3	12.7	190	18250	37.9	.	23.70	1.477	10.46	84	7.2	1.8	0.2	3.4	95.14	27.64	0.002	37.23	5.56	6.73	334.21	20	1.4
95-CO-25	39.46922	105.33741	1	7.76	3.7	10.5	370	2816	14.0	.	46.14	12.268	9.30	192	21.1	4.3	2.82	0.62	55.25	15.73	0.002	3.59	0.12	6.57	243.77	20	15.4
95-CO-26	39.44772	105.35160	1	7.57	8.1	10.2	390	2988	6.9	.	44.72	10.702	12.77	183	23.3	4.9	0.31	0.68	107.36	10.24	0.008	2.00	2.85	7.68	248.49	273	10
95-CO-27	39.43005	105.35192	4	7.65	5.1	11.9	490	6466	47.9	.	49.79	11.795	12.03	184	30.5	6.7	1.59	2.24	84.95	24.36	0.002	11.90	2.37	5.37	213.90	585	0.5

Appendix B - Sampling and Testing Results

Sample$	LAT	LONG	Rock	pH	DO	Temp	SpCond	^{222}Rn	U	^{226}Ra	Ca	Mg	Na	HCO3	SO4	Cl	NO3	F	Ba	Cu	Fe	Li	Mn	Si	Sr	Zn	Trans
			Type		(mg/L)	°C	(umhos/cm)	(pCi/L)	(µg/L)	(pCi/L)	(mg/L)	(mg/L)	(mg/L)	(mg/L)	(mg/L)	(mg/L)	(mg/L)	(mg/L)	(µg/L)	(µg/L)	(mg/L)	(µg/L)	(µg/L)	(mg/L)	(µg/L)	(µg/L)	(ft^2/day)
95-CO-28	39.48976	105.33393	1	7	5.5	8.5	975	2985	3.0	.	93.67	22.514	11.78	181	13.9	93.2	13.12	0.25	104.19	15.07	0.002	6.14	0.12	10.97	527.10	20	14.4
95-CO-29	39.49283	105.33439	1	6.91	6.7	8.4	710	3346	3.2	.	66.65	16.661	13.98	109	20.2	42.6	20.6	0.25	240.15	37.81	0.002	9.71	0.12	11.67	350.84	20	
95-CO-30	39.49462	105.32938	1	7.16	.	7.6	305	6552	7.5	.	31.87	11.002	8.00	156	5.1	6.8	0.36	0.53	125.51	13.09	0.002	6.05	0.12	8.79	186.96	20	14.5
95-CO-31	39.49363	105.32698	1	6.65	.	8.2	370	5276	5.9	.	40.79	9.115	9.4	148	6.7	17.3	2.93	0.47	69.32	65.11	0.002	7.21	0.12	10.77	218.7	20	70
95-CO-32	39.48736	105.37188	1	7.06	.	9.5	160	2935	5.3	.	24.23	5.281	8.19	111	13.1	1.8	0.18	0.54	39.91	6.75	0.002	3.93	19.83	9.55	107.5	20	49
95-CO-33	39.47921	105.37384	1	8.02	.	13.2	370	2770	5.0	.	24.13	10.274	31.78	179	15.4	5.9	0.1	3.42	98.78	15.53	0.002	13.03	0.43	6.06	488.7	20	0.13
95-CO-34	39.48211	105.33348	1	6.85	.	9.3	285	2771	1.7	.	34.28	5.443	8.35	109	13.5	14.2	2.04	0.25	94.75	29.28	0.002	5.53	10.86	9.27	160.1	176.4	2.6
95-CO-35	39.48116	105.33204	1	6.89	5.5	10.4	415	1605	8.5	.	48.51	9.146	10.89	132	12	42.9	0.62	0.38	29.16	128.5	0.002	3.73	2.97	10.23	448.1	20	2.5
95-CO-36	39.47321	105.33378	1	6.94	5.1	10.3	290	2646	5.8	.	32.4	8.445	8.56	128	10.4	5	1.43	0.52	43.67	29.39	0.002	2.9	0.12	8.19	204.8	20	1.2
95-CO-37	39.48611	105.33375	1	7.54	2.8	9.0	360	2563	9.5	.	47.65	9.521	8.68	176	9.9	10.7	2.55	0.79	41.68	88.34	0.002	2	1.4	6.59	693.5	20	3.4
95-CO-38	39.47722	105.33096	1	7.67	0.3	12.1	1200	879	9.6	.	209.69	2.999	44.16	77	491.2	3.6	0.65	2.63	11.61	55.9	0.002	3.63	0.12	8.07	5467	20	2.3
95-CO-39	39.48033	105.40352	4	6.81	7.7	11.8	200	3741	7.3	.	22.13	3.937	5.6	55	12.4	9.6	1.64	2.05	15.35	47.88	0.002	3.63	0.35	8.72	83.99	20	272
95-CO-40	39.47085	105.33659	1	8.19	2.7	11.4	330	1577	13.9	.	25.42	10.335	5.57	146	22.2	2.2	0.1	2.79	62.07	25.42	0.002	7.09	5.19	6.32	863.78	480	3.9
95-CO-41	39.48238	105.40422	4	6.69	8.3	11.4	140	8009	0.4	.	13.84	2.037	5.17	43	11.11	1.6	0.45	2.05	3.40	11.36	0.002	5.18	0.26	10.24	63.82	20	5.9
95-CO-42	39.48073	105.40248	4	6.43	6.5	9	210	3499	1.9	.	22.70	3.332	5.69	49	12.6	10	2.99	1.66	10.70	49.31	0.002	5.09	1.14	7.62	63.95	20	1.2
95-CO-43	39.48028	105.33000	1	7.52	2.8	9.9	910	1613	8.3	.	91.48	18.7	13.96	143	22.4	112.9	7.88	0.82	202.4	2.71	0.002	5.76	0.42	8.53	965.2	630.4	0.95
95-CO-44	39.44861	105.35028	1	6.94	6.4	7.5	610	4964	8.3	.	59	14.1	13.98	234	26.6	6.6	1.65	0.6	143	75	0.002	1	0.12	8.1	314	20	123

APPENDIX C

FITEQL INPUT AND OUTPUT FILES

INPUT FILE: Well 9-1-CO-38

```
': PROGRAM: FITEQL Version 3.2
': DATE: 03-13-1996
'Graph Information
1
1
1
1
1
10
4       1       2      34       1       0
160 X-Psi       -1.000  0.000E+00
  4 UO2[2+]     -9.000  1.000E-09
200 YOH(wk)     -4.100  7.770E-05
100 XOH(str)    -6.800  1.600E-07
300 U(ads)       0.000  0.000E+00
  3 H2CO3[2-]   -3.860  1.380E-04
 50 H[+]         0.000  0.000E+00

 50 H[+]          0.000    50   1
 51 OH[-]       -14.000    50  -1
  3 H2CO3         0.000     3   1
 31 HCO3[-]      -6.300     3   1   50  -1
 32 CO3[2-]     -16.600     3   1   50  -2
  4 UO2[2+]       0.000     4   1
401 UO2OH        -5.200     4   1   50  -1
402 UO2(OH)2    -10.300     4   1   50  -2
403 UO2(OH)3    -19.200     4   1   50  -3
404 UO2(OH)4    -33.000     4   1   50  -4
405 UO2)2(OH)    -2.700     4   2   50  -1
406 UO2)2(OH)2   -5.620     4   2   50  -2
407 UO2)3(OH)4  -11.900     4   3   50  -4
408 UO2)3(OH)5  -15.550     4   3   50  -5
409 UO2)3(OH)7  -31.000     4   3   50  -7
410 UO2)4(OH)7  -21.900     4   4   50  -7
412 UO2(CO3)     -6.900     4   1    3   1   50  -2
413 UO2(CO3)2   -16.200     4   1    3   2   50  -4
414 UO2(CO3)3   -28.170     4   1    3   3   50  -6
415 UO2-CO3-OH  -17.780     4   2    3   1   50  -5
101 XOH2[+]       6.510   160   1  100   1   50   1
100 XOH           0.000   100   1
102 XO[-]        -9.130   160  -1  100   1   50  -1
103 X(O2)UO2CO  -12.930   160  -2    4   1  100   1  300   1    3   1   50  -4
104 X(O2)UO2     -2.570     4   1  100   1  300   1   50  -2
105 XCO3H         2.900   100   1    3   1
106 XCO3[-]      -5.090   160  -1  100   1    3   1   50  -1
205 YCO3H         2.900   200   1    3   1
206 YCO3[-]      -5.090   160  -1  200   1    3   1   50  -1
201 YOH2[+]       6.510   160   1  200   1   50   1
200 YOH           0.000   200   1
202 YO[-]        -9.130   160  -1  200   1   50  -1
203 Y(O2)UO2CO  -17.020   160  -2    4   1  200   1  300   1    3   1   50  -4
204 Y(O2)UO2     -6.280     4   1  200   1  300   1   50  -2

50 H[+]
51 OH[-]
3 H2CO3
31 HCO3[-]
```

```
32 CO3[2-]
4 UO2[2+]
401 UO2OH
402 UO2(OH)2
403 UO2(OH)3
404 UO2(OH)4
405 UO2)2(OH)
406 UO2)2(OH)2
407 UO2)3(OH)4
408 UO2)3(OH)5
409 UO2)3(OH)7
410 UO2)4(OH)7
412 UO2(CO3)
413 UO2(CO3)2
414 UO2(CO3)3
415 UO2-CO3-OH
101 XOH2[+]
100 XOH
102 XO[-]
103 X(O2)UO2CO
104 X(O2)UO2
105 XCO3H
106 XCO3[-]
205 YCO3H
206 YCO3[-]
201 YOH2[+]
200 YOH
202 YO[-]
203 Y(O2)UO2CO
204 Y(O2)UO2

2  600.0000    0.0108
0.1000    1.0000

0        0        0
1        1        1        0
300    0   'Total Conc. data for Component: U(ads)
0.000E+00
50    1   'Log Free Conc. data for Component: H[+]
   -7.1000
0        0
```

```
'Graph Information
3   50    1    1 'X Axis Series Type: Species Conc. Range: [ 1
1 ]
5  103    1    1 3 'Y Axis Series( 1 ) Type: Species Conc. Range: [ 1
1 ] Format: Both
5  104    1    1 3 'Y Axis Series( 2 ) Type: Species Conc. Range: [ 1
1 ] Format: Both
5  203    1    1 3 'Y Axis Series( 3 ) Type: Species Conc. Range: [ 1
1 ] Format: Both
5  204    1    1 3 'Y Axis Series( 4 ) Type: Species Conc. Range: [ 1
1 ] Format: Both
4  300    1    1 3 'Y Axis Series( 5 ) Type: Component Sum Range: [ 1
1 ] Format: Both
1  160    0    0 3 'Y Axis Series( 6 ) Type: None Range: [ 0
0 ] Format: Both
3  1.000E+01  1.000E+00  1.000E+00 'X Axis Scale: -log Max
Min
Step
1  1.000E-09  0.000E+00  1.000E-09 'Y Axis Scale: linear Max
Min
Step
Adsorption of 10-6 U[VI] on ferrihydrite vs. pH                 'Graph Title
pH                                                              'X - Axis Title
U(VI) adsorbed                                                  'Y - Axis Title
```

FITEQL OUTPUT FILE: WELL 91-CO-38

```
FITEQL32.EXE Version 3.2 (January 15, 1996) 03-13-1996 12:11:00
Input File:      WELL381.F32
Output File:     WELL381.OUT

TABLE 1:  Chemical Equilibrium Problem

TABLE 1.1  Components
  # ID   COMPONENT  X           LOG X     T           TYPE
  1  160 X-Psi      1.000D-01   -1.000    0.000D+00    I -T
  2    4 UO2[2+]    1.000D-09   -9.000    1.000D-09    I -T
  3  200 YOH(wk)    7.943D-05   -4.100    7.770D-05    I -T
  4  100 XOH(str)   1.585D-07   -6.800    1.600D-07    I -T
  5  300 U(ads)     1.000D+00    0.000    0.000D+00   II -T,X
  6    3 H2CO3[2-]  1.380D-04   -3.860    1.380D-04  III -X
  7   50 H[+]       1.000D+00    0.000    0.000D+00  III -X
```

TABLE 1.2.1: Species, log K, and Stoichiometry Matrix A

	ID#	NAME	LOG K	X-Psi	UO2[2+]	YOH(wk)	XOH(str	U(ads)	H2CO3[2
1	50	H[+]	0.000	0.000	0.000	0.000	0.000	0.000	0.000
2	51	OH[-]	-14.000	0.000	0.000	0.000	0.000	0.000	0.000
3	3	H2CO3	0.000	0.000	0.000	0.000	0.000	0.000	1.000
4	31	HCO3[-]	-6.300	0.000	0.000	0.000	0.000	0.000	1.000
5	32	CO3[2-]	-16.600	0.000	0.000	0.000	0.000	0.000	1.000
6	4	UO2[2+]	0.000	0.000	1.000	0.000	0.000	0.000	0.000
7	401	UO2OH	-5.200	0.000	1.000	0.000	0.000	0.000	0.000
8	402	UO2(OH)2	-10.300	0.000	1.000	0.000	0.000	0.000	0.000
9	403	UO2(OH)3	-19.200	0.000	1.000	0.000	0.000	0.000	0.000
10	404	UO2(OH)4	-33.000	0.000	1.000	0.000	0.000	0.000	0.000
11	405	UO2)2(OH)	-2.700	0.000	2.000	0.000	0.000	0.000	0.000
12	406	UO2)2(OH)2	-5.620	0.000	2.000	0.000	0.000	0.000	0.000
13	407	UO2)3(OH)4	-11.900	0.000	3.000	0.000	0.000	0.000	0.000
14	408	UO2)3(OH)5	-15.550	0.000	3.000	0.000	0.000	0.000	0.000
15	409	UO2)3(OH)7	-31.000	0.000	3.000	0.000	0.000	0.000	0.000
16	410	UO2)4(OH)7	-21.900	0.000	4.000	0.000	0.000	0.000	0.000
17	412	UO2(CO3)	-6.900	0.000	1.000	0.000	0.000	0.000	1.000
18	413	UO2(CO3)2	-16.200	0.000	1.000	0.000	0.000	0.000	2.000
19	414	UO2(CO3)3	-28.170	0.000	1.000	0.000	0.000	0.000	3.000
20	415	UO2-CO3-OH	-17.780	0.000	2.000	0.000	0.000	0.000	1.000
21	101	XOH2[+]	6.510	1.000	0.000	0.000	1.000	0.000	0.000
22	100	XOH	0.000	0.000	0.000	0.000	1.000	0.000	0.000
23	102	XO[-]	-9.130	-1.000	0.000	0.000	1.000	0.000	0.000
24	103	X(O2)UO2CO	-12.930	-2.000	1.000	0.000	1.000	1.000	1.000
25	104	X(O2)UO2	-2.570	0.000	1.000	0.000	1.000	1.000	0.000
26	105	XCO3H	2.900	0.000	0.000	0.000	1.000	0.000	1.000
27	106	XCO3[-]	-5.090	-1.000	0.000	0.000	1.000	0.000	1.000
28	205	YCO3H	2.900	0.000	0.000	1.000	0.000	0.000	1.000
29	206	YCO3[-]	-5.090	-1.000	0.000	1.000	0.000	0.000	1.000
30	201	YOH2[+]	6.510	1.000	0.000	1.000	0.000	0.000	0.000
31	200	YOH	0.000	0.000	0.000	1.000	0.000	0.000	0.000
32	202	YO[-]	-9.130	-1.000	0.000	1.000	0.000	0.000	0.000
33	203	Y(O2)UO2CO	-17.020	-2.000	1.000	1.000	0.000	1.000	1.000
34	204	Y(O2)UO2	-6.280	0.000	1.000	1.000	0.000	1.000	0.000

TABLE 1.2.1: Species, log K, and Stoichiometry Matrix A

	ID#	NAME	H[+]
1	50	H[+]	1.000
2	51	OH[-]	-1.000
3	3	H2CO3	0.000
4	31	HCO3[-]	-1.000
5	32	CO3[2-]	-2.000
6	4	UO2[2+]	0.000
7	401	UO2OH	-1.000
8	402	UO2(OH)2	-2.000
9	403	UO2(OH)3	-3.000
10	404	UO2(OH)4	-4.000
11	405	UO2)2(OH)	-1.000
12	406	UO2)2(OH)2	-2.000
13	407	UO2)3(OH)4	-4.000
14	408	UO2)3(OH)5	-5.000
15	409	UO2)3(OH)7	-7.000
16	410	UO2)4(OH)7	-7.000
17	412	UO2(CO3)	-2.000
18	413	UO2(CO3)2	-4.000
19	414	UO2(CO3)3	-6.000
20	415	UO2-CO3-OH	-5.000

21	101	XOH2[+]	1.000
22	100	XOH	0.000
23	102	XO[-]	-1.000
24	103	X(O2)UO2CO	-4.000
25	104	X(O2)UO2	-2.000
26	105	XCO3H	0.000
27	106	XCO3[-]	-1.000
28	205	YCO3H	0.000
29	206	YCO3[-]	-1.000
30	201	YOH2[+]	1.000
31	200	YOH	0.000
32	202	YO[-]	-1.000
33	203	Y(O2)UO2CO	-4.000
34	204	Y(O2)UO2	-2.000

TABLE 1.2.2 Species, log K, and Stoichiometry Matrix B

	ID#	NAME	LOG K	X-Psi	UO2[2+]	YOH(wk)	XOH(str	U(ads)	H2CO3[2
1	50	H[+]	0.000	0.000	0.000	0.000	0.000	0.000	0.000
2	51	OH[-]	-14.000	0.000	0.000	0.000	0.000	0.000	0.000
3	3	H2CO3	0.000	0.000	0.000	0.000	0.000	0.000	1.000
4	31	HCO3[-]	-6.300	0.000	0.000	0.000	0.000	0.000	1.000
5	32	CO3[2-]	-16.600	0.000	0.000	0.000	0.000	0.000	1.000
6	4	UO2[2+]	0.000	0.000	1.000	0.000	0.000	0.000	0.000
7	401	UO2OH	-5.200	0.000	1.000	0.000	0.000	0.000	0.000
8	402	UO2(OH)2	-10.300	0.000	1.000	0.000	0.000	0.000	0.000
9	403	UO2(OH)3	-19.200	0.000	1.000	0.000	0.000	0.000	0.000
10	404	UO2(OH)4	-33.000	0.000	1.000	0.000	0.000	0.000	0.000
11	405	UO2)2(OH)	-2.700	0.000	2.000	0.000	0.000	0.000	0.000
12	406	UO2)2(OH)2	-5.620	0.000	2.000	0.000	0.000	0.000	0.000
13	407	UO2)3(OH)4	-11.900	0.000	3.000	0.000	0.000	0.000	0.000
14	408	UO2)3(OH)5	-15.550	0.000	3.000	0.000	0.000	0.000	0.000
15	409	UO2)3(OH)7	-31.000	0.000	3.000	0.000	0.000	0.000	0.000
16	410	UO2)4(OH)7	-21.900	0.000	4.000	0.000	0.000	0.000	0.000
17	412	UO2(CO3)	-6.900	0.000	1.000	0.000	0.000	0.000	1.000
18	413	UO2(CO3)2	-16.200	0.000	1.000	0.000	0.000	0.000	2.000
19	414	UO2(CO3)3	-28.170	0.000	1.000	0.000	0.000	0.000	3.000
20	415	UO2-CO3-OH	-17.780	0.000	2.000	0.000	0.000	0.000	1.000
21	101	XOH2[+]	6.510	1.000	0.000	0.000	1.000	0.000	0.000
22	100	XOH	0.000	0.000	0.000	0.000	1.000	0.000	0.000
23	102	XO[-]	-9.130	-1.000	0.000	0.000	1.000	0.000	0.000
24	103	X(O2)UO2CO	-12.930	-2.000	1.000	0.000	1.000	1.000	1.000
25	104	X(O2)UO2	-2.570	0.000	1.000	0.000	1.000	1.000	0.000
26	105	XCO3H	2.900	0.000	0.000	0.000	1.000	0.000	1.000
27	106	XCO3[-]	-5.090	-1.000	0.000	0.000	1.000	0.000	1.000
28	205	YCO3H	2.900	0.000	0.000	1.000	0.000	0.000	1.000
29	206	YCO3[-]	-5.090	-1.000	0.000	1.000	0.000	0.000	1.000
30	201	YOH2[+]	6.510	1.000	0.000	1.000	0.000	0.000	0.000
31	200	YOH	0.000	0.000	0.000	1.000	0.000	0.000	0.000
32	202	YO[-]	-9.130	-1.000	0.000	1.000	0.000	0.000	0.000
33	203	Y(O2)UO2CO	-17.020	-2.000	1.000	1.000	0.000	1.000	1.000
34	204	Y(O2)UO2	-6.280	0.000	1.000	1.000	0.000	1.000	0.000

TABLE 1.2.2 Species, log K, and Stoichiometry Matrix B

	ID#	NAME	H[+]
1	50	H[+]	1.000
2	51	OH[-]	-1.000
3	3	H2CO3	0.000
4	31	HCO3[-]	-1.000
5	32	CO3[2-]	-2.000
6	4	UO2[2+]	0.000
7	401	UO2OH	-1.000
8	402	UO2(OH)2	-2.000
9	403	UO2(OH)3	-3.000
10	404	UO2(OH)4	-4.000
11	405	UO2)2(OH)	-1.000
12	406	UO2)2(OH)2	-2.000
13	407	UO2)3(OH)4	-4.000
14	408	UO2)3(OH)5	-5.000
15	409	UO2)3(OH)7	-7.000
16	410	UO2)4(OH)7	-7.000
17	412	UO2(CO3)	-2.000
18	413	UO2(CO3)2	-4.000
19	414	UO2(CO3)3	-6.000
20	415	UO2-CO3-OH	-5.000
21	101	XOH2[+]	1.000
22	100	XOH	0.000
23	102	XO[-]	-1.000
24	103	X(O2)UO2CO	-4.000
25	104	X(O2)UO2	-2.000
26	105	XCO3H	0.000
27	106	XCO3[-]	-1.000
28	205	YCO3H	0.000
29	206	YCO3[-]	-1.000
30	201	YOH2[+]	1.000
31	200	YOH	0.000
32	202	YO[-]	-1.000
33	203	Y(O2)UO2CO	-4.000
34	204	Y(O2)UO2	-2.000

TABLE 1.3: Electric Double Layer Model

Gouy - Chapman Model
S (M^2/G) = 6.000D+02 A (g/L) = 1.080D-02
Electrolyte Concentration (mol/L) = 1.000D-01
Electrolyte Valence = 1.000D+00

TABLE 2: Input Data for Verification -
Serial Data and Estimated Standard Deviation

TABLE 2.1 Total Concentration for Components

#	U(ads)
1	0.000D+00

TABLE 2.2 Free Concentration for Components

#	LOG H[+]
1	-7.100D+00

TABLE 2.4 Standard Deviation of Total Concentration

Component	Relative	Absolute
U(ads)	1.000D-02	1.000D-06

TABLE 2.5 Standard Deviation of Free Concentration

Component	Relative	Absolute
H[+]	2.303D-02	0.000D+00

0.00000

TABLE 4: Description of Chemical Equilibrium

TABLE 4.1 Description of Chemical Equilibrium: T, Y

	T U(ads)	Y U(ads)	T H2CO3[2-]	Y H2CO3[2-]	T H[+]	Y H[+]
1	0.000D+00	9.224D-10	1.380D-04	8.808D-04	0.000D+00	-8.707D-04

TABLE 4.2 Description of Chemical Equilibrium: log C

	H[+]	OH[-]	H2CO3	HCO3[-]	CO3[2-]	UO2[2+]
1	-7.100	-6.900	-3.860	-3.060	-6.260	-14.731

TABLE 4.2 Description of Chemical Equilibrium: log C

	UO2OH	UO2(OH)2	UO2(OH)3	UO2(OH)4	(UO2)2(OH)	(UO2)2(OH)2
1	-12.831	-10.831	-12.631	-19.331	-25.061	-20.881

TABLE 4.2 Description of Chemical Equilibrium: log C

	(UO2)3(OH)4	(UO2)3(OH)5	(UO2)3(OH)7	(UO2)4(OH)7	UO2(CO3)	UO2(CO3)2
1	-27.692	-24.242	-25.492	-31.123	-11.291	-10.251

TABLE 4.2 Description of Chemical Equilibrium: log C

	UO2(CO3)3	UO2-CO3-OH	XOH2[+]	XOH	XO[-]	X(O2)UO2CO
1	-11.881	-15.601	-7.948	-6.901	-8.473	-9.107

TABLE 4.2 Description of Chemical Equilibrium: log C

	X(O2)UO2	XCO3H	XCO3[-]	YCO3H	YCO3[-]	YOH2[+]
1	-10.002	-7.861	-8.293	-5.172	-5.605	-5.260

TABLE 4.2 Description of Chemical Equilibrium: log C

	YOH	YO[-]	Y(O2)UO2CO	Y(O2)UO2
1	-4.212	-5.785	-10.508	-11.023

TABLE 4.3 Description of Chemical Equilibrium: C (mol/L)

	H[+]	OH[-]	H2CO3	HCO3[-]	CO3[2-]	UO2[2+]
1	7.943D-08	1.259D-07	1.380D-04	8.710D-04	5.495D-07	1.859D-15

TABLE 4.3 Description of Chemical Equilibrium: C (mol/L)

	UO2OH	UO2(OH)2	UO2(OH)3	UO2(OH)4	(UO2)2(OH)	(UO2)2(OH)2
1	1.477D-13	1.477D-11	2.340D-13	4.670D-20	8.681D-26	1.314D-21

TABLE 4.3 Description of Chemical Equilibrium: C (mol/L)

	(UO2)3(OH)4	(UO2)3(OH)5	(UO2)3(OH)7	(UO2)4(OH)7	UO2(CO3)	UO2(CO3)2
1	2.032D-28	5.727D-25	3.220D-26	7.537D-32	5.120D-12	5.614D-11

TABLE 4.3 Description of Chemical Equilibrium: C (mol/L)

	UO2(CO3)3	UO2-CO3-OH	XOH2[+]	XOH	XO[-]	X(O2)UO2CO
1	1.316D-12	2.504D-16	1.126D-08	1.256D-07	3.362D-09	7.822D-10

TABLE 4.3 Description of Chemical Equilibrium: C (mol/L)

	X(O2)UO2	XCO3H	XCO3[-]	YCO3H	YCO3[-]	YOH2[+]
1	9.963D-11	1.378D-08	5.088D-09	6.727D-06	2.485D-06	5.500D-06

TABLE 4.3 Description of Chemical Equilibrium: C (mol/L)

```
      YOH         YO[-]      Y(O2)UO2CO Y(O2)UO2
 1     6.135D-05  1.642D-06  3.105D-11  9.486D-12

TABLE 4.4  Description of Chemical Equilibrium: log X
      X-Psi    UO2[2+] YOH(wk) XOH(str U(ads)  H2CO3[2 H[+]
 1     -0.457 -14.731  -4.212  -6.901   0.000  -3.860  -7.100

TABLE 4.5  Description of Chemical Equilibrium: X (mol/L)
      X-Psi       UO2[2+]     YOH(wk)     XOH(str)    U(ads)      H2CO3[2-]
 1     3.488D-01  1.859D-15  6.135D-05  1.256D-07  1.000D+00  1.380D-04

TABLE 4.5  Description of Chemical Equilibrium: X (mol/L)
      H[+]
 1     7.943D-08

TABLE 4.6  Description of Chemical Equilibrium: Electrostatics
      TO (mol/L) (C/M^2)     LOG XO      PSIO(V)
 1     1.375D-06  2.047D-02 -4.575D-01  2.706D-02


TABLE 4.8  Estimate Standard Deviation in Experimental Data: ST, SX
      ST          SX
      U(ads)      H[+]
 1     1.000D-06  1.829D-09

TABLE 5:  INTERMEDIATE QUANTITIES IN OPTIMIZATION PROCEDURE:
          VALUES FOR Y OF GROUP II COMPONENT: U(ads)

TABLE 5.1  Derivatives for Propagation of Error: (dY/dT), (dY/dX)
      (dY/dT)     (dY/dT)     (dY/dT)     (dY/dT)     (dY/dT)     (dY/dX)
      X-Psi       UO2[2+]     YOH(wk)     XOH(str)    U(ads)      U(ads)
 1     0.000D+00  0.000D+00  0.000D+00  0.000D+00  0.000D+00  0.000D+00

TABLE 5.1  Derivatives for Propagation of Error: (dY/dT), (dY/dX)
      (dY/dX)     (dY/dX)
      H2CO3[2-]   H[+]
 1     0.000D+00  0.000D+00

TABLE 5.2  Terms in Equation for Propagation of Error:
           ((dY/dT)*ST)^2,  ((dY/dX)*SX)^2
      T           X
      U(ads)      H[+]
 1     0.000D+00  0.000D+00

TABLE 5.3  Terms in Weighted Sum of Squares
      SY*SY       SY          Y           Y/SY        (Y/SY)^2    T
 1     0.000D+00  0.000D+00  0.000D+00  9.999D+37  9.999D+37  0.000D+00

TABLE 5.3  Terms in Weighted Sum of Squares
      Y/T
 1     9.999D+37

TABLE 6:  OPTIMIZATION PROCEDURE
          VALUES FOR Y OF GROUP II COMPONENT: U(ads)
```

APPENDIX D

"BATS" PROGRAM

Instructions:

1) Use model configuration in Appendix C, and save this as TEMPLATE.F32. Check values in TEMPLATE.F32, save as TEMPLATE.

2) Type "qbasic makebat". Use Shift F5 to run the module. The program will ask for pH and bicarbonate concentrations. When complete, exit Qbasic.

3) Type Vampire. The program will run through the batch file. Make sure it completes the run.

4) Type "qbasic outint", (Shift F5 to run), The program will ask for a file name. When complete, It will compile the data in a spreadsheet importable file with pH vs. bound U.

The quickbasic files are provided below for those who might wish to modify the template or do any other changes which would change the positioning of the lines in the in or output files.

Part 1: Makebat

```
OPEN "vampire.bat" FOR OUTPUT AS 1

INPUT "6-letter file name"; nf$
INPUT "H2CO3[2-] (log carb conc)"; h2co31: h2co32 = 10 ^ h2co31
INPUT "pH"; ph: ph = -ph

FOR u2 = -9 TO -1 STEP .5

OPEN "template" FOR INPUT AS 3

nfum = nfum + 1
nfum$ = STR$(nfum)
nfum$ = RIGHT$(nfum$, LEN(nfum$) - 1): REM get rid of blank at start
nf1$ = nf$ + nfum$ + ".f32"
PRINT #1, "fiteql32     " + nf1$

OPEN nf1$ FOR OUTPUT AS 2

FOR i = 1 TO 11
 INPUT #3, a$
 PRINT #2, a$
```

```
NEXT
INPUT #3, a$
PRINT #2, USING "     4 UO2[2+]     ##.### ##.###^^^^"; u2; 10 ^ u2

FOR i = 1 TO 3
 INPUT #3, a$
 PRINT #2, a$
NEXT
INPUT #3, a$
PRINT #2, USING "     3 H2CO3[2-]   ##.### ##.###^^^^"; h2co31; h2co32
FOR i = 1 TO 80
 INPUT #3, a$
 PRINT #2, a$
NEXT

INPUT #3, a$
PRINT #2, USING "   ##.####"; ph

FOR i = 1 TO 26
 INPUT #3, a$
 PRINT #2, a$
NEXT

CLOSE 2
CLOSE 3

NEXT u2

CLOSE 1
```

Part 2: OutInt

```
INPUT "Output file name"; onf$
OPEN onf$ FOR OUTPUT AS 1

PRINT #1, "LOG(U)     X(O2)UO2CO   X(O2)UO2    Y(O2)UO2CO    Y(O2)U02"

OPEN "vampire.bat" FOR INPUT AS 2

5 INPUT #2, a$
ON ERROR GOTO 10
b$ = RIGHT$(a$, 12)
c$ = LEFT$(b$, 8) + ".out"
6 IF LEFT$(c$, 1) = " " THEN c$ = RIGHT$(c$, LEN(c$) - 1): GOTO 6

OPEN c$ FOR INPUT AS 3

1 INPUT #3, a$
IF LEFT$(a$, 9) = "TABLE 1.1" THEN
 INPUT #3, b$, c$, d$
```

```
 logu = VAL(MID$(d$, 31, 9))
 GOTO 1
END IF

IF LEFT$(a$, 9) = "TABLE 4.2" THEN
 l = l + 1
 IF l = 4 THEN
  INPUT #3, b$, c$
  v1 = VAL(RIGHT$(c$, 9)): REM X...CO
 END IF
 IF l = 5 THEN
  INPUT #3, b$, c$
  v2 = VAL(MID$(c$, 5, 9)): REM X...
 END IF
 IF l = 6 THEN
  INPUT #3, b$, c$
  v3 = VAL(MID$(c$, 27, 9)): REM Y...CO
  v4 = VAL(RIGHT$(c$, 9)): REM Y...
 END IF
END IF

IF l = 6 THEN 3
GOTO 1

3 l = 0

PRINT #1, USING "###.###      ###.###     ###.###      ###.###      ###.###";
logu; v1; v2; v3; v4
CLOSE 3
GOTO 5

10 CLOSE 1
END: REM To here after end oif bat file
```

APPENDIX E

SURFACE COMPLEXATION MODEL CALCULATION WORKSHEET

Appendix E - Surface Complexation Model: Calculation Worksheet

Sample$	Rock	pH	Rn (pCi/L)	U ppb	Log Ueq (moles/L)	HCO_3 (mg/L)	Alk (moles/L)	Ct	H2CO3*	log H2CO3	Log Γ	Γ	Trans (ft2/day)	aperture (cm)	aperture (m)	Enrichment Calcs			
																U conc (ug/L)	^{238}U activity	iron-oxide g/L	iron oxide g/m2
95-CO-38	1	7.67	879	9.6	-7.39	76	0.0012	1.30E-03	5.30E-05	-4.28	-3.01	9.87E-04	2.3	0.016	1.57E-04	1154	381.99	2.30	0.18
95-CO-32	1	7.06	2935	5.3	-7.65	112	0.0018	2.15E-03	3.19E-04	-3.50	-3.32	4.84E-04	49	0.043	4.35E-04	566	187.28	15.67	3.41
95-CO-29	1	6.91	3346	3.2	-7.87	108	0.0018	2.20E-03	4.34E-04	-3.36	-3.48	3.34E-04				390	129.12	25.91	
95-CO-34	1	6.85	2771	1.7	-8.15	108	0.0018	2.27E-03	4.99E-04	-3.30	-3.69	2.06E-04	2.6	0.016	1.63E-04	242	79.94	34.66	2.83
95-CO-40	1	8.19	1577	13.9	-7.23	146	0.0024	2.40E-03	3.06E-05	-4.51	-3.07	8.50E-04	3.9	0.019	1.87E-04	995	329.16	4.79	0.45
95-CO-43	1	7.52	1613	8.3	-7.46	142	0.0023	2.46E-03	1.40E-04	-3.85	-3.23	5.88E-04	0.95	0.012	1.17E-04	688	227.56	7.09	0.41
91-CO-42	2	7.55	6321	17.1	-7.14	144	0.0024	2.49E-03	1.32E-04	-3.88	-3.02	9.49E-04	0.804	0.011	1.10E-04	1110	367.27	17.21	0.95
95-CO-36	1	6.94	2646	5.8	-7.61	128	0.0021	2.58E-03	4.80E-04	-3.32	-3.36	4.40E-04	1.2	0.013	1.26E-04	515	170.43	15.53	0.98
95-CO-35	1	6.89	1605	8.5	-7.45	132	0.0022	2.72E-03	5.56E-04	-3.25	-3.26	5.45E-04	2.5	0.016	1.61E-04	637	210.91	7.61	0.61
91-CO-29	1	7.90	3198	6.1	-7.59	165	0.0027	2.75E-03	6.74E-05	-4.17	-3.37	4.28E-04	1.072	0.012	1.22E-04	500	165.53	19.32	1.17
88-CO-44	2	6.60	1510	1.6	-8.17	114	0.0019	2.81E-03	9.38E-04	-3.03	-3.80	1.59E-04	109.88	0.057	5.69E-04	186	61.56	24.53	6.98
91-CO-28	1	7.85	2746	19.0	-7.10	171	0.0028	2.87E-03	7.87E-05	-4.10	-3.05	8.90E-04	1.072	0.012	1.22E-04	1041	344.51	7.97	0.48
95-CO-30	1	7.16	6552	7.5	-7.50	156	0.0026	2.91E-03	3.53E-04	-3.45	-3.33	4.67E-04	14.5	0.029	2.90E-04	546	180.62	36.27	5.25
95-CO-33	1	8.02	2770	5.0	-7.68	180	0.0030	2.99E-03	5.59E-05	-4.25	-3.47	3.40E-04	0.13	0.006	6.02E-05	398	131.78	21.02	0.63
91-CO-27	1	7.65	3646	17.0	-7.15	178	0.0029	3.03E-03	1.30E-04	-3.89	-3.11	7.81E-04	1.34	0.013	1.31E-04	914	302.47	12.05	0.79
95-CO-37	1	7.54	2563	9.5	-7.40	176	0.0029	3.05E-03	1.66E-04	-3.78	-3.28	5.23E-04	3.4	0.018	1.79E-04	612	202.48	12.66	1.13
91-CO-33	2	7.10	2081	2.7	-7.95	166	0.0027	3.15E-03	4.31E-04	-3.37	-3.69	2.05E-04	3.618	0.018	1.82E-04	240	79.50	26.17	2.39
92-CO-20	2	7.30	3197	18.6	-7.11	175	0.0029	3.15E-03	2.87E-04	-3.54	-3.10	7.95E-04				931	307.93	10.38	
95-CO-26	1	7.57	2988	6.9	-7.54	184	0.0030	3.17E-03	1.62E-04	-3.79	-3.40	4.00E-04	10	0.026	2.56E-04	468	154.75	19.31	2.47
95-CO-25	1	7.76	2816	14.0	-7.23	192	0.0031	3.25E-03	1.09E-04	-3.96	-3.20	6.36E-04	15.4	0.030	2.96E-04	744	246.08	11.44	1.69
92-CO-19	1	7.60	3714	21.5	-7.04	194	0.0032	3.33E-03	1.59E-04	-3.80	-3.08	8.26E-04	4.69	0.020	1.99E-04	966	319.76	11.62	1.15
91-CO-31	1	7.25	1604	15.0	-7.20	183	0.0030	3.33E-03	3.36E-04	-3.47	-3.19	6.46E-04	335	0.082	8.25E-04	756	250.23	6.41	2.64
91-CO-34	2	7.88	1022	39.0	-6.79	200	0.0033	3.35E-03	8.59E-05	-4.07	-2.92	1.22E-03	5.762	0.021	2.13E-04	1422	470.64	2.17	0.23
95-CO-31	1	6.65	5276	5.9	-7.61	148	0.0024	3.51E-03	1.08E-03	-2.97	-3.50	3.16E-04	70	0.049	4.90E-04	370	122.35	43.12	10.55
95-CO-28	1	7	2985	3.0	-7.90	180	0.0030	3.54E-03	5.88E-04	-3.23	-3.72	1.91E-04	14.4	0.029	2.89E-04	224	74.05	40.31	5.83
88-CO-45	1	6.63	3830	3.1	-7.89	149	0.0024	3.58E-03	1.14E-03	-2.94	-3.72	1.91E-04	375.2	0.086	8.57E-04	223	73.95	51.79	22.18
91-CO-03B	1	7.70	3825	40.0	-6.77	211	0.0035	3.58E-03	1.37E-04	-3.86	-2.94	1.15E-03	2.144	0.015	1.53E-04	1342	443.92	8.62	0.66
91-CO-35	2	7.30	1543	8.3	-7.46	199	0.0033	3.58E-03	3.26E-04	-3.49	-3.41	3.92E-04	2.278	0.016	1.56E-04	459	151.73	10.17	0.79
91-CO-15	1	7.80	2145	15.4	-7.19	218	0.0036	3.67E-03	1.13E-04	-3.95	-3.23	5.84E-04	1.474	0.014	1.35E-04	683	225.98	9.49	0.64
92-CO-21	2	7.35	4361	26.7	-6.95	217	0.0036	3.87E-03	3.17E-04	-3.50	-3.10	7.94E-04	3.752	0.018	1.85E-04	929	307.56	14.18	1.31
95-CO-07	1	7.55	2757	32.4	-6.87	234	0.0038	4.04E-03	2.15E-04	-3.67	-3.07	8.54E-04	6.2	0.022	2.18E-04	999	330.69	8.34	0.91
88-CO-43	2	7.11	4110	32.0	-6.87	234	0.0038	4.43E-03	5.94E-04	-3.23	-3.13	7.45E-04	160.8	0.065	6.46E-04	872	288.44	14.25	4.60
95-CO-15	1	7.35	8430	14.8	-7.21	250	0.0041	4.46E-03	3.65E-04	-3.44	-3.36	4.32E-04	0.93	0.012	1.16E-04	506	167.30	50.39	2.92
95-CO-44	1	6.94	4964	8.3	-7.46	234	0.0038	4.71E-03	8.78E-04	-3.06	-3.58	2.61E-04	123	0.059	5.91E-04	305	100.91	49.19	14.53
91-CO-41	2	7.00	4052	19.0	-7.10	282	0.0046	5.54E-03	9.22E-04	-3.04	-3.45	3.54E-04				415	137.19	29.54	
95-CO-03	1	7.2	11560	79.0	-6.48	326	0.0053	6.01E-03	6.72E-04	-3.17	-3.08	8.24E-04	2.3	0.016	1.57E-04	964	318.97	36.24	2.84
93-CO-01	4	7.61	4464	6.7	-7.55	20	0.0003	3.38E-04	1.58E-05	-4.80	-2.76	1.72E-03	4.288	0.019	1.93E-04	2013	666.20	6.70	0.65
91-CO-14	4	6.40	5471	0.8	-8.46	16	0.0003	4.71E-04	2.09E-04	-3.68	-3.42	3.82E-04				447	147.83	37.01	
95-CO-08	4	7.24	4286	3.4	-7.85	36	0.0006	6.57E-04	6.77E-05	-4.17	-3.02	9.49E-04				1111	367.56	11.66	
92-CO-16	4	6.90	20527	3.0	-7.91	35	0.0006	7.11E-04	1.43E-04	-3.85	-3.08	8.40E-04	10.854	0.026	2.63E-04	983	325.30	63.10	8.30
88-CO-29	4	6.30	6190	0.6	-8.62	22	0.0004	7.28E-04	3.64E-04	-3.44	-3.59	2.56E-04	1058.6	0.121	1.21E-03	299	98.92	62.58	37.87
92-CO-15a	4	7.30	7745	1.6	-8.17	41	0.0007	7.38E-04	6.71E-05	-4.17	-3.27	5.41E-04	0.804	0.011	1.10E-04	633	209.30	37.00	2.04
92-CO-11	4	7.40	15603	1.3	-8.27	43	0.0007	7.51E-04	5.53E-05	-4.26	-3.34	4.58E-04	64.32	0.048	4.76E-04	536	177.43	87.94	20.93
91-CO-22	4	6.55	7969	0.6	-8.63	31	0.0005	7.81E-04	2.81E-04	-3.55	-3.61	2.47E-04	2000	0.150	1.50E-03	289	95.49	83.46	62.44
95-CO-09	4	7.3	3669	3.7	-7.81	46	0.0008	8.28E-04	7.53E-05	-4.12	-3.03	9.32E-04	5	0.020	2.03E-04	1090	360.64	10.17	1.03
91-CO-24	4	6.60	7242	1.5	-8.20	36	0.0006	8.86E-04	2.96E-04	-3.53	-3.32	4.82E-04	4.556	0.020	1.97E-04	564	186.72	38.79	3.82
91-CO-09	4	6.88	9534	1.8	-8.12	44	0.0007	9.01E-04	1.88E-04	-3.73	-3.26	5.45E-04	656.6	0.103	1.03E-03	638	211.11	45.16	23.31
91-CO-19	4	6.40	4877	0.8	-8.47	31	0.0005	9.12E-04	4.04E-04	-3.39	-3.52	3.05E-04	0.804	0.011	1.10E-04	356	117.95	41.35	2.28
95-CO-41	4	6.69	8009	0.4	-8.74	42	0.0007	9.69E-04	2.80E-04	-3.55	-3.73	1.85E-04	5.9	0.021	2.15E-04	216	71.56	111.91	12.01
93-CO-04	4	7.40	15771	7.8	-7.48	55	0.0009	9.72E-04	7.15E-05	-4.15	-2.84	1.45E-03	21.44	0.033	3.30E-04	1691	559.47	28.19	4.65
91-CO-38a	4	7.10	11268	4.0	-7.77	87	0.0009	1.01E-03	1.38E-04	-3.86	-3.04	9.06E-04	17.42	0.031	3.08E-04	1059	350.57	32.14	4.95
91-CO-21	4	6.71	6151	0.7	-8.54	45	0.0007	1.01E-03	2.84E-04	-3.55	-3.59	2.55E-04				299	98.81	62.25	
91-CO-01B	4	6.40	10465	0.6	-8.63	35	0.0006	1.03E-03	4.56E-04	-3.34	-3.66	2.19E-04	2.144	0.015	1.53E-04	256	84.80	123.40	9.45
92-CO-17	4	6.80	5748	1.2	-8.30	49	0.0008	1.06E-03	2.54E-04	-3.59	-3.42	3.77E-04	129.98	0.060	6.02E-04	441	145.84	39.41	11.86
91-CO-17	4	6.26	11262	0.6	-8.58	31	0.0005	1.07E-03	5.61E-04	-3.25	-3.63	2.34E-04				274	90.73	124.13	
91-CO-20	4	6.84	13203	5.8	-7.61	51	0.0008	1.08E-03	2.42E-04	-3.62	-2.95	1.13E-03	2.68	0.017	1.65E-04	1322	437.43	30.18	2.49
88-CO-37	4	5.80	14800	1.3	-8.28	16	0.0003	1.09E-03	8.26E-04	-3.08	-3.41	3.87E-04	30.82	0.037	3.72E-04	453	149.95	98.70	18.38
91-CO-37	4	7.61	1517	1.7	-8.15	64	0.0010	1.10E-03	5.13E-05	-4.29	-3.32	4.78E-04	1.206	0.013	1.26E-04	560	185.19	8.19	0.52
91-CO-11	4	7.00	10404	0.9	-8.42	56	0.0009	1.10E-03	1.83E-04	-3.74	-3.52	3.01E-04	576.2	0.099	9.88E-04	353	116.65	89.19	44.08
92-CO-14	4	6.32	11809	1.5	-8.21	36	0.0006	1.15E-03	5.61E-04	-3.25	-3.38	4.19E-04	32.16	0.038	3.78E-04	490	162.23	72.79	13.75
95-CO-21	4	7.75	5352	4.5	-7.72	68	0.0011	1.15E-03	3.94E-05	-4.40	-3.04	9.22E-04				1079	357.06	14.99	
95-CO-39	4	6.81	3741	7.3	-7.51	54	0.0009	1.16E-03	2.73E-04	-3.56	-2.89	1.27E-03	272	0.077	7.70E-04	1491	493.32	7.58	2.92

Appendix E - Surface Complexation Model: Calculation Worksheet

Sample$	Rock	pH	Rn	U	Log Ueq	HCO_3	Alk	Ct	H2CO3*	log H2CO3	Log Γ	Γ	Trans	aperture (cm)	aperture (m)	Enrichment Calcs			
			(pCi/L)	ppb	(moles/L)	(mg/L)	(moles/L)						(ft2/day)			U conc (ug/L)	^{238}U activity	iron-oxide g/L	iron oxide g/m2
91-CO-25	4	6.38	22740	1.7	-8.15	40	0.0007	1.21E-03	5.50E-04	-3.26	-3.34	4.54E-04	32.16	0.038	3.78E-04	531	175.82	129.34	24.43
92-CO-09	4	7.75	17551	133.0	-6.25	78	0.0013	1.31E-03	4.49E-05	-4.35	-2.14	7.26E-03	0.536	0.010	9.65E-05	8496	2811.44	6.24	0.30
92-CO-01	4	6.90	21216	7.8	-7.48	65	0.0011	1.33E-03	2.67E-04	-3.57	-2.91	1.24E-03	4.422	0.019	1.95E-04	1446	478.65	44.33	4.32
95-CO-24	4	8.42	18250	37.9	-6.80	84	0.0014	1.37E-03	1.03E-05	-4.99	-2.47	3.36E-03	1.4	0.013	1.33E-04	3930	1300.48	14.03	0.93
95-CO-42	4	6.43	3499	1.9	-8.10	48	0.0008	1.37E-03	5.83E-04	-3.23	-3.34	4.57E-04	1.2	0.013	1.26E-04	535	176.90	19.78	1.25
91-CO-18	4	6.35	11428	0.9	-8.41	52	0.0009	1.61E-03	7.59E-04	-3.12	-3.62	2.41E-04	2000	0.150	1.50E-03	282	93.34	122.43	91.61
91-CO-10	4	6.60	12770	1.5	-8.20	68	0.0011	1.66E-03	5.55E-04	-3.26	-3.47	3.37E-04	2000	0.150	1.50E-03	394	130.51	97.85	73.21
95-CO-11	4	7.19	10125	5.8	-7.61	90	0.0015	1.66E-03	1.90E-04	-3.72	-3.06	8.73E-04	262	0.076	7.60E-04	1022	338.13	29.94	11.38
91-CO-26	4	7.55	2100	29.0	-6.91	99	0.0016	1.71E-03	9.11E-05	-4.04	-2.61	2.46E-03	0.938	0.012	1.16E-04	2883	953.95	2.20	0.13
91-CO-23	4	6.62	9460	4.3	-7.74	73	0.0012	1.77E-03	5.74E-04	-3.24	-3.17	6.77E-04	8.04	0.024	2.38E-04	792	262.03	36.10	4.30
95-CO-14	4	8.25	8815	11.7	-7.31	112	0.0018	1.84E-03	2.04E-05	-4.69	-2.89	1.30E-03	1.7	0.014	1.42E-04	1518	502.37	17.55	1.24
95-CO-22	4	7.62	6290	8.0	-7.47	108	0.0018	1.85E-03	8.45E-05	-4.07	-3.00	1.00E-03	2.4	0.016	1.59E-04	1171	387.50	16.23	1.29
95-CO-12	4	7.2	8613	5.6	-7.63	102	0.0017	1.88E-03	2.10E-04	-3.68	-3.11	7.75E-04	4.4	0.019	1.95E-04	906	299.92	28.72	2.79
95-CO-19	4	7.81	4213	13.7	-7.24	116	0.0019	1.95E-03	5.86E-05	-4.23	-2.86	1.37E-03	1.1	0.012	1.23E-04	1604	530.73	7.94	0.49
95-CO-20	4	8.13	8631	13.0	-7.26	120	0.0020	1.98E-03	2.89E-05	-4.54	-2.88	1.31E-03	106	0.056	5.62E-04	1531	506.50	17.04	4.79
95-CO-18	4	7.14	3176	22.2	-7.03	108	0.0018	2.02E-03	2.56E-04	-3.59	-2.74	1.82E-03	5.7	0.021	2.12E-04	2131	705.18	4.50	0.48
95-CO-02	4	7.42	7743	175.0	-6.13	122	0.0020	2.15E-03	1.51E-04	-3.82	-2.21	6.12E-03				7163	2370.39	3.27	
91-CO-12	4	7.00	22211	75.0	-6.50	113	0.0018	2.22E-03	3.69E-04	-3.43	-2.44	3.61E-03	0.402	0.009	8.77E-05	4218	1395.73	15.91	0.70
95-CO-23	4	7.33	7216	4.1	-7.76	126	0.0021	2.26E-03	1.93E-04	-3.72	-3.28	5.28E-04	367	0.085	8.50E-04	618	204.43	35.30	15.01
95-CO-17	4	6.47	5677	7.9	-7.48	84	0.0014	2.31E-03	9.31E-04	-3.03	-3.09	8.13E-04	13.2	0.028	2.81E-04	951	314.62	18.04	2.53
91-CO-13	4	7.30	8490	9.7	-7.39	143	0.0023	2.58E-03	2.34E-04	-3.63	-3.08	8.32E-04	37.52	0.040	3.98E-04	973	322.02	26.36	5.24
95-CO-05	4	7.04	4514	4.1	-7.76	136	0.0022	2.63E-03	4.05E-04	-3.39	-3.35	4.46E-04	178	0.067	6.68E-04	522	172.65	26.14	8.73
91-CO-05	4	6.93	10700	20.0	-7.08	130	0.0021	2.64E-03	5.01E-04	-3.30	-2.88	1.31E-03	0.804	0.011	1.10E-04	1537	508.64	21.04	1.16
92-CO-18	4	7.90	3355	8.3	-7.46	158	0.0026	2.64E-03	6.48E-05	-4.19	-3.14	7.28E-04	2.144	0.015	1.53E-04	852	281.77	11.91	0.91
88-CO-42	4	6.28	1340	0.5	-8.67	82	0.0013	2.76E-03	1.41E-03	-2.85	-4.05	8.87E-05	348.4	0.084	8.36E-04	104	34.35	39.01	16.30
91-CO-06	4	7.90	7200	24.0	-7.00	166	0.0027	2.77E-03	6.79E-05	-4.17	-2.85	1.40E-03	4.422	0.019	1.95E-04	1637	541.81	13.29	1.30
91-CO-08	4	6.71	10100	1.7	-8.15	126	0.0021	2.87E-03	8.03E-04	-3.10	-3.67	2.12E-04	2000	0.150	1.50E-03	248	81.98	123.20	92.18
95-CO-06	4	6.98	2743	2.9	-7.91	148	0.0024	2.93E-03	5.07E-04	-3.30	-3.52	3.04E-04	820	0.111	1.11E-03	356	117.82	23.28	12.94
91-CO-07	4	6.99	10700	11.0	-7.34	149	0.0024	2.95E-03	5.00E-04	-3.30	-3.11	7.71E-04	1.206	0.013	1.26E-04	902	298.62	35.83	2.27
95-CO-13	4	7.33	9667	8.5	-7.45	170	0.0028	3.04E-03	2.60E-04	-3.59	-3.21	6.20E-04	2.9	0.017	1.69E-04	725	240.02	40.28	3.41
95-CO-27	4	7.65	6466	47.9	-6.70	184	0.0030	3.14E-03	1.34E-04	-3.87	-2.73	1.87E-03	0.5	0.009	9.43E-05	2190	724.56	8.92	0.42
91-CO-16	4	7.50	13411	22.0	-7.03	182	0.0030	3.17E-03	1.88E-04	-3.73	-2.95	1.12E-03	2.814	0.017	1.68E-04	1309	433.22	30.96	2.60
92-CO-13	4	6.60	3391	0.4	-8.75	143	0.0023	3.52E-03	1.17E-03	-2.93	-4.27	5.32E-05	119.26	0.058	5.85E-04	62	20.59	164.66	48.14
95-CO-04	4	7.45	14055	24.0	-7.00	214	0.0035	3.75E-03	2.48E-04	-3.61	-3.03	9.27E-04				1085	358.89	39.16	
95-CO-16	4	7.72	8290	11.5	-7.32	252	0.0041	4.28E-03	1.57E-04	-3.81	-3.35	4.48E-04	7.4	0.023	2.31E-04	524	173.52	47.77	5.53
88-CO-34	3	7.10	8390	0.87	-8.44	14	0.0002	2.73E-04	3.74E-05	-4.43	-3.35	4.48E-04				524	173.28	48.42	
88-CO-22	3	7.40	3890	0.73	-8.51	16	0.0003	2.82E-04	2.07E-05	-4.68	-3.40	3.95E-04	3.216	0.018	1.75E-04	463	153.06	25.41	2.23
88-CO-24	3	6.72	15850	0.33	-8.86	21	0.0003	4.66E-04	1.28E-04	-3.89	-3.72	1.92E-04	4.154	0.019	1.91E-04	224	74.26	213.44	20.38
89CO-20	3	6.01	6368	1.7	-8.15	17	0.0003	8.43E-04	5.57E-04	-3.25	-3.33	4.69E-04	3.752	0.018	1.85E-04	549	181.54	35.08	3.24
89CO-12	3	6.30	27240	2.2	-8.03	27	0.0004	8.87E-04	4.43E-04	-3.35	-3.26	5.55E-04	2.278	0.016	1.56E-04	650	214.96	126.72	9.90
91-CO-40	3	7.00	13200	7.2	-7.52	47.75	0.0008	9.38E-04	1.56E-04	-3.81	-2.93	1.18E-03	6.03	0.022	2.16E-04	1386	458.59	28.78	3.11
88-CO-26	3	7.40	4100	28.0	-6.93	53	0.0009	9.45E-04	6.96E-05	-4.16	-2.55	2.80E-03	388.6	0.087	8.67E-04	3278	1084.54	3.78	1.64
88-CO-31	3	6.62	138700	110.0	-6.34	44	0.0007	1.06E-03	3.43E-04	-3.46	-2.23	5.90E-03	46.9	0.043	4.28E-04	6903	2284.22	60.72	13.01
88-CO-27	3	5.90	24040	0.54	-8.64	19	0.0003	1.07E-03	7.66E-04	-3.12	-3.75	1.77E-04	50.92	0.044	4.40E-04	207	68.66	350.13	77.08
88-CO-23	3	6.23	11930	0.93	-8.41	32	0.0005	1.14E-03	6.15E-04	-3.21	-3.60	2.51E-04	30.82	0.037	3.72E-04	293	97.01	122.98	22.90
88-CO-30	3	5.80	6800	0.14	-9.22	17	0.0003	1.16E-03	8.85E-04	-3.05	-4.22	6.02E-05				70	23.29	292.01	
89CO-11	3	6.48	30934	6.7	-7.55	49	0.0008	1.33E-03	5.28E-04	-3.28	-3.06	8.67E-04	33.5	0.038	3.83E-04	1014	335.55	92.19	17.65
89CO-18	3	7.42	12283	1.1	-8.33	89	0.0015	1.57E-03	1.11E-04	-3.96	-3.68	2.07E-04	2.814	0.017	1.68E-04	243	80.31	152.94	12.83
89CO-03	3	6.40	1516	222.2	-6.03	58	0.0009	1.70E-03	7.54E-04	-3.12	-2.21	6.11E-03				7143	2363.47	0.64	
89CO-08	3	6.00	8995	144.9	-6.22	35	0.0006	1.71E-03	1.14E-03	-2.94	-2.32	4.75E-03	3.484	0.018	1.80E-04	5553	1837.47	4.90	0.44
89CO-09	3	6.47	5496	21.5	-7.04	62	0.0010	1.71E-03	6.90E-04	-3.16	-2.84	1.46E-03	281.4	0.078	7.78E-04	1707	564.72	9.73	3.79
88-CO-33	3	7.91	7590	71.0	-6.53	104	0.0017	1.74E-03	4.16E-05	-4.38	-2.52	3.04E-03	0.804	0.011	1.10E-04	3560	1177.85	6.44	0.36
88-CO-41	3	6.71	22100	3.1	-7.88	79	0.0013	1.80E-03	5.05E-04	-3.30	-3.43	3.71E-04	11.256	0.027	2.66E-04	434	143.61	153.88	20.48
91-CO-32	3	6.40	5315	2.1	-8.05	65	0.0011	1.91E-03	8.47E-04	-3.07	-3.59	2.59E-04				302	100.09	53.10	
89CO-05	3	6.40	10590	111.1	-6.33	76	0.0013	2.24E-03	9.93E-04	-3.00	-2.53	2.96E-03	2.144	0.015	1.53E-04	3467	1147.36	9.23	0.71
91-CO-36	3	7.51	3329	5.8	-7.61	132	0.0022	2.29E-03	1.33E-04	-3.88	-3.39	4.10E-04	1.34	0.013	1.31E-04	480	158.85	20.96	1.37
89CO-04	3	6.50	9340	158.7	-6.18	86	0.0014	2.30E-03	8.89E-04	-3.05	-2.45	3.57E-03	8.71	0.024	2.44E-04	4177	1382.03	6.76	0.83
88-CO-38	3	6.70	12500	48.0	-6.70	103	0.0017	2.36E-03	6.73E-04	-3.17	-2.79	1.63E-03	81.74	0.052	5.15E-04	1905	630.20	19.83	5.11
89CO-06	3	6.90	1012	618.6	-5.59	131	0.0022	2.69E-03	5.40E-04	-3.27	-2.19	6.40E-03	469	0.092	9.23E-04	7491	2478.86	0.41	0.19
88-CO-50	3	6.88	1640	3.4	-7.84	138	0.0023	2.86E-03	5.95E-04	-3.23	-3.72	1.90E-04	308.2	0.080	8.02E-04	222	73.59	22.29	8.94
91-CO-30	3	7.70	966	4.8	-7.70	177	0.0029	3.01E-03	1.15E-04	-3.94	-3.66	2.20E-04	2.948	0.017	1.70E-04	258	85.24	11.33	0.97

APPENDIX F

SEQUENTIAL EXTRACTION TEST RESULTS

Appendix F - Sequential Extraction Test Results

Sample	EPOXY CONTROL	FD1-B	FD1-E	FD6-D (host)	FD5-J (host)
SA Fracture (in^2)	0	2.25	2	4.5	3
SA Fracture (cm^2)	0	15	13	29	19
Mass Rock	50	97	70	17	69
Bulk U conc. (as ppm U3O8)	nd	2	3	3	<1
Bulk U conc. (as ppm U)	nd	0.57	0.85	0.85	<0.28
Fracture Filling Mineral Thickness	N/A (underneath)	N/A (fresh Ypp)	N/A (altered Ypp host)	host rock	host rock
Mineral	epoxy	Ypp	Ypp (altered)	host rock	host rock
Extraction#1 (1M MgNO3)					
Volume extractant	0.04	0.02	0.02	0.02	0.02
Uranium Conc. (ppb)	2.4	15	3.1	3.1	2.8
mass ext (ug)	0.10	0.30	0.06	0.06	0.06
Extraction#2 (0.5 M NaHCO3/Na2CO3)					
Volume extractant	0.04	0.02	0.02	0.02	0.02
Uranium Conc. (ppb)	5	60	8	25	7
mass ext (ug)	0.20	1.20	0.17	0.50	0.15
Extraction#3 (1M NaOAc to pH 5)					
Volume extractant	0.04	0.02	0.02	0.02	0.02
Uranium Conc. (ppb)	6	107	19	67	34
mass ext (ug)	0.26	2.14	0.38	1.34	0.68
Extraction#4 (0.04M NH2OH.HCl in 25% Acetic Acid)					
Volume extractant (L)	0.035	0.035	0.035	0.035	0.035
Uranium Conc. (ppb)	223	503	117	640	62
mass U ext (ug)	7.8	17.6	4.095	22.4	2.17
Fe Conc. (ppm)	10	88	41	199	57
Mn Conc. (ppm)	8	8	2	51	29
mass Fe extracted (mg)	0.4	3.1	1.4	7.0	2.0
mass Mn extracted (mg)	0.3	0.3	0.1	1.8	1.0
mass Fe+Mn extracted (mg)	0.6	3.3	1.5	8.8	3.0
mass as ferrihydrite (Fe2O3.H20) (mg)	1.2	10.0	4.6	22.5	6.5
mass as birnessite (MnO2) (mg)	0.4	0.4	0.1	2.8	1.6
total mass sorbent (mg)	1.6	10.4	4.7	25.4	8.1
iron mass basis (ug U/g Fe2O3)	**6755**	**1766**	**882**	**994**	**336**
manganese mass basis (ug U/g MnO2)	**18309**	**41297**	**43509**	**7933**	**1352**
sorbent mass basis (ug U/g Fe2O3+MnO2)	**4935**	**1694**	**864**	**883**	**269**
Total					
mass U ext (ug)	8.36	21.25	4.70	24.30	3.05
total mass basis (ug U/g bulk rock)	0.167	0.219	0.067	1.430	0.044
iron mass basis (ug UO2/g Fe2O3)	**7233**	**2131**	**1013**	**1078**	**473**
manganese mass basis (ug UO2/g MnO2)	**19604**	**49836**	**49969**	**8607**	**1901**
sorbent mass basis (ug UO2/g Fe2O3+MnO2)	**5284**	**2044**	**993**	**958**	**379**
SA basis (pCi U-238/m2)	na	4836	1204	2766	521
activity of Ra extracted (pCi)	0.2	2.6	0.6	1.6	1.5
SA basis (pCi Ra/m2)	na	1791	465	551	775
approx activity of 238-U extracted.	2.8	7.0	1.6	8.0	1.0
Ra/U activity ratio (percent)	7	37	39	20	149
%ug U extracted:					
Extn#1	1.15	1.41	1.32	0.26	1.83
Extn#2	2.39	5.65	3.53	2.06	4.78
Extn#3	3.06	10.07	8.08	5.51	22.28
Extn#4	93.39	82.87	87.07	92.17	71.10

Appendix F - Sequential Extraction Test Results

Sample	FD1-C	FD6-J
SA Fracture (in^2)	2.75	2.5
SA Fracture (cm^2)	18	16
Mass Rock	25	43
Bulk U conc. (as ppm U3O8)	nd	3
Bulk U conc. (as ppm U)	nd	0.85
Fracture Filling Mineral Thickness	bare to 0.2 mm	0.1 to 0.2 mm
Mineral	chlorite	chlorite
Extraction#1 (1M MgNO3)		
Volume extractant	0.02	0.02
Uranium Conc. (ppb)	2.2	3.1
mass ext (ug)	0.04	0.06
Extraction#2 (0.5 M NaHCO3/Na2CO3)		
Volume extractant	0.02	0.02
Uranium Conc. (ppb)	20	42
mass ext (ug)	0.40	0.84
Extraction#3 (1M NaOAc to pH 5)		
Volume extractant	0.02	0.02
Uranium Conc. (ppb)	38	90
mass ext (ug)	0.76	1.80
Extraction#4 (0.04M NH2OH.HCl in 25% Acetic Acid)		
Volume extractant (L)	0.035	0.035
Uranium Conc. (ppb)	141	222
mass U ext (ug)	4.935	7.77
Fe Conc. (ppm)	81	214
Mn Conc. (ppm)	33	30
mass Fe extracted (mg)	2.8	7.5
mass Mn extracted (mg)	1.2	1.1
mass Fe+Mn extracted (mg)	4.0	8.5
mass as ferrihydrite (Fe2O3.H20) (mg)	9.2	24.2
mass as birnessite (MnO2) (mg)	1.8	1.7
total mass sorbent (mg)	11.0	25.9
iron mass basis (ug U/g Fe2O3)	**538**	**321**
manganese mass basis (ug U/g MnO2)	**2701**	**4678**
sorbent mass basis (ug U/g Fe2O3+MnO2)	**449**	**300**
Total		
mass U ext (ug)	6.14	10.47
total mass basis (ug U/g bulk rock)	0.246	0.244
iron mass basis (ug UO2/g Fe2O3)	**669**	**432**
manganese mass basis (ug UO2/g MnO2)	**3360**	**6305**
sorbent mass basis (ug UO2/g Fe2O3+MnO2)	**558**	**404**
SA basis (pCi U-238/m2)	1143	2145
activity of Ra extracted (pCi)	1.1	1.8
SA basis (pCi Ra/m2)	620	1116
approx activity of 238-U extracted.	2.0	3.5
Ra/U activity ratio (percent)	54	52
%ug U extracted:		
Extn#1	0.72	0.59
Extn#2	6.52	8.02
Extn#3	12.38	17.19
Extn#4	80.39	74.20

Appendix F - Sequential Extraction Test Results

Sample	FD1-H	FD1-K	FD1-N	FD1-P	FD5-B
SA Fracture (in^2)	2.25	2.25	5	3	3
SA Fracture (cm^2)	15	15	32	19	19
Mass Rock	78	52	40	41	47
Bulk U conc. (as ppm U3O8)	3	6	4	4	5
Bulk U conc. (as ppm U)	0.85	1.70	1.13	1.13	1.41
Fracture Filling Mineral Thickness	bare to 0.1 mm	stains to 0.3 mm	stains to 0.2 mm	stains to 0.2 mm	0.1 mm
Mineral	hematite, limonite and	limonite	limonite, chlorite and	black oxide, limonite	limonite
Extraction#1 (1M MgNO3)					
Volume extractant	0.02	0.02	0.02	0.02	0.02
Uranium Conc. (ppb)	2.7	12	7.3	3.5	8.4
mass ext (ug)	0.05	0.24	0.15	0.07	0.17
Extraction#2 (0.5 M NaHCO3/Na2CO3)					
Volume extractant	0.02	0.02	0.02	0.02	0.02
Uranium Conc. (ppb)	11	471	283	315	301
mass ext (ug)	0.22	9.42	5.66	6.30	6.02
Extraction#3 (1M NaOAc to pH 5)					
Volume extractant	0.03	0.02	0.02	0.02	0.02
Uranium Conc. (ppb)	24	747	296	140	67
mass ext (ug)	0.72	14.94	5.92	2.80	1.34
Extraction#4 (0.04M NH2OH.HCl in 25% Acetic Acid)					
Volume extractant (L)	0.035	0.035	0.035	0.035	0.035
Uranium Conc. (ppb)	172	2242	874	887	225
mass U ext (ug)	6.02	78.47	30.59	31.045	7.875
Fe Conc. (ppm)	168	311	289	362	55
Mn Conc. (ppm)	34	45	207	803	34
mass Fe extracted (mg)	5.9	10.9	10.1	12.7	1.9
mass Mn extracted (mg)	1.2	1.6	7.2	28.1	1.2
mass Fe+Mn extracted (mg)	7.1	12.5	17.4	40.8	3.1
mass as ferrihydrite (Fe2O3.H20) (mg)	19.0	35.2	32.7	41.0	6.2
mass as birnessite (MnO2) (mg)	1.9	2.5	11.5	44.5	1.9
total mass sorbent (mg)	20.9	37.7	44.2	85.5	8.1
iron mass basis (ug U/g Fe2O3)	**316**	**2228**	**934**	**757**	**1264**
manganese mass basis (ug U/g MnO2)	**3198**	**31497**	**2669**	**698**	**4184**
sorbent mass basis (ug U/g Fe2O3+MnO2)	**288**	**2080**	**692**	**363**	**971**
Total					
mass U ext (ug)	7.01	103.07	42.32	40.22	15.40
total mass basis (ug U/g bulk rock)	0.090	1.982	1.058	0.981	0.328
iron mass basis (ug UO2/g Fe2O3)	**369**	**2926**	**1293**	**981**	**2472**
manganese mass basis (ug UO2/g MnO2)	**3726**	**41371**	**3692**	**905**	**8183**
sorbent mass basis (ug UO2/g Fe2O3+MnO2)	**335**	**2733**	**957**	**471**	**1899**
SA basis (pCi U-238/m2)	1596	23460	4334	6865	2629
activity of Ra extracted (pCi)	1.4	9.1	6	11	2.7
SA basis (pCi Ra/m2)	964	6269	1860	5683	1395
approx activity of 238-U extracted	2.3	34.1	14.0	13.3	5.1
Ra/U activity ratio (percent)	60	27	43	83	53
%ug U extracted:					
Extn#1	0.77	0.23	0.35	0.17	1.09
Extn#2	3.14	9.14	13.38	15.67	39.08
Extn#3	10.27	14.50	13.99	6.96	8.70
Extn#4	85.83	76.13	72.29	77.20	51.13

Appendix F - Sequential Extraction Test Results

Sample	FD5-D	FD5-G	FD5-G (phase1)	FD5-I	FD5-J (phase1)
SA Fracture (in^2)	2.5	3	4.5	3	2.3
SA Fracture (cm^2)	16	19	29	19	15
Mass Rock	54	69	29	53.9	27
Bulk U conc. (as ppm U3O8)	3	<1	<1	2	2
Bulk U conc. (as ppm U)	0.85	<0.28	<0.28	0.57	0.57
Fracture Filling Mineral Thickness	stains to 0.2 mm	stains	stains to 0.1 mm	0.2 to 0.5 mm	stains to 0.1 mm
Mineral	limonite, hematite,	limonite, hematite	limonite/clay	limonite	hematite
Extraction#1 (1M MgNO3)					
Volume extractant	0.04	0.04	0.02	0.02	0.02
Uranium Conc. (ppb)	4	2.8	49	4.5	51
mass ext (ug)	0.16	0.11	0.98	0.09	1.02
Extraction#2 (0.5 M NaHCO3/Na2CO3)					
Volume extractant	0.04	0.04	0.02	0.02	0.02
Uranium Conc. (ppb)	216	12	272	121	38
mass ext (ug)	8.64	0.48	5.44	2.42	0.76
Extraction#3 (1M NaOAc to pH 5)					
Volume extractant	0.04	0.04	0.02	0.02	0.02
Uranium Conc. (ppb)	105	29	222	66	24
mass ext (ug)	4.20	1.16	4.44	1.32	0.48
Extraction#4 (0.04M NH2OH.HCl in 25% Acetic Acid)					
Volume extractant (L)	0.035	0.035	0.020	0.035	0.020
Uranium Conc. (ppb)	845	152	603	139	214
mass U ext (ug)	29.575	5.32	12.06	4.865	4.28
Fe Conc. (ppm)	407	156	489	22	235
Mn Conc. (ppm)	255	105	105	16	90
mass Fe extracted (mg)	14.2	5.5	9.8	0.8	4.7
mass Mn extracted (mg)	8.9	3.7	2.1	0.6	1.8
mass Fe+Mn extracted (mg)	23.2	9.1	11.9	1.3	6.5
mass as ferrihydrite (Fe2O3.H20) (mg)	46.1	17.7	31.7	2.5	15.2
mass as birnessite (MnO2) (mg)	14.1	5.8	3.3	0.9	2.8
total mass sorbent (mg)	60.2	23.5	35.0	3.4	18.1
iron mass basis (ug U/g Fe2O3)	**642**	**301**	**381**	**1952**	**281**
manganese mass basis (ug U/g MnO2)	**2095**	**915**	**3631**	**5492**	**1503**
sorbent mass basis (ug U/g Fe2O3+MnO2)	**491**	**227**	**345**	**1440**	**237**
Total					
mass U ext (ug)	42.58	7.07	22.92	8.70	6.54
total mass basis (ug U/g bulk rock)	0.788	0.102	0.790	0.161	0.242
iron mass basis (ug UO2/g Fe2O3)	**923**	**400**	**724**	**3489**	**430**
manganese mass basis (ug UO2/g MnO2)	**3016**	**1217**	**6900**	**9816**	**2296**
sorbent mass basis (ug UO2/g Fe2O3+MnO2)	**707**	**301**	**655**	**2574**	**362**
SA basis (pCi U-238/m2)	8721	1207	2608	1484	1456
activity of Ra extracted (pCi)	12	1.4		2.3	
SA basis (pCi Ra/m2)	7440	723	na	1188	na
approx activity of 238-U extracted.	14.1	2.3	7.6	2.9	2.2
Ra/U activity ratio (percent)	85	60	-	80	na
%ug U extracted:					
Extn#1	0.38	1.58	4.28	1.04	15.60
Extn#2	20.29	6.79	23.73	27.83	11.62
Extn#3	9.86	16.40	19.37	15.18	7.31
Extn#4	69.47	75.23	52.62	55.95	65.46

Appendix F - Sequential Extraction Test Results

Sample	FD5-K (phaseI)	FD5-L	FD5-M	FD6-A (phaseI)	FD6-C
SA Fracture (in^2)	5	2	3	1.5	3
SA Fracture (cm^2)	32	13	19	10	19
Mass Rock	14	36	43	32	16
Bulk U conc. (as ppm U3O8)	nd	2	2	2	3
Bulk U conc. (as ppm U)	nd	0.57	0.57	0.57	0.85
Fracture Filling Mineral Thickness	thick	0.1 mm	stains to 0.1 mm	thick	0.1 to 0.3 mm
Mineral	limonite	?Mn oxides (purple to	limonite	limonite	limonite, hematite
Extraction#1 (1M MgNO3)					
Volume extractant	0.02	0.02	0.04	0.02	0.02
Uranium Conc. (ppb)	49	1.8	20	111	6
mass ext (ug)	0.98	0.04	0.80	2.22	0.12
Extraction#2 (0.5 M NaHCO3/Na2CO3)					
Volume extractant	0.02	0.02	0.04	0.02	0.02
Uranium Conc. (ppb)	1186	136	53	1744	1258
mass ext (ug)	23.72	2.72	2.12	34.88	25.16
Extraction#3 (1M NaOAc to pH 5)					
Volume extractant	0.02	0.02	0.04	0.02	0.02
Uranium Conc. (ppb)	905	89	62	769	454
mass ext (ug)	18.10	1.78	2.48	15.38	9.08
Extraction#4 (0.04M NH2OH.HCl in 25% Acetic Acid)					
Volume extractant (L)	0.020	0.035	0.035	0.020	0.035
Uranium Conc. (ppb)	2343	159	427	3441	1029
mass U ext (ug)	46.86	5.565	14.945	68.82	36.015
Fe Conc. (ppm)	524	318	16	411	210
Mn Conc. (ppm)	1600	649	311	600	283
mass Fe extracted (mg)	10.5	11.1	0.6	8.2	7.4
mass Mn extracted (mg)	32.0	22.7	10.9	12.0	9.9
mass Fe+Mn extracted (mg)	42.5	33.8	11.4	20.2	17.3
mass as ferrihydrite (Fe2O3.H20) (mg)	33.9	36.0	1.8	26.6	23.8
mass as birnessite (MnO2) (mg)	50.6	35.9	17.2	19.0	15.7
total mass sorbent (mg)	84.5	72.0	19.0	45.6	39.5
iron mass basis (ug U/g Fe2O3)	**1382**	**154**	**8246**	**2587**	**1514**
manganese mass basis (ug U/g MnO2)	**926**	**155**	**868**	**3626**	**2299**
sorbent mass basis (ug U/g Fe2O3+MnO2)	**554**	**77**	**785**	**1510**	**913**
Total					
mass U ext (ug)	89.66	10.10	20.35	121.30	70.38
total mass basis (ug U/g bulk rock)	6.404	0.281	0.473	3.791	4.398
iron mass basis (ug UO2/g Fe2O3)	**2644**	**280**	**11226**	**4560**	**2959**
manganese mass basis (ug UO2/g MnO2)	**1771**	**281**	**1182**	**6390**	**4492**
sorbent mass basis (ug UO2/g Fe2O3+MnO2)	**1061**	**140**	**1069**	**2661**	**1784**
SA basis (pCi U-238/m2)	9183	2586	3473	41414	12014
activity of Ra extracted (pCi)		2.8	3.8	14.7	15
SA basis (pCi Ra/m2)	na	2170	1963	15190	7750
approx activity of 238-U extracted.	29.6	3.3	6.7	40.1	23.3
Ra/U activity ratio (percent)	na	84	57	37	65
%ug U extracted:					
Extn#1	1.09	0.36	3.93	1.83	0.17
Extn#2	26.46	26.93	10.42	28.76	35.75
Extn#3	20.19	17.62	12.19	12.68	12.90
Extn#4	52.26	55.09	73.46	56.74	51.18

Appendix F - Sequential Extraction Test Results

Sample	FD6-D (phaseI)	FD6-E	FD6-F	FD6-I
SA Fracture (in^2)	4.5	5	4	2.5
SA Fracture (cm^2)	29	32	26	16
Mass Rock	92	43	48	57
Bulk U conc. (as ppm U3O8)	3	4	3	2
Bulk U conc. (as ppm U)	0.85	1.13	0.85	0.57
Fracture Filling Mineral Thickness	stains to 0.2 mm	stains to 0.2 mm	0.1 to 0.3 mm	stains to 0.2 mm
Mineral	hematite/limonite	limonite, hematite,	hematite, limonite	limonite, tr. hematite
Extraction#1 (1M MgNO3)				
Volume extractant	0.04	0.03	0.03	0.02
Uranium Conc. (ppb)	104	4	2.8	6.3
mass ext (ug)	4.16	0.12	0.08	0.13
Extraction#2 (0.5 M NaHCO3/Na2CO3)				
Volume extractant	0.04	0.03	0.03	0.02
Uranium Conc. (ppb)	223	494	308	46
mass ext (ug)	8.92	14.82	9.24	0.92
Extraction#3 (1M NaOAc to pH 5)				
Volume extractant	0.04	0.03	0.03	0.02
Uranium Conc. (ppb)	449	328	280	52
mass ext (ug)	17.96	9.84	8.40	1.04
Extraction#4 (0.04M NH2OH.HCl in 25% Acetic Acid)				
Volume extractant (L)	0.040	0.035	0.035	0.035
Uranium Conc. (ppb)	1963	838	729	177
mass U ext (ug)	78.52	29.33	25.515	6.195
Fe Conc. (ppm)	528	305	214	168
Mn Conc. (ppm)	227	286	309	57
mass Fe extracted (mg)	21.1	10.7	7.5	5.9
mass Mn extracted (mg)	9.1	10.0	10.8	2.0
mass Fe+Mn extracted (mg)	30.2	20.7	18.3	7.9
mass as ferrihydrite (Fe2O3.H20) (mg)	68.4	34.5	24.2	19.0
mass as birnessite (MnO2) (mg)	14.4	15.8	17.1	3.2
total mass sorbent (mg)	82.7	50.4	41.3	22.2
iron mass basis (ug U/g Fe2O3)	**1149**	**849**	**1053**	**326**
manganese mass basis (ug U/g MnO2)	**5467**	**1852**	**1491**	**1963**
sorbent mass basis (ug U/g Fe2O3+MnO2)	**949**	**582**	**617**	**279**
Total				
mass U ext (ug)	109.56	54.11	43.24	8.28
total mass basis (ug U/g bulk rock)	1.191	1.258	0.901	0.145
iron mass basis (ug UO2/g Fe2O3)	**1603**	**1566**	**1784**	**435**
manganese mass basis (ug UO2/g MnO2)	**7628**	**3417**	**2528**	**2624**
sorbent mass basis (ug UO2/g Fe2O3+MnO2)	**1325**	**1074**	**1046**	**373**
SA basis (pCi U-238/m2)	12468	5542	5536	1696
activity of Ra extracted (pCi)	5.3	12	6.7	1.5
SA basis (pCi Ra/m2)	1826	3720	2596	930
approx activity of 238-U extracted.	36.2	17.9	14.3	2.7
Ra/U activity ratio (percent)	15	67	47	55
%ug U extracted:				
Extn#1	3.80	0.22	0.19	1.52
Extn#2	8.14	27.39	21.37	11.11
Extn#3	16.39	18.19	19.43	12.56
Extn#4	71.67	54.20	59.01	74.81

Summary - Extraction Tests

Sample	Avg controls	Max	Min	SD
SA Fracture (in^2)	2.35	4.50	0.00	1.64
SA Fracture (cm^2)	15.16	29.03	0.00	10.55
Mass Rock	60.60	97.00	17.00	29.57
Bulk U conc. (as ppm U3O8)	2.67	3.00	2.00	0.58
Bulk U conc. (as ppm U)	0.75	0.85	0.57	0.16
Fracture Filling Mineral Thickness				
Mineral				
Extraction#1 (1M MgNO3)				
Volume extractant	0.02	0.04	0.02	0.01
Uranium Conc. (ppb)	5.28	15.00	2.40	5.44
mass ext (ug)	0.12	0.30	0.06	0.10
Extraction#2 (0.5 M NaHCO3/Na2CO3)				
Volume extractant	0.02	0.04	0.02	0.01
Uranium Conc. (ppb)	21.12	60.00	5.00	23.14
mass ext (ug)	0.44	1.20	0.15	0.45
Extraction#3 (1M NaOAc to pH 5)				
Volume extractant	0.02	0.04	0.02	0.01
Uranium Conc. (ppb)	46.68	107.00	6.40	40.62
mass ext (ug)	0.96	2.14	0.26	0.78
Extraction#4 (0.04M NH2OH.HCl in 25% Acetic Acid)				
Volume extractant (L)	0.04	0.04	0.04	0.00
Uranium Conc. (ppb)	309.00	640.00	62.00	251.23
mass U ext (ug)	10.82	22.40	2.17	8.79
Fe Conc. (ppm)	79.04	199.00	10.20	72.70
Mn Conc. (ppm)	19.42	51.00	1.70	20.48
mass Fe extracted (mg)	2.77	6.97	0.36	2.54
mass Mn extracted (mg)	0.68	1.79	0.06	0.72
mass Fe+Mn extracted (mg)	3.45	8.75	0.63	3.17
mass as ferrihydrite (Fe2O3.H20) (mg)	8.95	22.54	1.16	8.24
mass as birnessite (MnO2) (mg)	1.08	2.82	0.09	1.13
total mass sorbent (mg)	10.03	25.36	1.58	9.20
iron mass basis (ug U/g Fe2O3)	**2147**	**6755**	**336**	**2626**
manganese mass basis (ug U/g MnO2)	**22480**	**43509**	**1352**	**19182**
sorbent mass basis (ug U/g Fe2O3+MnO2)	**1729**	**4935**	**269**	**1862**
Total				
mass U ext (ug)	12.33	24.30	3.05	9.78
total mass basis (ug U/g bulk rock)	0.39	1.43	0.04	0.59
iron mass basis (ug U/g Fe2O3)	**2386**	**7233**	**473**	**2776**
manganese mass basis (ug U/g MnO2)	**25983**	**49969**	**1901**	**22731**
sorbent mass basis (ug U/g Fe2O3+MnO2)	**1931**	**5284**	**379**	**1968**
SA basis (pCi 238-U/m2)	2332	4836	521	1916
activity of Ra extracted (pCi)	1.30	2.60	0.20	0.94
SA basis (pCi Ra/m2)	895.56	1791.11	465.00	611.17
approx activity of 238-U extracted.	4.07	8.03	1.01	3.23
Ra/U activity ratio (percent)	50.32	148.75	7.24	56.53
Summary				
%ug U extracted:				
Extn#1	1.19	1.83	0.26	0.58
Extn#2	3.68	5.65	2.06	1.53
Extn#3	9.80	22.28	3.06	7.46
Extn#4	85.32	93.39	71.10	8.99

Summary - Extraction Tests

Sample	AVG Smectite	Max	Min	SD
SA Fracture (in^2)	2.625	2.75	2.5	0.18
SA Fracture (cm^2)	17	18	16	1.14
Mass Rock	34	43	25	12.73
Bulk U conc. (as ppm U3O8)	3	3	3	
Bulk U conc. (as ppm U)	0.85	0.85	0.85	
Fracture Filling Mineral Thickness				
Mineral				
Extraction#1 (1M MgNO3)				
Volume extractant	0.02	0.02	0.02	0.00
Uranium Conc. (ppb)	2.65	3.1		0.64
mass ext (ug)	0.05	0.06	0.04	0.01
Extraction#2 (0.5 M NaHCO3/Na2CO3)				
Volume extractant	0.02	0.02	0.02	0
Uranium Conc. (ppb)	31	42	20	16
mass ext (ug)	0.62	0.84	0.40	0.31
Extraction#3 (1M NaOAc to pH 5)				
Volume extractant	0.02	0.02	0.02	0
Uranium Conc. (ppb)	64	90	38	37
mass ext (ug)	1.28	1.80	0.76	0.74
Extraction#4 (0.04M NH2OH.HCl in 25% Acetic Acid)				
Volume extractant (L)	0.035	0.035	0.035	0.000
Uranium Conc. (ppb)	182	222	141	57
mass U ext (ug)	6.3525	7.77	4.935	2.0
Fe Conc. (ppm)	148	214	81	94
Mn Conc. (ppm)	32	33	30	2
mass Fe extracted (mg)	5.2	7.5	2.8	3.3
mass Mn extracted (mg)	1.1	1.2	1.1	0.1
mass Fe+Mn extracted (mg)	6.3	8.5	4.0	3.2
mass as ferrihydrite (Fe2O3.H20) (mg)	16.7	24.2	9.2	10.7
mass as birnessite (MnO2) (mg)	1.7	1.8	1.7	0.1
total mass sorbent (mg)	18.5	25.9	11.0	10.5
iron mass basis (ug U/g Fe2O3)	**429**	**538**	**321**	**154**
manganese mass basis (ug U/g MnO2)	**3690**	**4678**	**2701**	**1398**
sorbent mass basis (ug U/g Fe2O3+MnO2)	**374**	**449**	**300**	**105**
Total				
mass U ext (ug)	8.31	10.47	6.14	3.06
total mass basis (ug U/g bulk rock)	0.245	0.246	0.244	0.001
iron mass basis (ug U/g Fe2O3)	**551**	**669**	**432**	**168**
manganese mass basis (ug U/g MnO2)	**4833**	**6305**	**3360**	**2082**
sorbent mass basis (ug U/g Fe2O3+MnO2)	**481**	**558**	**404**	**109**
SA basis (pCi 238-U/m2)	1644	2145	1143	708
activity of Ra extracted (pCi)	1.5	1.8	1.1	0.5
SA basis (pCi Ra/m2)	868	1116	620	351
approx activity of 238-U extracted.	2.7	3.5	2.0	1.0
Ra/U activity ratio (percent)	53	54	52	2
Summary				
%ug U extracted:				
Extn#1	0.65	0.72	0.59	0.09
Extn#2	7.27	8.02	6.52	1.06
Extn#3	14.78	17.19	12.38	3.40
Extn#4	77.29	80.39	74.20	4.38

Summary - Extraction Tests

Sample	Avg Fe-oxides	Max	Min	SD
SA Fracture (in^2)	3.23	5.00	1.50	1.10
SA Fracture (cm^2)	21	32	10	7
Mass Rock	45.9	92.0	14.0	19.6
Bulk U conc. (as ppm U3O8)	3.125	6	2	1.204159458
Bulk U conc. (as ppm U)	0.88	1.70	0.57	0.34
Fracture Filling Mineral Thickness				
Mineral				
Extraction#1 (1M MgNO3)				
Volume extractant	0.025263158	0.04	0.02	0.00841191
Uranium Conc. (ppb)	23.68947368	111	1.8	33.92116505
mass ext (ug)	0.62	4.16	0.04	1.02
Extraction#2 (0.5 M NaHCO3/Na2CO3)				
Volume extractant	0.025263158	0.04	0.02	0.00841191
Uranium Conc. (ppb)	394	1744	11	478
mass ext (ug)	8.83	34.88	0.22	9.53
Extraction#3 (1M NaOAc to pH 5)				
Volume extractant	0.025789474	0.04	0.02	0.008377078
Uranium Conc. (ppb)	269	905	24	277
mass ext (ug)	6.39	18.10	0.48	6.15
Extraction#4 (0.04M NH2OH.HCl in 25% Acetic Acid)				
Volume extractant (L)	0.032	0.040	0.020	0.007
Uranium Conc. (ppb)	919	3441	139	928
mass U ext (ug)	27.46657895	78.52	4.28	24.84439474
Fe Conc. (ppm)	273	528	16	157
Mn Conc. (ppm)	317	1600	16	382
mass Fe extracted (mg)	8.4	21.1	0.6	4.9
mass Mn extracted (mg)	9.3	32.0	0.6	9.2
mass Fe+Mn extracted (mg)	17.6	42.5	1.3	12.0
mass as ferrihydrite (Fe2O3.H20) (mg)	27.1	68.4	1.8	16.0
mass as birnessite (MnO2) (mg)	14.6	50.6	0.9	14.6
total mass sorbent (mg)	41.8	85.5	3.4	25.5
iron mass basis (ug U/g Fe2O3)	**1385**	**8246**	**154**	**1801**
manganese mass basis (ug U/g MnO2)	**3923**	**31497**	**155**	**6853**
sorbent mass basis (ug U/g Fe2O3+MnO2)	**705**	**2080**	**77**	**516**
Total				
mass U ext (ug)	43.30	121.30	6.54	38.21
total mass basis (ug U/g bulk rock)	1.335	6.404	0.090	1.707
iron mass basis (ug U/g Fe2O3)	**2161**	**11226**	**280**	**2512**
manganese mass basis (ug U/g MnO2)	**5865**	**41371**	**281**	**9012**
sorbent mass basis (ug U/g Fe2O3+MnO2)	**1133**	**2733**	**140**	**830**
SA basis (pCi 238-U/m2)	7804	41414	1207	9830
activity of Ra extracted (pCi)	6.73125	15	1.4	4.885040941
SA basis (pCi Ra/m2)	3854	15190	723	3844
approx activity of 238-U extracted.	14.3	40.1	2.2	12.6
Ra/U activity ratio (percent)	57	85	15	21
Summary				
%ug U extracted:				
Extn#1	2.03	15.60	0.17	3.54
Extn#2	19.32	39.08	3.14	10.34
Extn#3	13.93	20.19	6.96	4.10
Extn#4	64.72	85.83	51.13	11.04

Extraction 1 - Metals by ICP-AES

Sample ID	Ag	Al	B	Ba	Be	Ca	Cd	Co	Cr	Cu	Fe	K	Li	Mg	Mo	Mn	Na	Ni	Pb	Sr	Sb	Ti	V	Zn
	ppb	ppm	ppb	ppb	ppb	ppm	ppb	ppb	ppb	ppb	ppm	ppm	ppb	ppm	ppb	ppm	ppm	ppb	ppb	ppm	ppb	ppb	ppb	ppb
epoxy control extn#1	<6.5	<0.075	<31.5	20	<1	14.7	32.9	46.3	<15.5	71.0	<0.5	1.9	<43	Saturated	172	0.6	<18	104.9	<125	0.04	<140	4.67	153	<80
kss fd1-b ext#1	<6.5	<0.075	<31.5	59	<1	32.8	39.3	57.5	<15.5	103.1	<0.5	3.7	<43	Saturated	197	1.0	<18	102.6	<125	0.07	<140	<3.5	154	<80
kss fd1-c ext#1	<6.5	<0.075	<31.5	237	<1	58.5	35.7	37.8	<15.5	153.4	<0.5	3.8	<43	Saturated	181	3.2	<18	114.5	<125	0.21	<140	5.35	153	81
kss fd1-d ext#1	<6.5	<0.075	<31.5	199	<1	282.0	35.6	64.3	<15.5	80.4	<0.5	10.7	<43	Saturated	182	1.1	<18	100.6	<125	0.72	<140	<3.5	157	112
kss fd1-e ext#1	<6.5	<0.075	<31.5	28	<1	53.5	36.1	62.2	<15.5	93.2	<0.5	4.0	<43	Saturated	187	0.8	<18	110.6	<125	0.13	<140	<3.5	157	<80
kss fd1-h ext#1	<6.5	<0.075	<31.5	58	<1	122.5	35.3	31.2	<15.5	73.1	<0.5	6.0	<43	Saturated	170	2.7	<18	100.3	<125	0.31	<140	<3.5	165	<80
kss fd1-k ext#1	<6.5	<0.075	<31.5	47	<1	161.0	39.2	31.3	<15.5	96.0	<0.5	8.0	<43	Saturated	197	4.8	<18	97.9	<125	0.30	<140	<3.5	148	347
kss fd1-n ext#1	8.10	<0.075	<31.5	17	<1	232.5	34.3	21.3	<15.5	81.8	<0.5	15.5	61.5	Saturated	173	4.6	<18	99.8	<125	0.35	<140	<3.5	149	108
kss fd1-p ext#1	<6.5	<0.075	<31.5	101	<1	319.5	39.3	<13	<15.5	60.4	<0.5	93.4	65.2	Saturated	186	6.9	<18	95.4	<125	0.56	<140	<3.5	167	392
kss fd1-q ext#1	<6.5	<0.075	<31.5	140	<1	210.5	39.3	35.9	<15.5	95.4	<0.5	17.2	72.2	Saturated	211	1.0	<18	106.5	<125	0.38	<140	<3.5	146	80
kss fd5-b ext#1	<6.5	<0.075	<31.5	68	<1	94.0	36.9	72.1	<15.5	85.9	<0.5	5.1	<43	Saturated	201	1.9	<18	179.0	<125	0.13	<140	<3.5	144	124
kss fd5-d ext#1	<6.5	<0.075	<31.5	285	<1	97.0	40.0	24.0	<15.5	74.7	<0.5	20.0	<43	Saturated	200	5.1	<18	107.3	<125	0.19	<140	<3.5	175	100
kss fd5-g ext#1	<6.5	<0.075	<31.5	108	<1	71.5	37.2	19.5	<15.5	84.1	<0.5	7.4	<43	Saturated	187	3.4	<18	99.9	<125	0.14	<140	<3.5	162	103
kss fd5-i ext#1	<6.5	<0.075	<31.5	176	<1	65.5	32.4	53.2	<15.5	66.2	<0.5	6.5	45.3	Saturated	148	1.0	<18	90.2	<125	0.13	<140	<3.5	150	<80
kss fd5-j ext#1	<6.5	<0.075	<31.5	125	<1	88.5	40.7	40.0	<15.5	106.5	<0.5	10.3	<43	Saturated	206	1.4	<18	91.9	<125	0.19	<140	<3.5	149	80
kss fd5-l ext#1	<6.5	<0.075	<31.5	79	<1	191.0	35.0	23.8	<15.5	80.6	<0.5	24.4	60.5	Saturated	190	6.4	<18	75.9	<125	0.63	<140	<3.5	153	84
kss fd5-m ext#1	<6.5	<0.075	<31.5	15	<1	69.5	35.1	18.1	<15.5	92.5	<0.5	6.6	48.3	Saturated	202	0.7	<18	62.2	<125	0.09	<140	<3.5	147	80
kss fd6-d ext#1	<6.5	<0.075	<31.5	483	<1	99.0	35.8	67.6	<15.5	94.5	<0.5	4.9	<43	Saturated	191	1.9	<18	104.8	<125	0.29	<140	<3.5	160	101
kss fd6-e ext#1	<6.5	<0.075	<31.5	382	<1	141.0	38.8	25.4	<15.5	61.3	<0.5	15.7	<43	Saturated	172	7.6	<18	92.6	<125	0.34	<140	<3.5	157	324
kss fd6-e ext#1(dupl)	<6.5	<0.075	<31.5	378	<1	141.5	37.1	19.4	<15.5	65.3	<0.5	16.5	<43	Saturated	177	7.6	<18	91.0	<125	0.34	<140	<3.5	160	322
kss fd6-f ext#1	<6.5	<0.075	<31.5	297	<1	61.5	35.4	28.3	<15.5	<30.5	<0.5	16.6	58.0	Saturated	194	3.7	<18	83.3	<125	0.18	<140	<3.5	171	<80
kss fd6-g ext#1	<6.5	<0.075	<31.5	304	<1	114.0	37.2	22.7	<15.5	58.1	<0.5	7.5	<43	Saturated	184	5.3	<18	106.8	<125	0.31	<140	<3.5	164	113
kss fd6-i ext#1	<6.5	<0.075	<31.5	1502	<1	335.0	41.8	22.1	<15.5	60.4	<0.5	15.5	<43	Saturated	199	6.5	<18	96.2	<125	0.79	<140	<3.5	167	82
kss fd6-i ext#1	<6.5	<0.075	<31.5	1385	<1	307.5	42.4	20.2	<15.5	79.4	<0.5	13.1	59.4	Saturated	206	5.8	<18	81.8	<125	0.72	<140	<3.5	144	85
kss fd6-j ext#1	<6.5	<0.075	<31.5	2010	<1	475.5	33.9	36.0	<15.5	65.8	<0.5	18.6	<43	Saturated	183	3.6	<18	90.8	<125	1.19	<140	<3.5	154	<80
kss fd6-l ext#1	<6.5	0.243	<31.5	1201	<1	112.0	38.5	81.1	<15.5	63.0	<0.5	14.5	53.1	Saturated	195	13.3	<18	104.7	<125	0.24	<140	<3.5	160	500

Extraction 2 - Metals by ICP-AES

Sample ID	Ag	Al	B	Ba	Be	Ca	Cd	Co	Cr	Cu	Fe	K	Li	Mg	Mo	Mn	Na	Ni	Pb	Sr	Sb	Ti	V	Zn
	ppb	ppm	ppb	ppb	ppb	ppm	ppb	ppb	ppb	ppb	ppm	ppm	ppb	ppm	ppb	ppm	ppm	ppb	ppb	ppm	ppb	ppb	ppb	ppb
epoxy control ext#2	<6.5	0.198	128	51.8	<1	4.3	<5.5	<13	42.2	50	<0.5	13.3	130	11.3	<29.5	<0.05	8086	<26.4	<125	0.20	<140	79.9	<11.5	<80
kss fd1-b ext#2	<6.5	<0.075	101	58.1	<1	5.5	<5.5	16.8	46.1	196	0.89	22.8	192	85.3	38	<0.05	9711	<26.4	<125	0.21	<140	84.4	<11.5	<80
kss fd1-c ext#2	<6.5	<0.075	<31.5	53.5	<1	7.6	<5.5	<13	44.3	442	0.74	16.3	181	62.5	38	0.24	10303	<26.4	<125	0.22	<140	84.2	<11.5	<80
kss fd1-c ext#2 (rep)	<6.5	0.204	98	53.9	<1	7.5	<5.5	15.0	48.4	411	0.74	14.9	103	61.0	42	0.24	13880	<26.4	<125	0.21	<140	88.7	<11.5	<80
kss fd1-d ext#2	<6.5	<0.075	98	52.4	<1	15.3	<5.5	17.1	35.2	164	<0.5	22.7	135	220.3	<29.5	<0.05	8372	<26.4	<125	0.21	<140	77.1	<11.5	<80
kss fd1-e ext#2	<6.5	0.102	<31.5	53.2	<1	10.3	<5.5	17.1	36.3	88	<0.5	16.9	122	77.4	34	<0.05	9147	<26.4	<125	0.19	<140	80.8	<11.5	<80
kss fd1-e ext#2 (rep)	<6.5	0.283	189	49.4	<1	9.7	<5.5	21.9	47.2	90	<0.5	13.4	111	71.8	<29.5	<0.05	12559	<26.4	<125	0.18	<140	79.3	<11.5	<80
kss fd1-h ext#2	<6.5	0.124	104	33.4	1	15.5	<5.5	<13	36.3	60	0.53	12.2	129	152.8	42	0.07	13964	<26.4	<125	0.19	<140	74.2	<11.5	<80
kss fd1-k ext#2	16.01	<0.075	392	13.5	<1	15.8	<5.5	<13	42.1	190	<0.5	17.9	209	181.3	350	0.12	10005	<26.4	<125	0.18	336	76.9	<11.5	<80
kss fd1-k ext#2 (rep)	<6.5	<0.075	32	14.0	<1	15.6	<5.5	<13	31.3	73	<0.5	15.3	125	179.1	328	0.12	14800	<26.4	<125	0.17	<140	79.3	<11.5	<80
kss fd1-n ext#2	<6.5	0.096	229	<3.5	<1	13.4	<5.5	<13	35.0	116	0.56	19.5	143	158.1	383	<0.05	14176	<26.4	<125	0.05	<140	75.8	<11.5	<80
kss fd1-p ext#2	<6.5	<0.075	<31.5	5.3	<1	24.2	<5.5	<13	40.5	48	<0.5	58.9	159	471.4	625	<0.05	9991	<26.4	<125	0.14	<140	66.6	<11.5	<80
kss fd1-q ext#2	<6.5	<0.075	92	51.4	<1	13.5	<5.5	<13	37.4	88	<0.5	23.5	162	120.6	<29.5	<0.05	8950	<26.4	<125	0.16	<140	72.2	<11.5	<80
kss fd5-b ext#2	<6.5	0.083	<31.5	39.2	<1	14.8	<5.5	<13	41.1	44	<0.5	15.8	117	171.8	<29.5	<0.05	8655	<26.4	<125	0.18	<140	79.1	<11.5	<80
kss fd5-d ext#2	7.03	0.114	301	16.7	1	10.2	<5.5	<13	46.4	125	0.50	27.2	186	112.9	106	0.06	8961	<26.4	<125	0.15	<140	75.8	<11.5	<80
kss fd5-g ext#2	<6.5	0.076	<31.5	10.6	<1	9.7	<5.5	<13	33.9	78	0.52	11.7	119	77.0	48	0.12	14677	<26.4	<125	0.16	<140	75.5	<11.5	<80
kss fd5-i ext#2	<6.5	0.131	139	52.7	1	13.6	<5.5	<13	44.5	97	<0.5	20.8	136	105.4	<29.5	<0.05	8485	<26.4	<125	0.19	<140	76.4	<11.5	<80
kss fd5-j ext#2	<6.5	0.252	59	61.5	<1	12.8	<5.5	<13	38.4	58	0.54	21.6	112	99.2	33	0.08	8417	<26.4	<125	0.15	<140	88.2	<11.5	<80
kss fd5-l ext#2	<6.5	0.246	119	15.2	<1	15.1	<5.5	<13	41.7	78	1.24	27.1	135	140.9	389	0.59	8338	<26.4	<125	0.08	<140	77.4	<11.5	<80
kss fd5-m ext$2	<6.5	<0.075	296	11.2	1	7.9	<5.5	<13	36.0	93	<0.5	10.9	146	79.2	50	0.19	14884	<26.4	<125	0.16	<140	74.3	<11.5	<80
kss fd6-c ext#2	<6.5	0.221	60	18.9	<1	11.4	<5.5	<13	44.7	44	<0.5	20.3	118	228.5	853	0.09	8656	<26.4	<125	0.09	<140	71.3	<11.5	<80
kss fd6-d ext#2	<6.5	0.236	105	108.9	<1	13.0	<5.5	15.6	40.5	121	0.62	19.9	135	138.4	35	0.05	8516	<26.4	<125	0.21	<140	77.2	<11.5	<80
kss fd6-e ext#2	<6.5	0.188	96	11.5	<1	14.1	<5.5	<13	43.0	41	<0.5	24.0	110	161.0	423	0.10	8244	<26.4	<125	0.11	<140	73.3	<11.5	<80
kss fd6-f ext#2	<6.5	0.100	188	9.8	<1	9.5	<5.5	<13	35.2	61	0.53	14.3	136	96.6	647	0.08	14022	<26.4	<125	0.09	<140	72.7	<11.5	<80
kss fd6-g ext#2	<6.5	<0.075	<31.5	6.4	<1	13.6	<5.5	<13	48.3	84	<0.5	17.4	135	106.9	107	0.10	9442	<26.4	<125	0.11	<140	84.0	<11.5	<80
kss fd6-i ext#2	<6.5	0.086	127	23.5	1	14.5	5.67	<13	35.3	85	0.51	17.0	130	196.6	75	0.11	13965	<26.4	<125	0.04	<140	74.8	<11.5	<80
kss fd6-j ext#2	<6.5	<0.075	<31.5	18.0	2	11.0	<5.5	<13	43.9	77	<0.5	16.8	129	268.0	38	0.08	16766	<26.4	<125	0.02	<140	82.4	<11.5	<80

Extraction 3 - Metals by ICP-AES

Sample ID	Ag	Al	B	Ba	Be	Ca	Cd	Co	Cr	Cu	Fe	K	Li	Mg	Mo	Mn	Na	Ni	Pb	Sr	Sb	Ti	V	Zn
	ppb	ppm	ppb	ppb	ppb	ppm	ppb	ppb	ppb	ppb	ppm	ppm	ppb	ppm	ppb	ppm	ppm	ppb	ppb	ppm	ppb	ppb	ppb	ppb
epoxy ext3	<6.5	0.08	265	42.2	1.00	14.7	<5.5	44.8	<15.5	<30.5	<0.5	30.3	121	8.2	88.4	0.22	12996	56.6	<125	0.053	<140	<3.5	<11.5	<80
kss fd1b ext3	<6.5	0.17	219	67.5	8.25	53.0	<5.5	47.1	<15.5	59.7	1.00	36.5	109	13.8	84.4	1.53	12157	41.0	<125	0.121	<140	<3.5	<11.5	<80
kss fd1c ext3	<6.5	0.53	233	109.8	6.88	25.1	<5.5	46.0	<15.5	310.4	1.86	38.6	135	25.9	98.2	4.33	12487	69.0	<125	0.167	<140	<3.5	<11.5	228
kss fd1d ext3	<6.5	1.05	253	105.3	91.23	345.3	<5.5	60.4	<15.5	65.3	2.03	44.0	145	82.8	<29.5	7.53	12920	43.6	143	0.414	<140	<3.5	<11.5	536
kss fd1e ext3	<6.5	0.17	265	34.3	6.66	28.9	<5.5	38.0	<15.5	40.8	<0.5	35.0	123	25.6	37.2	0.30	11790	42.4	<125	0.096	<140	<3.5	<11.5	<80
kss fd1e ext3 (dupl)	<6.5	0.46	236	30.9	6.01	29.0	<5.5	43.8	<15.5	31.9	<0.5	26.4	90	26.0	48.6	0.30	13942	57.7	<125	0.090	<140	4.53	<11.5	<80
kss fd1h ext3	<6.5	0.44	230	27.9	8.48	38.6	<5.5	40.8	<15.5	<30.5	<0.5	28.7	107	28.1	45.8	2.77	12404	55.2	<125	0.127	<140	<3.5	<11.5	101
kss fd1k ext3	<6.5	1.42	292	169.9	12.56	61.1	49.4	35.3	<15.5	35.5	0.64	35.9	88	52.7	52.8	7.15	15244	65.5	<125	0.209	<140	<3.5	<11.5	807
kss fd1n ext3	<6.5	1.57	226	64.3	37.92	101.9	<5.5	17.1	<15.5	85.0	0.89	33.3	116	83.1	91.3	11.36	12522	57.0	<125	0.351	<140	<3.5	<11.5	379
kss fd1p ext3	<6.5	1.48	256	189.9	52.63	46.4	7.4	<13	<15.5	<30.5	1.59	46.2	140	78.8	73.3	12.69	12036	94.1	<125	0.326	<140	<3.5	<11.5	689
kss fd1q ext3	<6.5	0.44	263	123.7	32.07	167.4	<5.5	34.5	<15.5	<30.5	11.18	32.3	105	72.3	62.4	5.42	13570	51.2	<125	0.345	<140	<3.5	<11.5	150
kss fd5b ext3	<6.5	0.39	226	63.6	7.49	76.0	<5.5	67.3	<15.5	<30.5	<0.5	27.1	130	53.8	36.2	1.90	10339	64.4	<125	0.129	<140	<3.5	<11.5	88
kss fd5d ext3	<6.5	1.44	296	336.1	41.07	38.8	6.1	<13	<15.5	45.9	<0.5	32.4	120	60.1	81.6	5.89	12313	39.8	<125	0.163	<140	<3.5	<11.5	178
kss fd5g ext3	<6.5	0.49	250	259.4	7.50	35.0	<5.5	15.5	<15.5	65.1	<0.5	32.3	116	30.6	47.5	7.25	12223	56.2	<125	0.148	<140	<3.5	<11.5	376
kss fd5i ext3	<6.5	0.38	325	210.1	16.60	70.5	<5.5	46.5	<15.5	37.3	<0.5	32.3	113	86.7	73.4	1.05	12032	75.6	<125	0.176	<140	<3.5	<11.5	<80
kss fd5j ext3	<6.5	0.72	244	167.8	3.45	63.1	7.7	33.8	<15.5	39.2	0.90	36.6	133	43.0	76.9	3.35	11438	207.1	<125	0.166	<140	<3.5	<11.5	125
kss fd5j ext3 (dupl)	<6.5	1.08	232	174.2	2.88	64.3	6.5	26.2	<15.5	36.6	0.88	32.3	94	43.2	32.9	3.42	13546	229.8	<125	0.174	<140	3.59	<11.5	119
kss fd5l ext3	<6.5	1.39	406	642.1	33.62	64.2	9.6	22.6	<15.5	113.6	1.39	34.6	127	63.3	48.7	36.64	13251	82.1	<125	0.882	<140	<3.5	<11.5	1545
kss fd5m ext3	29.8	0.66	260	456.3	7.69	1720.9	5.5	23.6	<15.5	<30.5	2.05	33.4	139	116.2	61.1	92.06	13274	48.1	<125	0.705	<140	<3.5	<11.5	240
kss fd6c ext3	<6.5	3.00	243	1133.4	15.65	36.2	<5.5	54.7	<15.5	63.8	<0.5	33.8	129	120.5	69.4	12.70	12692	56.4	<125	0.244	<140	<3.5	<11.5	410
kss fd6d ext3	<6.5	0.98	251	436.7	4.99	88.4	<5.5	43.5	<15.5	68.9	0.81	29.4	115	103.8	<29.5	2.57	12869	60.2	<125	0.315	<140	<3.5	<11.5	137
kss fd6e ext3	<6.5	2.01	263	825.8	25.97	63.8	10.5	15.0	<15.5	60.8	<0.5	34.0	113	135.5	64.9	13.35	12865	51.9	<125	0.341	<140	<3.5	<11.5	917
kss fd6f ext3	<6.5	0.77	261	1168.9	9.09	47.5	<5.5	<13	<15.5	62.5	0.53	33.7	109	99.6	57.0	14.59	13694	66.1	<125	0.312	<140	<3.5	<11.5	371
kss fd6g ext3	<6.5	0.87	260	625.3	6.08	85.8	<5.5	<13	<15.5	92.4	<0.5	31.7	105	108.3	51.2	10.06	14090	53.8	<125	0.342	<140	<3.5	<11.5	310
kss fd6i ext3	<6.5	2.11	275	1056.3	17.94	126.0	13.0	<13	<15.5	43.9	0.88	32.4	102	112.9	29.5	10.15	14506	59.2	<125	0.412	<140	<3.5	<11.5	360
kss fd6j ext3	<6.5	2.51	303	1327.7	34.06	217.2	7.1	21.3	<15.5	58.3	0.63	29.7	133	169.6	68.9	6.01	12231	62.0	<125	0.647	<140	<3.5	<11.5	128

Extraction 4 - Metals by ICP-AES

Sample ID	Ag	Al	B	Ba	Be	Ca	Cd	Co	Cr	Cu	Fe	K	Li	Mg	Mo	Mn	Na	Ni	Pb	Sr	Sb	Ti	V	Zn
	ppb	ppm	ppb	ppb	ppb	ppm	ppb	ppb	ppb	ppb	ppm	ppm	ppb	ppm	ppb	ppm	ppm	ppb	ppb	ppm	ppb	ppb	ppb	ppb
epoxy ext4	<13	133	708	840	27.6	102	18.4	613	<31	68.2	10	5.4	226	51.1	154	5.2	46	156	285	0.352	<280	19.1	26.4	278
kss fd1k ext4	<13	155	901	583	72.1	75	43.8	585	<31	<61	311	6.3	282	14.6	391	45.4	202	179	850	0.173	<280	31.2	<23	2675
kss fd5d ext4	<13	475	732	6648	271.2	140	82.1	747	<31	90.8	407	17.9	593	69.9	258	255.3	229	229	935	0.629	<280	<7	31.7	3658
kss fd5i ext4	21.9	279	2614	3041	91.2	138	25.4	718	<31	89.3	22	8.4	209	58.1	251	15.8	118	263	596	0.238	<280	37.9	71.2	351
kss fd6i ext4	<13	301	270	3791	119.9	97	56.3	549	<31	<61	168	8.8	530	80.3	140	56.7	256	177	797	0.306	<280	11.4	51.4	2073
kss fd1b ext4	<13	155	570	653	27.8	131	24.2	877	<31	124.3	88	5.4	278	15.3	209	7.7	57	167	770	0.279	<280	298.9	26.8	395
kss fd1c ext4	<13	504	290	1006	48.2	65	32.7	497	<31	289.5	81	4.5	518	10.4	163	32.7	93	184	659	0.239	<280	494.6	60.7	1641
kss fd1e ext4	<13	317	1060	236	37.1	68	28.3	865	<31	66.1	41	5.1	290	13.5	212	1.7	106	154	700	0.089	<280	310.1	46.1	425
kss fd1e ext4 (dupl)	<13	316	985	166	36.6	68	27.2	879	<31	102.2	41	8.6	271	13.6	291	1.7	258	162	482	0.093	<280	315.2	52.6	433
kss fd1h ext4	<13	399	758	463	115.3	148	46.8	1358	<31	<61	168	6.7	413	28.4	236	34.1	181	180	489	0.228	<280	15.6	44.3	1729
kss fd1n ext4	<13	93	445	740	193.0	99	42.8	686	<31	<61	289	9.1	377	35.6	303	206.9	242	165	631	0.397	<280	<7	<23	2091
kss fd1p ext4	24	514	642	19660	248.3	193	68.5	588	<31	<61	362	28.6	508	34.8	270	803.4	438	181	1184	1.532	<280	<7	<23	5218
kss fd5b ext4	<13	267	920	1266	53.7	126	36.1	1044	<31	107.2	55	9.9	232	40.1	218	33.7	93	292	778	0.299	<280	13.2	46.7	1005
kss fd5g ext4	<13	404	869	1378	126.9	122	45.8	656	<31	103.3	156	9.8	393	30.5	303	105.2	165	274	623	0.260	<280	63.9	57.6	2660
kss fd5j ext4	39	197	1189	1242	29.3	99	34.7	577	<31	110.5	57	8.1	287	18.6	333	29.0	119	155	569	0.111	<280	530.1	36.9	1044
kss fd5l ext4	39	55	751	8928	150.9	77	39.3	745	<31	90.1	318	16.7	240	47.4	296	649.1	149	232	338	3.146	<280	<7	<23	3809
kss fd5m ext4 (dupl)	17	279	85	3200	54.8	1513	30.5	498	<31	133.5	16	19.1	237	146.5	278	311.6	480	159	253	0.840	<280	<7	66.7	626
kss fd5m-ext4	121	280	820	4181	55.5	1529	28.6	498	<31	79.2	16	11.2	255	146.2	361	311.0	186	151	673	0.831	<280	<7	78.6	653
kss fd6c ext4	<13	201	758	20498	111.7	247	49.0	902	<31	249.4	210	10.1	400	32.2	271	283.1	160	198	516	1.184	<280	<7	166.7	3908
kss fd6d ext4	<13	393	530	1540	88.0	187	37.3	686	<31	89.7	199	7.9	454	87.4	117	51.4	135	322	614	0.378	<280	12.6	59.0	1478
kss fd6e ext4	<13	379	786	5834	154.5	208	64.7	750	<31	150.1	305	11.8	294	72.3	233	286.1	267	181	426	0.408	<280	<7	59.8	4520
kss fd6e ext4 (dupl)	<13	383	639	5790	156.7	210	70.8	750	<31	185.4	310	16.4	278	74.2	208	293.4	456	146	625	0.415	<280	<7	69.8	4513
kss fd6f ext4	<13	377	309	10395	50.7	83	43.1	840	<31	64.1	214	9.3	233	66.0	313	308.9	155	170	391	0.299	<280	<7	35.9	1658
kss fd6j ext4	<13	333	1493	3398	239.7	126	54.0	612	<31	67.3	214	11.4	767	105.6	170	29.8	391	165	<250	0.431	<280	11.9	54.4	1695
kss fd6-a (phase 1)	<65	39	3416	36316	168.1	228	55.1	530	<155	921.2	411	19.0	659	115.6	448	601.6	1132	655	2053	1.651	<1500	<35	<115	7204
kss fd6-d (phase 1)	<65	70	1961	8859	287.0	172	90.1	265	<155	584.7	528	<15	1094	60.4	660	226.7	1099	741	1199	0.397	<1500	<35	<115	5585
kss fd5-f (phase 1)	<65	38	1933	2639	325.5	82	58.8	265	<155	653.0	489	<15	554	16.4	438	102.8	705	655	1688	0.127	<1500	86.3	249.7	5414
kss fd5-j (phase 1)	<65	64	2918	2211	169.1	105	<55	240	<155	537.2	235	20.1	764	27.4	<300	87.9	802	914	<1250	0.196	<1500	109.3	<115	3649
kss fd5-k (phase 1)	174	8	3659	16987	465.1	4014	101.4	2334	<155	354.2	524	112.7	496	434.8	<300	1598.9	1728	2114	1842	3.843	<1500	<35	<115	44573